Characterization of the chloroplast protein import receptors in the single-cell C_4 species *Bienertia sinuspersici*

by

Shiu Cheung Lung

A thesis

presented to the University of Waterloo

in fulfillment of the

thesis requirement for the degree of

Doctor of Philosophy

in

Biology

Waterloo, Ontario, Canada, 2012

Author's declaration

I hereby declare that I am the sole author of this thesis. This is a true copy of the thesis, including any required final revisions, as accepted by my examiners.

I understand that my thesis may be made electronically available to the public.

Abstract

Bienertia sinuspersici is one of the three currently known land plants which perform C_4 photosynthesis without the conventional dual-cell system, but rather through intracellular compartmentation of organelles and enzymes within individual photosynthetic cells. Whilst earlier works have involved anatomical and molecular techniques to understand the unique organelle partitioning, the lack of technology for gene manipulation and organelle purification has precluded biochemical characterization of this novel single-cell C_4 model. Of particular interest is the unknown mechanism(s) leading to the differential accumulation of photosynthetic enzymes in the dimorphic chloroplasts within the same cells, which implicates the selective import of precursor proteins into the organelles.

The first part of this thesis describes the establishment of multiple cell biology techniques for studying the single-cell C_4 model. First, procedures have been optimized for isolating a homogenous population of chlorenchyma protoplasts from *B. sinuspersici*. Cell viability and preservation of the complex organelle compartmentation were confirmed by cytochemical staining and transient expression of fluorescent fusion proteins. The versatility of this highly efficient gene manipulation system was exemplified by the sorting of various fusion proteins to their respective subcellular locations. The isolation of intact chlorenchyma protoplasts has also led to the successful purification of the dimorphic chloroplasts. A protocol has been optimized for hypo-osmotic lysis of isolated protoplasts and concomitant separation of the central chloroplasts embedded in discrete ball structures and the peripheral chloroplasts adhered to the vacuole surface. The dimorphic chloroplasts were further purified to high homogeneity as evaluated by immunoblotting of their respective protein markers.

The second part of this thesis reports the identification and characterization of the chloroplast protein import receptors Toc159 and Toc34 in *B. sinuspersici*. Protein expression profiling revealed independent regulation of two identified Toc159 isoforms during leaf development, implicating their different substrate selectivities. Several subcellular localization approaches consistently demonstrated the co-existence of a cytosolic form of Toc159, which was found to interact with actin filaments and microtubules. This unique localization pattern is pertinent to the concurrent discovery of a novel mechanism for the reversible targeting of Toc159 to the chloroplast surface. Multiple computational methods predicted a chloroplastic transit peptide-like sorting signal at the carboxyl end of Toc159, which was experimentally demonstrated to guide passenger proteins to the chloroplast envelope or stroma depending on its orientation.

Collectively, the data in this thesis point to a chloroplast protein import model proposing that a novel sorting signal guides the movement of the Toc159 receptor to and from the chloroplast surface for preprotein targeting which may be assisted by the cytoskeleton. In light of the established gene manipulation and organelle purification techniques, the mechanism for selective protein import into dimorphic chloroplasts can be studied in the future.

Acknowledgements

First and foremost, I would like to thank my primary supervisor, Dr. Simon Chuong, for his invaluable guidance and constructive criticisms throughout my PhD study, taking me on a journey of discovery, wonderment and learning. His enthusiasm and unobtrusive way of supervision were just perfect for bringing in inspirations and novel ideas to my project. In addition, I am deeply indebted to my co-supervisor, Prof. Barb Moffatt, for her critical insights, continual encouragement and tremendous support at various levels, making my academic pursuit that memorable and my learning experience that fruitful in the past four years.

I would like to express my gratitude to my committee members, Dr. Brendan McConkey and Dr. Matt Smith, for their insightful feedback and ongoing advice. Without Matt's helpful support and his generous sharing of expertise, the completion of this thesis would not have been possible. I would also like to thank my external examiners, Prof. Danny Schnell and Dr. Betsy Daub, for devoting their precious time to review my thesis and provide valuable feedback and suggestions.

I would also like to extend my appreciation to my many colleagues and friends at the University of Waterloo, including but not limited to: Makoto Yanagisawa, Sarah Schoor, Jennifer Northmore, Dr. Ayumu Kondo, Sanghyun Lee, Katja Engel, Ishari Waduwara-Jayabahu, Yong Li, Tony Facciuolo, Zhenyu Cheng.

Last but not least, I sincerely thank my parents and my uncle Saiwan for their great support and encouragement.

Table of contents

List of figures

List of tables

List of abbreviations

ADP	Adenosine diphosphate
APS	Ammonium persulfate
ATP	Adenosine triphosphate
bp	Basepair(s)
BCA	Bicinchoninic acid
BLAST	Basic Local Alignment Search Tool
BSA	Bovine serum albumin
BYA	Billion years ago
CA	Carbonic anhydrase
CAM	Crassulacean acid metabolism
CCC	Central cytoplasmic compartment
C-Chl	Central chloroplast
CDCFDA	5-(and-6)-Carboxy-2',7'-dichlorofluorescein diacetate
cDNA	Complementary deoxyribonucleic acid
cICAT	Cleavable stable isotope coded affinity tags
ClpC	Caseinolytic protease, subunit C
CoA	Coenzyme A
CS	Cleavage site of stromal processing peptidase
CT	C-Terminal tail
cTP	Chloroplastic transit peptide
Cyt-f	Cytochrome f
Da	Dalton
DAPI	4',6-Diamidino-2-phenylindole

DNA	Deoxyribonucleic acid
ECL	Enhanced chemiluminescence
EDTA	Ethylene diamine tetraacetic acid
EGFP	Enhanced green fluorescent protein
EGTA	Ethylene glycol tetraacetic acid
Fd	Ferredoxin
FDA	Fluorescein diacetate
FNR	Ferredoxin:$NADP^+$ reductase
GFP	Green fluorescent protein
GTP	Guanosine triphosphate
HEPES	(4-(2-Hydroxyethyl)-1-piperazineethanesulfonic acid
Hip	Heat shock protein 70-interacting protein
Hop	Heat shock protein70/heat shock protein 90-organizing protein
Hsp	Heat shock protein
IMAC	Immobilized metal ion affinity chromatography
iTRAQ	Isobaric tag for relative and absolute quantitation
kb	Kilobase
LB	Luria-Bertani
LC-MS	Liquid chromatography-mass spectrometry
LTQ	Linear ion trap triple quadrupole
MAP4	Microtubule-associated protein 4
MDH	Malate dehydrogenase
ME	Malic enzyme
MES	2-(N-morpholino)ethanesulfonic acid

MGDG	Monogalactosyldiacylglycerol
MOPS	4-morpholinepropanesulfonic acid
mRNA	Messenger ribonucleic acid
NAD	Nicotinamide adenine dinucleotide
NADP(H)	Nicotinamide adenine dinucleotide phosphate (reduced)
NLS	Nuclear localization signal
OAA	oxaloacetate
OD	Optical density
OEP	Outer envelope protein
PAGE	Polyacrylamide gel electrophoresis
PBS	Phosphate-buffered saline
P-Chl	Peripheral chloroplasts
PCC	Peripheral cytoplasmic compartment
PCR	Polymerase chain reaction
PEG	Polyethylene glycol
PEP	Phosphoenolpyruvate
PEPC	Phosphoenolpyruvate carboxylase
PEP-CK	Phosphoenolpyruvate carboxykinase
pI	Isoelectric point
PIPES	Piperazine-N,N'-bis(2-ethanesulfonic acid)
POTRA	Polypeptide-transport-associated
PPDB	Plant Proteome Database
PPDK	Pyruvate orthophosphate dikinase
PsaD	Photosystem I subunit II protein
PsbO	Photosystem II manganese-stabilizing protein

PSI	Position-Specific Iterative
PTS	Peroxisomal targeting signal
PVDF	Polyvinylidene fluoride
RACE	Rapid amplification of cDNA ends
RbcL	Ribulose 1,5-bisphosphate carboxylase/oxygenase large-subunit
RbcS	Ribulose 1,5-bisphosphate carboxylase/oxygenase small-subunit
RNA	Ribonucleic acid
rpm	Revolutions per minute
RT-PCR	Reverse transcription polymerase chain reaction
Rubisco	Ribulose 1,5-bisphosphate carboxylase/oxygenase
SD	Standard deviation
SDS	Sodium dodecyl sulfate
SE	Standard error
TBS	Tris-buffered saline
T-DNA	Transfer DNA
TEMED	Tetramethylethylenediamine
Ti	Tumor-inducing
Tic	Translocon at the inner envelope membrane of chloroplasts
TMD	Transmembrane domain
Toc	Translocon at the outer envelope membrane of chloroplasts
TP	Transit peptide

Chapter 1. General introduction

1.1 Photosynthesis

The synthesis of carbohydrates from carbon dioxide and water at the expense of energy (i.e. ATP) and reducing power (i.e. NADPH) generated from the energy of sunlight is referred to as photosynthesis (Taiz and Zeiger, 2010). Photosynthesis is therefore a process of energy conversion from light to the chemical bonds of carbohydrates. Since heterotrophic organisms cannot perform the reduction of carbon dioxide to organic compounds, photosynthetic organisms (and other autotrophs) are the primary source of energy for all forms of life. Although the light-harvesting machinery is more or less similar among photosynthetic organisms, there are more variations in the enzymatic reactions for carbon fixation, from the typical C_3 photosynthesis to the more specialized pathways of crassulacean acid metabolism (CAM) and C_4 photosynthesis (Table 1.1). Sage et al. (1999) have estimated that the vast majority (i.e. 250,000 species) of higher plants perform C_3 photosynthesis in contrast to merely 30,000 species (i.e. 10%) of CAM plants and 7,500 species (i.e. 3%) of C_4 plants. In spite of the fewer C_4 species in the floristic spectrum, they contribute to about 30% of primary terrestrial productivity on a global scale (Gillion and Yakir, 2001) and more than 80% in warm temperate to tropical grasslands (Tieszen et al., 1979; Bird et al., 1994). In hot and arid habitats, the relatively higher photosynthetic efficiencies of C_4 species are attributed to their evolutionary development of a series of anatomical and biochemical modifications of leaves. The biochemistry of C_3, C_4 and CAM pathways is briefly outlined in the following sections and the recent discovery of the terrestrial single-cell C_4 species as the major focus in this research is also introduced.

Table 1.1	**Timeline for the discovery of the four photosynthesis pathways**		
Pathways	**Year**	**Workers**	**The discovery**
C_3	1956	Calvin	Radioactively labeled $^{14}CO_2$ was applied to algal suspensions to elucidate the carbon fixation pathway
CAM	1960	Ranson and Thomas	The sequence of biochemical reactions was described to account for the early landmark observations of a daily reciprocal relationship of acid and sugar contents in green CAM tissues in late 1800's
C_4	1966	Hatch and Slack	Exposure of sugarcane leaves to $^{14}CO_2$ led to the discovery of 4-carbon acids (malate, aspartate and oxaloacetate) as initial photosynthetic products
Single-cell C_4	2001	Voznesenskaya et al.	C_4 photosynthetic features without the Kranz-type leaf anatomy was first discovered in *Suaeda aralocaspica*
	2002	Freitag and Stichler	A different subcellular compartmentation system was discovered in another C_4 species without Kranz-type leaf anatomy, *Bienertia cycloptera*
	2005	Akhani et al.	The third single-cell C_4 species, *Bienertia sinuspersici*, was found in a different habitat from Southwest Asia

1.1.1 C_3 photosynthesis

The classification of photosynthesis into C_3 and C_4 metabolism is based on the number of carbons in the first stable product after the initial fixation of CO_2. In the 1950's, Melvin Calvin first identified the carbon assimilation intermediates by paper chromatography after application of the radioactively labeled $^{14}CO_2$ to green algal suspensions (Calvin, 1956). In the Calvin cycle, the enzyme ribulose-1,5-bisphosphate carboxylase/oxygenase (Rubisco) initiates the carboxylation of the CO_2 acceptor ribulose-1,5-bisphosphate (RuBP), into a 3-carbon compound, 3-phosphoglycerate, which further leads to the formation of triose phosphates (i.e. glyceraldehyde phosphate and dihydroxyacetone phosphate) at the expenses of ATP and NADPH. In the regenerative phase, a series of reactions convert five-sixths of the triose phosphates into the initial CO_2 acceptor, RuBP, whilst one-sixth of the carbon is removed from the cycle for the synthesis of sugars and other organic compounds.

The rate of photosynthesis is generally limited by CO_2 availability rather than the availability of light, and thus photosynthetic organisms have evolved to express high levels of Rubisco, which represents ~40% of the total protein in C_3 plants, making it the most abundant protein in the biosphere (Malkin and Niyogi, 2000). The requirement of high Rubisco abundance is attributed to its inefficiency from a low turnover rate for CO_2 fixation and a poor specificity in distinguishing CO_2 from O_2, with the latter being far more damaging than a competitive inhibitor. Although carboxylation proceeds ca. 3 times faster than oxygenation, the atmospheric concentration of O_2 is more than 600-fold higher than that of CO_2 (Malkin and Niyogi, 2000). As a result, the oxygenase activity of Rubisco diverts approximately 50% of RuBP from the biosynthesis of sugars in the Calvin cycle through the process of

photorespiration (Ogren, 1984). To make matters worse, the oxygenation reaction also leads to the formation of the toxic intermediate 2-phosphoglycolate, which has to be rapidly hydrolyzed to glycolate and further metabolized to recover the fixed carbon lost at the expense of ATP through the C_2 oxidative photosynthetic carbon cycle (Tolbert, 1981).

Previously, down-regulation of Rubisco expression using an anti-sense construct indicated that the rate of carbon flux through the C_3 cycle is profoundly limited by the unfavorable catalytic properties of Rubisco, particularly under high light and temperature conditions (Stitt and Schulze, 1994). Hence, with an ultimate goal to increase crop productivity, research has been targeted on the Rubisco-associated bottlenecks (for review, see Raines, 2011), including the inhibition of Rubisco-mediated oxygenation reactions (Lieman-Hurwitz et al., 2003) and the recent engineering of a photorepiratory bypass in the chloroplasts (Peterhansel and Maurino, 2011). While attempts to improve the C_3 cycle are ongoing, alternative approaches to boost photosynthetic yields have been focused on engineering C_3 plants with C_4 photosynthetic capability.

1.1.2 C_4 photosynthesis

Given the limitation of Rubisco as stated above, a number of plants have evolved a series of anatomical and biochemical modifications to concentrate CO_2 at the site of Rubisco-catalyzed carbon fixation. The fossil records and estimations using molecular tools suggested that C_4 photosynthesis first arose in grasses dating back 24-35 million years ago (Sage, 2004), and the evolutionary process in other C_4 monocot and dicot lineages was substantially promoted due to the drastic decrease in atmospheric CO_2 levels by ca. 25 million years ago

(Zachos et al., 2001). The independent evolution of C_4 pathways from at least 45 origins in 19 families of angiosperms (Sage, 2004) has resulted in considerable variation in the biochemistry of C_4 pathways. Currently, C_4 species are further classified biochemically into three major families, including the $NADP^+$-malic enzyme (NADP-ME), NAD^+-malic enzyme (NAD-ME) and phosphoenolpyruvate carboxykinase (PEP-CK) subtypes, which were grouped based on the major decarboxylation enzyme activity present in each species (Gutierrez et al., 1974).

1.1.2.1 The C_4 cycle

Terrestrial C_4 plants possess an additional major cell type containing chloroplasts (i.e. the bundle sheath cells) as compared to C_3 plants. These additional cells surround the vascular tissues in addition to outer layers of mesophyll cells (Taiz and Zeiger, 2010), leading to an extraordinary leaf arrangement, which is commonly referred to as the Kranz anatomy (Figure 1.1, upper panel). The Kranz anatomy is critical to the biochemistry of the initial carbon influx such that the mesophyll cells are responsible for initial fixation of CO_2 into a C_4 acid and the bundle sheath cells for subsequent breakdown of C_4 acids and Rubisco-mediated re-fixation of the liberated CO_2 under an O_2-limited environment. As an example, Figure 1.1 illustrates the biochemical pathways of C_4 photosynthesis in maize, an NADP-ME subtype of C_4 species. In all C_4 species, the photosynthetic cycle begins in the mesophyll cells with the carboxylation of phosphoenolpyruvate (PEP) into the 4-carbon compound oxaloacetate (Malkin and Niyogi, 2000). The reaction is not prone to inhibition by O_2 due to the fact that the enzyme phosphoenolpyruvate carboxylase (PEPC) utilizes the hydrated form (HCO_3^-) rather than the gaseous form of CO_2. Oxaloacetate is either reduced to malate (NADP-ME

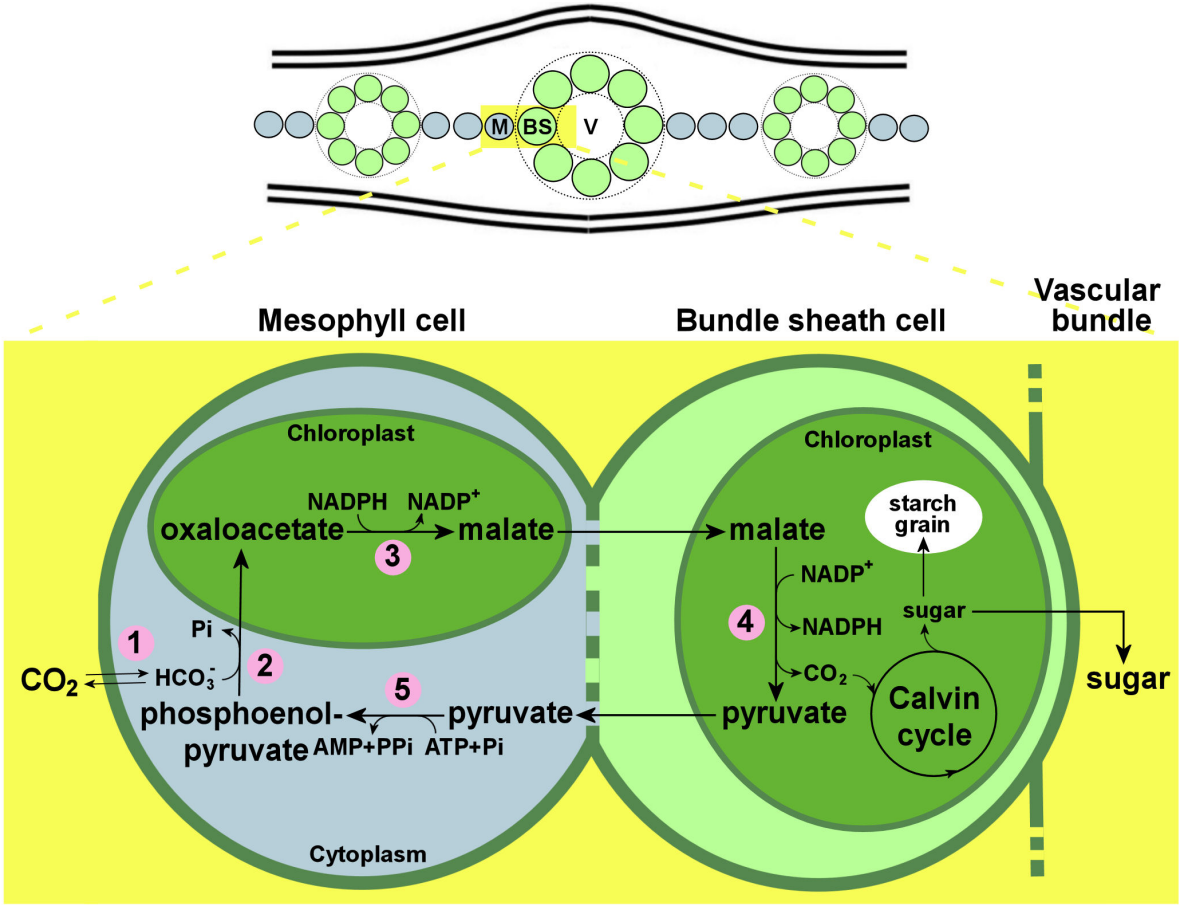

Figure 1.1 The NADP-ME subtype of C_4 photosynthetic pathway

A schematic representation illustrates the cross-section of a maize leaf featuring an additional chloroplast-containing cell type, the bundle sheath (BS) cells, surrounding the vascular bundles (V), and the mesophyll (M) cells in the outer layers (upper panel). The lower panel summarizes the C_4 photosynthetic pathways in a NADP-ME subtype of C_4 species. 1, carbonic anhydrase (CA); 2, phosphoenolpyruvate carboxylase (PEPC); 3, $NADP^+$-malate dehydrogenase (NADP-MDH); 4, $NADP^+$-malic enzyme (NADP-ME); 5, pyruvate-orthophosphate dikinase (PPDK).

subtype) or transaminated to aspartate (NAD-ME and PEP-CK subtypes) and the resulting C_4 acid is transported via plasmodesmata to the bundle sheath cells for the liberation of CO_2 by the respective decarboxylation enzymes. While the thickened and sometimes suberized cell wall prevents gaseous diffusion into the bundle sheath cell, the breakdown of C_4 acids in the bundle sheath cells effectively concentrates CO_2 and favors the carboxylation reaction of Rubisco for the productive carbon assimilation in the Calvin cycle. The C_4 cycle is eventually completed by the regeneration of the initial carbon acceptor, PEP, at the expense of ATP in the mesophyll cells, catalyzed by pyruvate orthophosphate dikinase (PPDK). Although the high energy investment implicates the need for adequate sunlight for efficient photochemistry, plants do benefit from the C_4 pathway under CO_2-limiting conditions such as higher temperature which reduces CO_2 solubility relative to O_2 and low humidity which promotes stomatal closure. As a consequence of higher photosynthetic efficiency under these conditions, the advantageous CO_2-concentrating mechanism has intrigued scientists to over-express C_4 enzymes including PEPC (Ku et al., 1999), NADP-ME (Takeuchi et al., 2000) and PPDK (Fukayama et al., 2001) in rice as the first steps toward boosting food productivity in the future. Despite some initial success in engineering C_4 biochemistry into C_3 plants, the introduction of the Kranz anatomy remains the biggest hurdle (Surridge, 2002).

1.1.2.2 C_4 compartmentation in the dual-cell anatomy

Haberlandt (1884) first documented the Kranz anatomy and proposed some unknown co-operative functions between the mesophyll and bundle sheath cells in photosynthesis. Although the kinetics studies using time-course labelling of $^{14}CO_2$ in sugarcane laid the foundation for defining the biochemistry of C_4 photosynthesis in the 1960's (Kortschak et al.,

1965; Hatch and Slack, 1966), the pathways were not described in relation to the dual-cell system. In fact, the C_4 acid decarboxylation and Rubisco-catalyzed re-fixation steps were not identified at the time of establishment of the first C_4 working model (Hatch and Slack, 1966). It was not until the 1970's that the relationship between C_4 biochemical pathways and Kranz anatomy was established following significant advances in the isolation of intact mesophyll and bundle sheath cells (for review, see Edwards et al., 2001). While earlier attempts to separate the dual-cell types using mechanical approaches of gentle grinding and filtration allowed studies of the intercellular compartmentation of enzymes, cross-contamination and breakage resistance of the isolated cells had precluded precise studies of the enzymology and subcellular fractionation (Edwards et al., 1970; Edwards and Black, 1971). These technical limitations were subsequently resolved using an enzymatic approach to digest the cell walls of mesophyll and bundle sheath cells with cellulase and pectinase followed by separation with an aqueous dextran-polyethylene glycol two-phase system (Kanai and Edwards, 1973). The successful isolation of intact protoplasts has led to explicit characterization of the intercellular and intracellular distributions of enzymes in relation to C_4 photosynthesis, photorespiration, glycolysis and nitrogen/sulphate assimilation (for review, see Edwards and Walker, 1983). In the 1990's, the enzymatic preparations of mesophyll and bundle sheath protoplasts have also been applied to study the regulation of photosynthetic enzymes in C_4 plants *in situ* (Pierre et al., 1992), *in vitro* (Giglioli-Guivarc'h et al., 1996) and *in planta* using transient gene expression systems (Sheen, 1991 and 1995; Imaizumi et al., 1997).

1.1.3 Crassulacean acid metabolism

Whilst the C_4 metabolism features the spatial compartmentation of initial carbon fixation and

the C_3 pathway between mesophyll and bundle sheath cells, respectively, the Crassulacean acid metabolism (CAM) species, which are predominantly found in extreme arid environments, separate the two fixation events temporally. The two processes are under the regulatory control of circadian rhythms, and coordinate with stomatal opening and closure to ensure maximal retention of water (Malkin and Niyogi, 2000). As briefly outlined in Figure 1.2, CAM plants open their stomata at night for gas exchange, and the initial PEPC-catalyzed carboxylation of PEP into oxaloacetate is essentially similar to that of the C_4 cycle. Oxaloacetate is reduced to malate, a 4-carbon acid, which is stored overnight in the central vacuole. During the day, the stored malate is decarboxylated by NADP-ME and the liberated CO_2 accumulates intracellularly at high levels as a result of closed stomata, which also prevents water loss. The high CO_2 concentration favors the carboxylation activity of Rubisco for biosynthesis of sugars via the Calvin cycle.

1.1.4 Single-cell C_4 photosynthesis

Two closely related Chenopodiaceae species (i.e. *Suaeda aralocaspica* and *Bienertia cycloptera*) have been found to exhibit C_4- or CAM-type carbon isotopic compositions, although neither species displays the characteristic Kranz anatomy of C_4 plants nor CAM-specific diurnal changes in leaf titratable acidity (Winter, 1981; Akhani et al., 1997; Freitag and Stichler, 2000, Sage, 2002). Subsequently, a series of anatomical, biochemical and physiological analyses of these species pointed to a novel type of C_4 mechanism (Voznesenskaya et al., 2001, 2002 and 2003; Freitag and Stichler, 2002). Following the recent discovery of *Bienertia sinuspersici* from Southwest Asia (Akhani et al., 2005), three terrestrial plant species are now known to perform single-cell C_4 photosynthesis, which

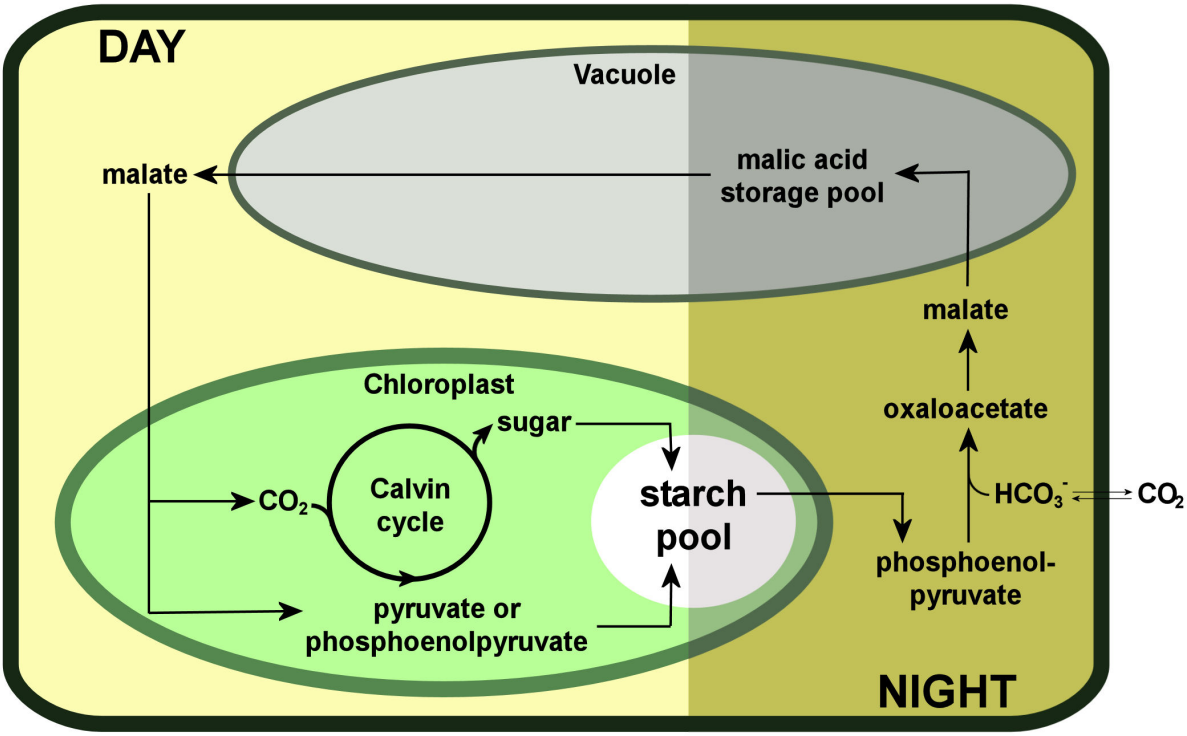

Figure 1.2 The Crassulacean acid metabolism pathway

A schematic diagram illustrates the Crassulacean acid metabolism pathway in a photosynthetic cell. The pathway features temporal separation of the processes of carbon dioxide acquisition and carbon fixation. At night, stomata open to take up carbon dioxide for fixation into malic acid which is stored in the central vacuole. In the heat of the day, the stomata close to conserve water and the malic acid in the vacuole is decarboxylated to release carbon dioxide for fixation in the Calvin cycle.

features a unique intracellular partitioning of organelles and enzymes in subcellular compartments of single photosynthetic cells compared to the intercellular compartmentation in the dual-cell or Kranz system of typical C_4 plants.

In spite of some morphological and anatomical variations, the three Chenopodiaceae species share common features that render the C_4 cycle operational within a single cell. In mature chloroplast-containing cells (i.e. chlorenchyma cells) of these species, the cytoplasm is divided into two compartments equivalent to the mesophyll and bundle sheath cells of Kranz-type C_4 species, respectively. In *Suaeda aralocaspica*, two types of chloroplasts are partitioned to opposite ends of individual elongated chlorenchyma cells resembling mesophyll and bundle sheath cells of Kranz-type species but without crosswalls. In the Bienertia system, the two compartments are connected by cytoplasmic channels, which limit inter-compartmental gas diffusion mimicking the function of thickened and/or suberized walls of bundle sheath cells. Regardless of the cellular details of the systems, subcellular organelles and key photosynthetic enzymes are partitioned within their respective cytoplasmic compartments in such a way that the compartment proximal to the entry point of atmospheric CO_2 is specialized for initial carbon fixation into C_4 acids and regeneration of the initial CO_2 acceptor PEP, whereas the compartment distal from the entry point of air is responsible for the decarboxylation of the C_4 acids and Rubisco-catalyzed re-fixation of the liberated CO_2 for carbon assimilation via the Calvin cycle.

The subcellular organelle distribution and biochemistry of the single-cell C_4 photosynthetic system of *B. sinuspersici*, used as a model plant for the current research, are more

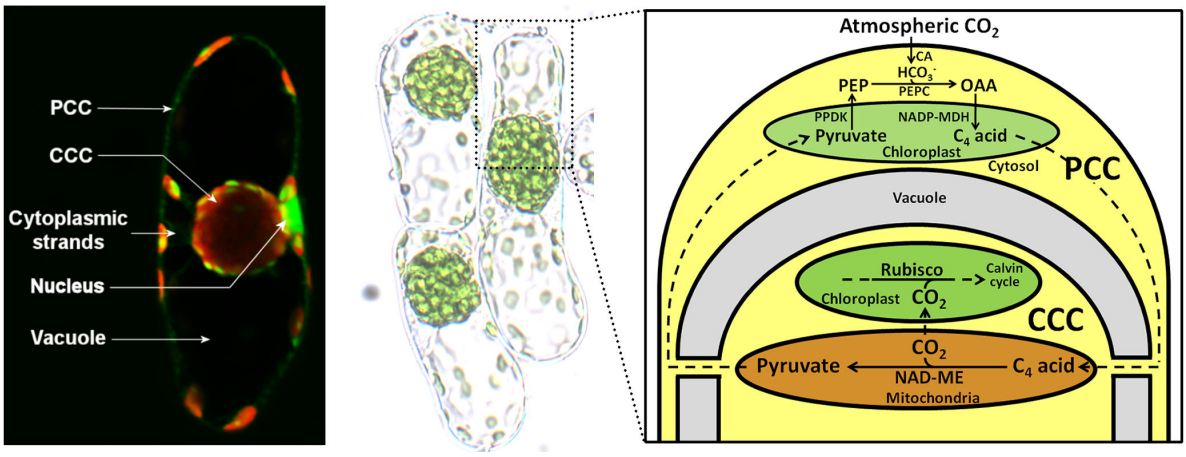

Figure 1.3 A single-cell C_4 model in *Bienertia sinuspersici*

An isolated chlorenchyma cell was stained with fluorescein diacetate (FDA) to illustrate the thin cytoplasmic layer in the periphery and the cytoplasmic strands under confocal laser scanning microscopy (left panel). The image shows a merge of FDA fluorescence and chlorophyll autofluorescence signals. In a mature chlorenchyma cell, the central vacuole separates the cytoplasm into the peripheral (PCC) and central (CCC) cytoplasmic compartment, which are interconnected with cytoplasmic strands. A bright field image of isolated chlorenchyma cells is shown in the middle panel. The right panel illustrates a schematic model of the single-cell C_4 photosynthetic pathways. CA, carbonic anhydrase; NAD-ME, NAD-malic enzyme; NADP-MDH, $NADP^+$-malate dehydrogenase; OAA, oxaloacetate; PEP, phosphoenolpyruvate; PEPC, phosphoenolpyruvate carboxylase; PPDK, pyruvate orthophosphate dikinase.

specifically illustrated in Figure 1.3, although previous studies have revealed similarities between the two Bienertia species (Voznesenskaya et al., 2002; Akhani et al., 2005). In *B. sinuspersici*, the central vascular bundles and water storage cells are surrounded by one or two layers of ellipsoid chlorenchyma cells, which are loosely packed with considerable intercellular space (Akhani et al., 2005; also see Figure 4.2B). Each chlorenchyma cell is divided into a large central cytoplasmic compartment (CCC) and a thin peripheral cytoplasmic compartment (PCC) (Figure 1.3, left panel). The CCC and PCC are separated by the large central vacuole, which is traversed by multiple cytoplasmic channels connecting the two compartments (Figure 1.3, left panel). The CCC is distinctively recognized as a large central ball containing mitochondria, peroxisomes and one distinct type of chloroplasts (also termed dimorphic chloroplasts, see section 1.2.2), whereas another type of chloroplasts is randomly distributed throughout the PCC. As illustrated in the working model (Figure 1.2, right panel), PEPC catalyzes the initial fixation of the hydrated form of CO_2 (i.e. HCO_3^-) to PEP and converts it into the 4-carbon intermediate oxaloacetate, which is reduced to a C_4 acid, malate. Malate diffuses via the cytoplasmic channels into the CCC, and is decarboxylated by NAD-ME to release pyruvate and enrich CO_2 in this compartment. In the CCC, carbon assimilation reactions are initiated by the carboxylation activity of Rubisco and continue through the Calvin cycle. The C_4 cycle is completed when pyruvate is shuttled back to the PCC for regeneration of the initial CO_2 acceptor, PEP, by the ATP-dependent enzyme PPDK.

While earlier works were aimed at supporting the hypothetical single-cell C_4 model with anatomical, ultrastructural and immunological evidence (Voznesenskaya et al., 2001, 2002,

2003 and 2005; Chuong et al., 2005), researchers have also initiated developmental studies of the rationale for the unique subcellular compartmentation (Chuong et al., 2006; Park et al., 2009). Chuong et al. (2006) used green fluorescent protein-tagged cytoskeleton markers in combination with cytoskeleton-disrupting drugs to demonstrate that a highly organized network of microtubules is associated with the dimorphic chloroplasts and is critical for organelle positioning in *B. sinuspersici* and *S. aralocaspica*. A number of fluorescent dyes were also used to monitor the changes in cell structure and organelle distribution throughout the development of chlorenchyma cells in *B. sinuspersici* (Park et al., 2009). Transcript and protein expression profiling further revealed that developmental regulation of the expression of the major photosynthetic and C_4 enzymes is mostly at the transcriptional level (Lara et al., 2008). Further understanding of the biochemistry and precise gene regulation mechanisms of the enzymes, however, awaited technological advancements in areas such as subcellular organelle purification and the establishment of an efficient transient gene expression system.

1.2 Plastids

In plants, plastids are the most prominent subcellular organelles, which play a crucial role in photosynthesis and other metabolic pathways including amino acid synthesis, lipid metabolism and nitrogen and sulfur assimilation (Keeling, 2004). In addition, plastids are found in virtually all algae, which are in indeed broadly referred to as a collection of non-plant eukaryotes possessing this organelle (Keeling, 2004). The phylogenetic relationship among plastid-containing organisms, as analyzed with the aid of molecular, morphological and biochemical markers, supported the current notion that plastids arose from a cyanobacterial ancestor (Keeling, 2004). Plastids and another type of endosymbiotic

organelle, mitochondria, are semi-autonomous since they retain a portion of their own ancestral genomes for gene expression and house the functional machinery (i.e. ribosomes and transfer RNAs) for protein synthesis (Harris et al., 1994). Analogous to the asexual mode of reproduction in their unicellular ancestor, plastids also proliferate by binary fission (for reviews, see Maple and Moller, 2007; Yang et al., 2008), which is mediated by the contractile activities of the inner (i.e. FtsZ1 and FtsZ2) and outer (i.e. PDV1 and PDV2) protein rings around the middle of the plastid envelope (Osteryoung and McAndrew, 2001; Miyagishima et al., 2006). The precise molecular mechanism for plastid fission, however, has not been clearly elucidated.

1.2.1 Plastid diversity

In plants and algae, plastids are functionally differentiated into several variants, which have distinctive protein complements, metabolite contents and suborganellar structures (Figure 1.4). The diverse members of the plastid family are, however, highly versatile in nature as is evident from their interconvertibility during plant development and in response to external cues (Figure 1.4). The smallest and least complicated form of plastids, known as proplastids, is commonly found in seeds and other meristematic tissues as the precursor form of all other plastid types (Keeling, 2004). The differentiation of proplastids into chloroplasts, the predominant form of plastids for photosynthesis, is triggered under light through the process of photomorpho-genesis. Upon illumination of dark-grown seedlings, the wavelength-specific receptor proteins (i.e. phytochrome and cryptochrome) are activated to promote the binding of active transcription factors (e.g. HY5) to the G-box sequences in target promoters, leading to the transcription of a number of photomorphogenesis-related genes (for review,

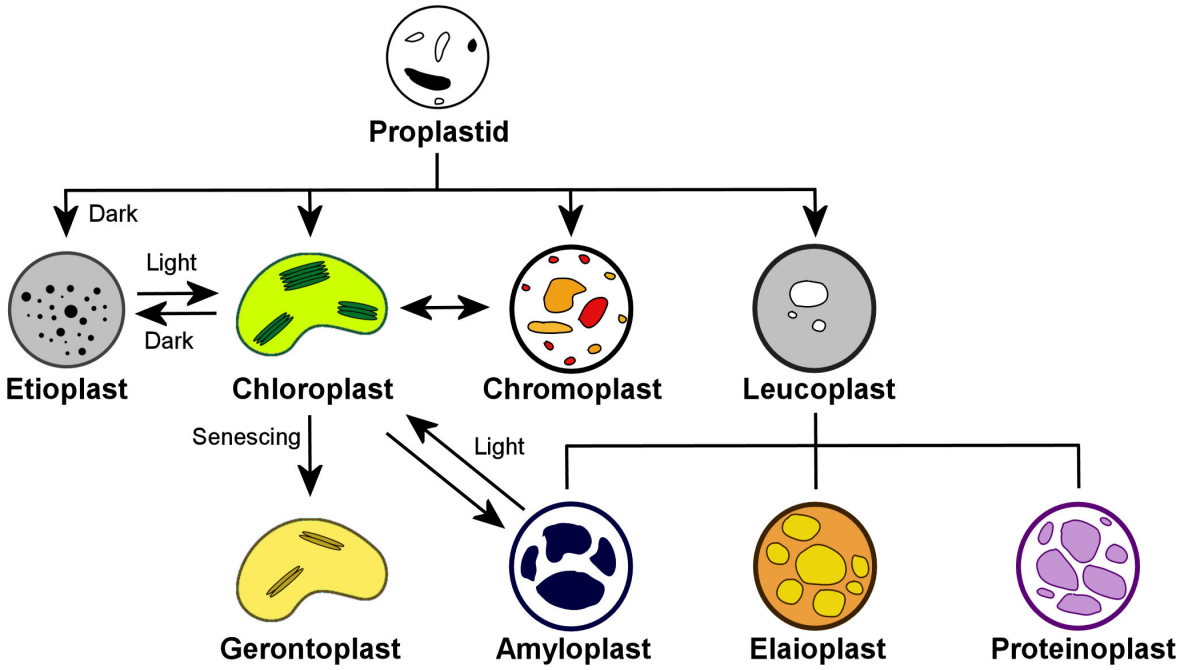

Figure 1.4 The diverse members of the plastid family

All plastid types are originally derived from proplastids. In some cases, the differentiated forms are inter-convertible in response to developmental and environmental cues. Arrows and branches indicate actual conversion and schematic sub-division of the plastid types, respectively.

see Waters and Langdale, 2009). The resulting assembly of photosynthetic machineries is accompanied by the development of an extensive intra-organellar membrane system for the capture of light in photochemical reactions. On the other hand, if seeds are germinated in the dark, the transition of proplastids into chloroplasts is arrested leading to the formation of etioplasts, which uniquely contain semi-crystalline branched tubules known as prolamellar bodies (Wise, 2006). Although light can trigger the differentiation of etioplasts into chloroplasts, the maintenance of chloroplast structure is light-dependent as evidenced from their reversion back to etioplasts after a prolonged period of darkness or inadequate illumination (Taiz and Zeiger, 2010). Developmentally, leaf yellowing is attributed to the transition of chloroplasts to gerontoplasts as a means to dismantle the photosynthetic apparatus and turnover the abundant protein and pigment contents during senescence (Krupinska, 2006). Whilst chloroplasts dominate in green tissues, the coloration of non-green tissues is produced by chromoplasts, which differentiate from chloroplasts (e.g. in ripening fruits) and occasionally from proplastids (Wise, 2006). The bright colors of chromoplasts are often ascribed to their carotenoid pigments, which are immobilized on supramolecular lipoprotein structures known as fibrils (Deruère et al., 1994). Other non-pigmented plastids are broadly classified into leucoplasts for storage of starch (i.e. amyloplasts), lipids (i.e. elaioplasts) and proteins (i.e. proteinoplasts). The abundance of starch granules and the deficiency of internal membranes distinguish amyloplasts of storage tissues from chloroplasts of photosynthetic tissues, although amyloplasts can be converted into chloroplasts as exemplified by the progressive greening of roots under illumination. In the root cap, the amyloplasts with densely packed starch grains are also specialized in the perception of gravity (Chen et al., 1999).

1.2.2 Chloroplast structure and functions

Chloroplasts are surrounded by a double-membrane envelope and contain highly elaborated and folded internal membrane systems (Figure 1.5). Each of the outer and inner envelope membranes is made up of a lipid bilayer distinctive from other organellar membranes with its unique composition of galactosyl diacylglycerides rather than phospholipids (Poincelot, 1976). The inner envelope membrane presumably acts as the actual physical barrier between the organelle interior and the cytosol controlling metabolite export and import to the chloroplast, because the outer envelope membrane is permeable to low molecular weight solutes (<600 Daltons) due to the presence of a number of porins (Flügg and Benz, 1984; Pottosin, 1992; Heiber et al., 1995). Interestingly, these porins are not simply general diffusion channels but exhibit distinct substrate selectivities as β-barrel proteins (Bölter and Soll, 2001). Thus, the inter-membrane space of the chloroplast envelope can function as a buffer zone between the organelle and the cytosol (Bölter and Soll, 2001). A current hypothesis proposes that the invagination of the inner envelope membranes leads to the development of intraorganellar membranes, possibly in a process of vesicle transfer as first evident from the appearance of the two membrane systems as a continuum in proplastids (for review, see Vothknecht and Westhoff, 2001). The internal membranes, known as thylakoids, are crucial for oxygenic photosynthesis and render cyanobacterial cells and chloroplasts structurally distinguishable from photosynthetic bacteria that perform anoxygenic photosynthesis. The thylakoids are composed of multiple appressed grana interconnected by prolonged extensions of lamellae forming an intricate membrane system (Figure 1.5), which is essential for the highly dynamic organization of the light-harvesting antenna, photosystems I and II, cytochrome b_6f complex and ATP synthase. The precise organization of these

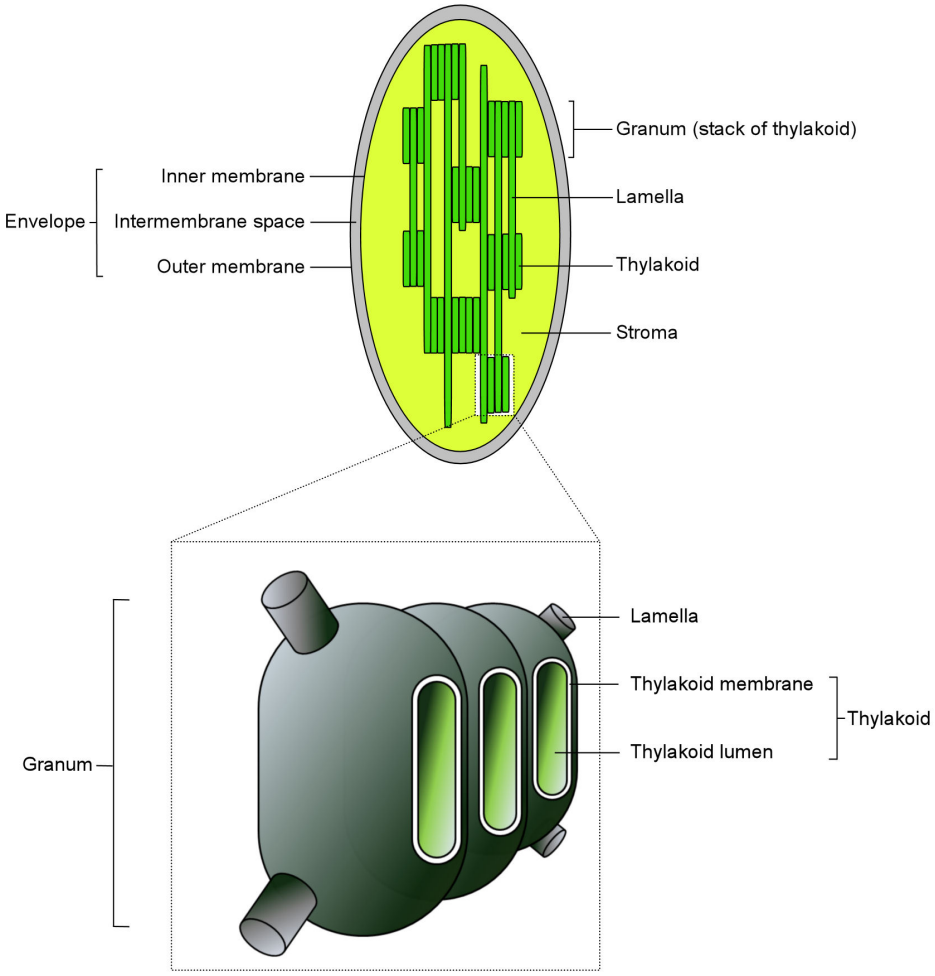

Figure 1.5 A schematic representation of chloroplast structure

The organelle is surrounded by an envelope consisting of the outer and inner membranes, and the region between the double membrane layers is known as intermembrane space. The internal membrane-bound compartment is called thylakoid, which is composed of a thylakoid membrane surrounding a thylakoid lumen. The thylakoid can be highly folded into stacks of appressed membranes, the grana, which are interconnected by the unstacked regions known as the lamella.

protein complexes on the thylakoid membrane is critical for the efficient transfer of light energy collected from the antenna systems and the flow of electrons to the reaction centers of both photosystems, leading to the production of ATP and NADPH in the photochemical reactions of photosynthesis. In contrast, the aqueous fluid surrounding the thylakoid membranes, known as stroma, primarily contains the soluble enzymes for the ATP- and NADPH-dependent chemical reactions of the Calvin cycle for carbon assimilation (see section 1.1.1).

Whilst chloroplasts are the best-known type of plastids for their major role in photosynthesis, they are also the site of a large number of other essential metabolic pathways. For instance, plastids are the primary site for de novo synthesis of fatty acids from the precursors acetyl-CoA and malonyl-CoA, with only a trace amount synthesized in mitochondria (Ohlrogge et al., 1993). While fatty acid synthesis in the plastids and the subsequent assembly of glycerolipids in the endoplasmic reticulum are essential for the biogenesis of all plastidial and extraplastidial membranes, the plastidial pathway of isoprenoid synthesis, on the other hand, leads to the production of carotenoids and other prenyl lipids, which play a crucial role in photosynthesis as well as oxidative stress (Dörmann, 2006). Other than lipid metabolism, a proportion of the reducing power generated from the photochemical reactions of photosynthesis also contributes to nitrogen assimilation in higher plants catalyzed by nitrite reductase, glutamine synthetase and glutamate synthase, which are localized in the plastids (Crawford, 1995; Lam et al., 1996). In non-green plastids, these enzymes are also capable of using the reducing power from the oxidative pentose-phosphate pathway (Neuhaus and Emes, 2000). Being a major site for nitrogen assimilation, plastids also concurrently harbor a wide

range of multi-specific aminotransferases for the synthesis of more than half of the twenty amino acids by the transfer of the α-amino group from glutamate (Forde and Lea, 2007). Moreover, the reduction of sulfate and its assimilation into cysteine take place primarily or exclusively in plastids (Pilon-Smits and Pilon, 2006).

1.2.3 The differentiation of dimorphic chloroplasts in C_4 species

Since the primary function of chloroplasts is photosynthesis, it is plausible that, in the Kranz-type C_4 species, chloroplasts have evolved into more differentiated forms for the division of labor between the mesophyll and bundle sheath cells. The most obvious evidence for the differentiation of dimorphic chloroplasts between the two cell types of C_4 plants apparently lies within their ultrastructural morphology (hence the name). In many terrestrial C_4 species, one type of dimorphic chloroplasts contains larger stacks of grana and higher granal index (i.e. higher ratio of the length of appressed thylakoid membranes to the total length of all thylakoid membranes) than the other type. This ultrastructural dimorphism of chloroplasts, however, varies among the C_4 subtypes in relation to the reductant and energy requirements in each of the dual cell types. As a general rule, the mesophyll chloroplasts of NADP-ME-subtype species typically have more well-developed grana (and thus photosystem II), so as to facilitate a linear electron flow for NADPH and ATP production, which fuels the reduction of oxaloacetate into malate and the regeneration of the CO_2 acceptor PEP in mesophyll cells (Edwards and Walker, 1983; Voznesenskaya et al., 1999). On the other hand, the bundle sheath chloroplasts contain fewer and less-developed grana, so as to facilitate a cyclic electron flow around photosystem I for less production of NADPH, which favors the $NADP^+$-dependent breakdown of C_4 acids in bundle sheath cells (Edwards and Walker, 1983;

Voznesenskaya et al., 1999). Comparatively, the difference in granal stacking is not as prominent in the NAD-ME and PEP-CK subtypes of C_4 species, although some Chenopodiaceae species do show more grana in bundle sheath chloroplasts than mesophyll chloroplasts (Gamaley and Voznesenskaya, 1986; Voznesenskaya et al., 2002, 2003 and 2005).

In addition to anatomical differences, functional differentiation of dimorphic chloroplasts at the biochemical level has been recently investigated using comparative proteomic approaches following mechanical separation of mesophyll and bundle sheath chloroplasts from maize (Majeran et al., 2005 and 2008; Majeran and van Wijk, 2009). Majeran et al. (2005) used three complementary techniques (i.e. comparative 2D-PAGE, cICAT and parallel LC-MS) to quantify the mesophyll to bundle sheath accumulation ratios of 125 soluble proteins from the isolated dimorphic chloroplasts at high confidence levels. Recently, the same research group (Majeran et al., 2008) also assigned similar relative accumulation ratios to more than 600 membrane proteins of the dimorphic chloroplasts using three comparative proteomics methods (i.e. blue-native gels, iTRAQ and LTQ-Orbitrap). As summarized in their recent review, a broad range of the identified soluble and membrane proteins demonstrated more or less differential accumulation between the mesophyll and bundle sheath chloroplasts (Majeran and van Wijk, 2009). Interestingly, in addition to some anticipated difference in relation to the C_4 metabolism and carbon fixation machineries, a substantial difference was also observed in other non-photosynthetic functions of the dimorphic chloroplasts, including the biosynthesis of amino acids, lipids, isoprenoids and jasmonate, and the exchange of a number of metabolites (Figure 1.6). To some extent, the

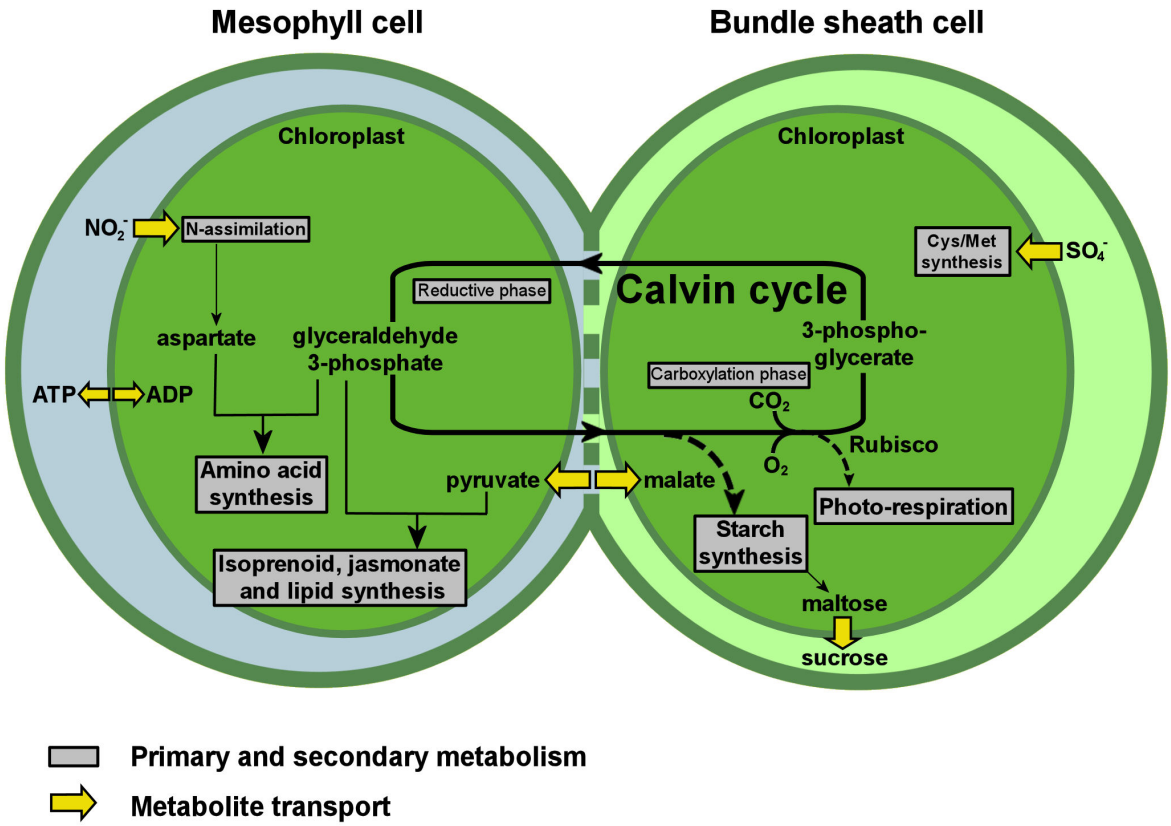

Figure 1.6

Figure legend on the next page

Figure 1.6 Distribution of major primary and secondary pathways and metabolite transporters between mesophyll and bundle-sheath chloroplasts

This schematic diagram illustrates the major difference between the mesophyll and bundle sheath chloroplasts of maize in the biochemical pathways and metabolite transports, other than the C_4 metabolism, as simplified from Majeran and van Wijk (2009). The major difference is centered around the reductive phase and the carboxylation phase of the Calvin cycle in the mesophyll and bundle sheath cells, respectively. In the mesophyll cell, the Calvin cycle intermediate glyceraldehyde 3-phosphate from the reduction of triose phosphate serves as the substrates for biosynthesis of amino acids, isoprenoids, jasmonate and lipids. In the bundle sheath cell, the carboxylation and oxygenation activities of Rubisco lead to carbon assimilation and photorespiration, respectively. As a result of sugar biosynthesis, starch biosynthetic enzymes including starch synthase and ADP-glucose pyrophosphorylase subunits accumulate preferentially in the bundle sheath cells. The preferential accumulation of enzymes in nitrogen import and assimilation in the mesophyll cell is in agreement with higher abundance of the reducing equivalents, NADPH, generated from non-cyclic electron flow. By contrast, sulfur assimilation occurs primarily in the bundle sheath chloroplasts. The distribution of primary carbon metabolism across the dual-cell types also requires a high exchange rate of metabolites, which is achieved by a number of specifically accumulated metabolite transporters such as maltose exporter, ATP/ADP translocator, 2-oxoglutarate/malate translocators, etc.

functional differentiation can be attributed to the redox imbalance between the dual-cell types. For instance, nitrogen import and assimilation are localized in mesophyll chloroplasts due to the high demand for reducing power, whereas sulfur assimilation in the bundle sheath chloroplasts favors the flow of cysteine (i.e. transport metabolite of reduced sulfur) to the mesophyll cells (Majeran and van Wijk, 2009). Similarly, lipid biosynthesis preferentially takes place in the mesophyll cells where NADPH and the carbon precursors such as pyruvate and malate are more abundant (Majeran and van Wijk, 2009).

Whilst the recent proteomics studies of the isolated dimorphic chloroplasts from maize have suggested their close structure-function relationships in the model Kranz-type C_4 species (Majeran et al., 2005 and 2008; Majeran and van Wijk, 2009), the differentiation of dimorphic chloroplasts in single-cell C_4 species has not been clearly elucidated. Analogous to the dimorphic chloroplasts from the NAD-ME-subtype of Chenopodiaceae species, the chloroplasts distal to the atmosphere have more well-developed grana than the ones proximal to the atmosphere as revealed by transmission electron microscopy in *B. cycloptera* (Voznesenskaya et al., 2002 and 2005) and *S. aralocaspica* (Voznesenskaya et al., 2003). Previous immunolocalization studies also confirmed partitioning of the major photosynthetic enzymes including Rubisco, PPDK and NADP-MDH between the dimorphic chloroplasts in the three single-cell C_4 species (Voznesenskaya et al., 2001, 2003 and 2005; Chuong et al., 2006; Boyd et al., 2007). In addition to these enzymes, a putative C_4-specific Na^+-dependent pyruvate transporter has recently been found to be more abundant in the preparation enriched with peripheral chloroplasts from *B. sinuspersici* (Offermann et al., 2011a). A thorough investigation of the biochemical and functional differentiation of dimorphic chloroplasts in

single-cell C_4 species, however, has awaited a more reliable technique for dimorphic chloroplast purification.

1.2.4 Plastid evolution

It is currently accepted that plastids and mitochondria are two endosymbiotic organelles, each of which arose from a monophyletic origin when a free-living bacterium was engulfed by a primitive eukaryote and retained in the host rather than being digested. The captured bacterium was progressively reduced to a double membrane-bound organelle and transmitted evolutionarily to the subsequent generations. The first endosymbiosis took place about 1.9 billion years ago (BYA) when a eukaryotic heterotroph entrapped an α-proteobacterial ancestor leading to the evolution of mitochondria (Hedges et al., 2004). In spite of the morphological and functional divergence of plastids, independent lines of evidence have led to a general consensus that all plastids, regardless of the host in which they reside, originated from a similar endosymbiotic event (Figure 1.7). This event happened about 1.6 BYA when a unicellular heterotrophic protist engulfed a photosynthetic cyanobacterium leading to the first appearance of plastids (for review, see Keeling, 2004). The early plastid-containing eukaryotes were subsequently split into the lineages of red and green algae about 1.5 BYA (Hedge et al., 2004; Yoon et al., 2004). Further diversification of the green lineage led to the evolution of land plants and the two algal groups (i.e. chlorophytes and charophytes). In comparison to the kingdom Plantae, plastid evolution in algae is far more complicated due to the presence of secondary plastids, which characteristically have one or two additional membranes enclosing the double membranes of primary plastids (Chan and Bhattacharya, 2010). These multi-membrane-bound plastids arose from the engulfment of a primary

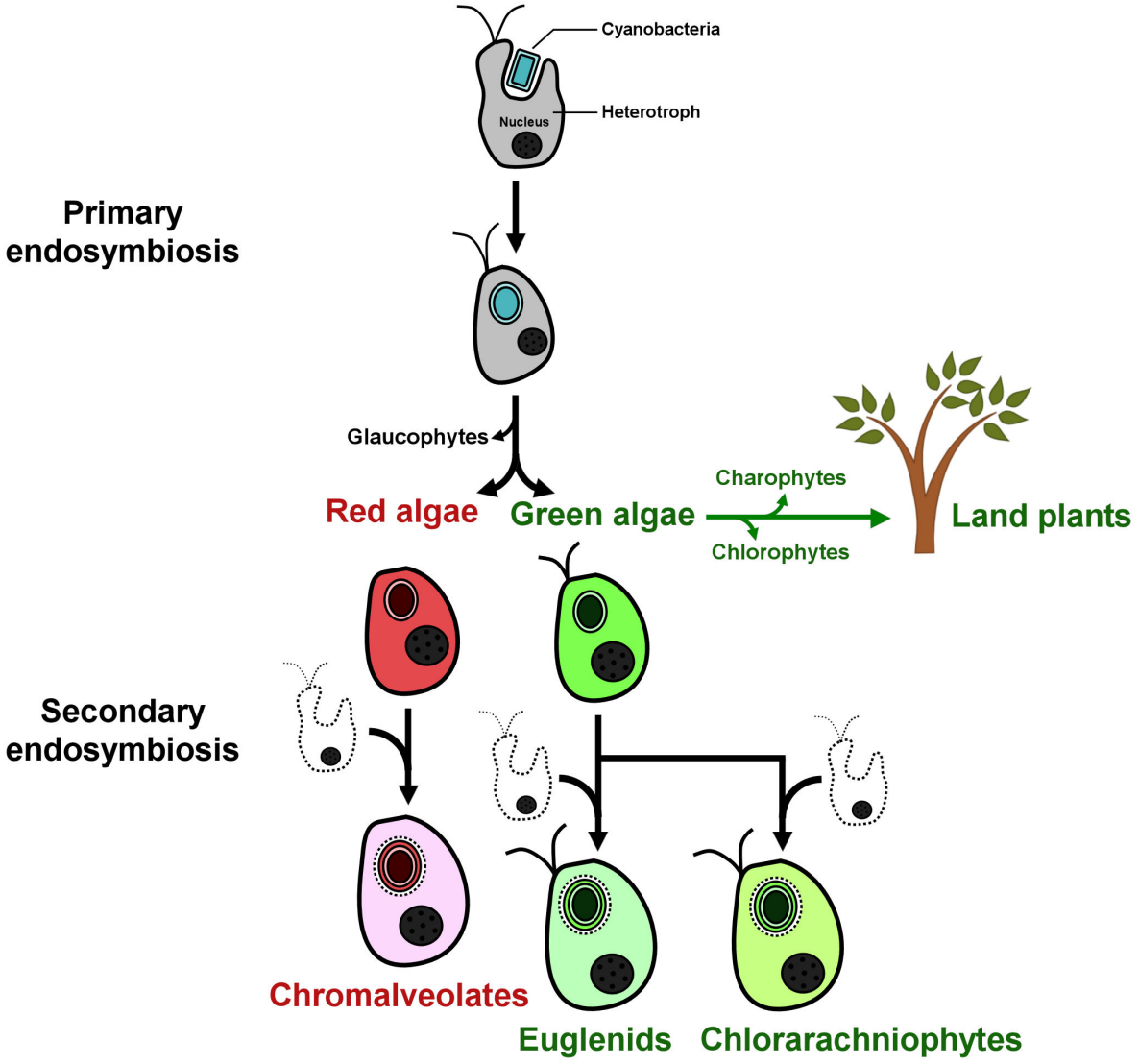

Figure 1.7 Endosymbiosis for the evolution of primary and secondary plastids

All plastid-containing eukaryotes are of the monophyletic origin and evolved originally through primary endosymbiosis when a gram-negative cyanobacterium was ingested by a heterotrophic eukaryote and retained in the cell rather than being digested. The engulfed cyanobacterium evolved into primary plastids. The primary plastid-containing eukaryotes were evolutionarily split into red and green algae, the latter of which evolved to form land plants. Some red and green algae contain secondary plastids bound by more than two membrane layers, which were believed to have developed from secondary endosymbiosis when a primary algal cell was eaten by another heterotroph.

plastid-bearing alga by another heterotroph at the event of secondary endosymbiosis (Figure 1.7), which also accounts for the diversity of red and green algae. While it is generally believed that the primary endosymbiotic event occurred only once as indicated by cytological, molecular and paleontological lines of evidence, there is currently no consensus view regarding the number of secondary endosymbioses that have occurred (Chan and Bhattacharya, 2010). In addition, attempts have been made to explain the extraordinary diversity of plastid types in dinoflagellates by various hypotheses of tertiary and serial secondary endosymbiosis (for review, see Keeling, 2004).

During the transition of the autonomous endosymbiont into a functional organelle, one of the critical steps was genome reduction, which involved the deletion of a substantial number of the redundant endosymbiont genes and the transfer of the majority of unique (e.g. photosynthesis-related) genes to the host nucleus (for review, see Dyall et al., 2004). Thus, modern-day plastids depend on the eukaryotic host genome for gene expression, as exemplified by the approximately 3,000 nuclear-encoded plastidial proteins in *Arabidopsis thaliana* (Leister, 2003; van Wijk, 2004). On the other hand, the plastidial genome encodes only 50~200 genes, primarily for photosynthesis and protein translation machineries (Glockner et al., 2000). In many cases, the multiprotein complexes of photosynthesis are assembled from both nucleus-encoded and plastid-encoded subunits. Due to the partitioning of genetic information, the plastidial and nuclear genomes must inevitably establish some forms of communication to ensure the correct stoichiometry of protein subunits and high dynamics of the complexes in response to developmental and external cues. To this end, multiple lines of evidence have recently emerged to support the existence of retrograde

signaling mechanisms by which chloroplast-derived signals modulate expression of nucleus-encoded genes. The current model proposes that a downstream retrograde signal is generated or perceived by a plastid-localized pentatricopeptide protein (i.e. GUN1) in developmentally impaired or stressed plastids in response to inhibition of plastid gene expression, accumulation of chlorophyll precursors and/or altered redox status (for reviews, see Gray et al., 2003; Jarvis, 2007). As a consequence of the massive transfer of the progenitor genome into the eukaryotic nuclear genome, effective intracellular protein targeting machineries also concurrently evolved for the relocation of the gene products to back to the organelles.

1.3 Protein import into chloroplasts

The majority of chloroplast proteins are encoded in the nucleus, synthesized on cytosolic ribosomes in the form of precursor proteins (preproteins), and post-translationally imported into the organelles. In a typical plant cell, several thousand polypeptides are sorted to the correct organelles and suborganellar compartments with the aid of targeting information embedded in the amino acid sequences (Raikhel and Chrispeels, 2000), which are referred to as “transit peptides” in the case of chloroplast preprotein targeting. Since the chloroplast envelopes are evolutionarily equivalent to the plasma membranes of primitive cyanobacteria, the current theory proposes that the envelope-specific sorting signals have been evolved from cyanobacterial sequences encoding the secretory virulence factors (Bruce, 2000). In fact, the protein channel for preprotein translocation at the outer membrane of chloroplasts (i.e. Toc75) and a putative channel for peptide secretion at the plasma membrane of cyanobacteria (i.e. SynToc75) share considerable similarities in terms of tertiary structures and gating properties (McFadden, 1999).

1.3.1 Transit peptides

Transit peptides are essential and sufficient N-terminal presequences for guiding nucleus-encoded preproteins into the chloroplast interior, although what makes them a chloroplast-specific sorting signal has been a long-standing question due to their high divergence in length, composition and organization (Bruce, 2000).

1.3.1.1 The nature of information encoded by transit peptides

The length of a transit peptide can range from 13 to 146 residues with a mean of 58 residues (Zhang and Glaser, 2002). No consensus sequence or conserved motif has been identified other than the generally conserved alanine immediately after the N-terminal methionine (Emanuelsson et al., 2007). Although it has been suggested that transit peptides are rich in hydroxylated residues (i.e. serine and threonine) and deficient in acidic residues (von Heijne et al., 1989), a recent global analysis of plant and algal transit peptide sequences showed that threonine is relatively underrepresented, whereas serine and alanine are amongst the most abundant amino acids (Patron and Waller, 2007). A similar trend in amino acid composition is also observed among the putative transit peptides from the single-cell C_4 model plant *B. sinuspersici* (Figure 1.8). Recently, alanine-substitution mutation studies and bioinformatics-based prediction were used to identify the critical sequence motifs of transit peptides, leading to the general classification of transit peptides into at least seven subgroups with distinctive motifs (Lee et al., 2006 and 2008).

Given the lack of sequence conservation, the nature of sorting information encoded by transit peptides has been alternatively implicated from a structural perspective. Transit peptides are

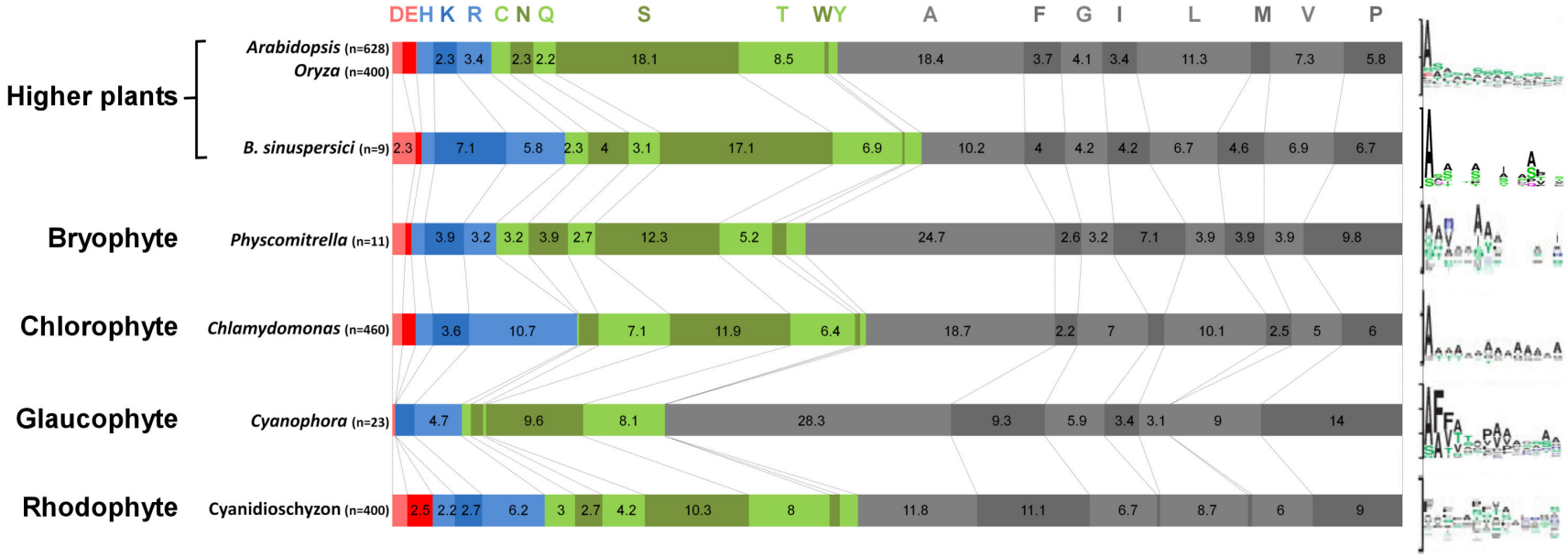

Figure 1.8 Amino acid compositions of chloroplastic transit peptides

The amino acid compositions were analyzed by Patron and Waller (2007), except that the ones in *Bienertia sinuspersici* were calculated using nine predicted chloroplastic transit peptides as deduced from identified full-length cDNA sequences (i.e. RbcS, PPDK, MDH, ferredoxin, two isoforms of FNR, pyruvate dehydrogenase E1-α and –β subunits, and Toc75). The numerical values within the bars represent the relative amino acid abundances (%), which are also shown in direct proportion to the lengths of the bars. The bars are shown in different colors depending on the amino acid properties (i.e. red, acidic; blue, basic; polar uncharged, green; hydrophobic, grey). The Logoplots (right panels) indicate amino acid positional frequencies of the N-terminal 14 residues of transit peptides. Sample sizes are shown in parentheses.

devoid of any regular secondary or tertiary structure in an aqueous environment (Krimm et al., 1999; Wienk et al., 1999), in agreement with the notion that they have evolved to become perfect random coils (von Heijne and Nishikawa, 1991). On the other hand, transit peptides tend to adopt α-helical structure(s) in membrane-mimicking environments with detergent micelles (Wienk et al., 1999 and 2000). Despite the unknown physiological relevance of the membrane-inducible secondary structures, it is widely accepted that the chloroplast envelope membranes, rather than merely forming a physical barrier, play an active role in preprotein targeting (Bruce, 2000 and 2001). This notion has been strengthened by the observed binding of transit peptides with artificial membranes devoid of protein components (Horniak et al., 1993; van't Hof and de Kruijff, 1995). The lipid-interacting activity of transit peptides is apparently chloroplast envelope-specific, as is evident from the impaired preprotein translocation upon enzymatic modification of the lipid composition of the outer envelope membrane (Kerber and Soll, 1992). Since the chloroplast envelope is the only cytoplasm-facing interphase composed of galactolipids and negatively charged phosphatidylglycerol (Joyard et al., 1991), the binding selectivity of transit peptides for the chloroplast envelope can be attributed to two specific modes of interactions (Bruce, 2000): (1) the ionic interaction of the basic transit peptides with the anionic phospholipids, and; (2) the hydrogen bonding between the hydroxyl groups of transit peptides and galactose headgroups of glycolipids.

1.3.1.2 Stromal processing peptidase cleavage of transit peptides

While the aforementioned functional motifs of transit peptides are more or less hypothetical, another better defined motif is located at the C-terminus of transit peptides specifically for downstream removal of the presequences from preproteins. Once the transit peptides emerge

in the chloroplast stroma during the translocation process, they are cleaved off by a specific zinc-binding metalloendopeptidase, known as the stromal processing peptidase (Richter and Lamppa, 1998). Pertinent to the broad substrate specificity of this enzyme, the cleavage recognition sites within the transit peptide sequences are also considerably variable. Earlier analysis of 32 transit peptides from various plant species has revealed that 30% of candidate sequences demonstrate a semi-conserved motif, (I/V)-X-(A/C)↓A (Gavel and von Heijne, 1990). However, later attempts to train a neural network using a larger dataset of annotated chloroplast protein sequences for cleavage site recognition were not successful, partly due to the fact that one or a few N-terminal residues of the mature proteins might be commonly removed by another stromal protease after the initial cleavage (Emanuelsson et al., 1999). The subsequent use of a motif-finding algorithm has led to the identification of the loosely conserved motif (VR↓AAAVXX) and the establishment of a sequence-based tool, ChloroP, for cleavage site prediction with a 60% success rate (Emanuelsson et al., 1999).

1.3.1.3 Prediction of protein subcellular localization

Since the function of a protein is closely linked to its subcellular localization, computational prediction of sorting signals has become an important tool for annotating unknown proteins in the first place. Among the popular sequence-based predictors including iPSORT (Nakai and Horton, 1999), ChloroP (Emanuelsson et al., 1999), TargetP (Emanuelsson et al., 2000), TMHMM (Krogh et al., 2001), SignalP (Bendtsen et al., 2004) and Predotar (Small et al., 2004), some use the machine learning methods (e.g. ChloroP, TargetP, SignalP) whereas others are based on homology searches of the actual sorting signals and/or the global properties such as amino acid compositions (Emanuelsson et al., 2007). Taking advantage of

various publicly accessible tools, Emanuelsson et al. (2007) have provided step-by-step instructions for the coupled use of various predictors in order to maximize the reliability of subcellular localization prediction. As a general rule of thumb, for the prediction of a chloroplast-localized protein, it is recommended that the sequence from a plant or algal source be first analyzed with TargetP to rule out other possible sorting signals, followed by the more specific analysis using ChloroP to identify the putative transit peptide and the cleavage site of stromal processing peptidase (Emanuelsson et al., 2007). Although the ChloroP predictor is known to provide 88% accuracy (Emanuelsson et al., 1999), other researchers have cautioned that the prediction results should only be taken as suggestions for further experimental analyses (Millar et al., 2009; Li and Chiu, 2010). Particularly, the co-existence of two endosymbiotic organelles (i.e. chloroplasts and mitochondria), which share substantial similarity in the nature of sorting signals and protein import machineries (Bruce, 2000; Schleiff and Becker, 2011), renders protein targeting more complicated in plant and algal cells. To make the situation more complex, at least 50 proteins have been identified to be dual-targeted to chloroplasts and mitochondria (Balsera et al., 2009a), under the guidance of a sorting signal with properties of both transit peptides and mitochondrial presequences (Chew et al., 2003; Pujol et al., 2007). Nonetheless, recent advances in high-throughput proteomics techniques have contributed to the deposition of protein subcellular localization databases such as the Plant Proteome DataBase (PPDB) and the SUB-cellular location database for *Arabidopsis* proteins (SUBA), which substantially facilitate cross-validation of prediction results from different approaches (for review, see Jorrín-Novo et al., 2009).

1.3.2 The general import apparatus

The plastid preprotein targeting pathway is initiated in the cytoplasm via the interaction of transit peptides with several cytosolic factors. First, the observed binding of transit peptides with Hsp70 (Heat shock protein, 70 kDa) suggests that these presequences might actively recruit molecular chaperones to keep the de novo synthesized preproteins in an import-competent, unfolded state (Ivey and Bruce, 2000; Zhang and Glaser, 2002). This theory is in line with the fact that the protein translocation channel at the outer envelope membrane has a minimal diameter that only allows threading of preprotein substrates in an extended conformation (Hinnah et al., 2002). The demonstrated translocation of small disulfide-bridged or cross-linked proteins, however, indicated some flexibility of the channel (Clark and Theg, 1997), and the unfoldase activity at the envelope might be of equal importance (Della-Cioppa et al., 1986; America et al., 1994). In addition, it has been reported that some transit peptides can be phosphorylated by a protein kinase in the cytosol (Waegemann and Soll, 1996; Martin et al., 2006), leading to the formation of phosphoserine and phosphothreonine as putative binding motifs for 14-3-3 proteins (May and Soll, 2000). The interaction of transit peptides with Hsp70 and 14-3-3 proteins leads to the formation of a guidance complex and thereby increases the efficiency and specificity of chloroplast import (May and Soll, 2000). However, this notion has been challenged by the results of point mutation studies of the phosphorylation sites which did not affect preprotein import *in vivo* (Nakrieko et al., 2004). While the physiological relevance of the guidance complex remains elusive, the interaction of other preproteins with Hsp90 and its recognition by an outer envelope membrane-bound protein with a tetratricopeptide repeat domain (i.e. Toc64) lead to an alternative route for the delivery of preproteins to the chloroplast surface (Qbadou et al.,

2006). Once the preproteins arrive at the chloroplast surface, transit peptides continue to mediate protein translocation across the chloroplast envelope, which is driven by the coordinate action of two multiprotein complexes (Figure 1.9), known as the Translocons at the outer envelope membrane of chloroplasts (Toc) and the Translocons at the inner envelope membrane of chloroplasts (Tic), which are all named according to their calculated molecular weights in kDa at the time of first discovery (e.g. Toc159 for 159 kDa; Schnell et al., 1997).

1.3.2.1 The import machinery at the outer envelope membrane

The core Toc complex is composed of two homologous GTPases (i.e. Toc159 and Toc34) and a channel protein (i.e. Toc75). Toc159 and Toc34 are also known as the Toc receptors for their critical role in preprotein recognition. Both receptors are composed of a C-terminal membrane-anchor (M) domain and a globular GTPase (G) domain (Hirsch et al., 1994; Kessler et al., 1994; Schnell et al., 1994; Seedorf et al., 1995). Whilst a short stretch of hydrophobic residues forms a single transmembrane α-helix in Toc34 (Kessler et al., 1994; Seedorf et al., 1995), how the bulky M-domain of Toc159 (i.e. ~50 kDa in pea) traverses the outer envelope membrane remains an open question due to the lack of any putative hydrophobic cluster and other structural data (Bölter et al., 1998; Chen et al., 2000). The high molecular weight of Toc159 compared to Toc34 is also due to an additional N-terminal acidic (A) domain of unknown function. The A-domain is intrinsically unstructured (Richardson et al., 2009) and highly susceptible to proteolytic cleavage (Bölter et al., 1998). In fact, at the time of first discovery of Toc159 from pea, it had been mistakenly identified as an 86 kDa protein with more than two-thirds of the A-domain sequence missing (Hirsch et al., 1994; Kessler et al., 1994; Schnell et al., 1994). It was not until the completion of the

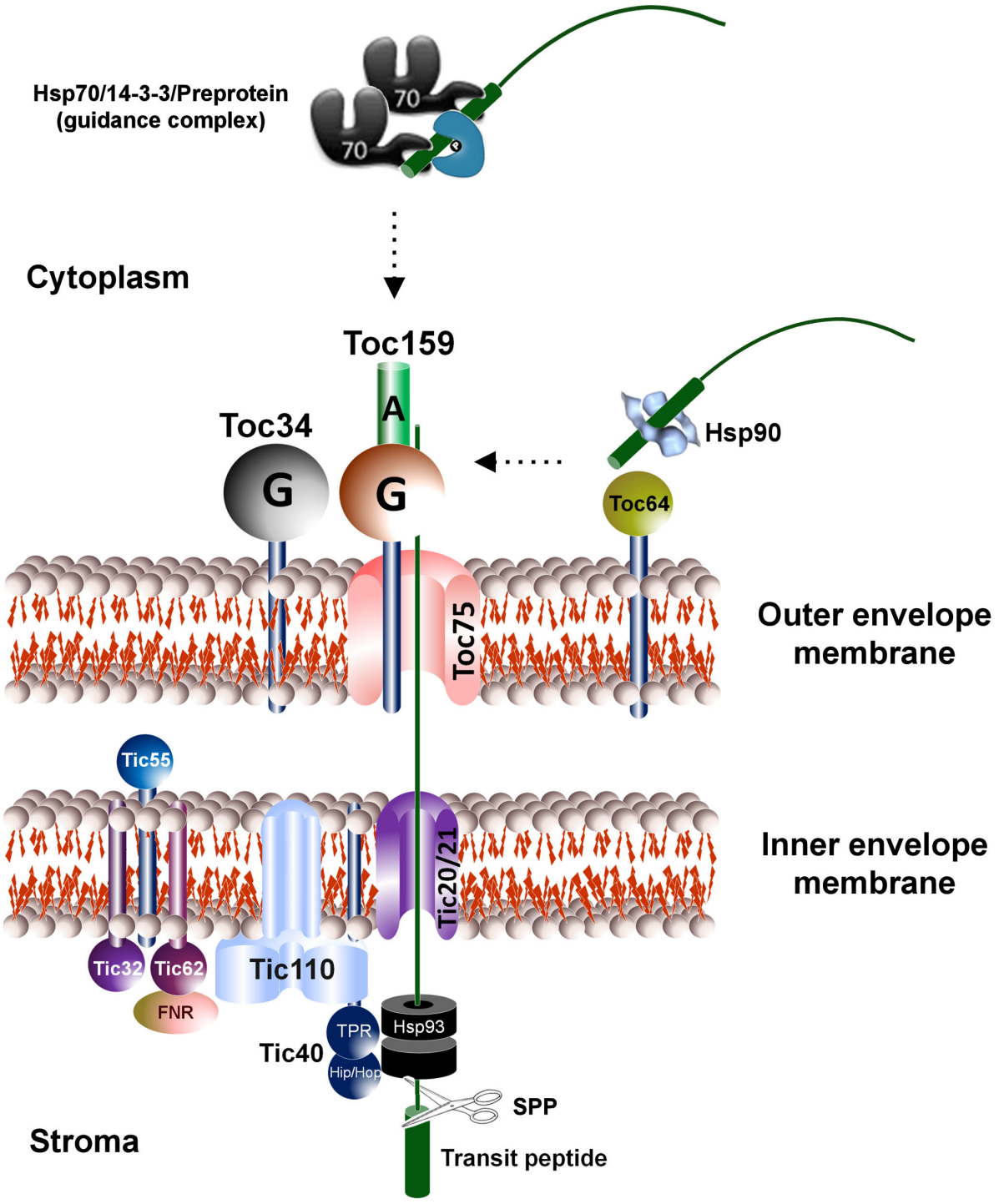

Figure 1.9

Figure legend on the next page

Figure 1.9 A schematic illustration of the chloroplast preprotein import apparatus

In the cytosol, a preprotein either form a guidance complex with Hsp70 and 14-3-3 adapter or interact with Hsp90 and Toc64. At the outer envelope membrane, the two GTPase receptors, Toc159 and Toc34, coordinate the targeting of the preprotein for translocation through the β-barrel protein channel Toc75. The preprotein is translocated across the inner envelope membrane through the major channel proteins Tic20/21, although Tic110 also forms a channel protein and functions to recruit Hsp93 chaperone in concert with the co-chaperone Tic40. The tetratricopeptide repeat (TPR) domain of Tic40 interacts with Tic110 and the Hip/Hop domain stimulates the ATP-dependent motor activity of Hsp93, which exerts a pulling effect for preprotein movement through the channels at both envelope membranes. Tic32, Tic55 and Tic62 play a role in redox regulation of the TIC machinery, for instance, by interacting with ferredoxin:$NADP^+$ oxidoreductase (FNR) to transmit the redox information from the photosynthetic electron transport chain. The transit peptide is eventually cleaved by the stromal processing peptidase (SPP).

Arabidopsis genome project that the full-length sequence was identified (Bölter et al., 1998; Chen et al., 2000). In contrast to Toc159 and Toc34, which project the bulk of their masses to the cytosolic side of the outer membrane, Toc75 is deeply embedded within this membrane, according to the data from proteolytic studies (Schnell et al., 1994; Tranel et al., 1995), and is predicted to form a β-barrel protein with 16 or 18 membrane-spanning β-strands (Sveshnikova et al., 2000; Schleiff et al., 2003a). While electrophysiological experiments indicated that the β-barrel structure of Toc75 forms a narrow, voltage-gated ion channel for preprotein translocation (Hinnah et al., 1997 and 2002), the predicted polypeptide-transport-associated (POTRA) domain at the N-terminus also suggests chaperone-like or preprotein recognition functions of Toc75 (Sanchez-Pulido et al., 2003; Ertel et al., 2005).

Earlier studies using isolated chloroplasts from pea revealed that the energy requirements for preprotein import can be separated into three steps. Initially, transit peptides are reversibly bound to the chloroplast surface in an energy-independent manner (Perry and Keegstra, 1994; Kouranov and Schnell, 1997). Next, the irreversible docking of the preproteins and their partial translocation across the outer envelope membrane through the Toc75 channel require a low concentration of ATP (i.e. <100 μM) in the intermembrane space (Olsen and Keegstra, 1992; Kessler et al., 1994) and supplementation with GTP (Young et al., 1999). This intermediate step can be further refined into three distinct sub-stages (Inoue and Akita, 2008). Finally, the arrested preprotein at this stage can be completely translocated across the inner envelope membrane into the stroma if a high concentration of ATP (i.e. 1 mM in pea) is present in the stroma (Pain and Blobel, 1987; Theg et al., 1989).

In spite of the substantial knowledge of Toc159 and Toc34 structures and the energy requirements during preprotein translocation, the molecular mechanism for initial preprotein recognition in relation to the specific roles of the two receptors remains an unsolved subject of controversy. Currently, there are two different hypotheses that can be outlined in the "targeting" and "motor" models (for reviews, see Inaba and Schnell, 2008; Jarvis, 2008; Balsera et al., 2009a). The "targeting" model considers Toc159 as the primary preprotein receptor (Smith, 2006), and was first proposed after the discovery of a cytosolic form of Toc159 (Hiltbrunner et al., 2001; Ivanova et al., 2004) and heterodimerization of Toc159 and Toc34 (Bauer et al., 2002; Smith et al., 2002a; Sun et al., 2002). This model is also in agreement with earlier findings that Toc159 could be cross-linked with preproteins during early stages of protein import (Perry and Keegstra, 1994; Ma et al., 1996), and that the formation of early import complex could be inhibited by antibody neutralization of Toc159 *in vitro* (Hirsch et al., 1994). In this model, the preprotein-bound Toc159 in the cytosol initially docks with Toc34 via weak homotypic interaction between their G-domains; next, GTP hydrolysis strengthens their interaction, induces the insertion of Toc159 into the outer envelope membrane, and initiates preprotein translocation. The subsequent exchange of GDP for GTP may release the free Toc159 back to the cytosol for another round of preprotein binding. On the other hand, the "motor" model proposes that the GTP-loaded Toc34 initiates the binding of the phosphorylated C-terminal part of a transit peptide, which in turn stimulates GTPase activity of Toc34 leading to the transfer of the preproteins to Toc159 (Jelic et al., 2002; Schleiff et al., 2002; Becker et al., 2004). This model argues that Toc159 exists solely in the membrane-bound form and functions as a GTP-driven motor for pushing preproteins through the Toc75 channel (Becker et al., 2004), as evidenced from the

preprotein translocation at the expense of GTP across an artificial membrane consisting of Toc159 and Toc75 only (Schleiff et al., 2003b). However, this notion has been recently challenged by the evidence that a mutant form of Toc159 with reduced GTPase activity could fully rescue the lethal T-DNA insertion line of *toc159* and support preprotein import into chloroplasts (Wang et al., 2008; Agne et al., 2009).

1.3.2.2 The selective recognition of precursor proteins

Although there is currently no consensus on which of the Toc receptors makes initial contact with transit peptides, biochemical and molecular genetic data from *Arabidopsis* have revealed a critical role for both Toc159 and Toc34 receptors in governing the substrate specificity of the Toc complex. The *Arabidopsis* genome encodes four Toc159 orthologues including AtToc159, AtToc132, AtToc120 and AtToc90 (Bölter et al., 1998; Bauer et al., 2000; Hiltbrunner et al., 2004), and two Toc34 orthologues including AtToc33 and AtToc34 (Li and Chen, 1997; Jarvis et al., 1998). Identification and characterization of various knockout mutants have revealed specific roles of each orthologue in preprotein recognition (Table 1.2). The null T-DNA insertion mutant of *toc159* is seedling-lethal and its cotyledons exhibit an albino phenotype in the absence of differentiated plastids, which is accompanied by the repression of major photosynthetic gene expression at the transcript and protein levels (Bauer et al., 2000). On the other hand, the homozygous knockout mutant of *toc120* is phenotypically indistinguishable from wildtype, and the equivalent mutant of *toc132* has displayed subtle chlorosis in young seedlings and other minor phenotypes in mature plants (Kubis et al., 2004). A lethal phenotype is only produced in double homozygote knock-out mutants of both *toc120* and *toc132* (Ivanova et al., 2004; Kubis et al., 2004); this can be

Table 1.2	The *Arabidopsis* knockout mutant phenotypes of Toc159 and Toc34 homologues	
Genotype	**Phenotype(s)**	**References**
Single mutants		
toc159 (*ppi2*)	Seedling-lethal; albino cotyledons; undifferentiated plastids	Bauer et al., 2000; Kubis et al., 2004
toc132	Very slight pale in young plants; yellow-green, reticulate in mature plants	Ivanova et al, 2004; Kubis et al., 2004
toc120	No phenotype	Ivanova et al, 2004; Kubis et al., 2004
toc90 (*ppi4*)	No phenotype	Hiltbrunner et al., 2004; Kubis et al., 2004
toc33 (*ppi1*)	Pale but improved steadily throughout development	Jarvis et al., 1998; Kubis et al., 2003
toc34 (*ppi3*)	Retarded root growth	Constan et al., 2004
Double mutants		
toc159/toc132	Embryo-lethal	Kubis et al., 2004; Hust and Gutensohn, 2006
toc120/toc132	Pale; almost as severe as *toc159* empty/aborted seeds in another study	Kubis et al., 2004; Ivanova et al, 2004
toc159/toc90	Paler than *toc159* single mutant	Hiltbrunner et al., 2004
toc120/toc90	No difference from *toc120* single mutant	Kubis et al., 2004
toc132/toc90	No difference from *toc132* single mutant	Kubis et al., 2004
toc33/toc34	Embryo-lethal due to post-fertilization defect	Constan et al., 2004; Hust and Gutensohn, 2006

partially rescued by complementation of either AtToc120 or AtToc132 but not AtToc159 (Kubis et al., 2004), indicating the functional redundancy of AtToc120 and AtToc132. In addition, *AtToc159* is expressed at a relatively high level in leaf tissues, whereas *AtToc120* and *AtToc132* are expressed weakly in different tissue types and stably across different developmental stages (Yu and Li, 2001; Ivanova et al., 2004; Kubis et al., 2004). Comparative transcriptomics analysis using the public microarray database consistently showed that *AtToc159* expression is relatively over-represented in rosette leaves and pollen, whereas *AtToc132* transcripts are relatively more abundant in roots, stamens and inflorescence shoot apices (Figure 1.10). The molecular genetic and expression data are also in agreement with *in vitro* biochemical observations. Smith et al. (2004) documented the binding of AtToc159 protein to immobilized fusion proteins with transit peptides of photosynthetic proteins, which can be competitively inhibited with recombinant photosynthetic preproteins but not non-photosynthetic preproteins. In contrast, the binding of AtToc132 with the transit peptide of a non-photosynthetic protein (pE1α) is stronger than that of Rubisco small-subunit (Ivanova et al., 2004). Recently, similar *in vitro* solid phase competition assays demonstrated that the substrate selectivities of AtToc159 and AtToc132 are regulated by their A-domains as evidenced from the non-specific association of the A-domain-less mutant proteins (i.e. AtToc159GM and AtToc132GM) with various preprotein substrates (Inoue et al., 2010). Interestingly, the lethal phenotype of the *toc120*/*toc132* double-knockout mutant can be partially rescued by overexpression of AtToc132GM, and the complementation effect is more even prominent after the addition of the A-domain of AtToc159 (Inoue et al., 2010).

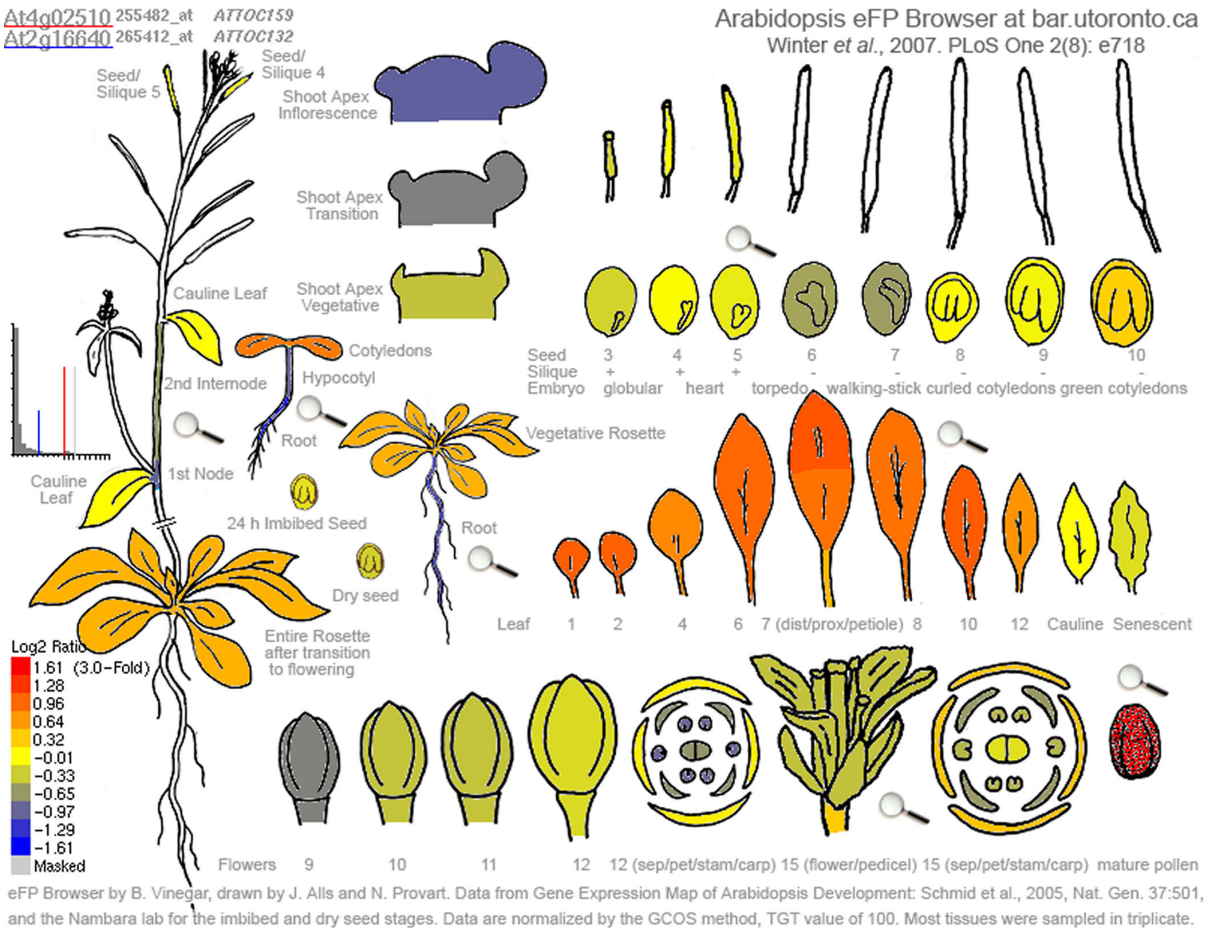

Figure 1.10 Pictographic representation of the comparative gene expression patterns of *AtToc159* and *AtToc132* in *Arabidopsis*

The data were collected using the *Arabidopsis* Electronic Fluorescent Pictograph (eFP) Browser which is publicly available at http://bar.utoronto.ca/efp/cgi-bin/efpWeb.cgi. Colors indicate the ratio of *AtToc159* to *AtToc132* (i.e. red indicates high ratio; blue indicates low ratio).

Co-immunoprecipitation studies further revealed that AtToc33 is predominantly found in the AtToc159-containing complex, whereas AtToc34 preferentially forms complexes with AtToc120 and AtToc132 (Ivanova et al., 2004). This observation is consistent with the phenotypes of their knockout mutants (Table 1.2). In spite of their reduced severity compared to *attoc159* mutants, homozygous knockout mutants of *attoc33* also exhibit slight chlorosis in young plants (Kubis et al., 2003). In contrast, *attoc34* mutants exhibit a less visible phenotype in photosynthetic tissues but have reduced root growth (Constan et al., 2004). Overall, numerous observations support the existence of different substrate-specific Toc complexes. Whilst the specific interaction between AtToc159 and AtToc33 favors the recognition of photosynthetic proteins, the interaction of the AtToc120/AtToc132 subgroup and AtToc34 is responsible for the recognition of non-photosynthetic proteins to ensure that these less abundant but essential proteins are not outcompeted during the active chloroplast differentiation (Bédard and Jarvis, 2005). However, a recent quantitative proteomic study of the *attoc159* knockout mutants indicated that the definition of AtToc159-dependent and AtToc159-independent substrates has been over-simplified, since a number of photosynthetic proteins also accumulate in the AtToc159-deficient plastids (Bischof et al., 2011).

1.3.2.3 The import machinery at the inner envelope membrane

While the physiological roles of Toc components await further clarification, there are more uncertainties regarding the identities and functions of the Tic complex (for reviews, see Jarvis, 2008; Benz et al., 2009; Li and Chiu, 2010). One of the uncertainties lies within the nature of the translocation channel(s) across the inner envelope membrane. In this regard, Tic20 and Tic21 have been considered excellent candidates since both proteins have four

predicted α-helical transmembrane helices which confer a structure analogous to some mitochondrial channel proteins (Rassow et al., 1999; Reumann and Keegstra, 1999; Teng et al., 2006). In fact, the knock-down mutants of either one of these Tic components exhibit significant defects in protein translocation across the inner envelope membrane (Chen et al., 2002; Teng et al., 2006). While the channel activity of Tic20 has been recently confirmed (Kovács-Bogdán et al., 2011), other studies have suggested that Tic21 functions as an iron permease, which can partially complement a yeast mutant with an iron uptake abnormality (Duy et al., 2007). Other than Tic20 and Tic21, Tic110 has been proposed to constitute a preprotein translocation channel as revealed from electrophysiological data after its incorporation into artificial membranes (Heins et al., 2002). In addition, Tic110 shares homology with the bacterial amino acid transporters and some mitochondrial channel proteins (Reumann and Keegstra, 1999). Molecular genetic data have also suggested that Tic110 is important for plastid biogenesis (Inaba et al., 2005). While a handful of topological approaches revealed that Tic110 consists of six transmembrane helices (Balsera et al., 2009b), earlier studies showed that Tic110 spans the inner envelope membrane twice only with short N-terminal hydrophobic domains (Jackson et al., 1998; Inaba et al., 2003). The bulk of Tic110 protein, on the other hand, is projected into the stroma for binding of transit peptides and recruitment of molecular chaperones (Kessler and Blobel, 1996; Akita et al., 1997; Nielsen et al., 1997; Inaba et al., 2003). Recently, comparative studies of Tic20 and Tic110 from two different plant species have consistently led to the conclusion that Tic110 functions as a general translocation pore, whereas the less abundant Tic20 has been electrophysiologically shown to function as an independent protein channel, possibly for the translocation of more specific substrates (Kovács-Bogdán et al., 2011).

While Tic110 may or may not constitute an important component of the protein channel, it has been shown to play an additional role in the assembly of the preprotein import motor comprising Hsp93/ClpC (Heat shock protein, 93 kDa; Caseinolytic protease subunit C) and Tic40. In the stroma, the motor complex mediates the binding of emerging preproteins and provides the driving force for their unidirectional movement through a ratchet-type mechanism (Kessler and Blobel, 1996; Akita et al., 1997; Nielsen et al., 1997; Jackson-Constan et al., 2001). Due to the absolute requirement of stromal ATP for preprotein translocation (see section 1.3.2.1), Hsp93/ClpC is believed to be the core component of the motor, given that it is the only ATPase identified to associate with the Tic complex (Kessler and Blobel, 1996; Akita et al., 1997; Nielsen et al., 1997). The direct association of Hsp93/ClpC with preproteins, however, has not been confirmed (Li and Chiu, 2010). In addition to the motor activity, Hsp93/ClpC may also function as a chaperone (Andersson et al., 2006) and a protease for the turnover of substrates (Shanklin et al., 1995; Halperin et al., 2001). The chaperone activity of Hsp93/ClpC might be regulated by Tic40, another component of the stromal translocation motor, which possesses a C-terminal domain structurally and functionally similar to other co-chaperones such as Hip (Hsp70-interacting protein) and Hop (Hsp70/Hsp90-organizing protein) (Stahl et al., 1999; Chou et al., 2003; Bédard et al., 2007). In addition, Tic40 has a putative tetratricopeptide repeat domain which directly interacts with Tic110 and triggers its release of the bound transit peptides for subsequent Hsp93/ClpC activities (Inaba et al., 2003). Although another stromal chaperone, Cpn60, also directly interacts with Tic110 in an ATP-dependent manner, the energy is only required for direct interaction with the mature form of processed proteins, suggesting that

Cpn60 might be a chaperone for protein folding rather than a component of the preprotein translocation motor (Kessler and Blobel, 1996).

In contrast to the mitochondrial translocons being assembled during preprotein translocation, a stable Toc/Tic supercomplex can be detected in the absence of preproteins (Akita et al., 1997; Kouranov et al., 1998; Nielsen et al., 1997). Nonetheless, Tic20 and Tic22 could not be co-immunoprecipitated with Tic110 (Kouranov et al., 1998), indicating that the assembly of a functional Tic complex exhibits certain dynamicity in response to some unknown factors (Bédard and Jarvis, 2005). For example, it is generally accepted that the Tic machinery is regulated in response to the intraorganellar redox status under the control of three Tic components, including Tic32, Tic55 and Tic62 (Bédard and Jarvis, 2005). The NAD(P)H-binding sites of Tic32 and Tic62 and the Rieske iron-sulfur centre of Tic55 implicate their putative functions in electron transfer processes (Caliebe et al., 1997; Küchler et al., 2002; Hörmann et al., 2004). More specifically, Tic32 interacts with calmodulin (Chigri et al., 2005) and Tic62 also has a binding site for ferredoxin:$NADP^+$ oxidoreductase (Stengel et al., 2008), suggesting that the regulation of Tic function may be modulated by calcium signals and the redox status of the photosynthetic electron transport chains.

1.3.3 The alternative chloroplast import pathways

TargetP analysis of the proteomics data from purified *Arabidopsis* chloroplasts has revealed that only 60% of identified plastid proteins have a predictable transit peptide and 8% might enter the secretory pathway (Kleffmann et al., 2004). Although the unexpected discrepancy might be attributed to experimental errors such as sample contamination and erroneous

prediction, a portion of the data are believed to reflect the physiological circumstances that the targeting of certain chloroplastic proteins is not mediated by transit peptides (Jarvis, 2008). In fact, the past decade has seen the discovery of a handful of alternative chloroplast-targeting pathways. For instance, a signal peptide for the secretory pathway is present in a stromal localized carbonic anhydrase (CAH1) which can be imported *in vitro* into pancreatic microsomes rather than isolated chloroplasts (Villarejo et al., 2005). Given the evidence of *N*-linked glycosylation, this enzyme is likely targeted to the chloroplast via the endoplasmic reticulum-Golgi pathway (Villarejo et al., 2005). Nanjo et al. (2006) have reported a similar pathway for another *N*-glycosylated protein, nucleotide pyrophosphate/phosphodiesterase. There are also two other known transit peptide-less proteins (i.e. Tic32 and the homologue of quinone oxidoreductase ceQORH) which are targeted the chloroplast in an ATP-dependent manner without using the functional Toc/Tic machinery (Miras et al., 2002 and 2007; Ferro et al., 2003). More interestingly, the major isoform (i.e. PORA) of the chloroplastic enzyme NADPH:protochlorophyllide oxidoreductase is imported after pre-binding with its substrate, protochlorophyllide (Reinboth et al., 1995 and 1997). The demonstrated non-canonical import mechanism is proposed as a means to stabilize the enzyme with the bound substrate and to minimize the toxicity effect of this substrate in the chloroplasts (Kim and Apel, 2004; Kim et al., 2005; Pollmann et al., 2007).

1.4 The targeting of outer envelope membrane proteins

According to the Plant Proteome Database (http://ppdb.tc.cornell.edu; Sun et al., 2009), the outer envelope membrane of chloroplasts contains approximately 30 different proteins, many of which function as transporters or channels. Although the mechanisms for the targeting of

these proteins to the chloroplast envelope have not been well elucidated, multiple pathways are apparent (for reviews, see Hofmann and Theg, 2005; Bölter and Soll, 2011). In this regard, the translocation channel Toc75 is amongst the best understood and the only known transit peptide-bearing outer envelope protein (OEP). Toc75 contains a bipartite targeting signal consisting of an N-terminal chloroplastic transit peptide and an unusual polyglycine stretch, the former of which is removed by the stromal processing peptidase to form an intermediate form of Toc75 (iToc75) (Tranel et al., 1995; Tranel and Keegstra, 1996). The second part of the presequence in iToc75 is further cleaved by an integral type I signal peptidase in the inner envelope membrane (Bölter et al., 2006). The transit peptide is essential and sufficient for protein targeting (Inoue et al., 2001), whereas the polyglycine stretch might function to prevent the further translocation of iToc75 into the stroma (Tranel et al., 1995; Tranel and Keegstra, 1996). Although the distantly related paralogue OEP80 (formerly named as Toc75-V) shares sequence and structural similarities with Toc75 (Eckart et al., 2002), this β-barrel protein contains a predicted transit peptide which is not cleavable (Inoue and Potter, 2004). Further experiments have demonstrated that OEP80 is neither associated with the Toc complex nor competed with the preprotein of Rubisco small-subunit (Inoue and Potter, 2004), suggesting that the targeting of OEP80 is different from that of Toc75. In fact, other integral β-barrel proteins at the outer envelope membrane, including OEP21, OEP24 and OEP37, are apparently self-inserted into the membrane (Bölter et al., 1999; Pohlmeyer et al., 1998; Goetze et al., 2006), although this notion has not been supported with adequate evidence (Bölter and Soll, 2011).

A number of helical transmembrane proteins constitute a large group of OEPs which have

been studied in some detail regarding their targeting to the outer envelope membrane (Table 1.3). Analogous to a number of similar membrane proteins in mitochondria and endoplasmic reticulum, these proteins characteristically contain a single hydrophobic α-helix which functions as a transmembrane domain (TMD) anchor and a sorting signal, despite some recent argument concerning the topology of Toc64 (Qbadou et al., 2007). Depending on whether the transmembrane domain is located at the N-terminus or C-terminus, these integral proteins can be broadly classified into the signal-anchored proteins (e.g. OEP7, OEP14, HKI, Toc64, CHUP1) and tail-anchored proteins (e.g. OMP24, HPL, Toc34 and OEP9), respectively. Although it was originally proposed that these proteins are spontaneously inserted into the destined membrane without any energy requirement or proteinaceous factor (Schleiff and Klösgen, 2001), numerous efforts have been made over the past decade to demonstrate some regulation in the targeting process. Bae et al. (2008) have contributed to the discovery of a chaperone-like *Arabidopsis* ankyrin repeat protein (i.e. AKR2A) which is essential for the biogenesis of chloroplast OEM proteins. The demonstrated binding of AKR2A to the targeting signals of several OEP proteins, together with the evidence of its direction association with chloroplasts *in vitro*, has led to the notion that AKR2A functions as a cytosolic mediator for the specific sorting of chloroplastic signal-anchored and tail-anchored proteins to the correct destination (Bae et al., 2008). To this end, the charge distribution of the residues adjacent to the TMD sequence also appears as the critical information to prevent the mis-targeting of Toc64 and OEP9 to the secretory route or mitochondria (Lee et al., 2001; Dhanoa et al., 2010). *In vitro* studies using reconstituted artificial membranes showed that the charge distribution of the TMD-flanking region, in addition to the lipid composition, determines the topology of the OEP7 protein (Schleiff et al.,

Table 1.3 Properties of the helical transmembrane proteins at the outer chloroplast envelope membrane

Protein	Species	Topology	Residues	Predicted transmembrane domain and flanking residues[1]	References
OEP7	*Arabidopsis*	N_{in}-C_{out}	64	1- MGKTSGAKQATVVVAAMALGWLAIEIAFKPFLDKFRSSIDKS -42	Lee et al., 2001
OEP14	Pea	N_{in}-C_{out}	65	1- MGKAKEAVVVAGALAFVWLAIELAFKPFLSQTRDSIDKS -39	Li et al., 1991; Li and Chen, 1996; Tu and Li, 2000
HKI	Spinach	N_{in}-C_{out}	498	1- MRKAAVGAAVVCTAAVCAAAAVLVRQRMKSSSKW -34	Wiese et al., 1999
Toc64	Pea	N_{in}-C_{out}	593	1- MKSMASPSSQIWVILGLGLAGIYVLTRKLTQAVKED -36	Sohrt and Soll, 2000; Lee et al., 2004; Hofmann and Theg, 2005
CHUP1	*Arabidopsis*	N_{in}-C_{out}	1004	1- MFVRIGFVVAASIAAVTVKRLNVKPSKPSKPSD -33	Oikawa et al., 2008
OMP24	Spinach	N.D.	148	88- NEDAQEDTNPLILWQIYALGGFIVLKWAWGKWQERKANNGS -128	Fischer et al., 1994
HPL	Tomato	N.D.	476	270- QLTEQEAIHNLLFILGFNAFGGFSIFLPTLLGNLGDEKNAD -310	Froehlich et al., 2001
Toc34	Pea	N_{out}-C_{in}	310	259- GPNPNQRGKLWIPLIFALQYLFLAKPIEALIRRDIAT -295	Chen and Schnell, 1997; Tsai et al., 1999; Qbadou et al., 2003; Dhanoa et al., 2010
OEP9	*Arabidopsis*	N_{out}-C_{in}	86	30- SGEKKHVLVGIGIVTIIFGVPWYLMTQGSKHQSHQ -64	Dhanoa et al., 2010

Remarks: This table was modified from Hofmann and Theg (2005).

[1]Predicted transmembrane domains are shaded in grey; Positively and negatively charged residues are shaded in yellow and green, respectively

[1]The numbers indicate start and end sites of sequences.

2001). Another homologue of OEP7 from pea (i.e. OEP14) can be efficiently inserted into liposomes with the assistance of Toc75 (Tu et al., 2004). Although OEP14 can compete with the import of Rubisco small-subunit, excess preproteins do not affect the binding or insertion of OEP14 suggesting that the targeting of OEP14 does not thoroughly overlap with the general import pathway (Tu et al., 2004). This is consistent with the earlier observation that OEP14 insertion could not be enhanced with the addition of up to 1 mM ATP (Li et al., 1991), which is generally required in the Toc/Tic-mediated pathway.

The mechanism for chloroplast targeting and membrane integration of Toc34 receptors also shares similar features with other signal-anchored and tail-anchored proteins. For instance, its topology is largely determined by the charge distribution surrounding the TMD and the lipid composition of the membrane (May and Soll, 1998; Schleiff et al., 2002; Qbadou et al., 2003). Important targeting information is also encoded within the C-terminal hydrophilic tail adjacent to the TMD as shown by the mis-localization of its deletion mutant protein (Chen and Schnell, 1997; Li and Chen, 1997; Dhanoa et al., 2010). On the other hand, the targeting of Toc34 is also uniquely dependent on its G-domain since the TMD sequence plus the hydrophilic C-terminal tail is not sufficient for chloroplast targeting *in planta* and *in vitro* (Chen and Schnell, 1997; Li and Chen, 1997; Tsai et al., 1999; Dhanoa et al., 2010), in agreement with the GTP requirement of Toc34 for membrane insertion (Seedorf et al., 1995; Chen and Schnell, 1997). Recently, Dhanoa et al. (2010) documented that the abolishment of dimerization and hydrolytic activity of the G-domain by site-specific mutation of its arginine finger does not affect Toc34 targeting, suggesting that the bound GTP may be more important for keeping the protein in an insertion-competent state rather than for providing

energy for the process. In analogy, membrane insertion of the homologous GTPase receptor Toc159 also relies on its G-domain in a GTP-dependent manner. Studies using G-domain mutants indicated that the productive insertion of Toc159 requires its intrinsic GTPase activity through homotypic interaction with Toc34 (Smith et al., 2002a). In spite of the functional similarity with Toc34, Toc159 is not a tail-anchored protein due to the lack of any predictable hydrophobic TMD sequence (Bölter et al., 1998; Chen et al., 2000). Nonetheless, numerous studies have shown that the C-terminal region of Toc159 interacts with the chloroplast envelope (Muckel and Soll, 1996; Bauer et al., 2002; Smith et al., 2002a), and this interaction is more efficient in the presence of the G-domain (Wallas et al., 2003). In addition, *in planta* experiments indicated that the C-terminal region alone (i.e. M-domain) is exclusively localized at the chloroplast envelope, suggesting the presence of an unknown chloroplast-targeting signal (Lee et al., 2003). The nature of targeting information in this region, however, has not been further elucidated.

1.5 Overall objectives

Although an understanding of the anatomy and biochemistry of the single-cell C_4 systems are beginning to emerge, our understanding of their overall development is in its infancy. In the single-cell C_4 system, the expression of key C_4 genes is under the control of a single nucleus and thus the targeting of nuclear-encoded proteins destined for the dimorphic chloroplasts might involve a selective import process to ensure the proper development of chloroplasts and functioning of the C_4 cycle. The operation of the single-cell C_4 pathway requires selective partitioning of key enzymes of the C_4 cycle as well as those of the C_3 pathway to the specific chloroplast types in separate intracellular compartments. Thus, the present study is based on an overall hypothesis that the differential protein accumulation in the dimorphic chloroplasts of the single-cell C_4 species *Bienertia sinuspersici* is mediated by the selective protein import via different Toc complexes and/or differential regulation of the Toc complexes in the individual subcellular compartments. Toward an ultimate goal of defining the precise mechanism of selective protein import in *B. sinuspersici*, this thesis focuses on two major themes as follows.

The first part of this thesis, as outlined in Chapters 3 and 4, was aimed at developing tools to better understand the novel single-cell C_4 photosynthetic mechanism. In order to achieve this goal, key technical challenges had to be overcome due to the unique intracellular arrangement and novelty of the system. Thus, the specific objectives of this research are:

1. Isolate a homogenous population of healthy chlorenchyma protoplasts with preserved organelle compartmentation from *B. sinuspersici*.
2. Establish an efficient system for transient gene expression in *B. sinuspersici*.

3. Purify the dimorphic chloroplasts from *B. sinuspersici*.

The second part of this thesis, as outlined in Chapters 5 and 6, was aimed at identifying and characterizing the chloroplast protein import receptors in *B. sinuspersici*. The following specific objectives are addressed:

4. Clone the cDNA sequences encoding the chloroplast protein import receptors Toc159 and Toc34 from *B. sinuspersici*.
5. Examine the subcellular localization patterns of the identified Toc159 and Toc34 homologues.
6. Study the mechanism for the targeting of Toc159 to the chloroplast surface.

Chapter 2. Materials and methods

2.1 Chemicals and supplies

All chemicals were of analytical grade and purchased from Sigma-Aldrich (Oakville, ON, Canada), BioShop Canada Inc. (Burlington, ON, Canada) or Fisher Scientific (Ottawa, ON, Canada), unless otherwise specified. All equipments and supplies for agarose and polyacrylamide gel electrophoresis and transblotting were purchased from Bio-Rad (Mississauga, ON, Canada). Molecular weight standards for electrophoresis included Quick-Load 100 bp DNA Ladder (New England Biolabs, Pickering, ON, Canada), 1 kb DNA Ladder RTU (GeneDireX, Toronto, ON, Canada), and Precision Plus Protein Standards (Bio-Rad, Mississauga, ON, Canada). All restriction enzymes, T4 DNA ligase and other modifying enzymes were purchased from New England Biolabs (Pickering, ON, Canada). PCR reactions for full-length cDNA identification and production of expression constructs were performed using the Phusion High-Fidelity DNA Polymerase (New England Biolabs, Pickering, ON, Canada; cat. no. F-530S), whereas RT-PCR and colony PCR were performed using T*aq* DNA Polymerase (New England Biolabs, Pickering, ON, Canada; cat. no. M0267S). DNA sequencing service was provided by the Sanger Sequencing Facility at The Centre for Applied Genomics (The Hospital for Sick Children, Toronto, ON, Canada). All partial sequences from cDNA cloning were subcloned into the pGEM®-T Easy Vector (Promega, Madison, WI, USA) prior to DNA sequencing. Custom DNA oligonucleotides were synthesized by Sigma Genosys (Oakville, ON, Canada) or Eurofins Scientific (Huntsville, AL, USA). Purification of plasmid DNA was performed using the EZ-10 Spin Column Plasmid DNA Minipreps or Midipreps Kits (Biobasic Inc., Markham, ON, Canada).

2.2 Plant propagation and growth conditions

Bienertia sinuspersici plants were propagated asexually by vegetative cuttings. Shoot branches of healthy 6-month-old seed-derived plants were excised, surface-sterilized with 0.5% (v/v) bleach, and cultured on ½ Murashige-Skoog basal medium containing Gamborg's vitamins (Sigma-Aldrich, Oakville, ON, Canada; cat. no. M0404) supplemented with 3% (w/v) sucrose and 0.7% (w/v) agar. Shoot cuttings were maintained in a controlled environmental chamber (Conviron Ltd., Winnipeg, MB, Canada) with a day/night regime of 14/10 h, 22/20 ^{o}C and a photon flux density of 20 μmol m^{-2} s^{-1} for 3 weeks. Rooted cuttings were transferred to 6-inch pots containing commercial potting soil and acclimated in a humidity dome in the greenhouse for 3 weeks, after which they were transferred to a controlled environmental chamber (Conviron Ltd., Winnipeg, MB, Canada) with a day/night regime of 14/10 h, 25/18 ^{o}C, and a photon flux density of approximately 350 μmol m^{-2} s^{-1}. The plants were watered and fertilized regularly with Miracle-Gro (24-8-16) and 150 mM NaCl.

Arabidopsis thaliana (ecotype Columbia) seeds were stratified at 4 ^{o}C in the dark for at least 48 h and sowed on 5-cm-tall cell packs containing a 1:1 soil mixture of Sunshine LC1 mix and Sunshine LG3 germination mix (SunGro Horticultural Inc., Bellevue, WA, USA). The plants were maintained in a controlled environmental chamber (Conviron Ltd., Winnipeg, MB, Canada) with a day/night regime of 16/8 h at 22 ^{o}C with a photon flux density of approximately 150 μmol m^{-2} s^{-1}. The seeds were germinated on the soil covered with plastic domes during the first week, and the seedlings were then watered and fertilized regularly

with 20:20:20 (N:P:K) fertilizer (Plant Products Co. Ltd., Brampton, ON, Canada). True leaves from 2- to 3-week-old plants were used for protoplast preparation.

2.3 Isolation of protoplasts from *B. sinuspersici*

The procedures for isolation and transfection of chlorenchyma protoplasts from *B. sinuspersici* were empirically optimized and modified from the protocol for *A. thaliana* protoplast isolation (Yoo et al., 2007). To isolate chlorenchyma cells, 20 mature (>2 cm in length) leaves (approximately 2 g fresh weight) were freshly harvested from 3- to 4-month-old vegetatively propagated plants and chlorenchyma cells were isolated from the leaves by gentle pressing using a mortar and pestle in 10 mL of cell-stabilizing (CS) buffer [0.7 M sucrose, 25 mM HEPES–KOH (pH 6.5), 5 mM KCl and 1 mM $CaCl_2$], unless otherwise specified. The cell suspension was transferred onto a piece of 40-µm nylon mesh filter (Sefar America Inc., Kansas City, MO, USA) and excess solution was removed by blotting with a stack of absorbent paper underneath. The isolated chlorenchyma cells were gently shaken off from the nylon mesh filter into a 60 mm petri plate containing 5 mL of enzyme solution, which was prepared as previously described (Yoo et al., 2007). Briefly, CS buffer was preheated at 70 ^{o}C for 5 min, and 1.5% (w/v) cellulase Onozuka R10 (Yakult Pharmaceutical, Tokyo, Japan) was subsequently added to the preheated buffer. The enzyme solution was incubated at 55 ^{o}C for 10 min and cooled down to room temperature, prior to the addition of 0.1% (w/v) bovine serum albumin (BSA; Sigma-Aldrich, Oakville, ON, Canada; cat. no. A7030). The chlorenchyma cells were incubated in the enzyme solution at room temperature in the dark without shaking. The progress of cellulase treatment was monitored under light microscopy such that the appearance of round-shaped protoplasts indicates complete cell

wall digestion, which was normally achieved within 4 h. The protoplast-washing steps were performed by floating the cells on top of the medium after centrifugation at 100*g* for 2 min in a swing-bucket rotor (A-8-11 for the refrigerated centrifuge 5417R; Eppendorf Canada Ltd., Mississauga, ON, Canada) and gently aspirating them with a micropipette. Typically, a homogenous population of chlorenchyma protoplasts was obtained after washing in 5 mL of CS buffer twice. The viability of the isolated protoplasts was assessed by vital staining and the protoplast yield was determined using a Neubauer-Levy haemocytometer (Hausser Scientific, Horsham, PA, USA).

2.4 Transfection of isolated protoplasts from *B. sinuspersici*

To prepare isolated protoplasts competent for polyethylene glycol (PEG)-mediated transfection, they were first incubated in W5 solution containing 2 mM MES-KOH (pH 5.7), 154 mM NaCl, 125 mM $CaCl_2$ and 5 mM KCl, and allowed to settle at the bottom of the tube sitting on ice for 30 min. The settled protoplasts were then resuspended in MES/Mg^{2+} buffer containing 4 mM MES (pH 5.7), 0.4 M sucrose and 15 mM $MgCl_2$ at a density of 2 x 10^5 protoplasts mL^{-1}. Approximately 1.5 x 10^4 protoplasts were mixed with 5 µg of plasmid DNA, unless otherwise specified. To initiate transfection, the protoplast/DNA mixture was gently mixed with 110 µL of PEG solution containing 40% (w/v) PEG4000 (Sigma-Aldrich, Oakville, ON, Canada; cat. no. 81240), 0.4 M sucrose and 100 mM $CaCl_2$, and incubated at room temperature for 5 min. The transfected protoplasts were incubated in W5 solution and allowed to settle at room temperature for 20 min. The supernatant was removed and the transfected protoplasts were resuspended in 1 mL of WI solution containing 4 mM MES-KOH (pH 6.5), 0.7 M sucrose and 5 mM KCl. The resuspended protoplasts were transferred

to a 35 mm petri plate and incubated in a growth chamber (Environmental Growth Chambers, OH, USA) at 23^{o}C with a photon flux density of approximately 30 μmol m^{-2} s^{-1} overnight.

2.5 Isolation and transfection of mesophyll protoplasts from *A. thaliana*

The procedures for isolation and transfection of mesophyll protoplasts from *A. thaliana* were modified from Yoo et al. (2007). Well-expanded true leaves from 2- to 3-week-old plants were freshly harvested and cut into 0.5- to 1-mm strips using a sharp razor blade on a piece of white paper with a glass plate underneath. Leaf strips from approximately 60 leaves were dipped into 10 mL of enzyme solution, which was prepared as follows: CS-mannitol buffer [0.4 M mannitol, 20 mM MES-KOH (pH 5.7) and 20 mM KCl] was preheated at 70 ^{o}C for 5 min, and 1.5% (w/v) cellulase Onozuka R10 and 0.4% (w/v) macerozyme R10 (Yakult Pharmaceutical, Tokyo, Japan) was subsequently added to the preheated buffer. The enzyme solution was incubated at 55 ^{o}C for 10 min and cooled down to room temperature, prior to the addition of 0.1% (w/v) BSA (Sigma-Aldrich, Oakville, ON, Canada; cat. no. A7030) and 10 mM $CaCl_2$. After 10-min vacuum infiltration in a desiccator, the cell suspension was incubated in the enzyme solution at room temperature in the dark without shaking for at least 3 h until the complete cell wall digestion as indicated by the occurrence of round-shaped protoplasts under light microscopy.

The isolated protoplasts were purified from the cell debris by filtration through a piece of 75-μm nylon mesh filter (Sefar America Inc., Kansas City, MO, USA). The filtrate was mixed with equal volume of W5 solution and centrifuged at 100*g* for 2 min. The protoplast pellets were resuspended in 4 mL of CS-sucrose buffer containing 0.4 M sucrose, 20 mM MES-

KOH (pH 5.7), 20 mM KCl and 10 mM $CaCl_2$, and centrifuged at 100*g* for 2 min. The supernatant and the pellet containing unhealthy protoplasts were removed carefully by aspiration without disturbing the healthy protoplasts on the floating layer, which were then resuspended in 1 mL of W5 solution by gentle swirling and allowed to settle on ice for 30 min. The settled protoplasts were then resuspended in MES/Mg^{2+} buffer containing 4 mM MES (pH 5.7), 0.4 M mannitol and 15 mM $MgCl_2$ at a density of 2 x 10^5 protoplasts mL^{-1}. In a standard reaction of PEG-mediated transfection, approximately 2 x 10^4 protoplasts were mixed with 10 µg of plasmid DNA and 110 µL of PEG solution containing 40% (w/v) PEG4000 (Sigma-Aldrich, Oakville, ON, Canada; cat. no. 81240), 0.4 M sucrose and 100 mM $CaCl_2$. After incubation at room temperature for 15 min, the transfected protoplasts were mixed with 440 µL of W5 solution and centrifuged at 100*g* for 2 min. The protoplast pellet was resuspended in 1 mL of WI solution containing 4 mM MES-KOH (pH 6.5), 0.5 M mannitol and 5 mM KCl. The resuspended protoplasts were transferred to a 35 mm petri plate and incubated in a growth chamber (Environmental Growth Chambers, OH, USA) at 23^oC with a photon flux density of approximately 30 µmol m^{-2} s^{-1} overnight. To allow sufficient materials for subsequent subfractionation and Western blot analysis, the standard procedures could be scaled up for transfection of 1.6 x 10^5 protoplasts with 40 µg of plasmid DNA, and the transfected protoplasts were cultured overnight in a 50 mm petri plate with 4 mL of WI solution.

2.6 Viability and organelle staining

Stock solutions of the following fluorescence stains were prepared: 0.2% (w/v) fluorescein diacetate (Sigma-Aldrich, Oakville, ON, Canada; cat. no. F5502) in acetone, 1% (w/v)

fluorescent brightener 28 (Sigma-Aldrich, Oakville, ON, Canada; cat. no. F3543) in distilled water, 1% (w/v) rhodamine 123 (Sigma-Aldrich, Oakville, ON, Canada; cat. no. R8004) in ethanol, and 1% (w/v) 4',6-diamidino-2-phenylindole (DAPI) dilactate (Sigma-Aldrich, Oakville, ON, Canada; cat. no. D9564) in dimethylformamide. Two hundred microliters of isolated protoplasts in CS-sucrose buffer were incubated with 4 µL of the staining stock solution at room temperature for 15 min, and then washed twice by centrifugation at 100*g* for 2 min and resuspension of the cells on the floating layer in 200 µL of CS-sucrose buffer. The stained cells were examined and imaged by confocal laser scanning microscopy.

For vacuolar staining, 200 µL of protoplasts were centrifuged at 100*g* for 2 min, and the floating protoplasts were collected and resuspended in 200 µL of acidic staining buffer containing 0.7 M sucrose, 50 mM sodium citrate (pH 4), 5 mM KCl and 1 mM $CaCl_2$. The protoplasts were stained with 1 µL of 10 mM 5-(and-6)-carboxy-2',7'-dichlorofluorescein diacetate (CDCFDA; Invitrogen, Burlington, ON, Canada; cat. no. C-369] at room temperature for 15 min, and washed twice by centrifugation at 100*g* for 2 min and resuspension of the cells on the floating layer in 200 µL of the acidic staining buffer. The stained protoplasts were observed under epifluorescence microscopy.

2.7 Biolistic transformation of onion epidermal cells

Tungsten microcarriers were coated with plasmid DNA essentially as previously described (Sanford et al., 1993). Briefly, 30 mg of tungsten M-17 particles (~1.1 µm in diameter; Bio-Rad, Mississauga, ON, Canada) were incubated in 70% (v/v) ethanol for 15 min, and washed three times with sterile distilled water. The washed tungsten particles were resuspended in

500 µL of 50% (v/v) glycerol and stored at -20 ^{o}C. One milligram of tungsten particles was coated with 5 µg of plasmid DNA in a suspension containing 16 mM spermidine and 0.1 M $CaCl_2$ by vigorous vortexing for 2 min and subsequent incubation for 10 min. The DNA-coated tungsten particles were collected by short-spinning, washed in 70% (v/v) and 100% (v/v) ethanol, and loaded onto the macrocarrier discs (Bio-Rad, Mississauga, ON, Canada). The plasmid DNA was bombarded into a 2.5 x 2.5 cm^2 section of onion bulb epidermis from a distance of 10 cm at a helium pressure of 1,100 p.s.i using a Biolistic PDS-1000/He particle-delivery system (Bio-Rad, Mississauga, ON, Canada) according to the manufacturer's instructions. The bombarded samples were incubated in petri plates on moist filter paper at room temperature in the dark for 16 h, and observed under epifluorescence microscopy.

2.8 Purification of dimorphic chloroplasts from *B. sinuspersici*

A protocol for purification of dimorphic chloroplasts from isolated chlorenchyma protoplasts of *B. sinuspersici* was established empirically in the present study. The isolated protoplasts were washed once in wash buffer containing 0.7 M sucrose, 25 mM HEPES-KOH (pH 6.5) and 5 mM KCl, and resuspended in an appropriate volume of wash buffer to obtain a cell density of 10^5 protoplasts mL^{-1}. All subsequent steps were carried out at 0~4 ^{o}C, unless otherwise specified. To separate the peripheral chloroplasts (P-Chls) and the central chloroplasts (C-Chls) by the hypo-osmotic shock method, 500 µL of protoplast suspension were prechilled on ice for 5 min and diluted with 1.25 mL of dilution buffer containing 25 mM HEPES-KOH (pH 6.5), 5 mM KCl, 2 mM EDTA, which had been equilibrated at room temperature, to obtain a final sucrose concentration of 0.2 M. The diluted protoplasts were

gently mixed by inverting the tube several times, and incubated at room temperature for 2 min. Following the osmotic lysis of protoplasts, the samples were immediately transferred onto ice with minimal agitation. During the 10-min incubation on ice, the released central cytoplasmic compartments (CCCs) were allowed to settle to the bottom of the tube, while the intact vacuoles carrying P-Chls floated to the top of the medium. The sedimentation of CCCs and the floating of vacuoles with associated P-Chls were enhanced by centrifugation at 100*g* for 4 min in a swinging-bucket rotor (A-8-11 for the refrigerated centrifuge 5417R; Eppendorf Canada Ltd., Mississauga, ON, Canada). The floating layer of vacuoles with P-Chls was carefully transferred to a fresh microfuge tube and the aqueous medium was aspirated off with a micropipette without disturbing the pellet containing CCCs. The CCC pellet was washed once with 2 mL of HS (pH 8) buffer [50 mM HEPES-KOH (pH 8) and 330 mM sorbitol] by gently tapping with an index finger, centrifuged at 100*g* for 2 min, and resuspended in 300 μL of dilution buffer. The CCCs were then dissociated by pipetting ten times up and down using a narrow bore 200-μL micropipette tip. To further purify C-Chls from the other organelles in CCCs, the dissociated CCCs were subjected to Percoll gradient centrifugation (see section 2.11). Similar Percoll gradients were used to isolate the loosely associated P-Chls from the vacuole surfaces.

2.9 Isolation of total chloroplasts from *B. sinuspersici*

The procedures for assembling a protoplast-rupturing device were modified according to the method described by Smith et al. (2002b). Briefly, the needle-fitting end of a 1-mL syringe barrel and the top part of a 500-μL microfuge tube were cut off to form a hollow tube and a slightly wider adaptor ring, respectively. A piece of 10-μm nylon mesh filter (Spectrum Lab

Inc., Rancho Dominguez, CA, USA) was fitted against the cut end of the hollow tube and held in place using the adaptor ring. All subsequent steps were carried out at 0~4 ^{o}C. The isolated protoplasts were collected by brief centrifugation at 100*g* for 2 min, and the cell pellet was resuspended in an appropriate volume of protoplast breakage buffer containing 20 mM tricine-KOH (pH 8.4), 330 mM sorbitol, 5 mM EDTA, 5 mM EGTA and 10 mM $NaHCO_3$, to obtain a cell density of 4 x 10^5 protoplasts mL^{-1}. Five hundred microliters of protoplast suspension were transferred into the protoplast-rupturing device and the plunger was replaced to force the suspension through the mesh. An equal volume of protoplast breakage buffer was then added to the protoplast-rupturing device for completing the breakage of residual protoplasts and CCCs on the mesh. To isolate total chloroplasts from the cell lysate, the pooled filtrates were subjected to Percoll gradient purification (see section 2.11).

2.10 Subfractionation of transfected *A. thaliana* protoplasts

The tranfected mesophyll protoplasts of *A. thaliana* in WI solution were mixed with equal volume of W5 solution and collected by brief centrifugation at 300*g* for 2 min. The cell pellet was resuspended in 300 µL of HS (pH 7.3) buffer containing 50 mM HEPES-KOH (pH 7.3) and 330 mM sorbitol. The resuspended protoplasts were lysed by passage through a layer of 10-µm nylon mesh using the protoplast-rupturing device (see section 2.9). Intact chloroplasts were isolated from the protoplast lysate by Percoll gradient purification (see section 2.11). For thermolysin treatment, the intact chloroplasts were resuspended in 50 µL of HS (pH 7.3) buffer and incubated with 10 µg of thermolysin (Sigma-Aldrich, Oakville, ON, Canada) on ice for 30 min. The reaction was stopped with 4 µL of 0.5 M EDTA prior to the re-isolation

of intact chloroplasts by Percoll gradient purification (see section 2.11). For alkaline extraction experiments, the intact chloroplasts were resuspended in 40 µL of HS (pH 7.3) buffer and incubated with 500 µL of 0.1 M Na_2CO_3 (pH 11.5) on ice for 10 min, followed by subfractionation of the chloroplast samples into the membrane and soluble fractions.

The isolated chloroplasts were subfractionated into the membrane and stromal fractions as described previously (Smith et al., 2002b). Briefly, 40 µL of isolated chloroplasts were hypo-osmotically lysed by incubation with 213 µL of 2 mM EDTA on ice for 10 min. To facilitate precipitation of chloroplast membranes, the lysed chloroplasts were mixed with 13.3 µL of 4 M NaCl. After centrifugation at 20,000*g*, 4 ^{o}C for 30 min, the membrane pellet was resuspended in 25 µL of solubilization buffer containing 50 mM Tris-HCl (pH 8), 5 mM EDTA and 0.2% (w/v) SDS, and the soluble proteins in the supernatant were concentrated by incubation with 4 volumes of ice-cold acetone at -20 ^{o}C for at least 1 h. The acetone-precipitated proteins were resuspended in 25 µL of solubilization buffer. Similarly, the total ruptured protoplasts were subfractionated into the insoluble and soluble fractions using the same procedures after hypo-osmotic lysis of the organelles with EDTA. The membrane pellets and acetone-precipitated soluble fractions were resuspended in solubilization buffer. The protein concentrations of all fractions were determined by bicinchoninic acid protein assays (see section 2.12).

2.11 Percoll gradient purification of chloroplasts

The chloroplast purification procedures were modified from Smith et al. (2002b). Briefly, up to 1 mL of chloroplast suspension was layered on a Percoll step gradient consisting of an

upper 500-µL Percoll solution [40% (v/v) Percoll, 50 mM HEPES-KOH (pH 7.3), 330 mM sorbitol, 1 mM $MgCl_2$, 1 mM $MnCl_2$ and 2 mM EDTA] and a lower 500-µL Percoll solution [85% (v/v) Percoll, 50 mM HEPES-KOH (pH 7.3) and 330 mM sorbitol]. The gradient was centrifuged at 2,500*g*, 4 ^{o}C for 10 min in a swinging-bucket rotor (A-8-11 for the refrigerated centrifuge 5417R; Eppendorf Canada Ltd., Mississauga, ON, Canada). The intact chloroplasts at the 40%/85% interface of the Percoll gradient were aspirated and diluted with 6 volumes of ice-cold HS (pH 7.3) buffer. The isolated chloroplasts were collected by centrifugation at 750*g*, 4 ^{o}C for 5 min and resuspended in 50 µL of ice-cold HS (pH 7.3) buffer.

2.12 Extraction of proteins from *B. sinuspersici* leaves

Fresh *B. sinuspersici* leaves were ground using a mortar and pestle on ice in 2 volumes of extraction buffer containing 100 mM Tris-HCl (pH 8), 150 mM NaCl, 1% (w/v) SDS, 1 mM EDTA, 1 mM phenylmethylsulfonyl fluoride and 1% (v/v) protease inhibitor cocktail (Sigma-Aldrich, Oakville, ON, Canada, cat. no. P9599). The crude extracts were clarified by centrifugation at 20,000*g*, 4 ^{o}C for 15 min) and the protein yields were quantified by bicinchoninic acid (BCA) assays (see section 2.13).

2.13 Protein quantification

Protein samples in detergent-containing buffers, including the protein extracts from total protoplasts and isolated chloroplasts, were quantified by using the BCA Protein Assay Kit (Pierce, Rockford, IL, USA), according to the manufacturer's instructions. In a BCA assay, the protein concentrations were estimated against standard solutions of BSA from 25 to

1,000 μg mL^{-1}. All other protein samples, including the recombinant proteins expressed in *E. coli*, were quantified by Bradford assays (Bradford, 1976) using the Protein Assay Dye Reagent Concentrate (Bio-Rad, Mississauga, ON, Canada), according to the manufacturer's instructions. In a Bradford assay, the protein concentrations were estimated against standard solutions of BSA from 1.25 to 15 μg mL^{-1}.

2.14 SDS-PAGE

Proteins were boiled with 6x SDS sample buffer [72 mM Tris–HCl (pH 6.8), 30% (v/v) glycerol, 2.% (w/v) SDS, 0.12% (w/v) bromophenol blue and 6% (v/v) β-mercaptoethanol] for 10 min, and resolved by polyacrylamide gel electrophoresis (PAGE) using the Mini-PROTEAN® III Electrophoresis Cell (Bio-Rad, Mississauga, ON, Canada). A 10% (w/v) resolving gel was cast with 2 mL of 30% (w/v) acrylamide/bisacrylamide (37.5:1), 2.25 mL of 1 M Tris-HCl (pH 8.8), 1.66 mL of distilled water, 60 μL of 10% (w/v) SDS, 30 μL of 10% (w/v) APS and 3 μL of TEMED. A 12% (w/v) resolving gel was cast with 2.4 mL of 30% (w/v) acrylamide/bisacrylamide, 2.25 mL of 1 M Tris-HCl (pH 8.8), 1.26 mL of distilled water, 60 μL of 10% (w/v) SDS, 30 μL of 10% (w/v) APS and 3 μL of TEMED. A 4.8% (w/v) stacking gel was cast with 400 μL of 30% (w/v) acrylamide/bisacrylamide, 312.5 μL of 1M Tris-HCl (pH 6.8), 1.75 mL of distilled water, 25 μL of 10% (w/v) SDS, 12.5 μL of 10% (w/v) APS and 2.5 μL of TEMED. Gel electrophoresis was run at 140 V in running buffer [24.8 mM Tris, 0.192 M glycine and 0.1% (w/v) SDS] until the dye front ran off the gel.

2.15 Western blot analysis

Resolved proteins from SDS-PAGE were electroblotted onto polyvinylidene difluoride (PVDF) membrane (Bio-Rad, Mississauga, ON, Canada) in transfer buffer [48 mM Tris, 39 mM glycine, 20% (v/v) methanol and 0.0375% (w/v) SDS] at room temperature, 15 V for 40 min using the Trans-Blot® SD Semi-Dry Electrophoretic Transfer Cell (Bio-Rad, Mississauga, ON, Canada). The blot was incubated in blocking solution containing TBS-T buffer [25 mM Tris-HCl (pH 7.4), 137 mM NaCl, 2.7 mM KCl, 0.05% (v/v) Tween-20] and 2% (w/v) ECL-Advance Blocking Agent (GE Healthcare, Baie d'Urfe, QC, Canada) or 5% (w/v) skim milk powder (for ECL-Plus detection) at room temperature for 1 h. The blot was probed in blocking solution with primary antibody against enhanced green fluorescent protein (EGFP; 1:4,000), pyruvate orthophosphate dikinase (PPDK; 1:4,000; courtesy of Dr. Chris Chastain from Minnesota State University Moorhead), large-subunit of Rubisco (RbcL; 1:5,000; Agrisera, Vannas, Sweden; cat. no. AS03-037), Photosystem II manganese-stabilizing protein (PsbO; 1:5,000; courtesy of Dr. Marilyn Griffith from University of Waterloo), cytochrome f (Cyt-f; 1:1,000; Agrisera, Vannas, Sweden; cat. no. AS08-306), Photosystem I subunit II (PsaD; 1:500; Agrisera, Vannas, Sweden; cat. no. AS09-461), BsToc159 (1:32,000), BsToc132 (1:4,000), AtToc34 (1:16,000; Agrisera, Vannas, Sweden; cat. no. AS07-238), phosphoenolpyruvate carboxylase (PEPC; 1:10,000; Chemicon, Temecula, CA, USA), actin (1:3,000; MP Biomedicals, Solon, OH, USA) or β-tubulin (1:1,000; Sigma-Aldrich, Oakville, ON, Canada; cat. no. T4026) at 4 ^{o}C overnight. After washing with three changes of TBS-T solution for a total of 30 min, the blot was probed in blocking solution with a horseradish peroxidase-conjugated anti-mouse (against actin and β-tubulin antibodies; Sigma-Aldrich, Oakville, ON, Canada, cat. no. A4416) or anti-rabbit

(otherwise; Sigma-Aldrich, Oakville, ON, Canada, cat. no. A6154) secondary antibody (1:10,000 for ECL-Plus detection or 1:800,000 for ECL-Advance detection) at room temperature for 2 h. The blot was washed with three changes of TBS-T solution for a total of 30 min, and the signals were detected with Amersham ECL-Plus Solution (for PPDK, RbcL, PsbO, Cyt-f, PsaD or PEPC; GE Healthcare, Baie d'Urfe, QC, Canada) or Amersham ECL-Advance Solution (otherwise; GE Healthcare, Baie d'Urfe, QC, Canada), according to the manufacturer's instructions. Luminescence was detected by exposing the membrane to Amersham Hyperfilm ECL films (GE Healthcare, Baie d'Urfe, QC, Canada), which were developed using a CP1000 Agfa photodeveloper (AGFA, Pointe Claire, QC, Canada). The films were scanned and processed using Adobe Photoshop CS (Adobe Systems Inc., Seattle, WA, USA). The intensities of immunoreactive bands were densitometrically quantified using the gel-analyzer function of Image J software v.1.46 (National Institutes of Health, USA).

2.16 Cloning of cDNAs encoding Toc receptors from *B. sinuspersici*

Primers were designed based on the conserved regions in the alignment of open reading frames of Toc homologues from different plant species, which were initially retrieved by BLASTp search using the Toc159 and Toc34 amino acid sequences from *P. sativum*. Sequences of primers used for cDNA cloning are shown in Table 2.1 and their binding positions are illustrated in Figure 2.1. Partial cDNA fragments were amplified by reverse-transcription PCR from mature leaf cDNA of *B. sinuspersici* using the Protoscript II RT-PCR Kit (New England BioLabs, Ipswich, MA, USA) according to the manufacturer's instructions. The full-length cDNA clones were obtained by 5′ and 3′ rapid amplification of cDNA ends (RACE) using the First Choice RLM-RACE kit (Ambion, Austin, TX, USA),

Table 2.1 List of oligonucleotides used for cDNA cloning

Name	Start	End	Nucleotide sequence (5' to 3')	Orientation
Toc159F1	+1,720	+1,739	AGGATTGATGGCCAGATTGT	Sense
Toc159R1	+3,106	+3,125	AATGGTGGCAGCTGGTCATA	Anti-sense
Toc159F3	+3,217	+3,239	CAGAAGAAGCAATGGAGAGAGGA	Sense
Toc159R3	+3,476	+3,497	TATCCACAGTCATGGTCCCAAC	Anti-sense
Toc159F5	+3,395	+3,416	ACAGTGACAACCCTGCTTATCG	Sense
Toc159F6	+3,451	+3,472	GCTAGGCCAGTTTTGGACACTC	Sense
Toc159F7	+486	+506	AACCAAAGAGGAGGAGGGTGT	Sense
Toc159R4	+1,842	+1,861	TGATGGTGCCAGGATCTGAG	Anti-sense
Toc159R7	+580	+601	TTATCCTTAGCAGCAGCACTTC	Anti-sense
Toc159F13	+1	+19	CGCCTCGAGATGGCGTCAGAAACTGCTT	Sense
Toc159R11	+4,202	+4,225	CGCAAGCTTCTAAAAGCAAATGACTGAGAACAA	Anti-sense
Toc132F2D	+2,118	+2,139	ATATGGTTTAATGCCATTGTKG	Sense
Toc132R2	+2,941	+2,963	TAGCGGTGAGTAGGGTTGTCAGA	Anti-sense
Toc132F5	+2,922	+2,943	TTTGCCAGTGTCCTTTGATTCT	Sense
Toc132F6	+1,453	+1,470	GCAGGTCTTGGTCGTGCT	Sense
Toc132R4	+2,262	+2,282	ACAGCATGTGATCGTTGAGTG	Anti-sense
Toc132R5	+1,547	+1,568	GTGGTGTCTTCAGCAACATTGG	Anti-sense
Toc132F8	-92	-71	CGCCTCGAGGATAGCCACATACTCCCTCCTC	Sense
Toc132R10	+3,920	+3,944	CGCGGATCCAACAAGAAAATTACACTGGCTATGC	Anti-sense
Toc34F3	+117	+137	GGTCCTTGTAATGGGGAAAGG	Sense
Toc34R1	+482	+503	TCTGGTGGAGAGAATTGAGCAT	Anti-sense
Toc34F4	+364	+384	CTGTATGTGGACCGATTGGATG	Sense
Toc34F5	+451	+472	ATATGGAAACGTGCTGCTGTTG	Sense
Toc34R3	+295	+319	CAATAGCACGATCATTCACATATCC	Anti-sense
Toc34R2	+275	+299	TATCCTCCCTCAACAAGACCTAGTG	Anti-sense
Toc34F8	-51	-32	CGCCTCGAGTTTTCACCCTTAAACGCCAAC	Sense
Toc34R6	+1,024	+1,045	CGCTCTAGAAAGTTTGCCACTACGGTGACTG	Anti-sense
5RACE-OP	N/A	N/A	GCTGATGGCGATGAATGAACACTG	Sense
5RACE-IP	N/A	N/A	CGCGGATCCGAACACTGCGTTTGCTGGCTTTGATG	Sense
3RACE-OP	N/A	N/A	GCGAGCACAGAATTAATACGACT	Anti-sense
3RACE-IP	N/A	N/A	CGCGGATCCGAATTAATACGACTCACTATAGG	Anti-sense

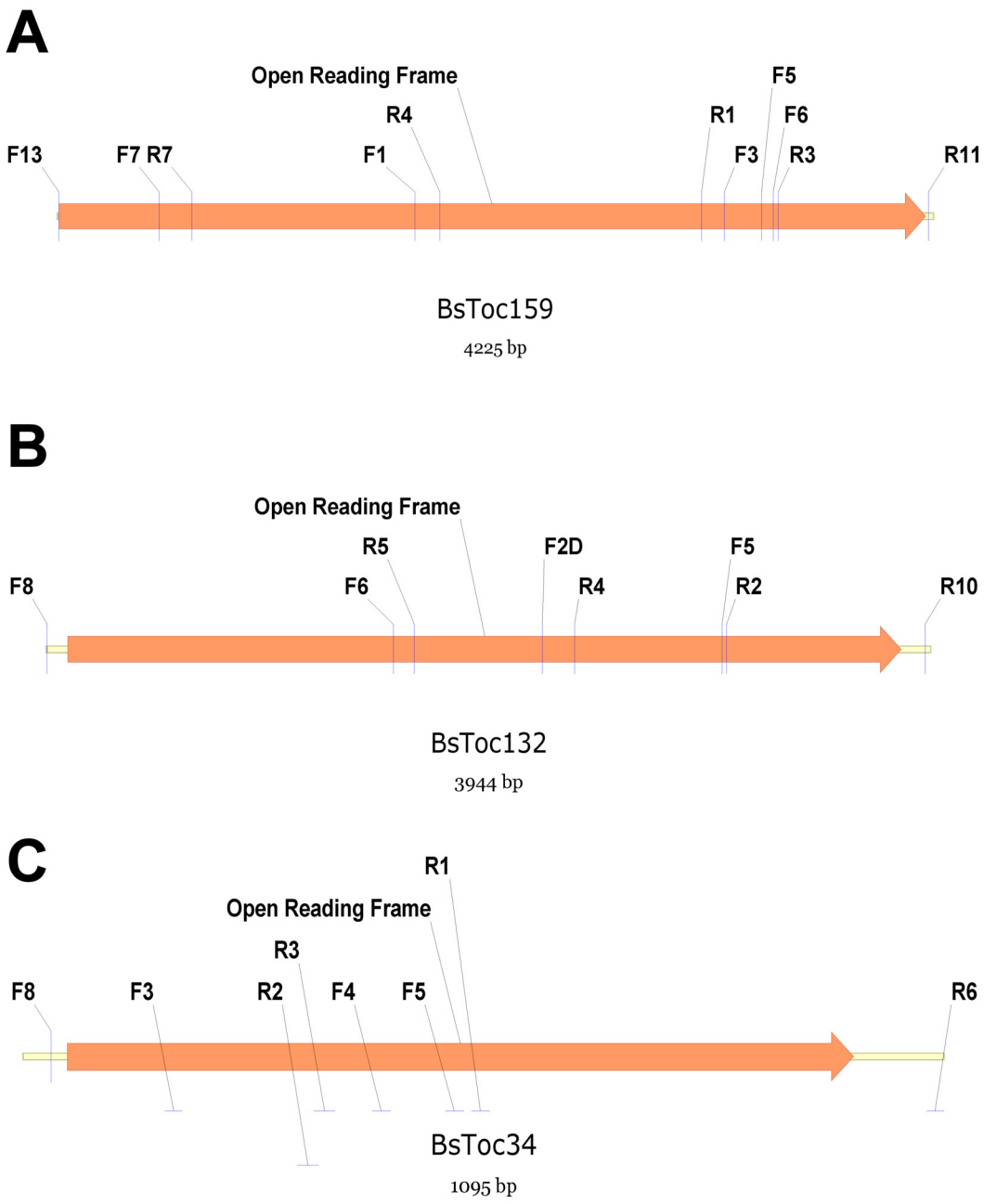

Figure 2.1 Cloning of cDNA encoding Toc receptors from *B. sinuspersici*

Primers used for cDNA cloning and the identified open reading frames are annotated using Vector NTI Advance™ 10.3.0 (Invitrogen).

(A) cDNA cloning of *BsToc159*.
(B) cDNA cloning of *BsToc132*.
(C) cDNA cloning of *BsToc34*.

following the manufacturer's protocol. A 280-bp fragment and a 1.4-kb fragment of BsToc159 were first identified after PCR amplification with Toc159F1/R1 and Toc159F3/R3, respectively. Toc159F5 and Toc159F6 were designed from the 280-bp sequence for 3'RACE by nested PCR. Toc159R4 was designed from the 1.4-kb sequence for PCR with Toc159-F7. Toc159R7 was designed from the resulting 1.2-kb sequence for 5'RACE by nested PCR. Full-length BsToc159 was amplified with Toc159F13/R11. A 825-bp fragment of BsToc132 was first identified after PCR amplification with Toc132F2D/R2. Toc132F5 was designed from the 825-bp sequence for 3'RACE. Toc132R4 was designed from the 825-bp sequence for PCR with Toc132F6. Toc132R5 was designed from the resulting sequence for 5'RACE. Full-length BsToc132 was amplified with Toc132F8/R10. A fragment of BsToc34 was first identified after PCR amplification with Toc34F3/R1. From the sequence, Toc34F4 and Toc34F5 were designed for 3'RACE by nested PCR and Toc34R2 and Toc34R3 were designed for 5'RACE by nested PCR. Full-length BsToc34 was amplified with Toc34F8/R6. Sequence data of the Toc receptor homologues can be found in the GenBank data library under the accession numbers: *BsToc159* (JQ739199), *BsToc132* (JQ739200) and *BsToc34* (JQ739201).

2.17 Construction of fluorescent protein fusion constructs

The construction of the GFP-talin and GFP-MAP4 plasmids has been described previously (Kost et al., 1998; Marc et al., 1998). The other EGFP fusion constructs for transient expression studies were produced by subcloning specific DNA fragments of interest at the 5'-end of EGFP sequence using pSAT6-35S:EGFP-N1 vector or the 3'-end of EGFP sequence using pSAT6-35S:EGFP-C1 vector (Appendix I), both of which were described

previously (Chung et al., 2005). The details of primers and subcloning vectors for the generation of each EGFP fusion construct can be found in Table 2.2. After identification of the cDNA sequences encoding NAD-malic enzyme, Rubisco small-subunit, ferredoxin, photosynthetic and non-photosynthetic isoforms of ferredoxin:$NADP^+$-oxidoreductase (Onda et al., 2000), PPDK and malate dehydrogenase from *B. sinuspersici*, their transit sequences were predicted using the ChloroP prediction program v1.1 (Emanuelsson et al., 1999; http://www.cbs.dtu.dk/services/ChloroP) and subcloned at the 5' end of EGFP. To generate the nuclear localization signal (NLS)-EGFP fusion construct, the EGFP-encoding sequence was PCR-amplified using a primer set with the simian virus (SV40)-like NLS sequence (i.e. PKKKRKV) introduced in the forward primer in frame with the N-terminus of EGFP. Similarly, the EGFP-peroxisomal targeting signal fusion construct was generated by PCR-amplifying the EGFP-encoding sequence using a primer set with the targeting signal (i.e. SKL) incorporated in the reverse primer in frame with the C-terminus of EGFP. The DNA sequences were reversed, if applicable, by rearranging the codon triplets and produced by assembly PCR reactions using multiple synthetic oligodeoxynucleotides (up to 68 bases long each), which were designed by the Assembly PCR Oligo Maker (Rydzanicz et al., 2005; http://startrek.ccs.yorku.ca/~pjohnson/AssemblyPCRoligomaker.html).

2.18 Construction of recombinant protein expression constructs

To raise specific antibodies, the entire protein of EGFP and the N-terminal regions of BsToc159 and BsToc132 were over-expressed and purified for rabbit immunization. The expression constructs were produced by subcloning specific DNA sequences into the *Bam*HI/*Xho*I sites of the pET-28a(+) expression vector (Novagen, Darmstadt, Germany;

Table 2.2 List of oligonucleotides used for the construction of EGFP fusion constructs

Fusion protein	Vector[1]	Oligonucleotide		
		Name	Sequence (5' to 3')[2]	Orientation
NLS-EGFP	N1	NLS-F	AT*ccatgg*TGCCAAAAAAGAAGAGAAAGGTAGAAGACCCC GTGATGGTGAGCAAGGGCGA	Sense
		NLS-R	CGC*gcggccgc*GTCACTGGATTTTGGTT	Anti-sense
EGFP-SKL	C1	SKL-F	AAA*ccatgg*TGAGCAAGGGCGAG	Sense
		SKL-R	AAA*ggatcc*CTACAGCTTGCTCTTGTACAGCTCGTCCATGC	Anti-sense
tME-EGFP	N1	METP-F	CGC*ccatgg*CAATGTCGATGATTTGTAATCGGAGT	Sense
		METP-R	ATA*ggatcc*CACGATGACCTTCAGAAGTAGTAAACG	Anti-sense
tRbcS-EGFP	N1	RbcS-TP-F	CGC*ccatgg*CAATGGCTTCTAGTTTGATGTCCAG	Sense
		RbcS-TP-R	CGC*gtcgac*CGCATTGGACTTTTCCACCGTT	Anti-sense
tFd-EGFP	N1	BsFd-F10	AAA*ccatgg*CAGCAACAACAACA	Sense
		BsFd-R11	AAA*ggatcc*CTTTGTAGGTTGCCATTGCTG	Anti-sense
tFNR(P)-EGFP	N1	BsFNR-F13	AAA*ccatgg*CTAACGCAGTCACAG	Sense
		BsFNR-R13	AAA*ggatcc*CTGAGGTGACTTGGGCCTTA	Anti-sense
tFNR(H)-EGFP	N1	BsFNR-F14	AAA*ccatgg*CTTATTCTGCCATCG	Sense
		BsFNR-R14	AAA*ggatcc*CTTGTTGCACAGACATGCAT	Anti-sense
tPPDK-EGFP	N1	BsPPDK-F2	AAA*ccatgg*CATTATGTTTCAAAGGA	Sense
		BsPPDK-R3	AAA*ggatcc*CCTGCTGTGTGGTGGTTGA	Anti-sense
tMDH-EGFP	N1	BsMDH-F2	AAA*ccatgg*CAGTAGCTGAGCTTTC	Sense
		BsMDH-R3	AAA*ggatcc*CAGCAAGGTTGCAACAAATCTT	Anti-sense
EGFP-Toc159	C1	Toc159F19	CGC*ctcgag*CTATGGCGTCAGAAACTGCTT	Sense
		Toc159R20	CGC*ggatcc*TTAATAAATAGAGTAGCTTGGACTG	Anti-sense
Toc159-EGFP	N1	Toc159F18	CGC*ctcgag*CATGGCGTCAGAAACTGCTT	Sense
		Toc159R19	CGC*ggatcc*CATAAATAGAGTAGCTTGGACTGACA	Anti-sense
EGFP-Toc132	C1	Toc132F12	CGC*ctcgag*CTATGGAAAATGGGGCGGGAGT	Sense
		Toc132R13	CGC*ggatcc*TCAATATCCAAGAGGATGCTCT	Anti-sense
Toc132-EGFP	N1	Toc132F11	CGC*ctcgag*CATGGAAAATGGGGCGGGAGT	Sense
		Toc132R12	CGC*ggatcc*CATATCCAAGAGGATGCTCTTGA	Anti-sense
EGFP-Toc34	C1	Toc34F12	CGC*ctcgag*CTATGGCTTCCCAAGTGGTTC	Sense
		Toc34R10	CGC*ggatcc*TCAGTACTTGCGCTTTGATACA	Anti-sense
Toc34-EGFP	N1	Toc34F11	CGC*ctcgag*CATGGCTTCCCAAGTGGTTC	Sense
		Toc34R9	CGC*ggatcc*CGTACTTGCGCTTTGATACATTCAT	Anti-sense

EGFP-Toc159$_{(1-1339)}$	C1	Toc159F19	CGC*ctcgag*CTATGGCGTCAGAAACTGCTT	Sense
		Toc159R29	AAA*ggatcc*TTAATTCCTTCCGACAGAAATCTG	Anti-sense
EGFP-Toc132$_{(1-1187)}$	C1	Toc132F12	CGC*ctcgag*CTATGGAAAATGGGGCGGGAGT	Sense
		Toc132R24	AAA*ggatcc*TCAAGACCGTCCCATCGGGAT	Anti-sense
EGFP-Toc159$_{(1340-1395)}$	C1	Toc159F28	AAA*ctcgag*CTTCAAAGATGGCTCTTCGTG	Sense
		Toc159R20	CGC*ggatcc*TTAATAAATAGAGTAGCTTGGACTG	Anti-sense
EGFP-Toc132$_{(1188-1239)}$	C1	Toc132F22	AAA*ctcgag*CTACAAATCTGGTTGCTCGTG	Sense
		Toc132R13	CGC*ggatcc*TCAATATCCAAGAGGATGCTCT	Anti-sense
OEP7-EGFP[3]	N1	AtOEP7S2	AACATG*ccatgg*GAAAAACTTCGGGAGCGAAACAGGCGAC TGTG	Sense
		AtOEP7A2	CTATGGCTAACCATCCTAACGCCATCGCTGCGACCACCA CAGTCGCCTGTTTCGC	Anti-sense
		AtOEP7S3	GCGTTAGGATGGTTAGCCATAGAGATCGCTTTCAAGCCT TTCCTCGATAAATTCCGC	Sense
		AtOEP7A3	GGTCTTTGGTTGGGTCAGATTTGTCGATTGAGGAGCGGA ATTTATCGAGGAAGG	Anti-sense
		AtOEP7S4	TCTGACCCAACCAAAGACCCCGATGACTTCGACACCGCC GCTACTGCAACCA	Sense
		AtOEP7A4	AAAA*ctgcag*AACAAACCCTCTTTGGATGTGGTTGCAGTAG CGGC	Anti-sense
EGFP-BsToc34G (i.e.34G)	C1	Toc34F12	CGC*ctcgag*CTATGGCTTCCCAAGTGGTTC	Sense
		Toc34R22	AAAA*ggtacc*GTGTCGTGCATTCGGGTTA	Anti-sense
EGFP-34G- BsToc159$_{(1340-1395)}$	C1-34G	Toc159F28	AAA*ctcgag*CTTCAAAGATGGCTCTTCGTG	Sense
		Toc159R20	CGC*ggtacc*TTAATAAATAGAGTAGCTTGGACTG	Anti-sense
EGFP-34G- BsToc132$_{(1188-1239)}$	C1-34G	Toc132F22	AAA*ctcgag*CTACAAATCTGGTTGCTCGTG	Sense
		Toc132R13	CGC*ggtacc*TCAATATCCAAGAGGATGCTCT	Anti-sense
EGFP-34G- AtToc159$_{(1447-1503)}$	C1-34G	AtToc159F2	AAA*ctcgag*CTTCAAAGATTGCGCTTCGTGCAGGACTTAAC AAC	Sense
		AtToc159R1	AAA*ggtacc*TTAGTACATGCTGTACTTGTCGTTC	Anti-sense
EGFP-34G- AtToc132$_{(1154-1206)}$	C1-34G	AtToc132F2	AAA*ctcgag*CTTCTAATTTAATTGCTCGTGCTAATCTGAACA AT	Sense
		AtToc132R1	AAA*ggtacc*TCATTGTCCATATTGCGTTTG	Anti-sense
EGFP-34G- RbcS$_{(55-1)}$[3]	C1-34G	AtSSU-S1a	AAA*ctcgag*CTTGCAACGTTAGAGGAGGCAACAGCACAATC TCCACTATTGACAACAAC	Sense
		AtSSU-A1	GTTTCCAAGCTTGGAGGAAGCGGCGAATGGGGCGGTGCG CTTAGCGTTGTTGTCAATAGTGGAGATTG	Antisense

		AtSSU-S2	CTTCCTCCAAGCTTGGAAACTTCCCTGCTGTCATGACTGC CCAGGCTCCGTCTGCCGTTATGACTGC	Sense
		AtSSU-A2	AAA*ggtacc*TTACATAGCGGAAGACATGAGAGAGGAAGCAG TCATAACGGCAGACG	Anti-sense
EGFP-34G-PPDK$_{(90\text{-}1)}$[3]	C1-34G	BsPPDK-S1	AAA*ggtacc*TCCGGACTCAGATCTCGAGCTGGGGACAGTAG AGGAAAAG	Sense
		BsPPDK-A1	GAACTGAGGTGGTTGTCTGCTGTCGTACAAAGGTAAAAC CTTTTCCTCTACTGTCCCC	Anti-sense
		BsPPDK-S2	GCAGACAACCACCTCAGTTCCAGACTCAATCTTGGCTATG GTCGATCAAAGAAACTCCC	Sense
		BsPPDK-A2	TTCCTCCTTCTGCATGGATGTCGTAAAGTGCTCTGGCTCTG GGAGTTTCTTTGATCGACC	Anti-sense
		BsPPDK-S3	GACATCCATGCAGAAGGAGGAACCGGTTCCAAGTTCGTC AGTTTAGTAATTGCCAAAGCTGT	Sense
		BsPPDK-A3	GTATGTGTAAGACCATACATCTTGTCTTGATATTGAACAC CACAGCTTTGGCAATTACTAAACTG	Anti-sense
		BsPPDK-S4	AGACAAGATGTATGGTCTTACACATACATTTGTAGATCCA GCTTCTAGAATCCTAATGGGAAAATT	Sense
		BsPPDK-A4	AAA*ggtacc*TTACATTGCTAAACAGAATTTTCCCATTAGGAT TCTAGAAGCTG	Anti-sense
EGFP-34G-Fd$_{(53\text{-}1)}$[3]	C1-34G	BsFd-S1	AAA*ctcgag*CTATGGCAACAATGAGAGGAGGACGAGCCGG TTCGAAGCTCGGG	Sense
		BsFd-A1	GTGGCATCATTGCAGCGAATGGGCAGTTCATGCCCCGGG CCAAGAACCCGAGCTTCGAACC	Anti-sense
		BsFd-S2	CGCTGCAATGATGCCACCACCAACCCAACCAAAGCCAGC CCTGACAACAGCCGCAATGGGAAT	Sense
		BsFd-A2	AAA*ggatcc*TTACATTGCTGCTGTTGTTGTTGTCATCATTCCC ATTGCGGCTGTTGT	Anti-sense
EGFP-34G-NAD-ME$_{(38\text{-}1)}$[3]	C1-34G	BsME-S1	AAAA*ggtacc*TCCGGACTCAGATCTCGAGCTCGTCATGGTG AATCTACTAC	Sense
		BsME-A1	AACTTGTATTCAATTGCTACAATCGTATCATGTCTCGAAA AAGTAGTAGATTCACCATGACGAGC	Anti-sense
		BsME-S2	TGATACGATTGTAGCAATTGAATACAAGTTGCGAAAAAT CTTGTCTTCGTCATTAAGAAGTCGGAA	Sense
		BsME-A2	AAAAGGATCCTTACATCGACATAATACAATTCCGACTTCT TAATGACGAAGAC	Anti-sense

NAD-ME$_{(1\text{-}38)}$-EGFP	N1	BsME-TP-F1	CGC*ccatgg*CAATGTCGATGATTTGTAATCGGAGT	Sense
		BsME-TP-R1	ATA*ggatcc*CACGATGACCTTCAGAAGTAGTAAACG	Anti-sense
EGFP-Fd$_{(54\text{-}151)}$	C1	BsFd-F11	AAAA*ctcgag*CTGCAACCTACAAAGTGACCCTCA	Sense
		BsFd-R13	AAAA*ctcgag*ATCTGAGTCCGGAGGTACCATTAAGCAGTAA GCTCTCTTCCTTG	Anti-sense
EGFP-Fd$_{(54\text{-}151)}$-Fd$_{(53\text{-}1)}$[3]	C1-Fd$_{(54\text{-}151)}$	BsFd-S1	AAA*ctcgag*CTATGGCAACAATGAGAGGAGGACGAGCCGG TTCGAAGCTCGGG	Sense
		BsFd-A1	GTGGCATCATTGCAGCGAATGGGCAGTTCATGCCCCGGG CCAAGAACCCGAGCTTCGAACC	Anti-sense
		BsFd-S2	CGCTGCAATGATGCCACCACCAACCCAACCAAAGCCAGC CCTGACAACAGCCGCAATGGGAAT	Sense
		BsFd-A2	AAA*ggatcc*TTACATTGCTGCTGTTGTTGTTGTCATCATTCCC ATTGCGGCTGTTGT	Anti-sense
Toc132$_{(1239\text{-}1188)}$-EGFP	N1	Toc132S1	CATG*ccatgg*TCTATGGACTTCCTCATGAGCAACGTCAGGG CATAATTAAGAG	Sense
		Toc132A1	TGCACCTGCAAAGCAAGAACAGCAAAAAGAGGCAGGAG TCTCTTAATTATGCCCTGACGTTGC	Anti-sense
		Toc132S2	TTCTTGCTTTGCAGGTGCAAGAAGCAAGTAACTTGCGTCT TAGTATCCAAGGATCAGGACGT	Sense
		Toc132A2	AAAA*gagctc*AGCACGCGCATTCAAGTTGTTACGTCCTGATC CTTGGATACTAAG	Anti-sense
Toc159$_{(1395\text{-}1340)}$-EGFP	N1	Toc159S1	CATG*ccatgg*TCTATATTTCTTACAGCCCAAGTGTCGGTCCTA AGTTCAAACAGT	Sense
		Toc159A1	GAGAAAGTGCAATAGCACCTAGAACTGGAATAGCAAGA GAGATATACTGTTTGAACTTAGGACCGAC	Anti-sense
		Toc159S2	TCTAGGTGCTATTGCACTTTCTCTCCATGATTCTAGCAGCA CAAAGGTGACAATTCAGGGAAGTCAA	Sense
		Toc159A2	AAAA*gagctc*AAGACGAACTGCCAAGTTATTCTTTTGACTTC CCTGAATTGTCACCT	Anti-sense

Remarks: [1] *pSAT6-35S:EGFP-N1 (i.e. N1) or pSAT6-35S:EGFP-C1 (i.e. C1) was used as primary subcloning vector.*
[2] *Restriction sites used for subcloning are italicized and showed in lower-case letters.*
[3] *These constructs were made by assembly PCR using multiple oligodeoxynucleotides.*

Appendix I): the A-domain of BsToc159$_{(1-629)}$ was PCR-amplified using Toc159F14 (5'-CGC GGA TCC ATG GCG TCA GAA ACT GCT T-3') and Toc132R14 (5'-CGC CTC GAG TTA ACG AGA TCC ATC TTG AGA TGA TAT A-3') primers the A-domain of BsToc132$_{(1-482)}$ was PCR-amplified using Toc132F7 (5'-CGC GGA TCC ATG GAA AAT GGG GCG GGA GT-3') and Toc132R7 (5'-CGC CTC GAG TTA TGC AGG AGG GGC AGC AGA-3') primers, and; the EGFP-encoding sequence was PCR-amplified using GFP-F1 (5'-AAA GGA TCC ATG GTG AGC AAG GGC GAG GAG-3') and GFP-R1(5'- AAA CTC GAG TCA CTT GTA CAG CTC GTC CAT G -3') primers.

To produce recombinant proteins for stromal processing peptidase assays, the sequences encoding EGFP fusions with the C-terminal tails of BsToc159 and BsToc132 were PCR-amplified from their respective pSAT6 constructs (see primers and constructs in Table 2.2), and subcloned into the *Bam*HI/*Xho*I sites of the pET-28a(+) expression vector (Novagen, Darmstadt, Germany; Appendix I). The EGFP-BsToc159$_{(1340-1395)}$ sequence was PCR-amplified using GFP-F1 and Toc159R20 primers, whereas the EGFP-BsToc132$_{(1188-1239)}$ sequence was PCR-amplified using GFP-F1 and Toc132R13.

2.19 Over-expression and purification of recombinant proteins

The expression vectors were transformed into the BL21-Codon-Plus (DE3)-RIPL strain of *E. coli* (Novagen, Darmstadt, Germany) by heat-shock transformation. For large-scale expression of recombinant proteins, 5 mL of LB broth supplemented with 30 mg L^{-1} kanamycin, 34 mg L^{-1} chloramphenicol and 25 mg L^{-1} streptomycin were inoculated with a single colony and incubated at 37 ^{o}C, 250 rpm for 16 h. Three milliliters of the overnight

starter culture was inoculated into 300 mL of LB broth supplemented with 30 μg mL^{-1} kanamycin and grown at 37 ^{o}C, 250 rpm to an optimum cell density of OD_{600} = 0.6~0.8. The culture was induced with 1 mM isopropyl β-D-thiogalactoside and incubated at room temperature, 200 rpm for 16 h. The cells were harvested by centrifugation at 10,000*g* for 5 min, and lysed by resuspension in 5 mL g^{-1} cell pellet of BugBuster® Protein Extraction Reagent (Novagen, Darmstadt, Germany) supplemented with 25 U mL^{-1} benzonase (Novagen, Darmstadt, Germany), 500 U mL^{-1} lysozyme (BioShop Canada Inc., Burlington, ON, Canada), 1 mM phenylmethylsulfonyl fluoride and 1% (v/v) protease inhibitor cocktail (EDTA-free; BioShop Canada Inc., Burlington, ON, Canada). After clarification of the cell lysates by centrifugation at 20,000*g*, 4 ^{o}C for 20 min, the hexahistidine-tagged recombinant proteins were purified by immobilized metal ion affinity chromatography (IMAC) using the Profinity™ IMAC Ni^{2+}-Charged Resins (Bio-Rad, Mississauga, ON, Canada), according to the manufacturer's instructions. Briefly, 500 μL of resins were incubated with the clarified cell lysate in a gravity-flow chromatography column (Bio-Rad, Mississauga, ON, Canada) at 4 ^{o}C for 30 min. After the flow-through was collected, the resins were washed with 10 column volumes of wash buffer containing 50 mM HEPES-KOH (pH 8) and 0.3 M NaCl, and the bound proteins were eluted in a stepwise gradient of elution buffer with increasing concentrations (20, 50, 100, 200 and 500 mM) of imidazole in wash buffer. The purified proteins were stored in 1X phosphate-buffered saline (1xPBS) containing 10 mM sodium phosphate (pH 7.4), 137 mM NaCl and 2.7 mM KCl after buffer exchange by ultra-filtration using the Nanosep 10K centrifugal device (Pall Life Sciences, Ann Arbor, MI, USA).

To remove the hexahistidine tags from the purified EGFP, 2 mg of eluted proteins were

incubated with 2 U mL^{-1} biotinylated thrombin (Novagen, Darmstadt, Germany) in thrombin cleavage buffer containing 20 mM Tris-HCl (pH 8.4), 150 mM NaCl and 2.5 mM $CaCl_2$ at room temperature for 16 h. To remove thrombin from the treated samples, the reaction mixture was incubated with 64 µL of streptavidin agarose (50% slurry; Novagen, Darmstadt, Germany) in a spin-filter column at room temperature for 30 min with gentle shaking. The filtrate was collected by brief centrifugation at 500*g* for 1 min. To remove the cleaved hexahistidine tags from the EGFP proteins, the thrombin-free filtrate was washed with 1xPBS buffer by ultra-filtration using the Nanosep 10K centrifugal device (Pall Life Sciences, Ann Arbor, MI, USA).

2.20 Production and affinity-purification of antibodies

For the production of polyclonal anti-sera against $BsToc159_{(1-629)}$ and $BsToc132_{(1-482)}$, the purified recombinant proteins were used for rabbit immunization at the Southern Alberta Cancer Research Institute (SACRI, Calgary, ON, Canada). The polyclonal anti-serum against EGFP was raised against the purified recombinant protein in a white New Zealand rabbit using a four-injection protocol. For the first injection, 500 µg of purified protein was mixed with an equal volume of Freund's complete adjuvant (Sigma-Aldrich, Oakville, ON, Canada; cat. no. F5881). Similarly, the three subsequent boost injections were performed with 250 µg of purified protein at 3-week intervals. The final bleed was collected 3 weeks after the final boost injection, and the crude anti-serum was obtained after blood coagulation at 4 ^{o}C overnight and clarification by centrifugation at 1,500*g*, 4^{o}C for 30 min.

Pure immunoglobulins were affinity-purified from the anti-sera by reversible binding to the

same antigenic recombinant proteins. Three milligrams of purified proteins were coupled to 1 mL of activated immunoaffinity support Affi-Gel 15 (Bio-Rad, Mississauga, ON, Canada) in 3 mL of 100 mM MOPS-KOH (pH 7.5) at 4 ^{o}C for 2 h. The uncoupled active esters were then blocked with 33.3 µL of 1 M ethanolamine-HCl (pH 8) at 4 ^{o}C for 1 h. The gel matrix was packed into a gravity-flow chromatography column (Bio-Rad, Mississauga, ON, Canada) and washed sequentially with 10 column volumes of 100 mM MOPS-KOH (pH 7.5), 1xPBS, elution buffer [100 mM glycine-HCl (pH 2.4) and 150 mM NaCl] and finally 1xPBS. Three milliliters of anti-serum were heated at 56 ^{o}C for 30 min to inactivate the complement factors, mixed with 200 µL of 1 M Tris-HCl (pH 8), and incubated with the antigen-coupled gel matrix at room temperature for 30 min. The gel matrix was washed with 10 column volumes of 1xPBS and the immobilized immunoglobulins were eluted with elution buffer in ten 1-mL fractions and immediately neutralized with 0.2 volume of 1 M Tris-HCl (pH 8). The active fractions were determined by SDS-PAGE and stored in frozen aliquots at -80 ^{o}C after dialysis against 1xPBS.

2.21 Stromal processing peptidase assays

Stromal extracts were prepared from isolated chloroplasts of *A. thaliana* mesophyll protoplasts essentially as described in section 2.10. The acetone-precipitated proteins were resuspended in 20 mM HEPES-KOH (pH 7.5). Ten nanograms of purified recombinant EGFP-BsToc159$_{(1340\text{-}1395)}$ or EGFP-BsToc132$_{(1188\text{-}1239)}$ were incubated with or without 10 µg of stromal proteins in 20 mM HEPES-KOH (pH 7.5) at 28 ^{o}C for 1.5 h. The reaction was stopped by boiling the samples with 0.2 volume of 6x SDS sample buffer, prior to Western blot analysis with EGFP antibody.

2.22 Cytoskeleton drug treatment of isolated protoplasts

A population of healthy chlorenchyma protoplasts was isolated from mature *B. sinuspersici* leaves as described above (see section 2.3). Stock solutions of 2 mM cytochalasin B (Serva, Heidelberg, Germany) or oryzalin (Crescent Chemical Co., Islandia, NY, USA) were prepared in 100% (v/v) dimethyl sulfoxide. Approximately 5 x 10^4 protoplasts were cultured in 100 µL of CS-sucrose buffer supplemented with 50 µM cytochalasin B or oryzalin at room temperature overnight in the dark. A negative control was set up with 2.5 µL of 100% (v/v) dimethyl sulfoxide. After centrifugation at 100*g* for 2 min, the floating layer of healthy protoplasts were resuspended in 100 µL of fractionation buffer containing 50 mM HEPES-KOH (pH 8), 0.8 M sorbitol, 1 mM $CaCl_2$ and 1% (v/v) protease inhibitor cocktail (Sigma-Aldrich, Oakville, ON, Canada, cat. no. P9599). The following steps were performed at 0~4 ^{o}C. Crude cell lysates were obtained using the protoplast-rupturing device as described above (see section 2.9), and subfractionated by differential speed centrifugation sequentially at 1,000*g* for 5 min, 5,000*g* for 10 min, and 20,000*g* for 15 min. The 1,000*g* and 5,000*g* supernatants were transferred into a fresh microfuge tube for further centrifugation, and the 20,000*g* supernatant was subjected to Western blot analysis. The pellet from each step was resuspended in original volume of fractionation buffer prior to Western blot analysis.

2.23 Co-immunoprecipitation assays

The following procedures were performed at room temperature, unless otherwise specified. Twenty microliters of Protein-G-sepharose slurry (Sigma-Aldrich, Oakville, ON, Canada; cat. no. P3296) were first packed into a spin chromatography column (Bio-Rad, Mississauga, ON, Canada), which facilitated the subsequent washing steps by centrifugation at 3,000*g* for 30 s.

The resin was washed with 200 µL of 1xPBS thrice and incubated with 5 µL of mouse anti-actin (MP Biomedicals, Solon, OH, USA) or 20 µL of mouse anti-β-tubulin (Sigma-Aldrich, Oakville, ON, Canada; cat. no. T4026) antibodies in 1xPBS for 30 min on a rotary shaker. A negative control was set up with 50 µL of 1xPBS only. To minimize the co-elution of the antibodies in the final steps, the immobilized antibodies were crosslinked to the protein-G-sepharose. Briefly, the resin was washed thrice with 500 µL of crosslinking buffer containing 0.2 M triethanolamine (pH 9) and 0.1 M sodium borate, and incubated with 500 µL of 20 mM dimethyl pimelimidate (Sigma-Aldrich, Oakville, ON, Canada) in 1xPBS for 45 min. The uncoupled sites were then blocked by incubation with 200 µL of blocking buffer containing 50 mM ethanolamine-HCl (pH 9) for 5 min and two changes of blocking buffer. The uncoupled antibodies were removed by incubation with 500 µL of elution buffer containing 100 mM glycine-HCl (pH 2.4) and 150 mM NaCl and two washes with 500 µL of 1xPBS.

Chlorenchyma cells were collected from approximately 0.5 g of mature *B. sinuspersici* leaves on a piece of 40-µm nylon mesh as described above (see section 2.3). The cells were ground using a mortar and pestle on ice in 1 mL of extraction buffer containing 1xPBS, 1% (w/v) n-dodecyl maltoside and 1% (v/v) protease inhibitor cocktail (Sigma-Aldrich, Oakville, ON, Canada, cat. no. P9599). The crude cell extract was clarified by centrifugation at 3,000*g*, 4 ^{o}C for 10 min. The antibody-coupled Protein-G-sepharose resin was first washed with 500 µL of extraction buffer, and incubated with 250 µL of solubilized crude extract (~1.5 mg total proteins mL^{-1}) for 30 min on a rotary shaker. The resin was washed five times with 150 µL of extraction buffer and the adsorbed proteins were eluted with three 15-µL changes of

elution buffer. The pooled eluents were immediately neutralized with 10 μL of 1 M Tris-HCl (pH 8) and boiled with 0.2 volume of 6x SDS sample buffer for SDS-PAGE and Western blot analysis.

2.24 Immunogold electron microscopy

Mature leaves of *B. sinuspersici* were sectioned in strips and vacuum-infiltrated using a desiccator at room temperature for 1 h in a fixative solution containing 50 mM PIPES-KOH (pH 7.2), 300 mM sorbitol, 2% (v/v) paraformaldehyde (Electron Microscopy Sciences, Burlington, ON, Canada) and 1.25% (v/v) glutaraldehyde (Electron Microscopy Sciences, Burlington, ON, Canada). After incubation at 4 ^{o}C for 16 h, the fixed specimens were washed for 15 min thrice in 50 mM PIPES-KOH (pH 7.2) and dehydrated with a graded ethanol series (i.e. 30%, 50%, 60%, 70%, 80%, 2x95% and 2x100%) for 15 min each. The dehydrated specimens were incubated with mixtures of London Resin (LR) White acrylic resin (Electron Microscopy Sciences, Burlington, ON, Canada) and 100% ethanol (1:3, 1:2, 1:1, 2:1, 3:1) for >12 h each, followed by infiltration in two changes of pure LR White (12~24 h each). The samples were finally placed in gelatine capsules (Canemco-Marivac, Lakefield, QC, Canada) filled with fresh LR white and polymerized at 65 ^{o}C overnight.

Ultra-thin (i.e. 60~80 nm) sections were made on an ultramicrotome equipped with a glass knife. The sections were mounted on 150-mesh nickel grids and blocked in TBST-BSA solution containing 25 mM Tris-HCl (pH 7.4), 137 mM NaCl, 2.7 mM KCl, 0.1% (v/v) Tween-20 and 1% (w/v) BSA at room temperature for 1 h. The sections were incubated with anti-BsToc159 (1:150), anti-BsToc132 (1:20) or anti-Toc34 (1:150) antibodies diluted in

TBST-BSA at 4 ^{o}C for 16 h. Negative controls were set up with no primary antibody. The sections were washed for 15 min thrice in TBST-BSA, and incubated with secondary anti-rabbit antibodies conjugated to 10-nm gold particles (1:100; Sigma-Aldrich, Oakville, ON, Canada) diluted in TBST-BSA at room temperature for 1 h. The sections were washed for 15 min thrice in TBST-BSA, stained in uranyl acetate saturated in 50% (v/v) ethanol for 10~15 s, and washed in a stream of 50% (v/v) ethanol. The sections were further stained with 0.4% (w/v) lead citrate in 0.1 N NaOH for ~10 s, and washed in a stream of degassed distilled water. The air-dried sections were observed under a transmission electron microscope (Philips CM-10) operated at 60 kV. All images were further processed and composed using Adobe Photoshop CS (Adobe Systems Inc., Seattle, WA, USA). Representative images were presented after similar results were obtained from at least three independent experiments. The relative abundance of gold particles representing envelope-associated and cytosolic signals in chlorenchyma cells was manually determined in 1.5 x 2 μm^2 areas of multiple electron micrographs from three individual blocks of specimens at a magnification of 64,000x.

2.25 Light and epifluorescence microscopy

Fifty microliters of stained or transfected protoplasts were examined in flat-bottomed depression slides using a Zeiss Axiophot microscope (Carl Zeiss Inc., Germany). Fluorescein diacetate and EGFP signals were detected using a 365-nm filter under UV illumination. Epifluorescence and bright field micrographs were acquired using a Q-Imaging digital camera (Quorum Technologies Inc., Guelph, ON, Canada). All images were processed and composed using Adobe Photoshop CS (Adobe Systems Inc., Seattle, WA, USA).

Representative images were presented after similar results were obtained from at least 3 independent experiments.

2.26 Confocal laser scanning microscopy

Approximately 100 µL of live protoplasts were imaged on 8-chamber Lab-Tek II chambered cover glass slides (Nalgene Nunc, Denmark) using an Olympus FV1000 confocal laser scanning microscope. Serial Z-stack images were acquired at 1-µm intervals using a 40X objective lens at a digital resolution of 1,024 x 1,024. The confocal excitation wavelength for chlorophyll autofluorescence was 649 nm and the emitted wavelength captured for the images was 666 nm. The fluorescence of DAPI and Fluorescent Brightener 28 were excited at 350 nm and the emission was detected at 470 nm. The fluorescence of EGFP, fluorescein diacetate, and rhodamine 123 was excited at 488 nm and the emission detected at a band path 495–540 nm. All images were further processed and composed using Adobe Photoshop CS (Adobe Systems Inc., Seattle, WA, USA). All experiments were repeated at least three times independently with similar results.

2.27 Phylogenetic analysis

The amino acid sequences of Toc159 and Toc 34 homologues were retrieved using BLASTp search. The deduced amino acid sequences were aligned using the ClustalW algorithm and the phylogenetic tree was constructed by the neighbor-joining method using the MEGA v5.05 program (Tamura et al., 2011). The reliability for internal branch was assessed using the bootstrapping method (2,000 bootstrap replicates).

Chapter 3. Establishing a protoplast isolation and transient gene expression method in *Bienertia sinuspersici*

3.1 Overview

Although transient gene expression using reporters such as green fluorescent protein is a versatile tool for examining gene functions and intracellular protein trafficking, the establishment of a highly efficient gene manipulation method remains a challenge in many plant species. A reliable transformation protocol has not yet been established for the three single-cell C_4 species, despite their potential of serving as model systems for their extraordinary C_4 photosynthetic metabolism. In this chapter, I report the first protocol optimized for isolating a large-scale and homogenous population of protoplasts from chlorenchyma cells of the single-cell C_4 species *Bienertia sinuspersici*. Cytochemical staining confirmed the preservation of the unusual subcellular compartmentation of organelles in chlorenchyma cells after cell wall digestion. The viability of isolated protoplasts was further confirmed by high efficiency of polyethylene glycol-mediated transfection for transient expression of reporter fluorescent proteins. Fluorescent fusion proteins tagged with various intracellular sorting signals demonstrated potential use of the transient gene expression system in subcellular protein localization and organelle dynamics studies. Further applications of the current protoplast isolation and transfection techniques in understanding the novel single-cell C_4 photosynthetic mechanism are discussed.

Remark: A version of this chapter has been published in: **Lung SC, Yanagisawa M, Chuong SDX** (2011) Protoplast isolation and transient gene expression in the single-cell C_4 species, *Bienertia sinuspersici*. Plant Cell Rep **30**: 473-484.

3.2 Introduction

Leaves of C_4 plant species generally consist of two anatomically and biochemically distinct photosynthetic cell types, mesophyll and bundle sheath, commonly known as Kranz anatomy. This dual-cell type system is considered an evolutionary adaptation because both cells function cooperatively to concentrate CO_2 at the site of ribulose 1,5-bisphosphate carboxylase/oxygenase (Rubisco), thereby reducing photorespiration (Hatch and Slack, 1970; Edwards and Huber, 1981). In C_4 photosynthesis, atmospheric CO_2 is initially converted into C_4 acids in the mesophyll cells by phosphoenolpyruvate carboxylase (PEPC), followed by the transport of C_4 acids to the bundle sheath cells with donation of CO_2 by C_4 acid decarboxylases (NAD-ME, NADP-ME or PEP-CK) to Rubisco for fixation via the Calvin cycle. The compartmentation of two different sets of biochemical reactions in two cell types allows C_4 plants to perform better than C_3 plants under CO_2 limiting conditions, as a result of higher rates of photosynthesis, and greater nitrogen and water use efficiency (Hatch, 1971; Edwards and Huber, 1981; Sage, 2001). The Kranz anatomy had been regarded as an indispensable feature of all terrestrial C_4 plant species until the discovery of three single-cell C_4 species in the Chenopodiaceae family, *Suaeda aralocaspica* (Voznesenskaya et al., 2001), *Bienertia cycloptera* (Voznesenskaya et al., 2002), and *B. sinuspersici* (Akhani et al., 2005; Voznesenskaya et al., 2005). These three chenopod species perform C_4 photosynthesis within individual chlorenchyma cells by partitioning chloroplasts and key photosynthetic enzymes in two intracellular cytoplasmic compartments, analogous to the mesophyll and bundle sheath cells in Kranz-type C_4 species, respectively. The discovery of the single-cell C_4 species thereby challenged the dual cell requirement for the operation of terrestrial C_4 photosynthesis (Edwards et al., 2004).

Despite some morphological and genetic differences between *B. sinuspersici* and *B. cycloptera*, the single-cell C_4 mechanisms of these two species are essentially similar (Voznesenskaya et al., 2002; Akhani et al., 2005; Voznesenskaya et al., 2005). In mature Bienertia leaves, the cytoplasm of each chlorenchyma cell is subdivided into the central cytoplasmic compartment (CCC) and the peripheral cytoplasmic compartment (PCC). The CCC forms a distinctive spherical structure in the centre of the cell tightly packed with chloroplasts and mitochondria, whereas the PCC comprises a thin layer of cytoplasm containing scattered chloroplasts and peroxisomes (Voznesenskaya et al., 2002). The two cytoplasmic compartments are spatially separated by a single central vacuole (Park et al., 2009), which is traversed by cytoplasmic channels (Voznesenskaya et al., 2005). Ultrastructural studies of chloroplasts of the CCC and PCC and immunolocalization of the key photosynthetic enzymes in the two cytoplasmic compartments have provided evidence for a novel single-cell C_4 photosynthetic model (Voznesenskaya et al., 2002 and 2005; Chuong et al., 2006). Given the extraordinary subcellular organization of Bienertia chlorenchyma cells, effort aimed at understanding the development and maintenance of the subcellular organelle compartmentation typically involves employing limited cell and molecular techniques (Chuong et al., 2006; Park et al., 2009). A study using real-time quantitative PCR and immunoblotting techniques to examine gene and protein expression in different stages of leaf development of *B. sinuspersici* has recently been documented (Lara et al., 2008). Further understanding of this novel photosynthetic model, however, has been precluded by the lack of technology available for manipulating gene expression in the single-cell C_4 species.

More recently, protoplast transfection has become one of the most reliable plant transformation methods for characterizing gene functions systematically (Sheen, 2001). Since the first reported success in protoplast preparation from tomato root tips (Cocking, 1960), protoplasts have been isolated from diverse tissues and different species. Despite the initial use of Ti plasmid from *Agrobacterium tumefaciens* for genetic engineering of plant protoplasts (Krens et al., 1982), Paszkowski et al. (1984) demonstrated stable gene integration into the genome of *Nicotiana tabacum* protoplasts using minimal *E. coli*-based cloning vectors independent of T-DNA borders. This finding has been considered as a significant contribution to achieving the high efficiency of plant protoplast transfection technologies (Davey et al., 2005). While earlier works have focused on the regeneration of stably transfected protoplasts to establish transgenic plants, protoplast-based transient assays are becoming more popular in plant research because they allow data collection in a much shorter period of time. For example, using the enhanced green fluorescent protein (EGFP) as a reporter, transient gene expression and intracellular protein trafficking can be monitored qualitatively and quantitatively in a nondestructive manner within hours post-transfection (Chen et al., 2006; Yoo et al., 2007). To date, plant protoplasts have been successfully transfected by microinjection (Neuhaus and Spangenberg, 1990), polyethylene glycol (PEG) treatment (Krens et al., 1982), and electroporation (Fromm et al., 1985). The latter two are amongst the more popular methods of choice, although their transfection efficiencies can vary substantially between different cell types and species and thus transfection conditions have to be optimized empirically.

In this chapter, I report the establishment of an efficient transient assay using leaf-derived protoplasts of *B. sinuspersici*, a model single-cell C_4 terrestrial plant. Procedures have been optimized for isolating a large number of viable protoplasts from healthy leaves with the integrity of the individual cytoplasmic compartments remaining intact. The healthiness of the isolated protoplasts was demonstrated by transient expression of the green fluorescent protein (GFP) reporter gene with over 80% transfection efficiency, which was comparable to those previously reported for rice and *Arabidopsis* (Chen et al., 2006; Yoo et al., 2007). The transient gene expression assays have been further extended to express various GFP fusion proteins that were selectively targeted to specific organelles of each subcellular compartment. Overall, the successful isolation of chlorenchyma protoplasts from *B. sinuspersici* can be applied to analyze the complex regulatory mechanisms governing the development of the single-cell C_4 system.

3.3 Results

3.3.1 Isolation of chlorenchyma cells

Isolation of transfection-competent protoplasts for transient gene expression requires a good source of healthy plant materials. I found that propagation of *B. sinuspersici* by vegetative cuttings under controlled environments is a reliable method to supply healthy starting materials for protoplast isolation (Figure 3.1A). A substantial amount of bushy branches were generated in a relatively short period of time when using vegetative propagation, allowing for a large-scale preparation of a homogenous population of protoplasts to meet specific experimental needs such as subcellular fractionation of organelles. Following the current protoplast isolation procedures, any batch-to-batch variation in protoplast yields might be attributed to the health of the starting leaf materials. Healthy leaves from 3- to 4-month-old plants that are ideal for protoplast isolation should appear turgid, dark olive green in color (Figure 3.1B) and covered with salt glands (Figure 3.1B inset). As a first step, I obtained chlorenchyma cells by gently squeezing the leaves with a mortar and pestle. The released chlorenchyma cells appeared homogenous without contamination from other tissues such as epidermis, water storage or vascular tissues (Figure 3.1C). The breakage of water storage cells increased the cell suspension volume substantially and thus I concentrated the isolated chlorenchyma cells on a piece of 40 μm of nylon mesh filter prior to cellulase treatment.

3.3.2 Enzymatic preparation of chlorenchyma protoplasts

I empirically optimized the components of the cell-stabilizing (CS) solution, which were

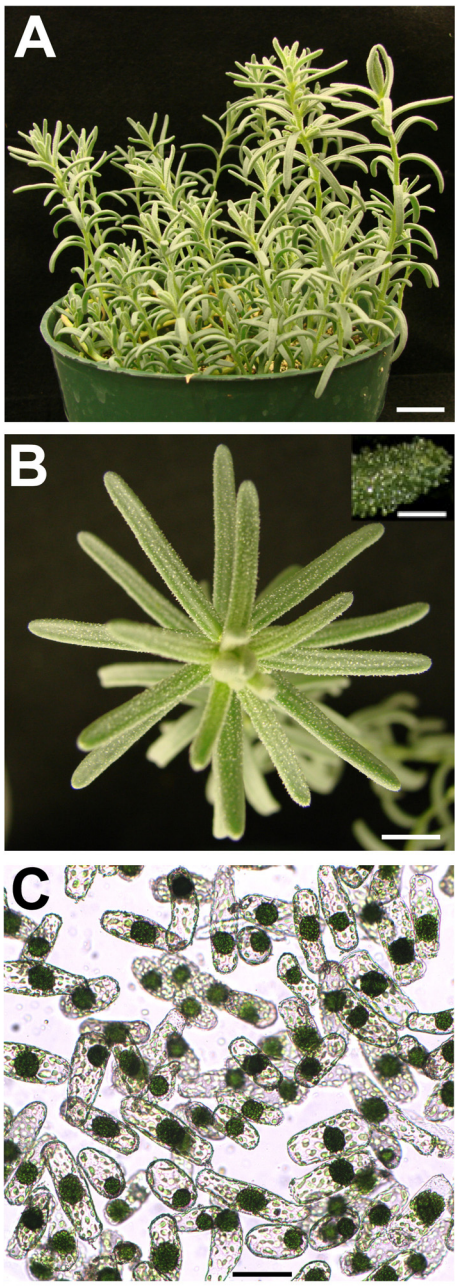

Figure 3.1 Preparation of chlorenchyma cells from *B. sinuspersici*

(A) Four-month-old *B. sinuspersici* plant was used for protoplast isolation. Scale bar = 20 mm.

(B) A healthy branch of *B. sinuspersici* plant contained turgid leaves with fuzzy salt glands suitable for protoplast isolation. The inset shows a close-up image of a leaf covered with salt glands. Scale bars = 5 mm or 0.1 mm (inset).

(C) A bright field image of chlorenchyma cells isolated from mature leaves. Scale bar = 50 µm.

found to be crucial for maintaining the integrity of the two cytoplasmic compartments and the distribution of their respective organelles in the resulting protoplasts. The best protoplast yield was obtained in weakly acidic pHs (Figure 3.2A). Although cellulase digestion of the cell wall was most active at pH 5.5, a significantly higher number of cells were broken at this pH resulting in a lower protoplast yield (Figure 3.2A). The acidic pH optimum of cellulase accounted for the absence of protoplasts when cell wall digestion was carried out at pH 7.5 (Figure 3.2A). At neutral pH, a high proportion of protoplasts had their CCC chloroplasts dispersed intracellularly whereas the undigested chlorenchyma cells appeared normal, suggesting that the weakly acidic pH might help to maintain the integrity of protoplasts when the cells were more or less stressed during cell wall removal. In addition to a suitable buffer, an osmoticum is commonly included in a protoplast isolation mixture for cell plasmolysis facilitating wall digestion and for counteracting the turgor pressure of cells as an osmotic pressure stabilizer. Accordingly, I investigated the effects of various concentrations of D-sorbitol, D-mannitol, D-glucose and sucrose on protoplast yields (Figure 3.2B). The integrity of cytoplasmic compartments and cell viability were best maintained in 0.7 M sucrose resulting in the highest yield of $1.8 \pm 0.2 \times 10^5$ protoplasts g^{-1} fresh weight (Figure 3.2B). Another technical advantage of isolating protoplasts in sucrose solution is that low-speed centrifugation of the sample in this medium enables the isolation of intact protoplasts on the floating layer from the broken protoplasts and cell debris in the pellet (Figure 3.3A). This differential separation also facilitates easy manipulation of subsequent procedures such as cytochemical staining of subcellular organelles and transfection for transient gene expression. In a higher concentration (i.e., 1 M) of sucrose, however, protoplasts appeared stressed as revealed by occasional clumping of PCC chloroplasts (Figure 3.3B). The 100*g* pellets in D-

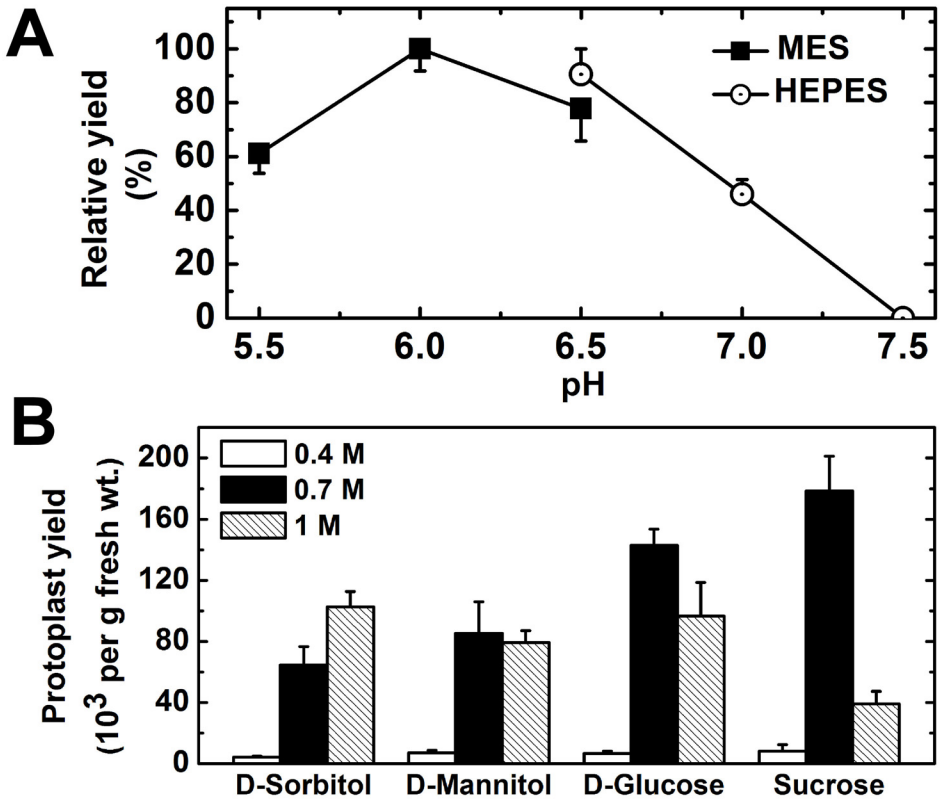

Figure 3.2 Optimization of pH and osmoticum for isolation of chlorenchyma protoplasts from *B. sinuspersici*

Chlorenchyma cells were digested with 1.5% (w/v) cellulase Onozuka R10 in cell-stabilizing buffer at room temperature in the dark for 4 h. Protoplast yields were determined using a haemocytometer and shown as the mean of three replicates (±SE).

(A) Protoplasts were isolated in a cell-stabilizing buffer containing 0.7 M sucrose and 25 mM MES or HEPES buffer at different pHs.

(B) Protoplasts were isolated in a cell-stabilizing buffer containing 25 mM HEPES-KOH (pH 6.5) and various concentrations of D-sorbitol, D-mannitol, D-glucose or sucrose.

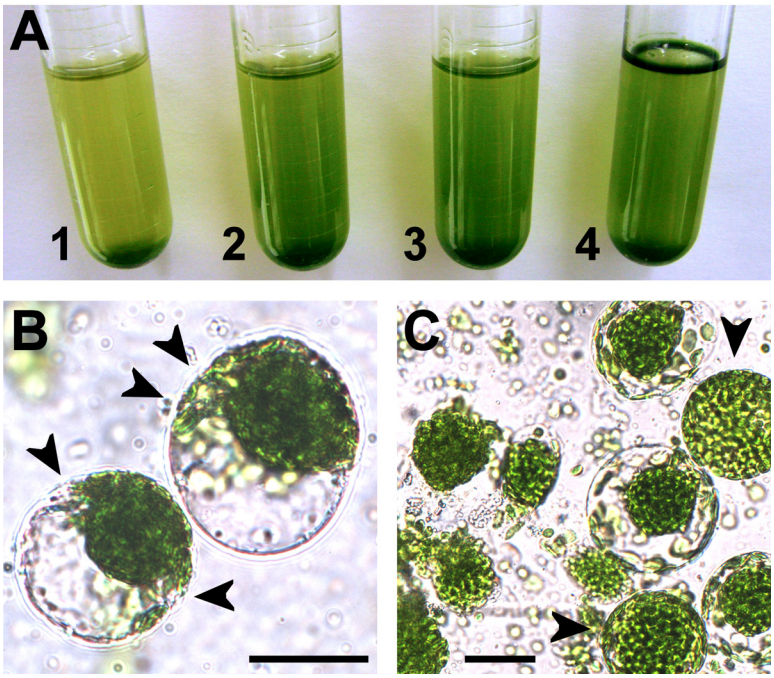

Figure 3.3 Isolation of chlorenchyma protoplasts from *B. sinuspersici* in different osmotica

(A) Protoplasts isolated in 0.7 M D-sorbitol (1), D-mannitol (2), D-glucose (3) or sucrose (4) were harvested as pellets (1-3) or a floating layer (4) by centrifugation at 100*g* for 2 min.

(B) A bright field image of protoplasts in 1 M sucrose. Arrowheads indicate clumping of chloroplasts in peripheral cytoplasmic compartments. Scale bar = 20 µm.

(C) A bright field image of pelleted protoplasts in 0.7 M D-mannitol. Arrowheads indicate protoplasts with dispersed central cytoplasmic compartment chloroplasts. Scale bar = 20 µm.

sorbitol, D-mannitol and D-glucose contained a mixture of intact and broken protoplasts as well as cell debris (Figure 3.3C). A large proportion of protoplasts isolated in D-sorbitol and D-mannitol had pronounced dispersal of CCC chloroplasts (Figure 3.3C).

Interestingly, during our preparation of transfection-competent protoplasts, I found that approximately 1–2% of the protoplasts appeared fused after 30-min incubation in the W5 salt solution on ice (Figure 3.4). In plants, protoplast fusion is relatively inefficient and often results from the use of inducing agents such as PEG and a pulse of electric field (Orczyk et al., 2003). This spontaneous fusion of protoplasts might be attributed to the overcrowding condition when the protoplasts settled to the bottom by gravity during the incubation. Fused protoplasts were easily distinguished by their increase in cell volumes and the presence of two CCCs within the same cell (Figure 3.4).

3.3.3 Intactness of isolated protoplasts

A homogenous population of round-shaped, intact protoplasts was obtained after 4-h cell wall digestion in 0.7 M sucrose buffer solution (Figure 3.5A). Over 90% of the isolated protoplasts remained viable as indicated by fluorescein diacetate staining (Figure 3.5B), which is routinely used to assess plant protoplast viability (Larkin, 1976). To further characterize the health of protoplasts and assess the integrity of the organelle distribution, I stained the cells with various cytochemical stains (Figure 3.6). Chlorophyll autofluorescence indicated no observable distortion of chloroplast distribution in protoplasts in comparison with untreated chlorenchyma cells; the CCC chloroplasts remained strictly confined to the central region of the cell whereas PCC chloroplasts were randomly scattered in the periphery

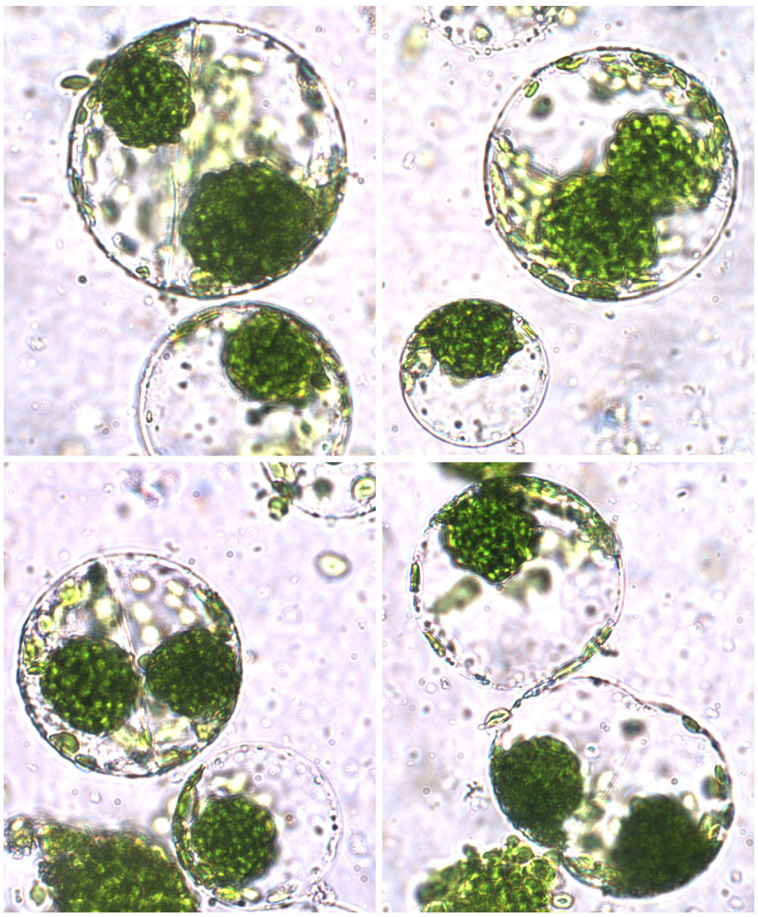

Figure 3.4 Occurrence of fused protoplasts during the preparation of transfection-competent protoplasts

Bright field images of protoplasts after incubation in W5 solution on ice for 30 min. Fused protoplasts are recognized by the presence of two central cytoplasmic compartments in the same cells. Scale bar = 20 µm.

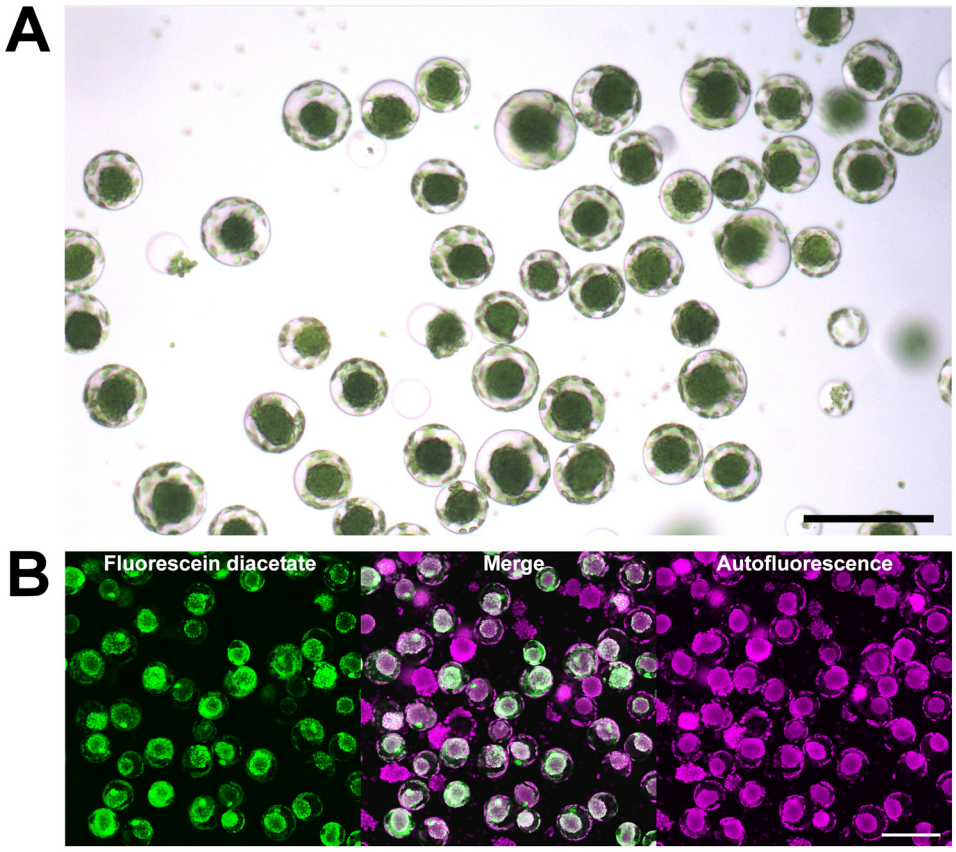

Figure 3.5 Viability of *B. sinuspersici* chlorenchyma protoplasts

(A) A bright field image of protoplasts which were isolated from chlorenchyma cells under 1.5% (w/v) cellulase Onozuka R10 treatment at room temperature in the dark for 4 h in cell-stabilizing buffer containing 0.7 M sucrose and 25 mM HEPES-KOH (pH 6.5). Scale bar = 50 µm.

(B) Isolated protoplasts were stained with the vital stain fluorescein diacetate and imaged under epifluorescence microscopy. Fluorescein diacetate staining (left panel), chlorophyll autofluorescence (middle panel) and a merge image (right panel) are shown. Scale bar = 50 µm.

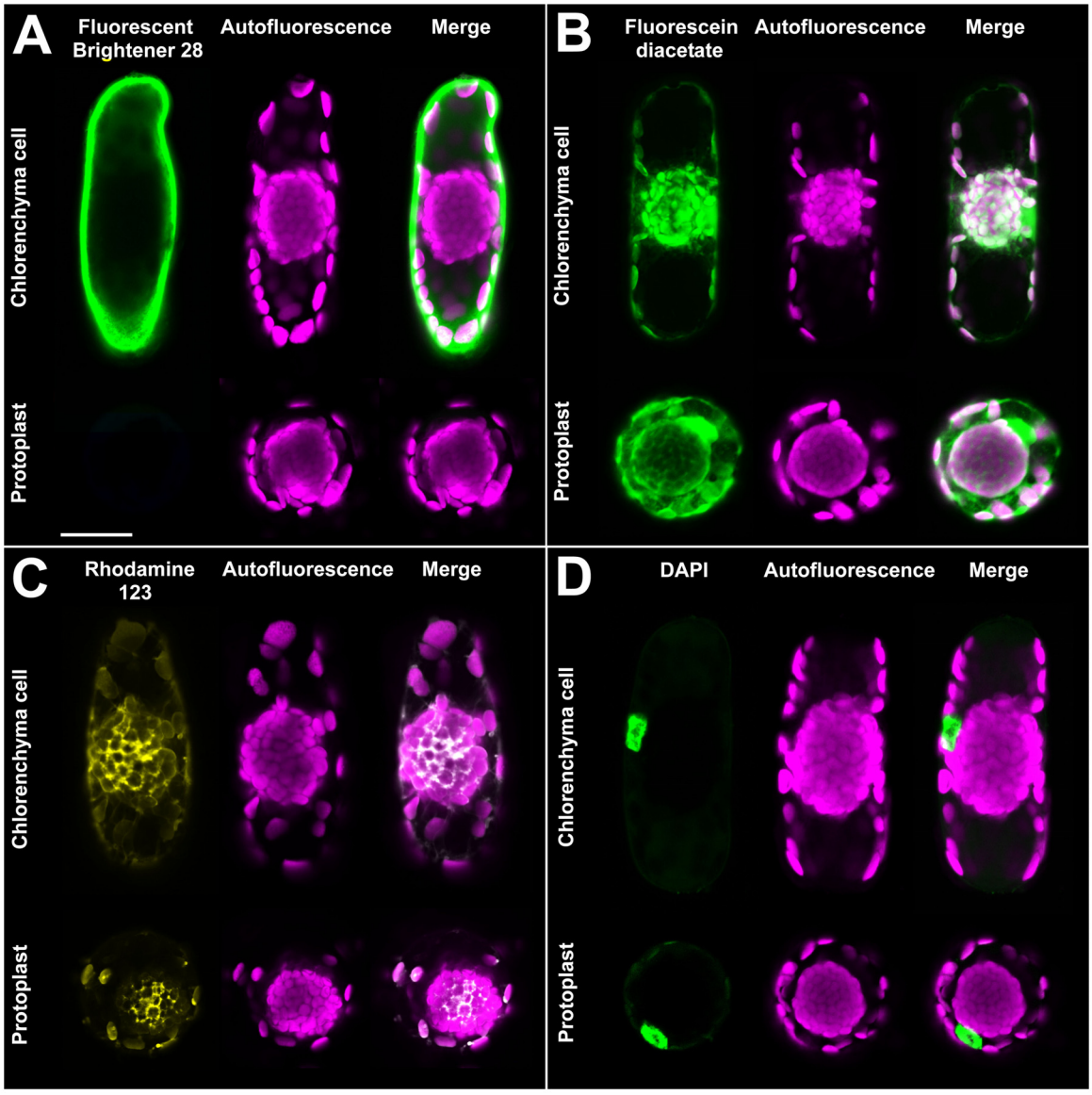

Figure 3.6

Figure legend on the next page

Figure 3.6 Fluorescence staining of subcellular organelles in chlorenchyma cells and protoplasts of *B. sinuspersici*

Isolated chlorenchyma cells and protoplasts were stained with different cytochemical stains and imaged under confocal laser scanning microscopy. Each image shows a representative result from at least three independent experiments. Fluorescence of cytochemical stains (left panels), chlorophyll autofluorescence (middle panels) and merged images (right panels) are shown. Chlorophyll autofluorescence was excited at 649 nm and emission was detected at 666 nm. Scale bar = 20 μm.

(A) Fluorescent brightener 28 stains cell wall. The fluorescence was excited at 350 nm and the emission was detected at 470 nm.
(B) Fluorescein diacetate stains cytoplasmic channels and diffuses into chloroplasts and nuclei in living cells. The fluorescence was excited at 490 nm and the emission was detected at 525 nm.
(C) Rhodamine 123 stains mitochondria in living cells. The fluorescence was excited at 511 nm and the emission was detected at 534 nm.
(D) DAPI dilactate primarily stains nucleic acids in nuclei. The fluorescence was excited at 350 nm and the emission was detected at 470 nm.

(Figure 3.6). Staining with Fluorescent Brightener 28, a cellulose-specific fluorescence dye, confirmed complete removal of the cell wall from protoplasts by 4-h cellulase treatment (Figure 3.6A). Transvacuolar cytoplasmic channels interconnecting PCC and CCC were preserved in protoplasts as indicated by staining with fluorescein diacetate, although strong fluorescence signals were also visualized in chloroplasts and nuclei due to intracellular diffusion (Figure 3.6B). Rhodamine 123 staining of both protoplasts and untreated chlorenchyma cells indicated that mitochondria were mainly concentrated in the central core of CCC and sparsely associated with PCC chloroplasts (Figure 3.6C), in agreement with earlier observations (Chuong et al., 2006). Nuclei in protoplasts remained specifically located between the CCC and PCC as visualized with the nucleic acid-binding dye 4',6-diamidino-2-phenylindole (DAPI) dilactate (Figure 3.6D).

3.3.4 Protoplast transfection

I initially attempted to transfect *B. sinuspersici* chlorenchyma protoplasts by electroporation. The various electroporation conditions tested (e.g. electroporation media, pulse parameters and durations) resulted in significant dispersal of CCC chloroplasts and protoplast lysis. In contrast, I found that the chemical method of transfection using PEG was more favorable for maintaining protoplast viability, as indicated by the maintenance of the complex subcellular organization and expression of the EGFP reporter gene. Typically, the PEG-mediated transfection of a 4.6-kb EGFP reporter gene construct, driven by the constitutive 35S promoter, resulted in over 80% of protoplasts producing the fluorescent signals when using the PEG method (Appendix II). It is, however, worthy of note that the transfection efficiency varies with a number of factors. For instance, lower transfection efficiency (e.g.

approximately 50%) might be anticipated with larger expression constructs such as an 8.8-kb plasmid encoding EGFP fusion with the full-length Toc159 protein (see Chapter 5). Apparently, the transfection efficiencies also varied with the duration of post-transfection incubation depending on the culture conditions. Yanagisawa (2012) showed that a maximum number of protoplasts expressing EGFP alone was achieved after 12-h incubation under low light intensity (30 μmol m^{-2} s^{-1}), whereas less than half of the protoplasts expressed the reporter gene after 12-h incubation in the dark, and a prolonged 18-h incubation was required to achieve the maximum transfection efficiency of over 80%.

To further investigate whether the isolated protoplasts could be transfected using metabolically more inert osmotica, the sucrose in the original recipe of transfection buffer was replaced with D-sorbitol or D-mannitol (Appendix II-C). It was found that the transfection efficiencies with the different tested osmotica varied insignificantly from 76.6% to 84.4% (Appendix II-C).

3.3.5 Transient expression of various EGFP fusion proteins

To demonstrate that the current protoplast-based transient expression system is a useful tool for studying subcellular localization of proteins, we produced various EGFP fusion constructs that targeted the fluorescence signals to different subcellular organelles (Appendix III). In the absence of targeting signal, EGFP protein resided mainly in the cytoplasm and diffused passively into the nuclei (Appendix III-A). A nuclear targeting signal (NLS) at the N-terminus, on the other hand, targeted the reporter protein exclusively to the nuclei (Appendix III-B). An extensive network of actin filaments was visualized throughout the

cytoplasm by probing with an EGFP fusion protein with talin (Appendix III-C), an actin-binding protein (Kost et al., 1998). Similarly, EGFP fusion with MAP4, a microtubule-associated protein (Marc et al., 1998), localized fluorescence signals to the microtubule network in the transfected protoplasts (Appendix III-D). Inclusion of the Ser-Lys-Leu (SKL) tripeptide, a PTS (Gould et al., 1989), at the C-terminal tail of EGFP resulted in distinctive fluorescence-labelled peroxisomes, which were found more abundant in the CCC than the PCC (Appendix III-E). The mitochondrial targeting signal of NAD-ME targeted the reporter protein exclusively to the mitochondria in CCC (Appendix III-F), whereas the transit peptide (TP) of Rubisco small-subunit (RbcS) guided the EGFP protein to the stroma of both CCC and PCC chloroplasts with similar efficiencies (Appendix III-G).

For a thorough evaluation of the plastid protein import efficiency in the isolated *B. sinuspersici* protoplasts, I produced additional EGFP fusion constructs expressing TPs of various chloroplast proteins including ferredoxin, photosynthetic and non-photosynthetic isoforms of ferredoxin:$NADP^+$ oxidoreductase (FNR), pyruvate orthophosphate dikinase (PPDK) and malate dehydrogenase (MDH). The constructs were designed based on the cDNA sequences identified from *B. sinuspersici* and TP lengths predicted using the ChloroP prediction program v1.1 (Emanuelsson et al., 1999; http://www.cbs.dtu.dk/services/ChloroP). In onion epidermal cells, transient expression of EGFP fusion with any of the tested TPs produced similar fluorescent signals in etioplasts and stromules (Figure 3.7, lower panels). In transfected *B. sinuspersici* protoplasts, on the other hand, the chloroplast-targeting efficiencies varied considerably with the TPs used (Figure 3.7, upper panels). Similar to the RbcS-TP (Appendix III-G), the TPs of both FNR isoforms directed EGFP efficiently to the

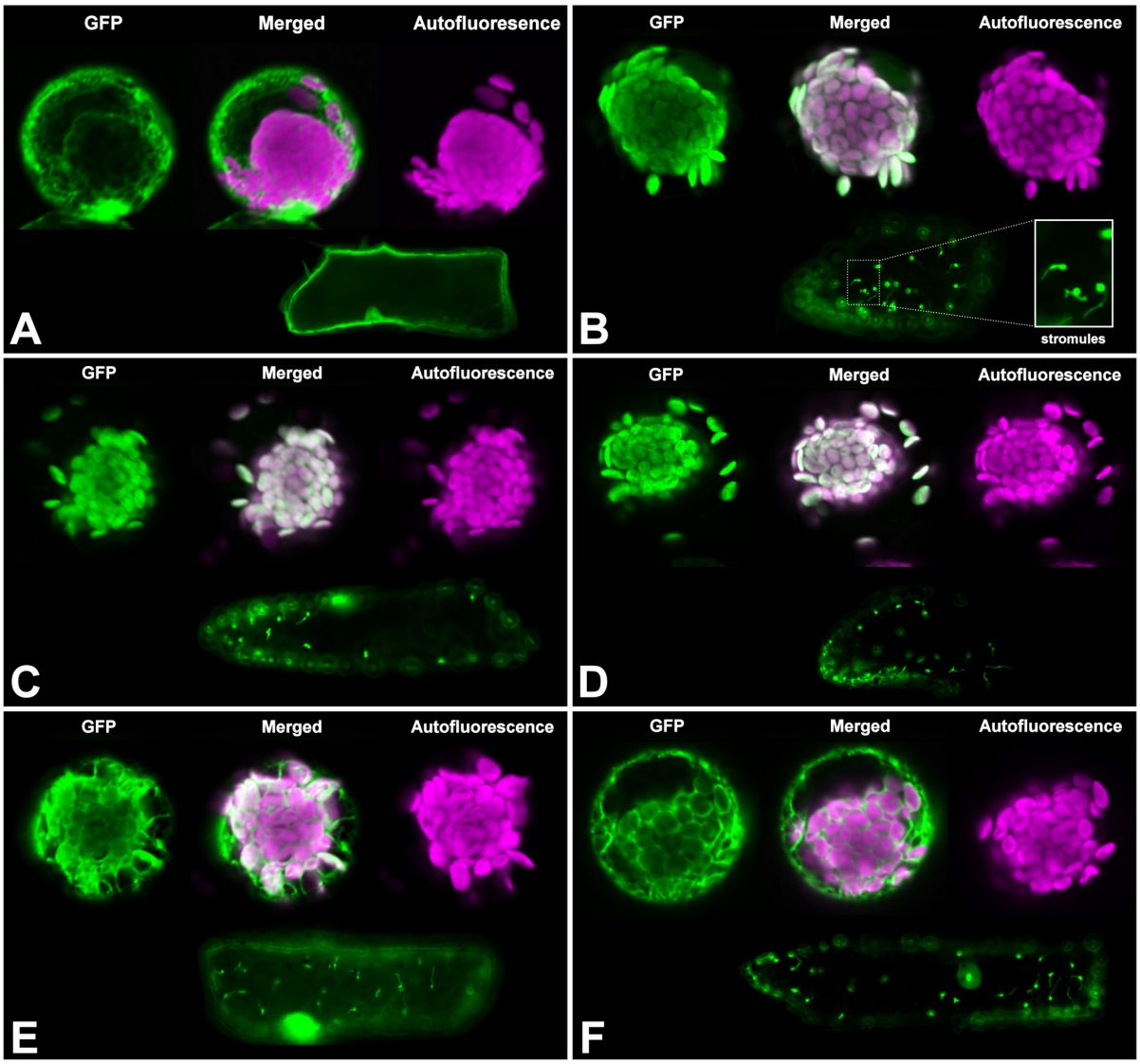

Figure 3.7

Figure legend on the next page

Figure 3.7 Transient expression of fluorescent protein fusion with chloroplastic transit peptides in chlorenchyma protoplasts of *B. sinuspersici* and onion epidermal cells

Isolated *B. sinuspersici* protoplasts and onion bulb epidermis were transfected with EGFP fusion constructs with a chloroplastic transit peptide at the N-terminus. Live protoplasts were visualized under confocal laser scanning microscopy and shown with EGFP fluorescence (upper left panels), chlorophyll autofluorescence (upper right panels) and merged images (upper middle panels). EGFP fluorescence in bombarded onion bulb epidermis was visualized under epifluorescence microscopy (lower panels). Images shown are representative results from at least three independent experiments.

(A) EGFP protein alone.
(B) EGFP fusion with the transit peptide of ferredoxin, i.e. tFd-EGFP. The inset shows a close-up image of stromules.
(C) EGFP fusion with the transit peptide of the photosynthetic isoform of ferredoxin: $NADP^+$ oxidoreductase, i.e. tFNR(P)-EGFP.
(D) EGFP fusion with the transit peptide of the non-photosynthetic isoform of ferredoxin: $NADP^+$ oxidoreductase, i.e. tFNR(H)-EGFP.
(E) EGFP fusion with the transit peptide of pyruvate orthophosphate dikinase, i.e. tPPDK-EGFP.
(F) EGFP fusion with the transit peptide of malate dehydrogenase, i.e. tMDH-EGFP.

both types of dimorphic chloroplasts (Figures 3.7C and 3.7D). Apparently, the targeting of EGFP to the two chloroplast types might be of slightly variable efficiencies when the TP of ferredoxin or PPDK was used, as evidenced by the weaker EGFP fluorescence in the central chloroplasts relative to their chlorophyll autofluorescence (Figures 3.7B and 3.7E). In the case of EGFP fusion with the TP of PPDK, the localization of fluorescent signal in peripheral chloroplasts was accompanied by a considerable amount of signal in the cytoplasm (Figure 3.7E). Similar cytoplasmic signals were more prominent with the TP of MDH, suggesting that EGFP was inefficiently targeted to the chloroplasts in isolated *B. sinuspersici* protoplasts (Figure 3.7F).

To confirm that our observation of fluorescent signals associated with the chloroplasts represents the targeting of EGFP into the stroma (Figure 3.7), I further investigated if the TPs were cleaved from the fusion proteins by Western blot analysis (Figure 3.8). The presence of both precursor proteins (~34 kDa) and EGFP proteins after maturation (~28 kDa) confirmed that the TPs indeed directed EGFP to the stroma of chloroplasts (Figure 3.8, lanes 1 and 3).

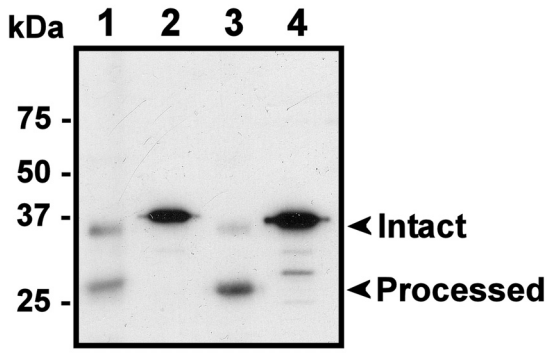

Figure 3.8 Western blot analysis demonstrating the import of EGFP protein into chloroplasts of tranfected protoplasts

Isolated *B. sinuspersici* protoplasts were transfected with EGFP construct which was either fused with the transit peptides of Rubisco small-subunit (lane 1) or ferredoxin (lane 3). The expected molecular masses for unprocessed and processed proteins of these fusion constructs are 34 and 28 kDa, respectively. Total protein extracts from transfected protoplasts were separated by SDS-PAGE, followed by immunoblotting with an anti-EGFP antibody. Purified recombinant fusion proteins of the aforementioned constructs, which contained a hexahistidine tag were used as controls (lanes 2 and 4). The hexahistidine tagged recombinant fusion constructs resulted in proteins of 37.5 (lane 2) and 37 (lane 4), respectively. Numbers to the left indicate the positions of protein standards, and the positions of unprocessed precursor proteins and processed (i.e. imported) proteins are indicated by arrowheads.

3.4 Discussion

3.4.1 The need for protoplast isolation and transfection

To date only fundamental anatomical and biochemical approaches have been used to examine the cellular mechanisms regulating organelle development and dynamics in chlorenchyma cells of the single-cell C_4 species, Bienertia (Voznesenskaya et al., 2005; Chuong et al., 2006; Lara et al., 2008; Park et al., 2009). Recently, biolistic bombardment of *B. sinuspersici* leaves was used to examine the role of cytoskeleton distribution in organelle partitioning by monitoring the expression of fluorescent fusion proteins (Chuong et al., 2006). Although biolistic transformation provided a sufficient number of transformed chlorenchyma cells for microscopic examination, further genetic manipulation using this method for other research purposes might not be feasible. To facilitate future work toward a better understanding of the single-cell C_4 mechanism, the present study was aimed at establishing a more efficient system for transient gene expression in *B. sinuspersici* chlorenchyma protoplasts. This protoplast-based transfection method permits high-throughput screening and quantitative assays when used in combination with an appropriate reporter protein such as EGFP. Since the transfection is performed in an isolated system, the genetically manipulated protoplasts are suitable for a diverse array of experimental goals, from gene function analyses and protein–protein interaction studies to examination of organelle dynamics and gene expression regulation in response to external stimuli.

3.4.2 Technical considerations for protoplast isolation

Due to the intricate nature of subcellular compartmentation and organelle distribution, the

isolation of *B. sinuspersici* chlorenchyma protoplasts requires the optimization of cell wall digestion conditions and CS buffer components by trial-and-error. Any unfavorable factors would cause significant cell lysis, dispersal of CCC chloroplasts and/or clumping of PCC chloroplasts. I started the protoplast isolation procedures by preparing chlorenchyma cells from fresh healthy mature leaves. Because the epidermis of any plant tissue protects the inner cells from enzyme digestion in typical protoplast isolation protocols, the source tissues are generally sliced into strips or the epidermis is peeled off mechanically or removed enzymatically (Davey et al., 2005). These steps are not only time-consuming but also yield-limiting if they are not carried out properly (Yoo et al., 2007). In *B. sinuspersici* leaves, however, the extensive intercellular spaces enable the loosely packed chlorenchyma cells to be readily released when the leaves are gently squeezed with a mortar and pestle. The released chlorenchyma cells appeared homogenous (Figure 3.1C), and thus protoplasts were subsequently obtained without using macerozyme (i.e. pectinase), which is routinely included in a protoplast digestion buffer to remove cell–cell adhesion (Davey et al., 2005). I obtained the best yield of $1.8 \pm 0.2 \times 10^5$ protoplast g^{-1} fresh weight when the isolated chlorenchyma cells were treated with cellulase under mildly acidic pHs (Figure 3.2A) and in the presence of 0.7 M sucrose (Figure 3.2B). This protoplast yield was apparently lower than that of mesophyll protoplasts from other species such as *Arabidopsis* with a reported yield of 10^7 protoplasts g^{-1} fresh weight (Yoo et al., 2007). This could be partially due to the presence of water storage cells in the succulent *B. sinuspersici* leaves, which make up the bulk of leaf fresh weight. The clumping of PCC chloroplasts in higher sucrose concentration suggested that the protoplasts were stressed by hyper-osmosis (Figure 3.3B). Recently, Yamada et al. (2009) have reported similar aggregation of chloroplasts in the C_4 finger millet mesophyll

cells, which might be induced by abscisic acid. Although sucrose serves as the best osmoticum in maintaining cell viability and the subcellular distribution of organelles in the two cytoplasmic compartments, successful protoplast isolation and transfection in D-sorbitol and D-mannitol (Figures 3.2B and Appendix II-C) demonstrated that these can be used as alternatives to the standard protocols if osmotically more inert osmoticum is preferred. For example, glucose and sucrose might hinder protoplast-based studies of photosynthetic gene promoters due to the potential metabolic repression of the gene transcription (Sheen, 1990). It is also well established that sucrose inhibits photosynthetic gene expression (Koch, 1996).

3.4.3 Proof of protoplast integrity and functionality

Subcellular staining with cytochemical probes (Figure 3.6) and transient expression of EGFP fusion proteins (Figure 3.7; Appendix III) confirmed that the removal of the cell wall did not affect the overall subcellular localization of organelles including the transvacuolar cytoplasmic channels, CCC and PCC chloroplasts, mitochondria, nucleus, actin filaments, microtubules, and peroxisomes. The integrity of the two cytoplasmic compartments and the subcellular distribution of organelles suggested that the isolated chlorenchyma protoplasts might be useful in the examination of organelle biogenesis and dynamics. For instance, movement of subcellular organelles in response to external stimuli or stresses can be monitored in an isolated system using the respective cytochemical stains or fluorescent protein probes. In addition, the protoplast transfection system also serves as a valuable tool for testing the subcellular localization of proteins, as shown here by the expression of EGFP fusion proteins with the various intracellular sorting signals (Figure 3.7; Appendix III).

3.4.4 Evaluation of selective protein import into dimorphic chloroplasts

In single-cell C_4 species, the major photosynthetic enzymes are localized to specific cytoplasmic compartments in relation to their C_4 metabolic functions (Voznesenskaya et al., 2002; Chuong et al., 2006). Selective protein import into chloroplasts remains one of the possibilities to account for the differential distribution of chloroplast proteins between the two cytoplasmic compartments (Offermann et al., 2011b). Taking advantage of the established fluorescent protein tagging system, I attempted to test this hypothesis for the first time (Figure 3.7; Appendix III-G). In this study, I showed that the efficiency of targeting EGFP into dimorphic chloroplasts varied considerably depending on the TPs used (Figure 3.7; Appendix III-G), implicating the presence of multiple regulatory mechanisms for different proteins. For instance, since it has been indicated that the plastid-encoded Rubisco large-subunit is overwhelmingly more abundant in central chloroplasts than in peripheral chloroplasts (Voznesenskaya et al., 2002), consistent with the anticipated higher abundance of the nuclear-encoded RbcS in central chloroplasts for the efficient assembly of functional Rubisco enzymes. However, RbcS-TP guided EGFP with equal efficiency into the central and peripheral chloroplasts (Appendix III-G), suggesting that this guiding signal might not be differentially recognized by the translocon receptors at the outer envelope of both chloroplast types. Rather, the selective targeting of mRNAs and differential regulation of RbcS at the transcript and protein levels among the two cytoplasmic compartments might be examined. On the other hand, the more efficient targeting of EGFP into the peripheral chloroplasts compared to the central chloroplasts using the TPs of ferredoxin or PPDK might be attributed to the selective recognition of these TPs by the translocon receptors (Figures 3.7B and 3.7E). Following the successful dimorphic chloroplast purification (see Chapter 4), this notion can

be further evaluated using other approaches such as *in vitro* protein import assays in the future.

3.4.5 Potential applications of isolated protoplasts

While EGFP fusion assays are suitable for determining the subcellular localization of proteins, functions of putative proteins can be implicated by predicting their potential interacting partners. The high transfection efficiency of this transient gene expression system allows co-transfection of different gene constructs for protein–protein interaction studies using bimolecular fluorescence complementation and fluorescence resonance energy transfer. A plant protoplast two-hybrid system (Ehlert et al., 2006) and a membrane protein-based split-ubiquitin system (Rahim et al., 2009) have been established recently for high-throughput analysis of a higher number of interacting partners. Establishment of an equivalent protein–protein interaction system using *B. sinuspersici* chlorenchyma protoplasts will help to study the regulation of single-cell C_4 photosynthesis at the protein level. The technique used for the isolation of a homogenous population of *B. sinuspersici* chlorenchyma protoplasts in the present study will also facilitate subcellular fractionation of organelles for a comprehensive analysis of their protein profiles using a proteomics approach. For instance, the successful separation of the two populations of chloroplasts, as detailed in the next chapter, will enable comparative analysis of the two chloroplast proteomes, which will provide important information on the respective roles of CCC and PCC in single-cell C_4 photosynthesis and other physiological perspectives, in analogy with the functional differentiation of maize mesophyll and bundle sheath chloroplasts (Majeran et al., 2005; Majeran et al., 2008).

It has been scientists' long-term desire to introduce C_4 photosynthesis into major C_3 agricultural crops. Despite the potential of incorporating the biochemistry of C_4 photosynthetic pathway into crop plants, the engineering of Kranz-leaf anatomy is considered the greatest hurdle due to the limitation of current technology (Surridge, 2002). The discovery of single-cell C_4 photosynthesis in three chenopod species, however, potentially provides new strategy for redesigning C_3-to-C_4 conversion in terrestrial plants. In this study, my initial observation of *B. sinuspersici* chlorenchyma protoplast fusion (Figure 3.4) implicated that somatic hybridization remains one of the potential strategies for generation of novel C_4 species. Given the earlier success in partial introduction of C_3–C_4 intermediate traits into somatic hybrids between *Moricandia arvensis* and *Brassica oleracea* (Ishikawa et al., 2003), attempts could be made to generate somatic hybrids and cybrids of *B. sinuspersici* with C_3 species in the future.

Chapter 4. Isolation of dimorphic chloroplasts from *Bienertia sinuspersici*

4.1 Overview

Bienertia sinuspersici is one of the three currently known terrestrial plant species which performs C_4 photosynthesis without the conventional dual-cell system, by partitioning two distinct types of chloroplasts in cytoplasmic compartments. I report herein a protocol for isolating the dimorphic chloroplasts from *B. sinuspersici*. Hypo-osmotically lysed protoplasts under the empirically optimized conditions released intact compartments containing the central chloroplasts in addition to intact vacuoles with adhering peripheral chloroplasts. The two chloroplast populations were further purified by Percoll step gradient centrifugation to high homogeneities as evaluated from the relative abundance of the respective protein markers. This protocol will open novel research directions toward understanding the differentiation of the dimorphic chloroplasts and other aspects of single-cell C_4 photosynthesis.

Remark: A version of this chapter has been published in: **Lung SC, Yanagisawa M, Chuong SDX** (2012) Isolation of dimorphic chloroplasts from the single-cell C_4 species *Bienertia sinuspersici*. Plant Methods **8**:8.

4.2 Introduction

The majority of terrestrial plants house chloroplasts primarily in one major leaf cell type (i.e. mesophyll cells), and perform C_3 photosynthesis to assimilate atmospheric CO_2 into a 3-carbon product, 3-phosphoglyceric acid. In C_4 species, on the other hand, a Kranz-type leaf anatomy featuring a second type of chlorenchyma cells surrounding the vascular bundles (i.e. bundle sheath cells) was recognized as early as in the late 1800's (Haberlandt, 1884). In these species, the initial carbon fixation into 4-carbon acids was first documented in the 1960's (Kortschak et al., 1965; Hatch and Slack, 1966). The physiological relevance of the Kranz anatomy in relation to the C_4 photosynthetic pathways, however, was not elucidated until the successful separation of the two types of chlorenchyma cells and their respective dimorphic chloroplasts. With the development of various mechanical and enzymatic methods for separating the mesophyll and bundle sheath cells, the biochemistry of C_4 cycles has been intensively studied over the past few decades focusing explicitly on characterizing the enzymatic properties and determining their precise subcellular locations in these cell types (for review, see Edwards et al., 2001), leading to the current C_4 model. In the C_4 model, atmospheric CO_2 is initially converted into C_4 acids by phosphoenolpyruvate carboxylase (PEPC) in mesophyll cells. The C_4 acids are broken down by a C_4 subtype-specific decarboxylation enzyme in bundle sheath cells, and the liberated CO_2 is subsequently re-fixed by ribulose-1,5-bisphosphate carboxylase/oxygenase (Rubisco). As a result, the C_4 pathway concentrates CO_2 at the site of Rubisco and minimizes photorespiration, which is a result of an unfavorable oxygenase activity of Rubisco with O_2 leading to the waste of energy.

The relationship between the Kranz anatomy and C_4 photosynthesis had been an accepted

indispensable feature of the system until the discovery of three terrestrial single-cell C_4 species, *Suaeda aralocaspica* (Voznesenskaya et al., 2001; formerly called *Borszczowia aralocaspica*), *Bienertia cycloptera* (Freitag and Stichler, 2002; Voznesenskaya et al., 2003), and *B. sinuspersici* (Akhani et al., 2005). In chlorenchyma cells of these succulent Chenopodiaceae species, the C_4 cycles are operational in the absence of Kranz anatomy due to the division of cytoplasm into two compartments. Cytoplasmic channels that connect the two compartments allow metabolite exchange but limit inter-compartmental gas diffusion, and resemble the function of plasmodesmata traversing the thickened and sometimes suberized bundle sheath cell wall. Each of the two cytoplasmic compartments house distinct types of dimorphic chloroplasts and different subsets of enzymes. Accordingly, the compartment proximal to the CO_2 entry point into leaves is specialized for carboxylation and regeneration of the initial carbon acceptor, phosphoenolpyruvate, whereas the second compartment distal to the CO_2 entry point is responsible for decarboxylation of C_4 acids and Rubisco-catalyzed re-fixation of the liberated CO_2. In agreement with the immunolocalization patterns of the major enzymes involved (Voznesenskaya et al., 2001 and 2002; Chuong et al., 2006), the two cytoplasmic compartments might be functionally equivalent to the mesophyll and bundle sheath cells of Kranz-type C_4 plants, respectively. Using differential speed centrifugation for the enrichment of each chloroplast type in subcellular fractions of *B. sinuspersici* leaves, Offermann et al. (2011a) have recently studied the protein distribution patterns of dimorphic chloroplasts and confirmed their functional similarities to the mesophyll and bundle sheath cells of Kranz-type C_4 plants, respectively. Thorough studies of the enzymology of the single-cell C_4 model, however, require homogenous preparations of the dimorphic chloroplasts with specific techniques based on the

unique cell anatomy, in analogy with the previous efforts of separation and subcellular fractionation of the dual cell types from Kranz-type C_4 plants (for review, see Edwards et al., 2001).

In this chapter, I present my empirically optimized protocol for separation of the two homogenous populations of dimorphic chloroplasts from isolated chlorenchyma protoplasts of *B. sinuspersici*. By reducing the osmotic potential of the culture medium to a suitable level, the isolated protoplasts were hypo-osmotically burst, concomitantly extruding one type of chloroplasts encased in one cytoplasmic compartment and another type of chloroplasts from the cell periphery adhered to the external surface of intact vacuoles. Following a centrifugation step, these two structures can be separated into the sedimented and floating fractions. Finally, two homogenous populations of dimorphic chloroplasts with minimal cross-contamination can be further purified by using a Percoll step gradient. Overall, this dimorphic chloroplast isolation protocol can be applied in multiple areas of research toward further understanding the development of single-cell C_4 systems.

4.3 Results

4.3.1 Rationale of the isolation procedures in relation to cell anatomy

To better describe each step of the isolation procedures as detailed in the subsequent sections, I first summarize the major cellular changes that take place in the chlorenchyma cells throughout the process (Figure 4.1). In a mature chlorenchyma cell, a large central vacuole (depicted in grey) separates the cytoplasm (yellow) into the peripheral (PCC) and the central (CCC) cytoplasmic compartments, which are interconnected by cytoplasmic channels traversing the vacuole (Figure 4.1A). The rounding of protoplasts by enzymatic digestion of the cell wall did not alter the integrity of the two cytoplasmic compartments and the cytoplasmic channels (Figure 4.1B). Reducing the osmotic potential of the cell-stabilizing buffer resulted in osmotic swelling of the protoplast and its central vacuole, disrupting the cytoplasmic channels and pushing the CCC against the plasma membrane (Figure 4.1C). The hypo-osmotic shock induced stretching of the plasma membrane beyond its extension limit eventually causing it to break releasing the intact CCC and an intact vacuole with attached peripheral chloroplasts (P-Chls; Figure 4.1D), in agreement with the previous observation that the two cytoplasmic compartments were separated by a single vacuole (Chuong et al., 2006; Park et al., 2009). Eventually, the central vacuole carrying P-Chls on the external surface (Figure 4.1E) and the isolated CCC containing central chloroplasts (C-Chls; Figure 4.1F) were separated into two discrete entities.

4.3.2 Isolation of chlorenchyma protoplasts

As a first step, I isolated chlorenchyma cells from *B. sinuspersici* leaves and enzymatically

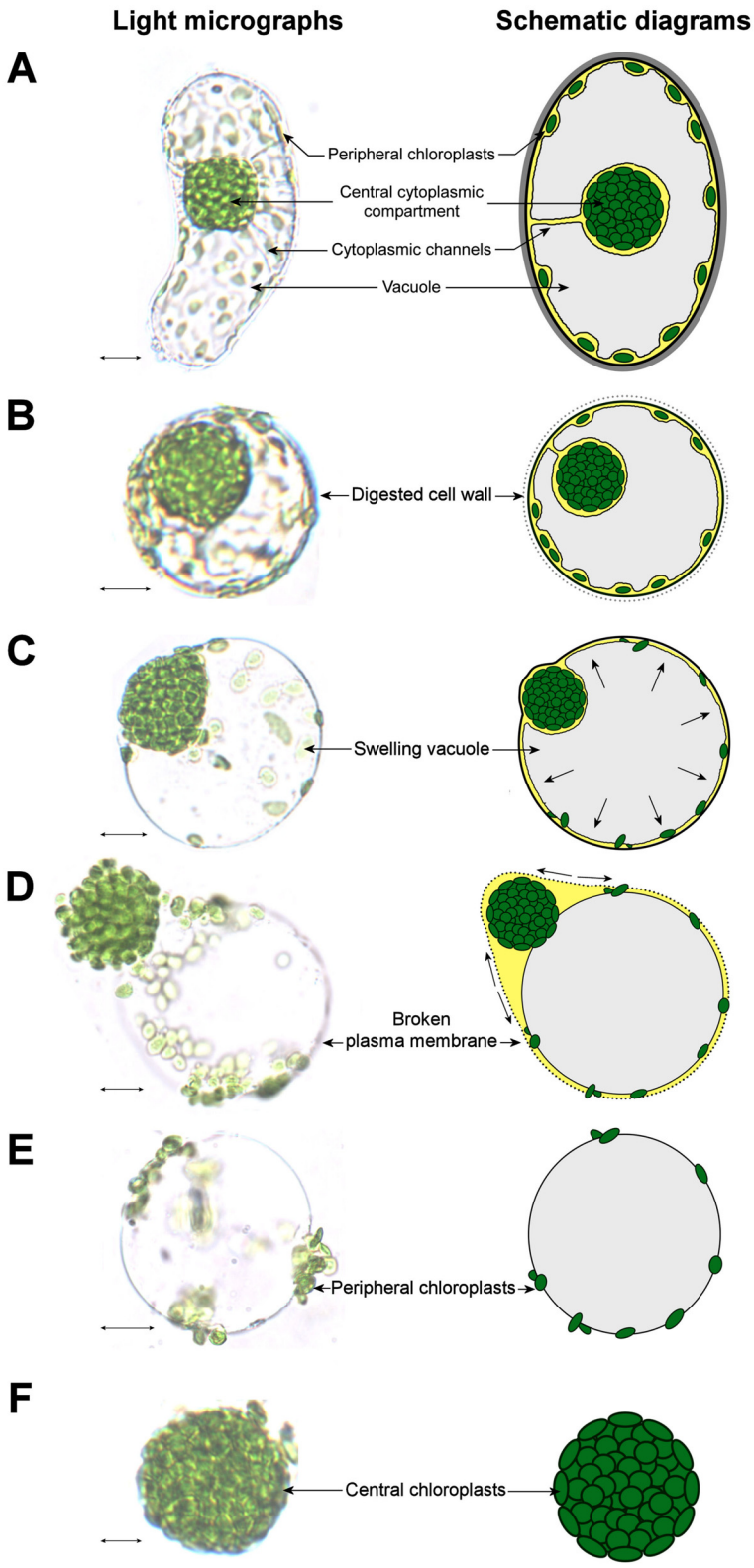

Figure 4.1

Figure legend on the next page

Figure 4.1 Illustration of the cellular and subcellular morphologies during the process of dimorphic chloroplast isolation

(A) A mature chlorenchyma cell. For clarity, only one cytoplasmic channel is illustrated despite the multiple occurrences in an actual cell. Scale bar = 10 μm.
(B) An isolated protoplast with digested cell wall. Scale bar = 10 μm.
(C) A swelling protoplast with increased osmotic pressure of the cell sap as indicated by arrows. Scale bar = 10 μm.
(D) A broken protoplast with torn plasma membrane as indicated by arrows. Scale bar = 10 μm.
(E) An intact vacuole carrying peripheral chloroplasts on the external surface. Scale bar = 10 μm.
(F) An isolated central cytoplasmic compartment. Scale bar = 5 μm.

prepared a homogenous population of healthy protoplasts. Detailed technical considerations on plant growth conditions and chlorenchyma protoplast isolation can be found in Chapter 3. Previously, progressive developmental variation had been identified at different stages of *B. sinuspersici* leaves in terms of the unique subcellular compartmentation and photosynthetic gene expression (Lara et al., 2008; Park et al., 2009). Similar developmental gradients were also observed across the base-to-tip dimension of leaves (Lara et al., 2008). Thus, these major sources of variability had to be taken into consideration in order to standardize the degree of C_4 functionality of the starting materials for dimorphic chloroplast isolation. To this end, *B. sinuspersici* plants were routinely propagated from vegetative cuttings, and entire leaves which were 2 cm or longer in length were collected from healthy branches of 3- to 4-month-old plants (Figure 4.2A). At this stage, the single-cell C_4 compartmentation has reached maturity as is evident by the presence of the distinctive subcellular distribution of dimorphic chloroplasts in the majority of chlorenchyma cells (Figure 4.2B). In a mature chlorenchyma cell, the C-Chls were densely packed into a large, spherical CCC structure, whereas the P-Chls were distributed throughout the thin layer of cytoplasm (PCC; Figure 4.2B). Following cell wall removal by cellulase treatment under the optimized conditions, the resulting protoplasts exhibited no observable changes in their unique chloroplast distribution, which was considered a prerequisite for subsequent preparations of pure dimorphic chloroplasts (Figure 4.2C). During the protoplast isolation, I occasionally observed vesicles with externally adhering P-Chls (Figure 4.2D). Given their potential of serving as an excellent source of pure P-Chls, I continued to optimize the conditions for inducing the formation of these P-Chl-containing vesicles from isolated protoplasts. To guarantee intactness and full functionality of the purified dimorphic chloroplasts, at least 90% viability

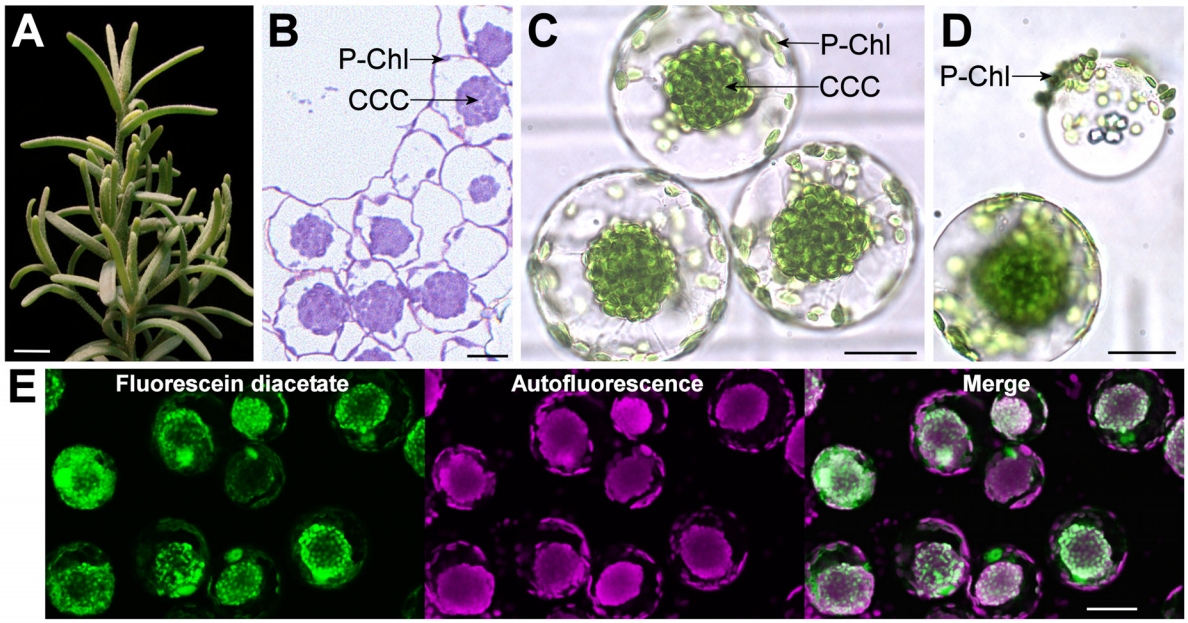

Figure 4.2 Isolation of chlorenchyma protoplasts from *B. sinuspersici*

(A) A healthy branch of vegetatively propagated *B. sinuspersici* suitable for protoplast isolation. Scale bar = 10 mm.

(B) A cross section of *B. sinuspersici* leaf showing chlorenchyma cells with two types of chloroplasts, i.e. the peripheral chloroplasts (P-Chls) in the peripheral cytoplasmic compartments and the central chloroplasts enclosed in the central cytoplasmic compartments (CCC). Scale bar = 20 µm.

(C) A bright field image of chlorenchyma protoplasts indicating the integrity of the two cytoplasmic compartments for subsequent isolation of the dimorphic chloroplasts. Scale bar = 20 µm.

(D) A bright field image of a protoplast and a vesicle with externally associated P-Chls. Scale bar = 20 µm

(E) Vital staining of isolated protoplasts imaged under epifluorescence microscopy. Fluorescein diacetate staining (left panel), chlorophyll autofluorescence (middle panel) and a merged image (right panel). Scale bar = 20 µm.

of the isolated protoplasts should be achieved prior to chloroplast separation as evaluated by fluorescein diacetate staining (Figure 4.2E).

4.3.3 Formation of vesicles from protoplasts by osmotic shock treatment

Preliminary trials suggested that the vesicles with adhering P-Chls could be derived from the swelling protoplasts in an osmotic potential-dependent manner. Accordingly, I carried out time-lapse imaging of the vesicle formation from isolated protoplasts subjected to hypo-osmotic shock treatments. I diluted the sucrose concentration of the protoplast culture medium from 0.7 M to various concentrations. When the sucrose concentration was decreased to 0.1 M, the isolated protoplasts expanded rapidly and lysed approximately 15 s after dilution, releasing the CCCs and vesicles with P-Chls (Figure 4.3A). The dense CCC structures gradually loosened and the encased C-Chls eventually started to dissociate from the CCC structures, whereas the vesicles continued to expand beyond the stretching limit of their membrane and eventually burst causing the P-Chls to adhere to strings of collapsed membrane which were inseparable from the CCC structures (Figure 4.3A). On the other hand, reducing the sucrose concentration to 0.2 M, the isolated protoplasts gradually swelled and lysed approximately 25 s after dilution, releasing the CCCs and P-Chl-carrying vesicles (Figure 4.3B). Under this condition, the majority of C-Chls remained tightly packed within the dense CCC structures and the vesicles continued to swell for a few seconds yet remained intact after cell lysis (Figure 4.3B). Subtle reduction of the sucrose concentration to 0.5 M did not burst the isolated protoplasts, although some vesicles were occasionally pinched off from the intact swelling protoplasts (Figure 4.3C). The majority of these vesicles, however, were not associated with any chloroplasts (Figure 4.3C).

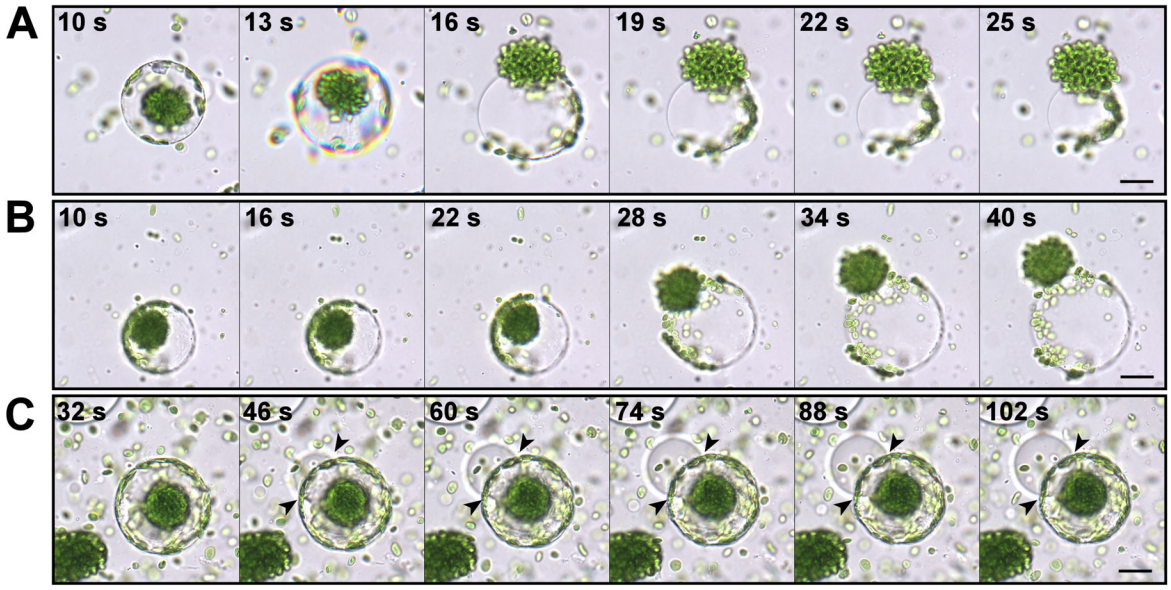

Figure 4.3 Time-lapse imaging of protoplasts subjected to osmotic swelling

(A) Diluting the cell-stabilizing buffer to a sucrose concentration of 0.1 M led to rapid swelling and bursting of both the protoplasts and their vacuoles. Scale bar = 20 µm.

(B) Lowering the osmotic potential of the cell-stabilizing buffer to the optimum 0.2 M sucrose resulted in protoplast lysis and the release of intact central cytoplasmic compartments and vacuoles with attached peripheral chloroplasts. Scale bar = 20 µm.

(C) Subtle dilution of the cell-stabilizing buffer to 0.5 M sucrose did not lyse the protoplasts while vesicles were slowly pinching off from the vacuoles of protoplasts as indicated by arrowheads. Scale bar = 20 µm.

4.3.4 The vacuolar origin of vesicles from lysed protoplasts

The time-lapse images clearly showed that the released vesicles from hypo-osmotically lysed protoplasts originally made up the bulk of cell volume (Figure 4.3), implying that these vesicles were derived from the large central vacuoles. Due to the unusual subcellular organization of *B. sinuspersici* chlorenchyma cells, I sought to confirm the vacuolar origin of the vesicles by staining with 5-(and-6)-carboxy-2',7'-dichlorofluorescein diacetate (CDCFDA), a pH-sensing vital probe for the vacuole lumen (Pringle et al., 1989). In a CDCFDA-stained protoplast, prominent fluorescent signals were typically found in the vacuole which occupied the massive cell content dividing the CCC and PCC (Figure 4.4A). Following hypo-osmotic shock treatment of CDCFDA-stained protoplasts, the persistence of fluorescent signals in the resulting vesicles indicated their vacuolar origin (Figures 4.4B and 4.4C). The occurrence of some patchy CDCFDA signals in other subcellular locations (Figure 4.4), similar to the observations from previous studies (Chuong et al., 2006; Park et al., 2009), might be attributed to the presence of reactive oxygen species (Nasr-Esfahani et al., 1990). In addition to the CDCFDA staining, the formation of prismatic and raphide crystals in the vesicles provided further evidence of their vacuolar origin (Figure 4.5). The occurrence of these crystals is a widespread phenomenon in plant vacuoles due to the accumulation of calcium oxalate as crystalline deposits (Franceschi and Nakata, 2005).

4.3.5 Dimorphic chloroplast subfractionation from lysed protoplasts

Given a promising strategy to separate CCCs and intact vacuoles with adhering P-Chls by osmotic treatment of isolated protoplasts, I further optimized the conditions for the best yields of homogenous populations of these two suborganellar structures. Since preliminary

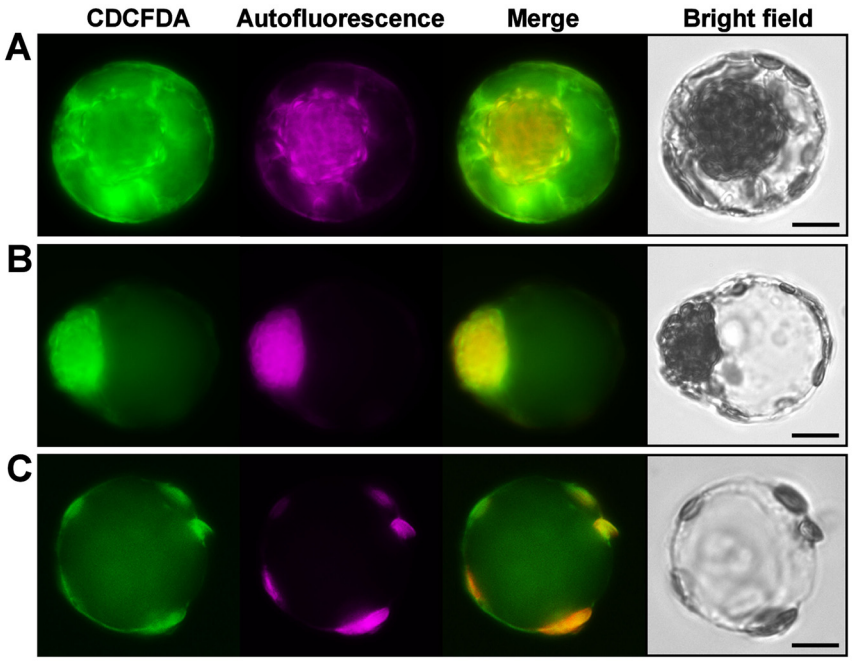

Figure 4.4 Vacuolar staining of chlorenchyma protoplasts and osmotically-derived vesicles

Isolated protoplasts were stained with 5-(and-6)-carboxy-2',7'-dichloro-fluorescein diacetate (CDCFDA) and lysed by osmotic swelling. The isolated protoplasts and induced vesicles were observed under light and epifluorescence microscopy. CDCFDA staining, chlorophyll autofluorescence, merged images of the two channels, and bright field images are shown. Scale bars = 10 μm.

(A) An isolated protoplast.
(B) A swelling protoplast before cell lysis.
(C) A vacuole-derived vesicle.

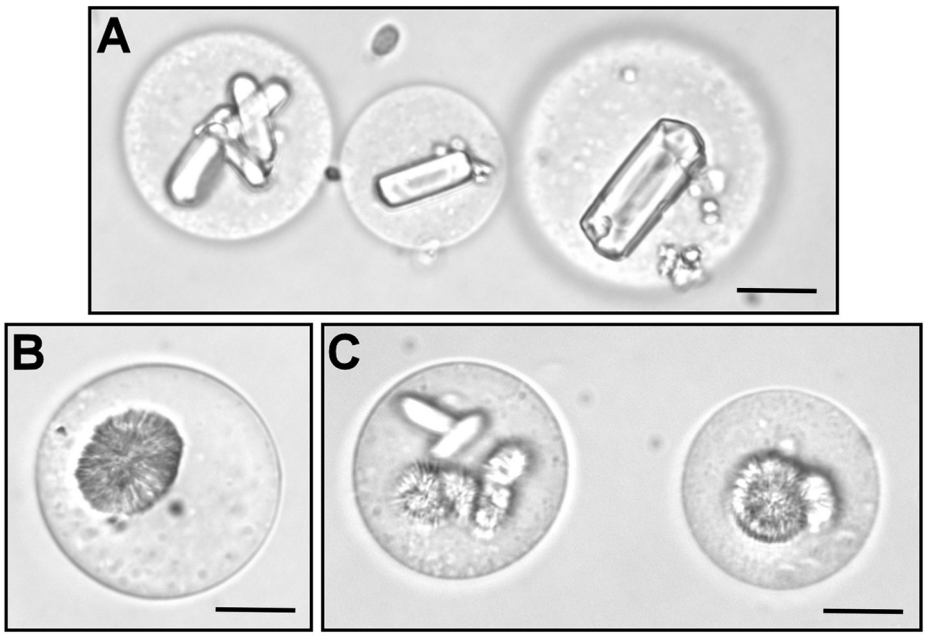

Figure 4.5 Formation of calcium oxalate crystals in the vacuole-derived vesicles

The vesicles were obtained from lysis of protoplasts by osmotic swelling at 0.2 M sucrose and isolated on the floating layer after centrifugation at 100*g* for 4 min. Formation of calcium oxalate crystals was induced by resuspension of the vesicles in cell stabilizing buffer with 0.7 M sucrose. Scale bars = 20 μm.

(A) A light micrograph of prismatic crystals.
(B) A light micrograph of raphide crystals.
(C) A light micrograph of both prismatic and raphide crystals.

trials suggested that the isolated protoplasts under an overcrowded condition responded heterogeneously to the osmotic shock, I routinely adjusted the cell density to 10^5 protoplasts mL^{-1} before treatment to ensure the highest percentage of protoplast lysis. Pre-conditioning of the isolated protoplasts at 0 ^oC potentially rendered their plasma membranes more brittle due to the reduced fluidity and facilitated the subsequent cell lysis. Rapid dilution of the isolated protoplasts at room temperature in an EDTA-containing buffer without the sucrose osmoticum resulted in stretching and fragmentation of the plasma membrane. This observation is considered a combined effect of protoplast swelling due to the reduced osmotic strength of buffer and the sudden alternation in membrane fluidity due to the thermal change and the chelation of divalent ions. At the optimal 0.2 M concentration of sucrose, 98% of isolated protoplasts were burst and approximately 80% of the released vacuoles remained intact (Figure 4.6). On the other hand, a relatively low percentages of protoplasts was lysed at higher sucrose concentrations (i.e. 0.3-0.7 M), whereas the released vacuoles at unfavorably low sucrose concentration (i.e. 0.1 M) were concomitantly burst (Figure 4.6). Taken together, I routinely lysed the isolated protoplasts by rapid dilution of the protoplast culture buffer to 0.2 M sucrose which provided the best yields of intact CCCs and intact P-Chl-containing vacuoles. Due to the substantial difference in densities of these two suborganellar structures, subsequent incubation on ice and low-speed centrifugation (100*g*, 4 min) led to their separation into the sedimented and floating fraction. The recovered pellets and floating layers contained a homogeneous population of CCCs (Figure 4.7A) and intact vacuoles with adhering P-Chls (Figure 4.7B), respectively. The CCCs could be easily dispersed mechanically by pipetting up and down following the cold treatment and the C-Chls released from the CCCs were further purified from other impurities on a typical two-

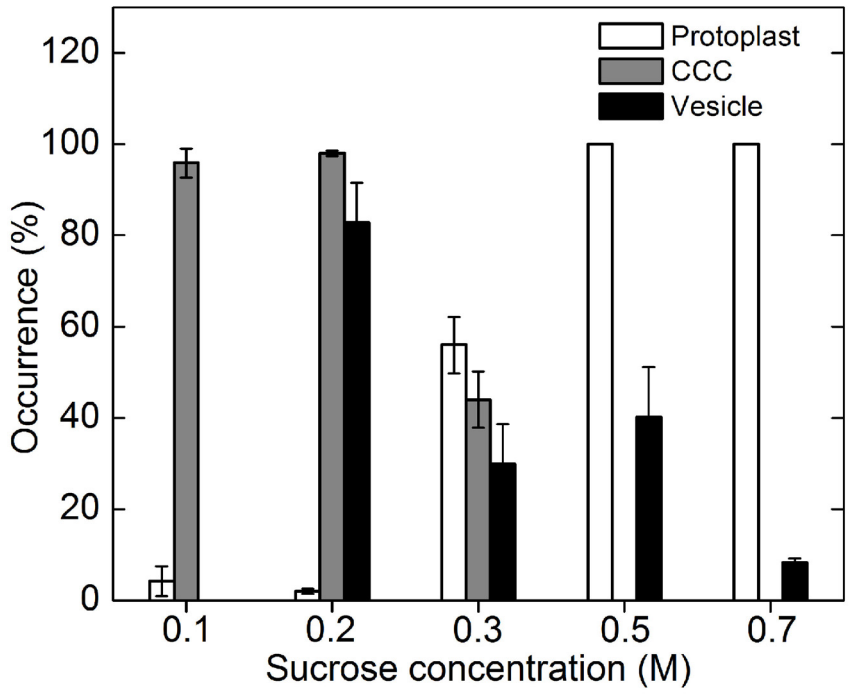

Figure 4.6 The release of central cytoplasmic compartments and vesicles from protoplasts under different osmotic conditions

The sucrose concentration of the cell stabilizing buffer was either undiluted (0.7 M) or diluted to 0.1, 0.2, 0.3 or 0.5 M, and the protoplasts were incubated on ice for 10 min. The number of intact protoplasts, central cytoplasmic compartments (CCC) and vacuole-derived vesicles were counted using a haemocytometer under light microscopy. The occurrence (%) is calculated from the number of protoplasts, CCC or vesicles after osmotic treatment divided by the number of protoplasts used. Each bar represents the mean value from three independent experiments (±SD).

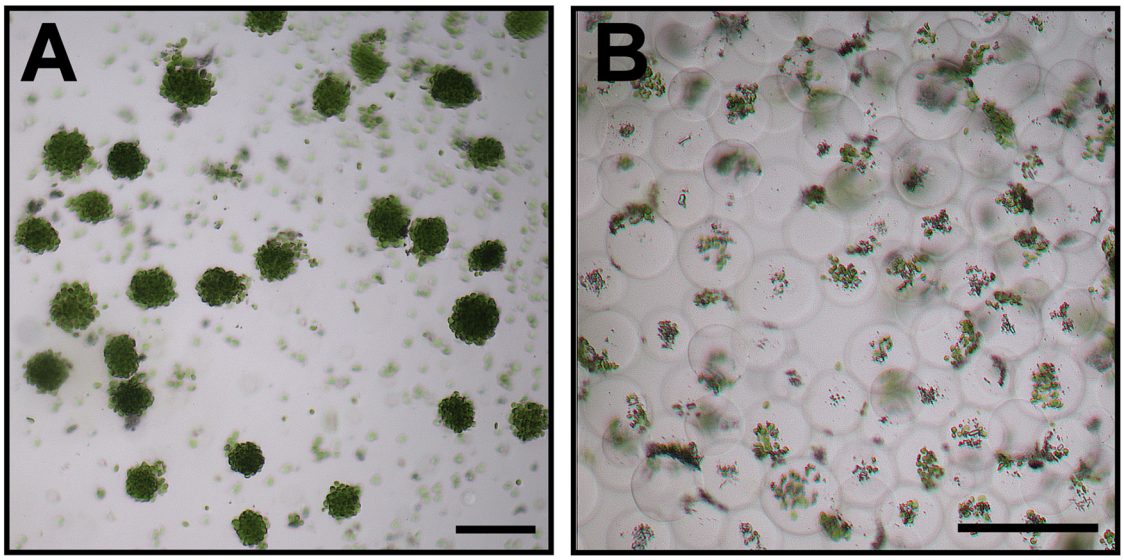

Figure 4.7 Bright field images of the isolated dimorphic chloroplast populations

(A) A homogenous population of central cytoplasmic compartments. Scale bar = 40 µm.
(B) A homogenous population of vacuole-derived vesicles carrying peripheral chloroplasts on the external surfaces. Scale bar = 40 µm.

step Percoll gradient. By centrifugation (2,500*g*, 10 min) of the P-Chl-containing vacuoles on a similar Percoll gradient, the loosely adhering P-Chls were easily dissociated from the vacuoles and entered the Percoll solutions. In both cases of C-Chls and P-Chls, the lower green band at the 40%/85% Percoll interface contained at least 50% of the loaded chloroplasts. The aspirated chloroplasts from this interface were confirmed to be pure and intact under phase contrast microscopy.

4.3.6 Evaluating cross-contamination of purified dimorphic chloroplasts

The purities of P-Chl and C-Chl preparations were evaluated from the relative abundances of their respective protein markers (Figure 4.8). Western blot analyses indicated that the immunoreactive band of pyruvate orthophosphate dikinase (PPDK) from P-Chls was two-fold more intense than that from C-Chls (Figure 4.8), whereas Rubisco large-subunit (RbcL) was almost exclusively found in C-Chls but rarely detectable in P-Chls (Figure 4.8). These protein distribution patterns are in agreement with the recent observations following the subcellular fractionation of P-Chls and C-Chls (Offermann et al., 2011a). In fact, previous immunolocalization experiments also revealed that the labelling of PPDK was mainly associated with the P-Chls, whereas RbcL was predominantly detected in the C-Chls (Chuong et al., 2006). The relative distribution of the photosystem II (Figure 4.8) and photosystem I (Figure 4.8) proteins in the dimorphic chloroplasts also correlated with the previous ultrastructural studies revealing that C-Chls had a higher granal index and generally greater sizes of grana stacks than P-Chls (Voznesenskaya et al., 2002). The Western blot analyses indicated that the C-Chls had slightly more photosystem II manganese-stabilizing proteins (PsbO; Figure 4.8), which are located predominantly in the stacked regions of

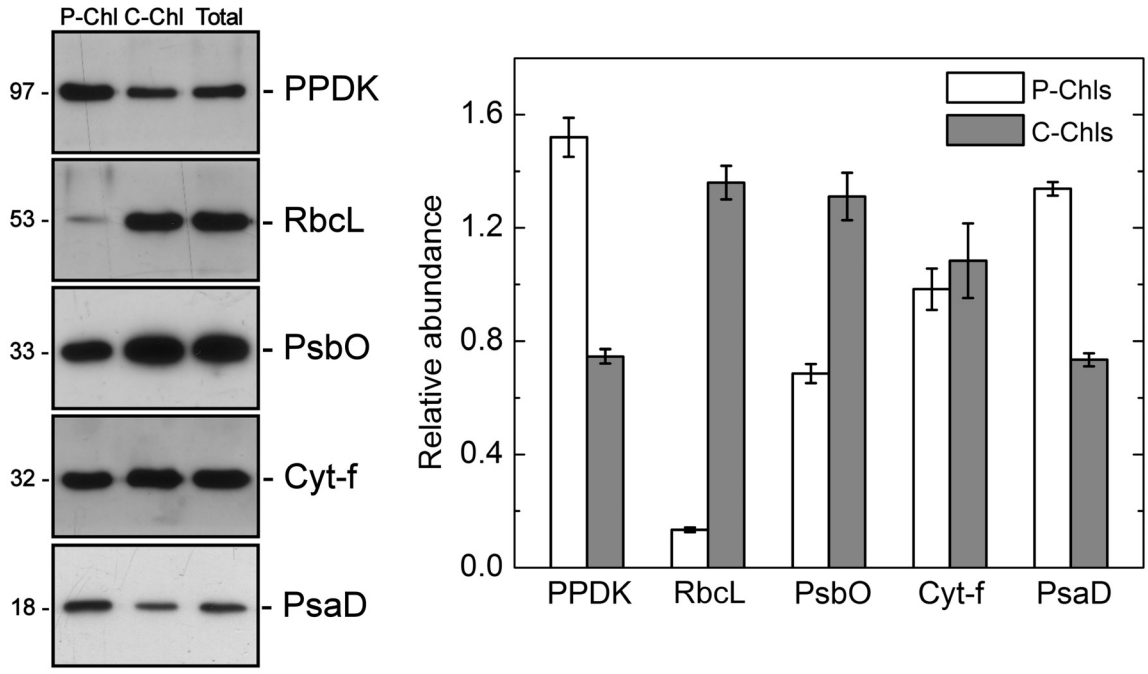

Figure 4.8 Western blot analyses of the isolated dimorphic chloroplast populations

Two micrograms of proteins from peripheral chloroplasts (P-Chl), central chloroplasts (C-Chl) and total chloroplasts (Total) were separated on SDS/12% PAGE, and immunoblotted onto nitrocellulose membranes for incubation with antibodies against pyruvate orthophosphate dikinase (PPDK), Rubisco large-subunit (RbcL), Photosystem II manganese-stabilizing protein (PsbO), Cytochrome f (Cyt-f) or Photosystem I subunit II protein (PsaD). Molecular weights are shown on the left in kilodaltons. The immunoblots were analyzed by densitometric quantification. The abundance of each protein in peripheral and central chloroplasts was calculated relative to that of total chloroplasts and shown with standard errors, after three (PsbO) or four (otherwise) independent experiments[1].

[1]A portion of the data for densitometric quantification was contributed by Dr. Makoto Yanagisawa.

thylakoid membrane. The P-Chls, on the other hand, contained more photosystem I subunit II proteins (PsaD; Figure 4.8), which are commonly found in the unstacked regions. The cytochrome f subunit of the cytochrome b6f complex, which is evenly distributed throughout the thylakoid membrane, was equally abundant in both types of chloroplasts (Figure 4.8). Overall, the electrophoretic analyses indicated minimal cross-contamination of the two isolated populations of dimorphic chloroplasts.

4.4 Discussion

4.4.1 Feasibility of isolating dimorphic chloroplasts from *B. sinuspersici*

In view of the chlorenchyma cell anatomies of the three currently known terrestrial single-cell C_4 species, isolation of dimorphic chloroplasts from the two Bienertia species is technically more feasible as compared to *S. aralocaspica*. Firstly, chlorenchyma cells of the two Bienertia species (i.e. *B. sinuspersici* and *B. cycloptera*) enclose one type of dimorphic chloroplasts within a distinctive spherical structure (CCC) at the centre of the cell and randomly distribute another type of chloroplasts in a thin layer of cytoplasm at the cell periphery (PCC). Separation of the dimorphic chloroplasts from chlorenchyma cells of these species is therefore technically more straightforward provided that the integrity of CCC can be preserved during the process. Secondly, the mature chlorenchyma cells of Bienertia species effectively limit gas diffusion by the formation of CCCs in the cell interior, as a means to reduce CO_2 leakage at the site of C_4 acid decarboxylation and exposure of Rubisco to O_2. At the cell periphery, the entire chlorenchyma cells are surrounded by extensive intercellular space to facilitate fixation of atmospheric CO_2 (Figure 2B; Vozensenskaya et al., 2002). Therefore, the loosely packed chlorenchyma cells can be readily isolated by squeezing the leaves in a mortar and pestle (see section 3.3.1). Technically, this rapid release of chlorenchyma cells devoid of contaminations such as epidermis, water storage and vacuolar tissues facilitates the subsequent isolation of pure and functional dimorphic chloroplasts. In contrast, mature leaves of *S. aralocaspica* partition dimorphic chloroplasts by localization of the first chloroplast type at one pole of the elongated chlorenchyma cells proximal to the atmosphere and the second chloroplast type at the opposite pole of the cells proximal to the

vascular tissues (Voznesenskaya et al., 2001). Thus, the operation of a single-cell C_4 cycle in this species depends primarily on the polarization of the dimorphic chloroplasts and the radial elongation of the cells for effective limitation of CO_2 and O_2 diffusion (Voznesenskaya et al., 2001 and 2003). Isolation of the two polarized chloroplast types solely based on the difference in their subcellular locations might be technically challenging, if not impossible. We speculate that, perhaps, any change in cell shape due to cell wall removal, as the first step in routine chloroplast isolation procedures, might distort the polarization of the dimorphic chloroplasts, although isolation of chlorenchyma protoplasts from *S. aralocaspica* has not yet been attempted. The leaf anatomy of *S. aralocaspica* also reveals absolute exclusion of intercellular air space toward the inner poles of chlorenchyma cells by tight cell-cell adhesion (Voznesenskaya et al., 2001 and 2003), suggesting that chlorenchyma cell isolation might be more difficult. Moreover, our successful plant propagation by vegetative cuttings added another technical advantage of using *B. sinuspersici* leaves for large-scale isolation of dimorphic chloroplasts with synchronized C_4 development.

4.4.2 Technical considerations for isolation of central chloroplasts

A reliable protocol for separating the dimorphic chloroplasts is primarily evaluated based on the criteria of no cross-contamination. The isolation of C-Chls is relatively effortless due to the confinement of these organelles within the large, dense CCC structures, which can be easily recovered from the cell lysates by low-speed centrifugation (Figure 4.7A). It is worthy of note, however, that the C-Chl preparation might be potentially contaminated with P-Chls due to incomplete protoplast lysis. In the previous chapter, I reported a low-speed centrifugation-based method for floatation of healthy, intact chlorenchyma protoplasts on a

sucrose medium and sedimentation of the stressed protoplasts (see section 3.3.2). In the present study, any protoplasts surviving from the osmotically-mediated lytic treatment might therefore be co-sedimented with the CCC fraction upon low-speed centrifugation leading to contamination of this fraction with P-Chls. Accordingly, I optimized the procedures for osmotic shock treatment and showed that the isolated protoplasts at a suitable cell density were almost exclusively burst under the defined chemical, thermal and osmotic conditions (Figure 4.6), leading to a homogenous preparation (Figure 4.7A) and satisfactory purity (Figure 4.8) of C-Chls. In addition to P-Chls, the potential contamination of C-Chl preparation with chloroplasts from immature chlorenchyma cells should be taken into account. The expression patterns of photosynthetic genes strongly suggested that these chloroplasts from immature chlorenchyma cells, as evidenced in the young leaf samples, might function in a C_3 default mode of photosynthetic and photorespiratory pathways (Lara et al., 2008). Since no chloroplast clumping was observed at this early stage of leaf development (Park et al., 2009), contamination due to chlorenchyma immaturity is not considered a concern in the preparation of C-Chls using our low-speed centrifugation-based method.

4.4.3 Technical considerations for isolation of peripheral chloroplasts

Purification of P-Chls from the protoplast lysates was technically more challenging as compared to the isolation of C-Chls. Recently, Offermann et al. (2011a) reported the first protocol for dimorphic chloroplast isolation from *B. sinuspersici* based on the differential centrifugation method. In my preliminary trial of various methods for dimorphic chloroplast isolation, similar centrifugation technique as reported by Offermann et al. (2011a) did not

provide satisfactory purity of P-Chls due to two major problems (data not shown). First, residual CCCs remained in the supernatant after the low-speed centrifugation leading to contamination of the P-Chl fraction. Attempts to increase the centrifugal force or duration of centrifugation, on the other hand, resulted in a considerable loss of P-Chls from the supernatant. More remarkably, the supernatant fraction of P-Chls was contaminated with C-Chls due to their dissociation from the CCC, which remains an unavoidable problem given the fact that the CCC is not confined by a membrane evident at the electron microscopic level. In fact, rapid dispersal of C-Chls was commonly observed when the chlorenchyma protoplasts were subjected to unfavorable culture conditions (see section 3.3.2) or mechanical disruption such as a gentle press on a microscopic slide (Offermann et al., 2011a). The integrity of CCC structures is primarily maintained by the association of C-Chls in the outer regions of CCCs with the surrounding cytoskeleton networks, of which the microtubule is considered the most important (Chuong et al., 2006). During the dimorphic chloroplast isolation, the instability of the CCCs might be attributed to a combined effect of osmotic swelling of C-Chls in the hypotonic medium and de-polymerization of microtubules by low temperature. Despite the contentious issue of cold treatment, chloroplast isolation at higher temperature is not recommended due to the potential risk of protein degradation and denaturation after cell lysis, particularly if chloroplasts are isolated for proteomics or enzymology studies. Similarly, chloroplasts for protein import studies should be isolated at low temperature due to the high susceptibility of the chloroplast protein import receptors to proteolysis (Bölter et al., 1998; Chen et al., 2000). Of relevance to preventing proteolytic degradation, the current chloroplast isolation method has an added advantage by confining the majority of proteolytic enzymes in the intact vacuoles.

Due to the considerable contamination of the P-Chls in the cell lysate with dissociated C-Chls when using the differential speed centrifugation method, I sought an alternative method for P-Chl purification by isolation of floating vacuoles as P-Chl carriers. The separation of plant vacuoles from isolated protoplasts is a common phenomenon in hypotonic solutions and was documented as early as when protoplasts were isolated for the first time from a plant source (Cocking, 1960). Since then, protoplast-based techniques for plant vacuole isolation have been well established (Gomez and Chrispeels, 1993; Robert et al., 2007). These isolated vacuoles are commonly surrounded by their tonoplasts with loosely adhering protoplasmic materials (Cocking, 1960), including the P-Chls in the present study (Figure 4.2D). Accordingly, I further optimized the conditions for isolating the vacuoles with adhering P-Chls since the floatation of P-Chls on a sucrose medium might effectively prevent their contamination with CCCs in the pellet or dissociated C-Chls in the supernatant. As expected, P-Chls prepared using this method contained barely detectable levels of RbcL, as revealed by immunoblot analysis, which was found almost exclusively in the C-Chl fraction (Figure 4.8). The striking difference in RbcL content between the dimorphic chloroplasts is in agreement with the quantitative immunogold transmission electron microscopic analysis showing that the RbcL signals were distributed between P-Chls and C-Chls at a ratio of 1:20 (Yanagisawa, 2012). This observation is substantially higher than the recent results reported by Offermann et al. (2011a) using the differential centrifugation method. In their study, Western blot analysis revealed the immunoreactive band intensities of RbcL for the P-Chl and C-Chl fractions at a ratio of 1: 3.5 (Offermann et al., 2011a), suggesting an impure preparation of P-Chls. Two possible sources of contamination in their P-Chl preparation with RbcL might be,

as discussed earlier, that the P-Chl fraction may be contaminated with unpelleted CCCs or dissociated C-Chls using the differential centrifugation method. Also, the C_3-like chloroplasts from immature chlorenchyma cells were inseparable from the P-Chls because neither type of chloroplasts forms intracellular clumping structures in immature cells. On the other hand, since vacuoles are not prominently found in young chlorenchyma cells (Park et al., 2009), the current vacuole-based method for preparation of P-Chls is less likely to be contaminated with C_3-like chloroplasts, as indicated by the low level of RbcL (Figure 4.8). Moreover, the unequal distribution of proteins associated with the photosystems (PsbO and PsaD) in the two chloroplast fractions presented here also supports earlier ultrastructural results showing that chloroplasts in the peripheral compartment have a lower granal index than those in the central compartment (Voznesenskaya et al., 2002).

4.4.4 Potential applications of isolated dimorphic chloroplasts

With the development of the current method to isolate two homogenous populations of dimorphic chloroplasts from *B. sinuspersici*, research can be carried out toward a thorough understanding of the single-cell C_4 mechanism. Enzymology of the C_4 photosynthetic and photorepiratory pathways can be explicitly characterized. Given the different subsets of enzymes in the two types of chloroplasts, the possibility of differential protein import can be evaluated by *in vitro* import assays and biochemical characterization of the protein import receptors at the chloroplast envelope using the isolated dimorphic chloroplasts. Recently, high-throughput proteomic analyses of the stroma (Majeran et al., 2005) and membrane fractions (Marjeran et al., 2008) of the purified mesophyll and bundle sheath cells from maize leaves have provided interesting insights into the different roles of dimorphic

chloroplasts in C_4 photosynthesis as well as in other plastid functions. Similar proteomic analysis of the isolated dimorphic chloroplasts from *B. sinuspersici* might allow an informative comparison of their respective roles in single-cell C_4 photosynthesis and other physiological metabolism. From another perspective, the concomitant isolation of intact vacuoles using the current method might also be useful. For instance, one might further rule out the possibility of crassulacean acid metabolism (CAM) in the single-cell C_4 species by characterization of the metabolite contents in the vacuoles. Alternatively, the regulation of photosynthetic enzymes in this single-cell C_4 species might be studied in relation to their turnover in vacuoles through the autophagic pathway (Yanagisawa, 2012).

Chapter 5. Identification and subcellular localization of Toc receptors from *Bienertia sinuspersici*

5.1 Overview

The single-cell C_4 species *Bienertia sinuspersici* partitions key photosynthetic enzymes between two types of chloroplasts in single photosynthetic cells, implicating a possible differential protein import mechanism. In the present study, two cDNA sequences (i.e. *BsToc159* and *BsToc132*) were identified to encode homologues of the chloroplast preprotein import receptor Toc159 as revealed from their phylogeny, conservation of the characteristic tripartite structures and the unusual properties of their N-terminal domains. Protein expression profiling indicated up-regulation of BsToc159 during the early development and subsequent differentiation of dimorphic chloroplasts, whereas the BsToc132 level was relatively stable. In contrast to the strict confinement of the homologous receptor BsToc34 to the chloroplast envelope, both Toc159 isoforms partitioned between the cytosolic and chloroplast envelope-associated forms, as revealed by immunogold localization, fluorescent protein tagging and subcellular fractionation experiments. Cytoskeleton-disrupting drug treatment and co-immunoprecipitation studies further suggested that the cytosolic forms of both Toc159 isoforms associated with actin filaments and more prominently, with microtubules. The current data support a hypothetical model proposing the cytoskeleton-assisted trafficking of Toc159 between the cytosol and chloroplasts for primary recognition of preproteins.

Remark: Parts of this chapter have been published in: **Lung SC, Chuong SDX** (2012) A transit peptide-like sorting signal at the C-terminus directs the *Bienertia sinuspersici* preprotein receptor Toc159 to the chloroplast outer membrane. Plant Cell, in press.

5.2 Introduction

Terrestrial plants primarily use the common C_3 photosynthetic pathway to fix atmospheric CO_2 to organic molecules required for all life forms. C_3 photosynthesis is, however, considered inefficient under CO_2-limiting conditions due to photorespiration, an energetically wasteful reaction caused by the oxygenase activity of ribulose-1,5-bisphosphate carboxylase/oxygenase (Rubisco). Therefore, a few plant species have evolved means to maximize their photosynthetic efficiencies by using a C_4 cycle to increase the levels of CO_2 at the site of Rubisco and limit the oxygenation process. The operation of the C_4 cycle requires the development of two morphologically distinct cell types, bundle sheath and mesophyll cells, commonly known as Kranz anatomy, and partitioning of a specific subset of enzymes in the two specialized cell types (Hatch and Slack, 1970; Edwards and Huber, 1981). *Bienertia sinuspersici* is one of three species in the Chenopodiaceae family, which perform the C_4 pathway in a single photosynthetic cell by sorting key C_4 enzymes and dimorphic chloroplasts located in two separate compartments of the same cell (Voznesenskaya et al., 2001 and 2002; Akhani et al., 2005). This intracellular organization of the cytoplasm within a single cell functions analogously to the mesophyll and bundle sheath cells in Kranz-type C_4 species. Previous studies confirmed that the major photosynthetic enzymes localized to the specific cytoplasmic compartments in relation to their C_4 metabolic functions (Voznesenskaya et al., 2002; Chuong et al., 2006). Although the spatial distribution of other chloroplast proteins between the two cytoplasmic compartments is not known, a considerable difference in the proteomes of the dimorphic chloroplasts is expected according to a high-throughput analysis of purified mesophyll and bundle sheath chloroplasts in maize, a Kranz-type C_4 plant (Majeran et al., 2005; Majeran et al., 2008). Whilst the biogenesis and

differentiation of dimorphic chloroplasts at the biochemical level remains an unresolved aspect of the novel single-cell C_4 model, it has been hypothesized that the partitioning of C_4 and other photosynthetic enzymes between the two chloroplast types may be mediated by a selective protein import mechanism (Offermann et al., 2011b).

All C_4 enzymes, similar to the majority of plastid proteins, are nuclear-encoded, translated in the cytosol, and post-translationally imported into the plastids under the guidance of the N-terminal transit peptides. The translocation of precursor proteins (preproteins) across the outer and inner membranes are mediated by the Translocons at the outer envelope membrane of chloroplasts (Toc) and the Translocons at the inner envelope membrane of chloroplasts (Tic), respectively (for recent reviews, see Inaba and Schnell, 2008; Jarvis, 2008). Among the many characterized components of the Toc and Tic complexes, Toc159 and Toc34 are the two homologous receptors which act in concert to coordinate initial preprotein recognition. Both receptors contain a GTPase domain (G-domain) projected into the cytosol and a C-terminal domain (M-domain) for membrane integration (Hirsch et al., 1994; Kessler et al., 1994; Schnell et al., 1994; Seedorf et al., 1995). While Toc34 is anchored by a single transmembrane α-helix (Kessler et al., 1994; Li and Chen, 1997), Toc159 does not have any hydrophobic cluster and partitions equally between the cytosolic and envelope-bound forms (Hiltbrunner et al., 2001; Ivanova et al., 2004). In addition to the G- and M-domains, Toc159 has an additional acidic domain (A-domain) at the N-terminus, which was recently found to be intrinsically unstructured (Richardson et al., 2009). The high variability of the N-terminal sequences implicates the substrate selectivity of Toc159 receptors (Inoue et al., 2010). Earlier works have also indicated the direct cross-linking of Toc159 with preproteins during the

formation of early import intermediates (Perry and Keegstra, 1994; Ma et al., 1996), which could be inhibited by Toc159 antibodies (Hirsch et al. 1994). Accordingly, the current "targeting" model is centered around Toc159 being the primary preprotein receptor (Smith, 2006). A contradictory model termed "motor model" challenged the existence of soluble Toc159 (Becker et al, 2004) and proposed that Toc34 is the primary preprotein receptor and Toc159 is a GTP-driven motor for preprotein translocation through the Toc75 channel (Sveshnikova et al., 2000; Schleiff et al., 2003b and 2003c). At the same time as the two competing models were being proposed, molecular genetics (Jarvis et al., 1998; Bauer, et al., 2000; Kubis et al., 2003; Constan et al., 2004; Ivanova et al., 2004; Kubis et al., 2004) and biochemical evidence (Ivanova et al., 2004; Smith et al., 2004) suggested that the multiple isoforms of Toc159 and Toc34 might specifically associate into Toc complexes of different substrate selectivities in *A. thaliana*. In this regard, the combination of AtToc159 and AtToc33 favors the translocation of photosynthetic proteins whilst the combination of AtToc120/132 subgroup and AtToc34 is specific for housekeeping proteins (for review, see Bédard and Jarvis, 2005), although a recent proteomics analysis of the *AtToc159* knockout mutants suggested that the definition of Toc159-specific substrates has been over-simplified (Bischof et al., 2011).

As a first initiative to study the chloroplast preprotein import machinery in a single-cell C_4 species, I identified cDNA sequences encoding two Toc159 isoforms and one Toc34 protein, of which the homology with the well-characterized counterparts in pea and *Arabidopsis* was deduced from the phylogenetic trees and the characteristic properties of domain structures. Multiple approaches consistently demonstrated the distinctive subcellular localization

patterns of BsToc159/132 and BsToc34. Together with the evidence of Toc159 interaction with actin filaments and microtubules, I propose that Toc159 traffics to and from the chloroplasts for preprotein targeting with the assistance of the cytoskeleton.

5.3 Results

5.3.1 Identification of cDNA sequences encoding the Toc receptors

As a first step toward understanding chloroplast protein import in the single-cell C_4 species, I identified the cDNA sequences encoding the homologues of the two chloroplast preprotein receptor families, Toc159 and Toc34, in *B. sinuspersici*. Earlier studies of preprotein recognition at the chloroplast envelope have focused on the Toc components in *P. sativum* (Hirsch et al., 1994; Kessler et al., 1994; Schnell et al., 1994). More recent research was also based on the orthologues from *A. thaliana* (Li and Chen, 1997; Bölter et al., 1998; Jarvis et al., 1998; Bauer et al., 2000) and on two *Spinacia oleracea* Toc34 isoforms (Voigt et al., 2005). To date, the identity of Toc receptor components in other plant species has not been studied. By conducting a BLASTp search using the primary sequences of *P. sativum* Toc159 and Toc34 as query, I retrieved homologous sequences of the two protein families from various plant species, designed gene-specific primers based on the conserved regions from nucleotide sequence alignments, and successfully cloned full-length cDNAs that encode two Toc159 homologues and one Toc34 homologue. Phylogenetic analyses of their deduced amino acid sequences indicated their similarities with other putative and demonstrated Toc159 (Figure 5.1) and Toc34 (Figure 5.2) proteins.

Similar to other reported Toc159 sequences, the tripartite structure which comprises an N-terminal A-domain, a central G-domain and a C-terminal M-domain is conserved in the two *B. sinuspersici* Toc159 homologues (Figure 5.1). The G-domains are highly conserved in both Toc159 (Figure 5.3A) and Toc34 (Figure 5.3B) homologues, with the maximum

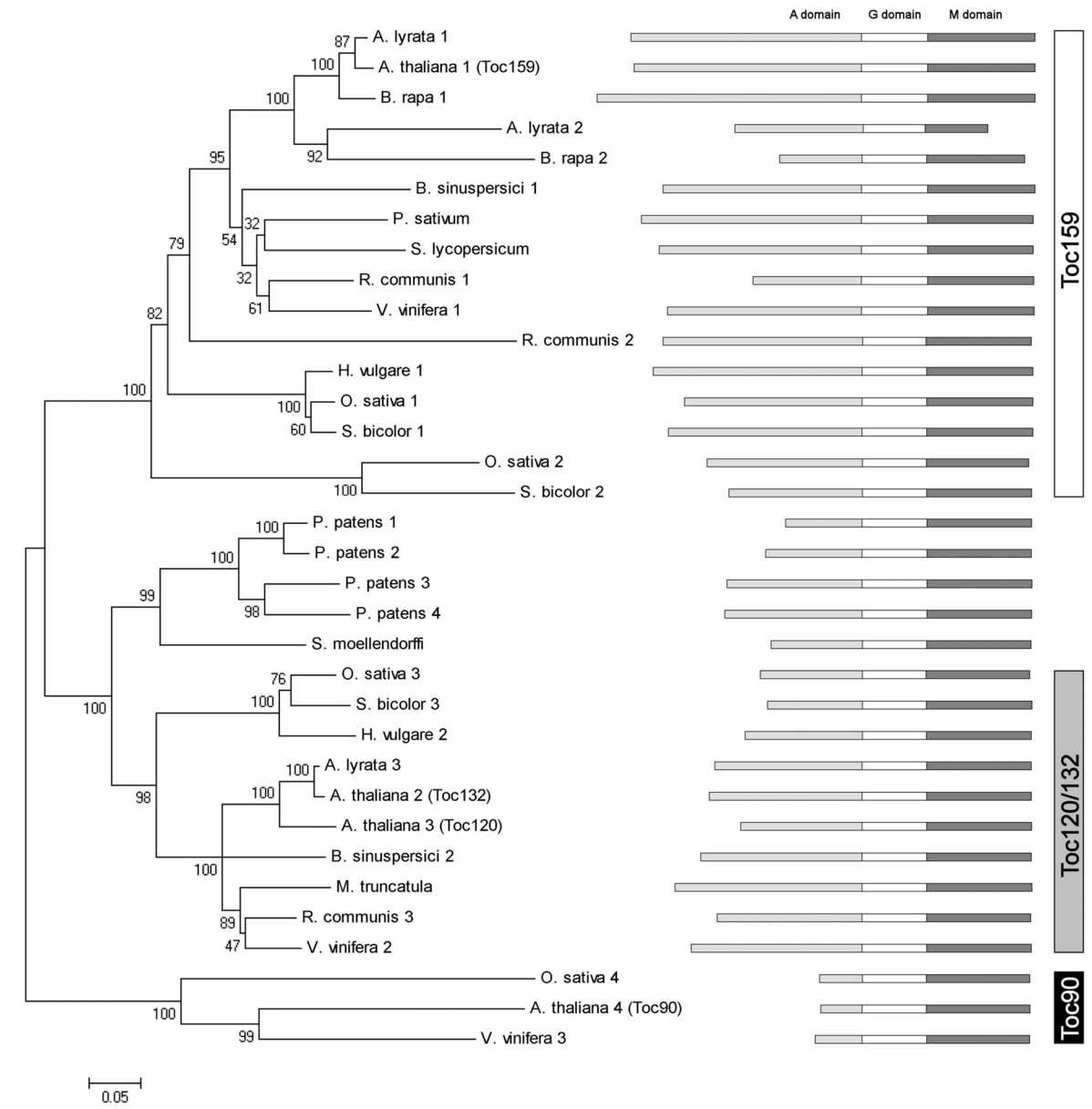

Figure 5.1

Figure legend on the next page

Figure 5.1 Phylogenetic analysis of putative and reported Toc159 homologues

A neighbor-joining tree of Toc159 homologues was constructed using the MEGA v5.05 program after sequence alignment with the ClustalW algorithm. The bootstrap values with 2,000 repetitions (%) are given at the respective nodes. The distance scale (substitutions per site) is shown in the bottom-left corner. The deduced amino acid sequences of Toc159 homologues were retrieved using BLASTp search. GenBank/EMBL accession numbers are shown in parentheses: *Arabidopsis lyrata* 1 (XP_002874910), *A. lyrata* 2 (XP_002874913), *A. lyrata* 3 (EFH62320), *A. thaliana* 1 (AC002330), *A. thaliana* 2 (AC005825), *A. thaliana* 3 (AB022217), *A. thaliana* 4 (AF296825), *Brassica rapa* 1 (AC232397), *B. rapa* 2 (AC232399), *Bienertia sinuspersici* 1 (JQ739199), *B. sinuspersici* 2 (JQ739200), *Hordeum vulgare* 1 (AK371279), *H. vulgare* 2 (AK367377), *Medicago truncatula* (AC147010), *Oryza sativa* 1 (AK102924), *O. sativa* 2 (AC092557), *O. sativa* 3 (AC020666), *O. sativa* 4 (AK241335), *Physcomitrella patens* 1 (XP_001770227), *P. patens* 2 (XP_001771331), *P. patens* 3 (AY496562), *P. patens* 4 (XP_001770228), *Pisum sativum* (AF262939), *Ricinus communis* 1 (XP_002531885), *R. communis* 2 (XP_002516922), *R. communis* 3 (XP_002528280), *Sorghum bicolor* 1 (XP_002440611), *S. bicolor* 2 (XP_002466147), *S. bicolor* 3 (XP_002464976), *Solanum lycopersicum* (EF647601), *Selaginella moellendorffi* (XP_002969262), *Vitis vinifera* 1 (AM485197), *V. vinifera* 2 (AM433085), *V. vinifera* 3 (AM431847).

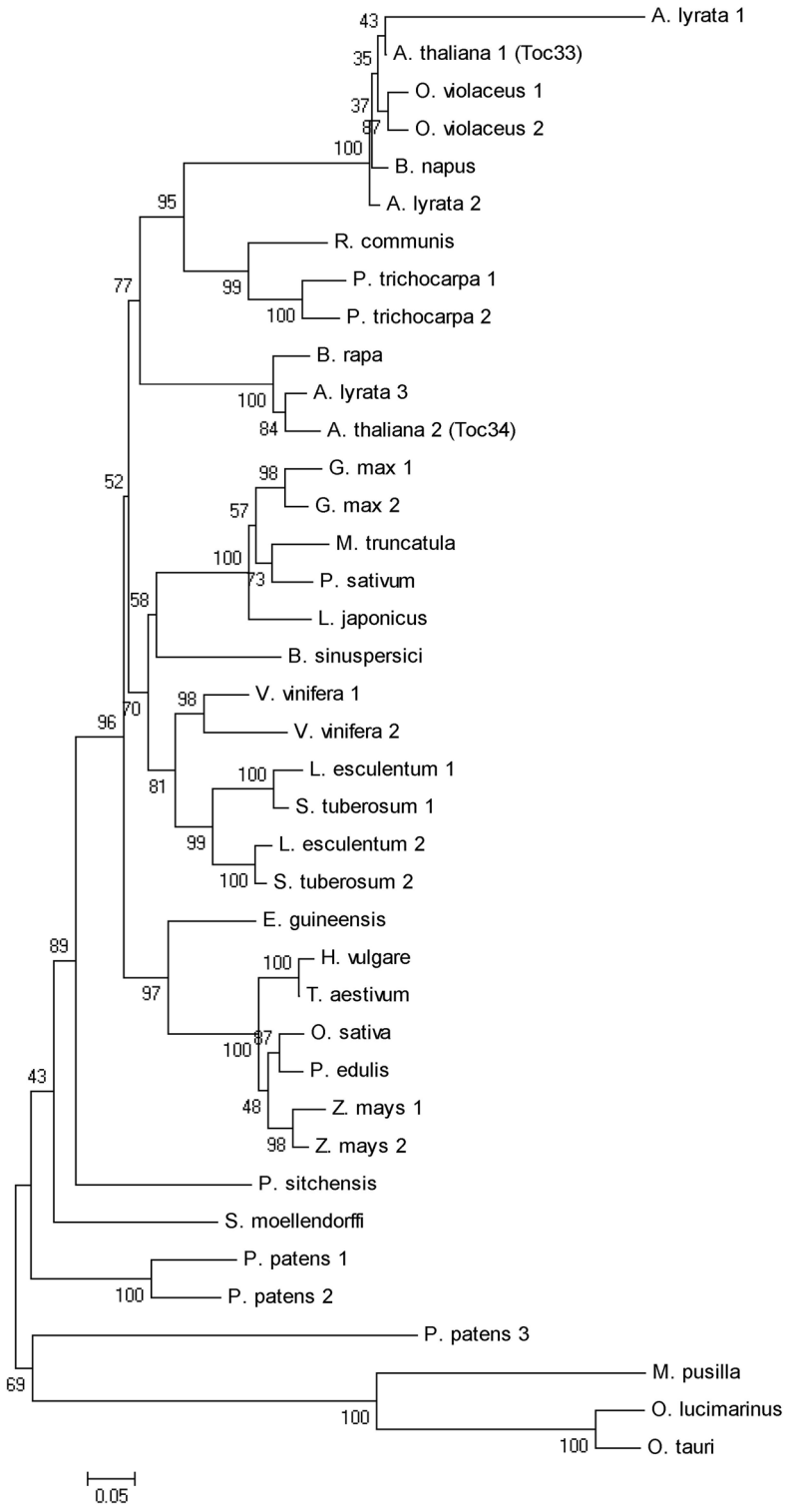

Figure 5.2

Figure legend on the next page

Figure 5.2 Phylogenetic analysis of putative and reported Toc34 homologues

A neighbor-joining tree of Toc34 homologues was constructed using the MEGA v5.05 program after sequence alignment with the ClustalW algorithm. The bootstrap values with 2,000 repetitions (%) are given at the respective nodes. The distance scale (substitutions per site) is shown in the bottom-left corner. The deduced amino acid sequences of Toc34 homologues were retrieved using BLASTp search. GenBank/EMBL accession numbers are shown in parentheses: *Arabidopsis lyrata* 1 (EFH58416), *A. lyrata* 2 (EFH68356), *A. lyrata* 3 (EFH49440), *A. thaliana* 1 (AJ010724), *A. thaliana* 2 (AJ132696), *Brassica napus* (AY332619), *B. rapa* (AC241048), *Bienertia sinuspersici* (JQ739201), *Elaeis guineensis* (EU285007), *Glycine max* 1 (BT093351), *G. max* 2 (BT099332), *Hordeum vulgare* (AK250670), *Lycopersicon esculentum* 1 (BT014489), *L. esculentum* 2 (BT013079), *L. japonicus* (AK338584), *Micromonas pusilla* (EEH61060), *Medicago truncatula* (AC149134), *Ostreococcus lucimarinus* (XP_001417009), *O. tauri* (CR954203), *Oryza sativa* (AK058676), *Orychophragmus violaceus* 1 (AF517947), *O. violaceus* 2 (AF517946), *Phyllostachys edulis* (FP093113), *Physcomitrella patens* 1 (AY496559), *P. patens* 2 (AY496561), *P. patens* 3 (AY496560), *Pisum sativum* (Q41009), *Picea sitchensis* (BT071210), *Populus trichocarpa* 1 (EEE81964), *P. trichocarpa* 2 (EEE99235), *Ricinus communis* (XP_002515131), *Selaginella moellendorffi* (GL377661), *Solanum tuberosum* 1 (DQ228327), *S. tuberosum* 2 (DQ191646), *Triticum aestivum* (AK331804), *Vitis vinifera* 1 (XP_002274573), *V. vinifera* 2 (XP_002278775), *Zea mays* 1 (AJ245968), *Z. mays* 2 (AJ271049).

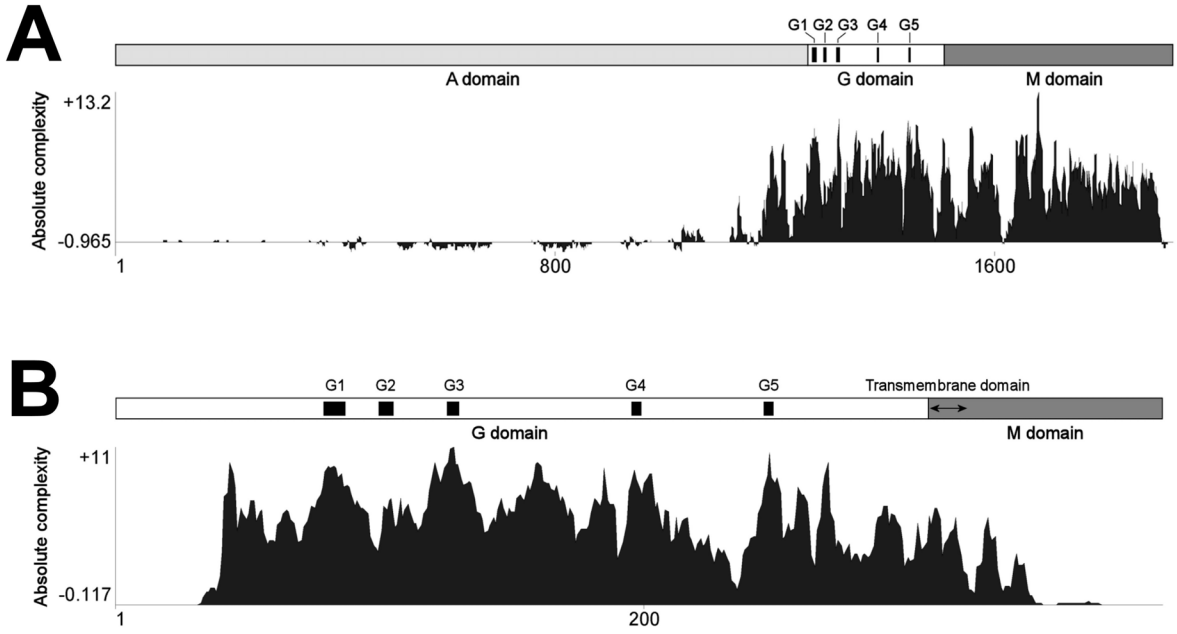

Figure 5.3 Absolute complexity plots of aligned Toc159 and Toc34 sequences

The absolute complexity indicates the average of pairwise alignment scores of each residue as computed using the AlignX module of Vector NTI Advance^{TM} 10.3.0 (Invitrogen) with the substitution matrix blosum62mt2. A more positive value indicates a higher degree of conservation. The positions of the conserved motifs G1-G5 of the GTPase superfamily and the transmembrane α-helix of Toc34 are indicated.

(A) An absolute complexity plot of Toc159 homologues.
(B) An absolute complexity plot of Toc34 homologues.

similarities within the G1, G3, G4 and G5 motifs typically found in the GTPase superfamily (Sun et al., 2002). The M-domains of Toc159 homologues are also conserved in the plant kingdom, although the physiological relevance of these domains is unknown (Figure 5.3A). Despite the lack of predictable membrane-spanning structures, the C-terminal regions of Toc159 are commonly termed "membrane anchors" solely due to their protease resistance, which implies their embedment in the outer membrane. In fact, the amino acid sequence alignment of Toc159 and Toc34 homologues shows that the transmembrane regions of Toc34 are partly substituted by less hydrophobic residues in the sequences of Toc159 (Figure 5.4).

The A-domains of Toc159 homologues are highly variable in length (Figure 5.1) and amino acid composition (Figure 5.3A) intra- and inter-specifically, correlating with the fact that this domain is fully dispensable (Lee et al., 2003), and plays an accessory role in regulating the substrate selectivity of the receptor (Inoue et al., 2010). The concept of preprotein specificity of the Toc159 receptors has arisen from the molecular genetics analysis of *A. thaliana* knockout mutants (Bauer, et al., 2000; Ivanova et al., 2004; Kubis et al., 2004) and *in vitro* binding studies (Smith et al., 2004), suggesting that the AtToc159 orthologue is specific for more abundant photosynthetic preproteins whereas AtToc132 and AtToc120 orthologues are functionally redundant for targeting non-photosynthetic, housekeeping preproteins. For an unknown physiological significance, the major isoforms of Toc159 also exhibit large blocks of protein tandem repeats in the A-domains (Figure 5.5), which are exemplified by eight imperfect homo-repeats of a 24-residue sequence in *P. sativum* (Chen et al., 2000) and four homo-repeats of a 47-residue sequence with less perfection in *A. thaliana* (Bölter et al.,

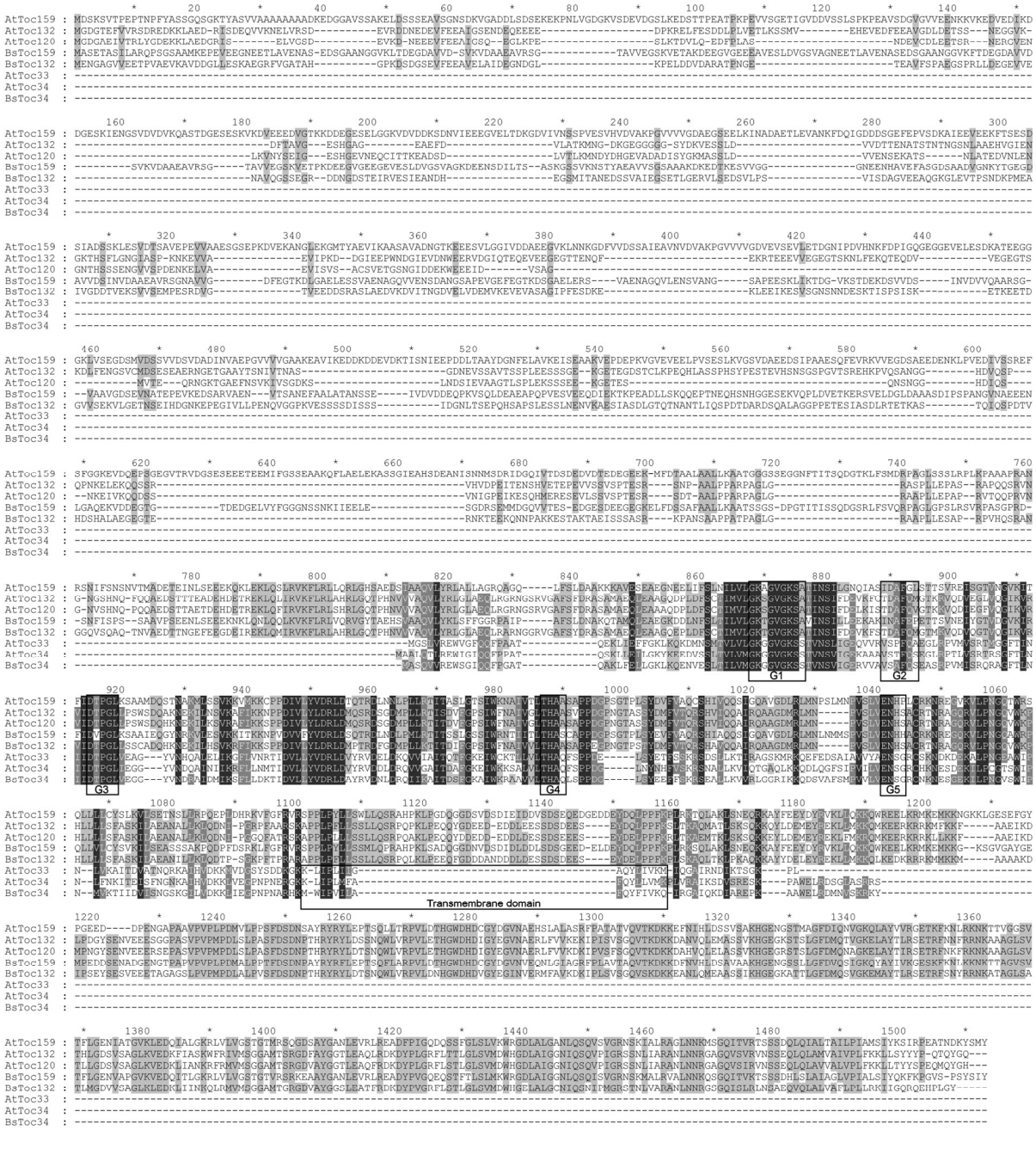

Figure 5.4

Figure legend on the next page

Figure 5.4 Deduced amino acid sequence alignment of Toc159 and Toc34 homologues from *B. sinuspersici* and *A. thaliana*

Alignment was performed using ClustalW v1.83 formatted in Genedoc (Multiple Sequence Alignment Editor and Shading Utility v2.6). The residues blocked with a white foreground on a black background are 100% conserved bases, residues with a white foreground on a dark grey background are 75% or more conserved bases, and residues aligned with a black foreground on a light grey background are 50-74% conserved bases. Conserved motifs of the GTPase superfamily and predicted transmembrane domains, if any, are boxed.

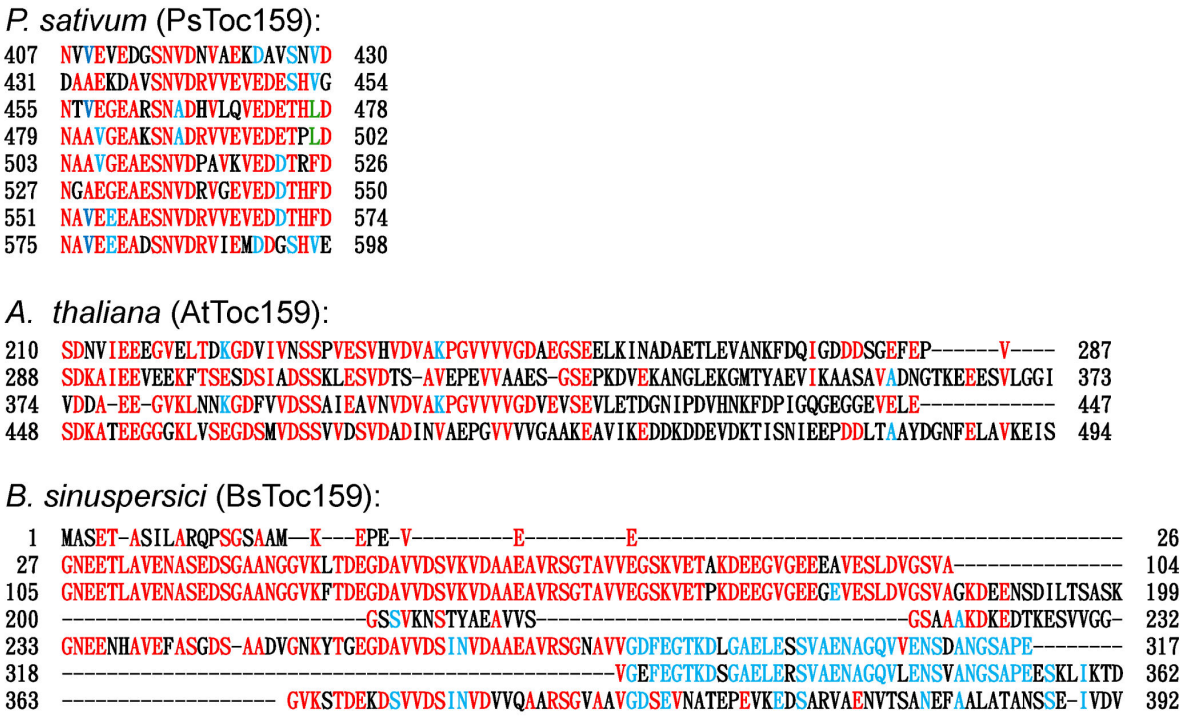

Figure 5.5 Alignment of tandem repeats in the A-domains of Toc159 homologues

The numbers to the left and right indicate the amino acid positions of the deduced Toc159 sequences. The tandem repeats are aligned vertically and the identical residues in the same column are shown in the same colors. Tandem repeats in the A-domains of PsToc159 (Chen et al., 2000) and AtToc159 (Bölter et al., 1998) have been previously reported.

1998). Similarly, from the deduced amino acid sequence of *B. sinuspersici* Toc159, a long stretch of sequence up to 79 residues has been found to be recurring, and a block of shorter repeats was also identified (Figure 5.5).

Pairwise homology comparison of the Toc159 sequences indicates that the two *B. sinuspersici* homologues share substantial identities with AtToc159 and AtToc132, respectively (Table 5.1). Thus, the two identified proteins in the present study have been named "BsToc159" and "BsToc132". While the present study confirmed the expression of multiple Toc159 isoforms in a plant species other than *A. thaliana*, the selectivity of Toc159 isoforms for specific subsets of preproteins is predicted to be universal in higher plants as the phylogenetic tree illustrates that multiple sequences retrieved from the same species separate into the "Toc159" clade and the "Toc120/132" clade, respectively (Figure 5.1). The two *A. thaliana* Toc34 isoforms (AtToc33 and AtToc34), on the other hand, fall into the same clade (Figure 5.2).

5.3.2 Protein expression profiles of Toc159 and Toc34

To confirm that the two identified Toc159 homologues are transcriptionally active for protein expression in *B. sinuspersici*, isoform-specific antibodies were raised against purified recombinant proteins of the highly variable A-domain regions at the N-termini (Appendix IV), which did not have any significant similarity found in PSI-BLAST. Western blot analysis detected immunoreactive bands of both Toc159 isoforms in crude leaf extracts of *B. sinuspersici* (Figure 5.6). The migration of BsToc159 and BsToc132 proteins during SDS-PAGE deviated from their theoretical molecular weights of 148 and 134 kDa, respectively

Table 5.1 Pairwise homology comparison of *B. sinuspersici* and *A. thaliana* Toc159 Isoforms

Isoform	Domain	Percentage of identical positions (%)					
		BsToc159	**BsToc132**	**AtToc159**	**AtToc132**	**AtToc120**	**AtToc90**
BsToc159	A domain	-	19.9	**25.5**	18.7	13.6	5.3
	G domain	-	57.1	**74.1**	55.5	55.9	44.0
	M domain	-	46.0	**72.2**	49.0	47.0	32.8
BsToc132	A domain	19.9	-	17.7	**30.0**	26.6	6.6
	G domain	57.1	-	59.1	**85.5**	85.1	50.0
	M domain	46.0	-	46.0	71.5	**71.6**	34.3

Protein sequence alignment was performed using the Align X program of Vector NTI Advance™ 10.3.0 (Invitrogen). The highest identities are showed in bold.

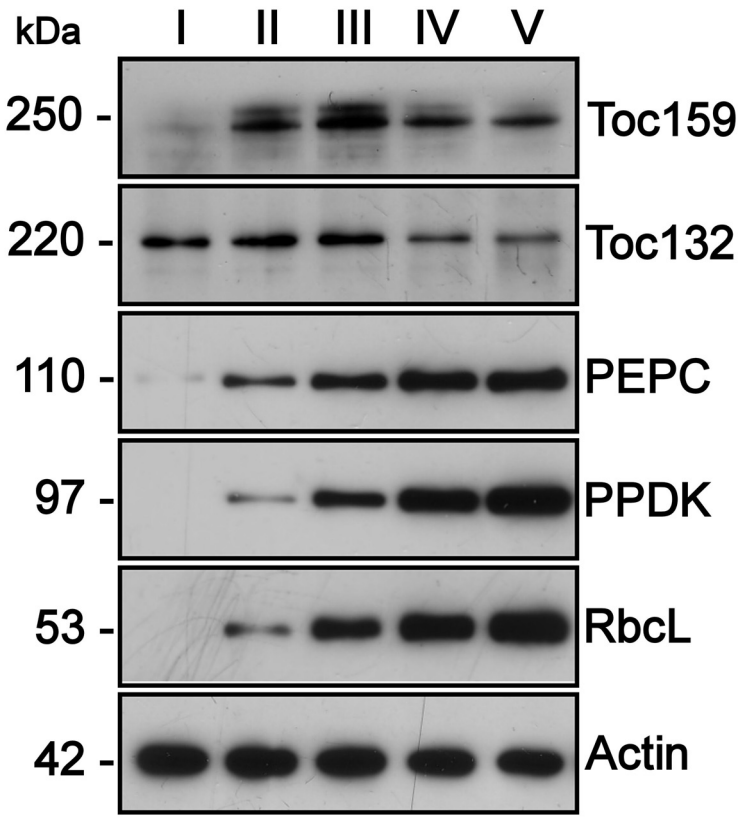

Figure 5.6 Expression profiles of Toc159 homologues and other proteins at different stages of leaf development in *B. sinuspersici*

For Western blot analysis, an equal amount (5 or 10 μg) of total proteins per lane was loaded for the same antibody used. Crude protein extracts were obtained from leaves of various lengths at stage I (<1 mm), stage II (2-3 mm), stage III (5-6 mm), stage IV (10-12 mm) and stage V (>20 mm). Numbers to the left indicate the positions of marker proteins in kilodaltons. PEPC, phosphoenolpyruvate carboxylase; PPDK, pyruvate orthophosphate dikinase; RbcL, Rubisco large-subunit.

(Figure 5.6). Similarly, the recombinant A-domains which were used for antibody production also exhibited unexpectedly low electrophoretic mobility. However, the identities of these pure *E. coli*-expressed proteins were confirmed by tandem mass spectrometry-based sequencing (Appendix V). Similar aberrant electrophoretic migration of A-domains (Richardson et al., 2009) and full-length proteins of Toc159 (Chen et al., 2000; Lee et al., 2003) has been attributed to their high acidity. The abundance of acidic residues might also account for the weak affinities of the A-domains to the immobilized metal affinity columns, as revealed by the elution of these proteins with relatively low concentrations of imidazole (Appendix VI).

Comparison of BsToc159 and BsToc132 protein amounts at different developmental stages of leaves revealed their different expression profiles in relation to their respective functions. The leaf primordia at the earliest developmental stage (stage I) contained proplastids that had not yet expressed the Rubisco large-subunit or imported photosynthetic enzymes such as pyruvate orthophosphate dikinase (Figure 5.6). BsToc132 was abundant at this stage, whereas BsToc159 was undetectable (Figure 5.6). A drastic increase in BsToc159 was observed at stages II and III when chloroplasts are actively accumulating photosynthetic enzymes whilst the amount of BsToc132 remained steady (Figure 5.6). Basal levels of both BsToc159 and BsToc132 were maintained at stages IV and V when leaves are primarily composed of mature chloroplasts (Figure 5.6). Thus, the expression profiles confirmed previous observations in *A. thaliana* that Toc159 and Toc132 exhibit substrate specificities for photosynthetic and housekeeping proteins, respectively (Bauer et al., 2000).

5.3.3 Distinctive subcellular localization patterns of Toc159 and Toc34

Since Toc159 and Toc34 have distinctive functions in both *P. sativum* and *A. thaliana*, I asked whether the homologues have different subcellular localization in *B. sinuspersici*. Immunogold micrographs revealed that the endogenous Toc34 proteins strictly reside at the chloroplast envelope (Figure 5.7), in agreement with the presence of a putative transmembrane α-helix in the Toc34 sequence (Figure 5.4). In addition to the localization of BsToc159 and BsToc132 to the chloroplast envelope, gold particles were approximately equally abundant in the inter-chloroplastic space (Figure 5.7). This observation is consistent with the previous subcellular localization studies showing that endogenous Toc159 or N-terminally truncated Toc159 fused to EGFP were localized to the intervening space between chloroplasts in *A. thaliana* (Hiltbrunner et al., 2001; Bauer et al., 2002). The presence of both soluble and membrane-associated forms of endogenous BsToc159 and BsToc132 was confirmed by Western blot analysis (Figure 5.8A). Densitometric analysis of the immunoreactive bands indicated that ca. 40% of both receptors were found in the soluble fractions (Figure 5.8B). Similar values of relative abundance were obtained from quantitative analysis of gold particles (Figure 5.8B).

To further support the notion that Toc159 is a soluble receptor that partitions between the cytosol and chloroplast envelopes, I confirmed the immunogold localization and immunoblotting data by transient expression of EGFP-tagged full-length Toc receptors in *B. sinuspersici* leaf-derived protoplasts (Figure 5.9). Confocal laser scanning microscopy revealed fluorescent signals of EGFP-BsToc159 and EGFP-BsToc132 in the intervening space between chloroplasts (Figure 5.9). The ring-like fluorescent signals of EGFP-BsToc34

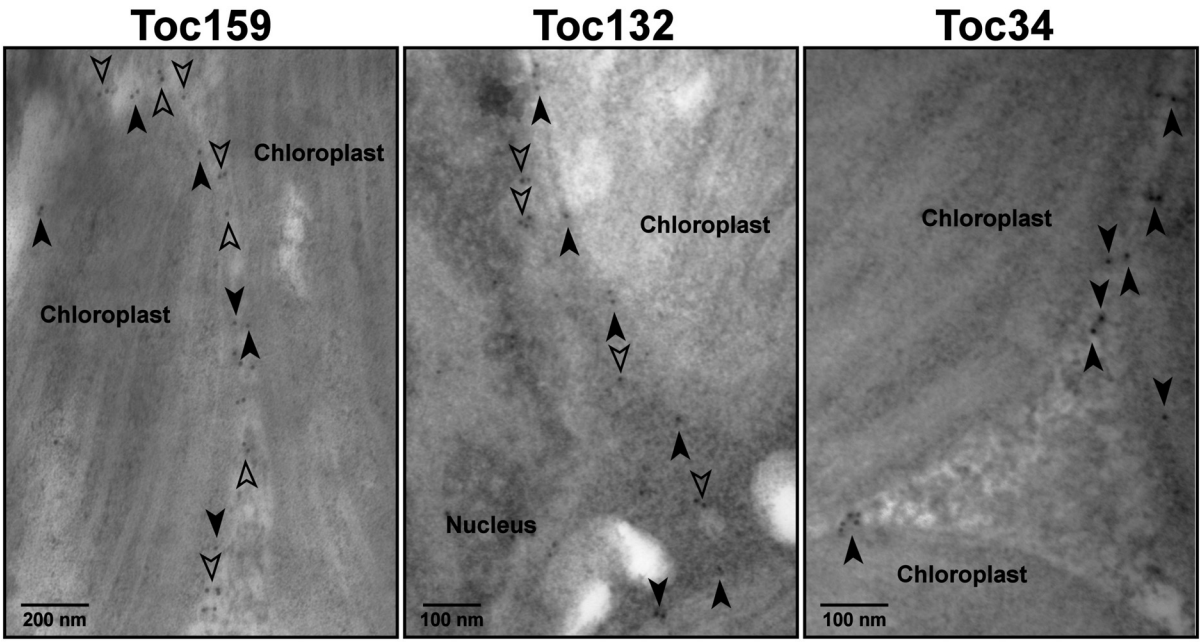

Figure 5.7 Immunogold localization of Toc159, Toc132 and Toc34 in mature leaves of *B. sinuspersici*

Immunogold labelling of mature leaves (>20 mm in length) was performed using isoform-specific antibodies against BsToc159 and BsToc132, and a commercial Toc34 antibody. Solid arrowheads indicate gold particles on the chloroplast envelopes, and open arrowheads indicate other gold particles in the inter-chloroplastic space.

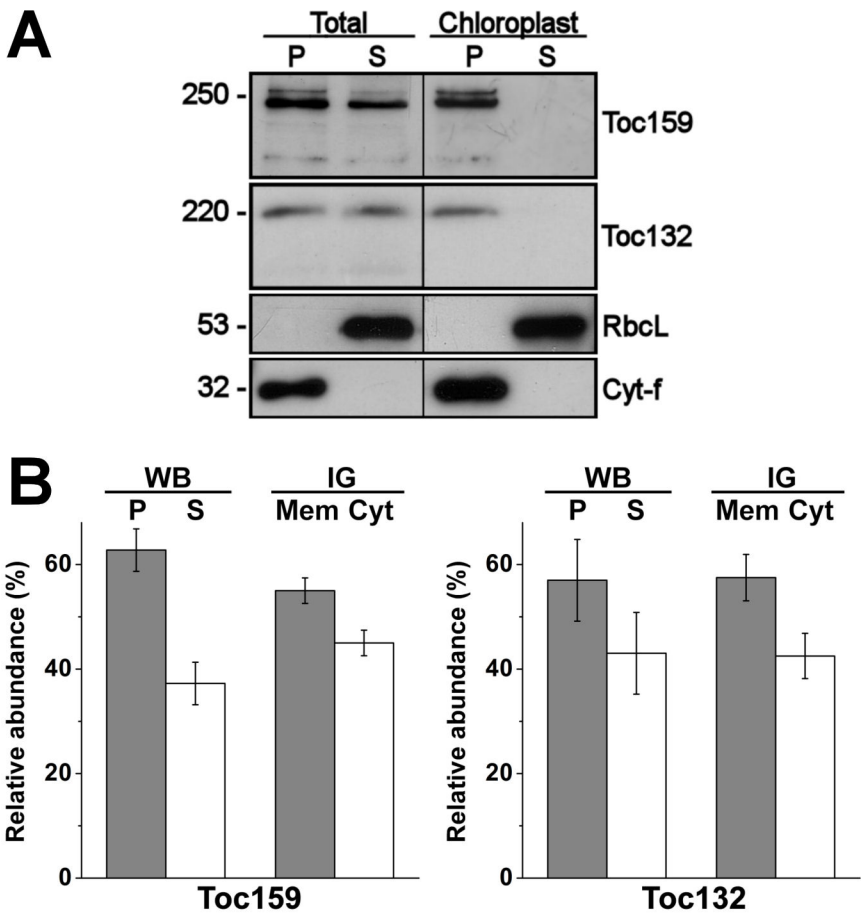

Figure 5.8 Relative abundance of endogenous Toc159 and Toc132 in insoluble and soluble fractions

(A) Western blot analysis of endogenous Toc159 and Toc132 in subcellular fractions. The total protoplasts or purified chloroplasts were subfractionated into the pellet (P) and soluble (S) fractions. Detection with antibodies against Rubisco large-subunit (RbcL) and cytochrome-f (Cyt-f) served as loading controls for the S and P fractions, respectively. Numbers to the left indicate the positions of marker proteins in kilodaltons.

(B) Relative abundance of endogenous Toc159 and Toc132. From Western blot analysis (WB), immunoreactive bands of the pellet (P) and soluble (S) fractions of the total protoplast extracts were analyzed by densitometric quantification. From immunogold localization (IG), the relative abundance of gold particles was determined by counting the number of membrane-associated (Mem) and cytosolic (Cyt) gold particles. All values are the mean of three replicates (±SE).

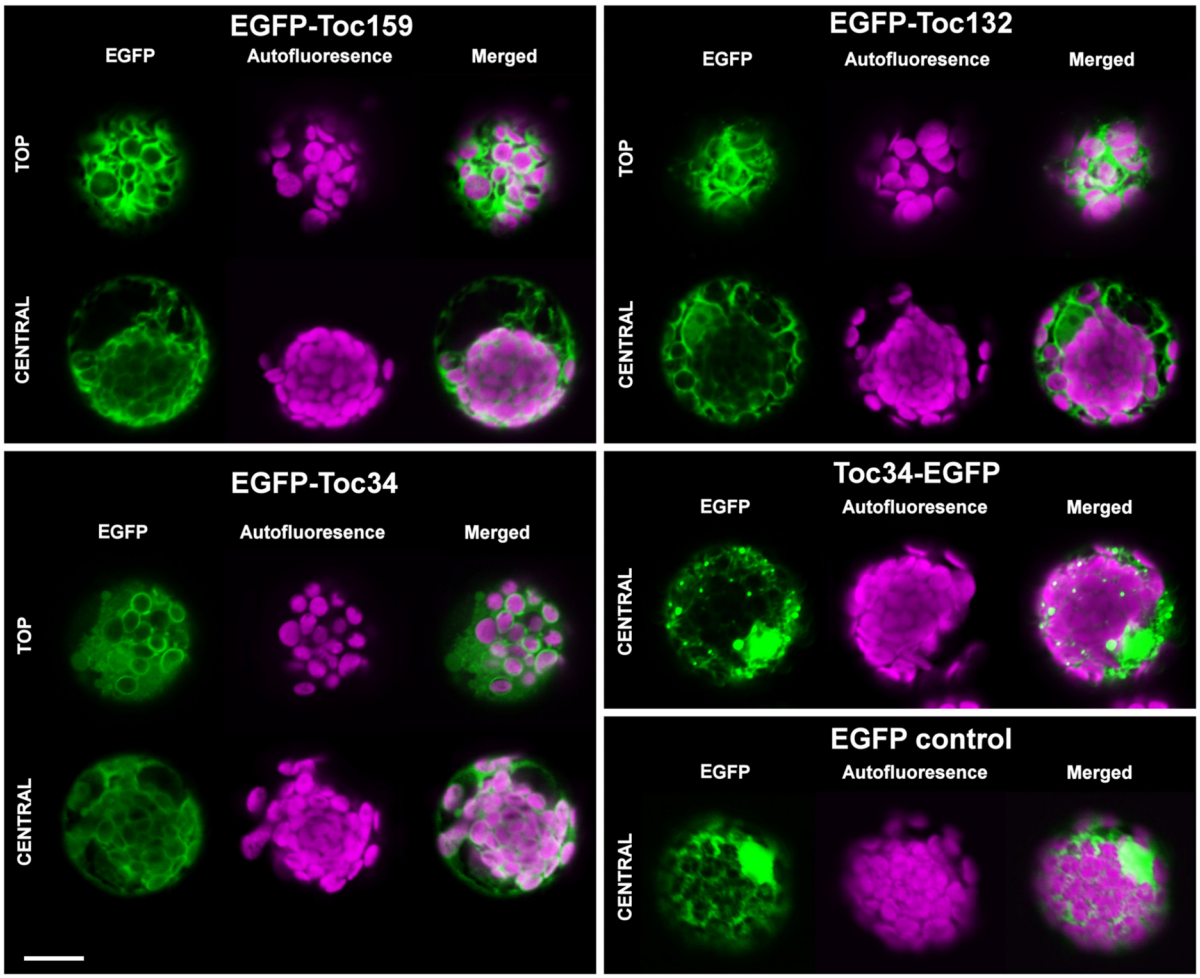

Figure 5.9 Transient expression of EGFP fusion proteins with Toc159, Toc132 and Toc34 in isolated *B. sinuspersici* chlorenchyma protoplasts

Entire Toc proteins were fused to the C-terminus of EGFP (i.e. EGFP-Toc159, EGFP-Toc132 and EGFP-Toc34) or the N-terminus of EGFP (i.e. Toc34-EGFP) for constitutive 35S-driven expression following PEG-mediated transfection of isolated protoplasts. Representative images showing central and/or top focal planes of EGFP fluorescence, chlorophyll autofluorescence and a merge of the two channels are shown. Scale bar = 10 µm.

(Figure 5.9), on the other hand, appeared similar to the immuolabelled fluorescent signals of Toc34 (Dhanoa et al., 2010) and Toc75 (Hiltbrunner et al., 2001), both of which are integral Toc components of the outer chloroplast membrane. Fusion of BsToc34 at the N-terminus of EGFP (i.e. BsToc34-EGFP), however, produced punctate structures of variable sizes (Figure 5.9). Since the C-terminal transmembrane domain of Toc34 and its flanking sequences contain important sorting information and the protein is integrated into the outer chloroplast membrane with an N_{out}-C_{in} topology (Qbadou et al., 2003; Dhanoa et al., 2010), the addition of a bulky tag (i.e. 27 kDa) to the C-terminus might result in mistargeting of the fusion protein and formation of insoluble aggregates. Fusion constructs of BsToc159 and BsToc132 with a C-terminal EGFP (i.e. BsToc159-EGFP and BsToc132-EGFP) did not produce any fluorescent signal in either *B. sinuspersici* or *A. thaliana* protoplasts in repeated experiments using different sequencing-verified clones. Concomitantly, the negative results from Western blot analysis of the transfected protoplasts indicated the absence of EGFP fusion proteins and ruled out the possibility of signal abolishment simply due to protein misfolding. Since the chloroplast-targeting signals of BsToc159 and BsToc132 are embedded at the C-terminal ends (see Chapter 6), I speculated that the addition of a sizable protein (i.e. 27 kDa) at the C-terminus might mask the sorting information, leading to the mislocalization of the BsToc159 and BsToc132 fusion proteins. The mistargeted proteins might therefore be turned over in the proteasome-mediated degradation pathway, which might also account for the absence of EGFP signals in immunoblots.

In addition, biolistic bombardment of onion epidermal cells with the EGFP-BsToc159 and EGFP-BsToc132 constructs resulted in diffuse fluorescent signals indistinguishable from that

of the EGFP null vector, whereas EGFP-Toc34 labelled punctate and occasionally elongated structures (Figure 5.10). A construct of ferredoxin TP fusion with EGFP produced similar punctate structures with elongated extensions that resembled stromules (Figure 5.10 inset).

Taken together, the distinctive subcellular localization patterns of the Toc receptors as revealed by multiple approaches suggest that Toc34 is solely a chloroplast envelope-associated protein, whereas the two Toc159 isoforms also exist as non-membrane-associated, soluble receptors. It is thus likely that the targeting of Toc159 to the chloroplast envelope is mediated by a pathway different from that of the tail-anchored proteins (e.g. Toc34), although some sorting information might similarly reside at the C-terminus of Toc159.

5.3.4 Association of Toc159 receptors with the cytoskeleton

Since immunogold localization studies revealed that considerable signals of BsToc159 and BsToc132 were not localized to the chloroplast membrane but confined within the inter-chloroplastic space in close proximity to the envelope (Figure 5.7), I continued to investigate the nature of this association. First, to determine if the non-membrane-associated form of Toc159 was truly soluble under physiological conditions, protoplast lysates were sub-fractionated in protoplast-culturing medium by differential speed centrifugation, and the various subcellular fractions were subjected to Western blot analysis using anti-BsToc159 and anti-BsToc132 antibodies (Figure 5.11A). In contrast to the solubilization of ca. 40% of both Toc159 isoforms upon high-salt (i.e. 500 mM NaCl) treatment (Figure 5.8), the sub-fractionation of protoplast lysates under milder conditions resulted in the majority of the proteins being associated with the 1,000*g* pellets (Figure 5.11A, upper panels). This

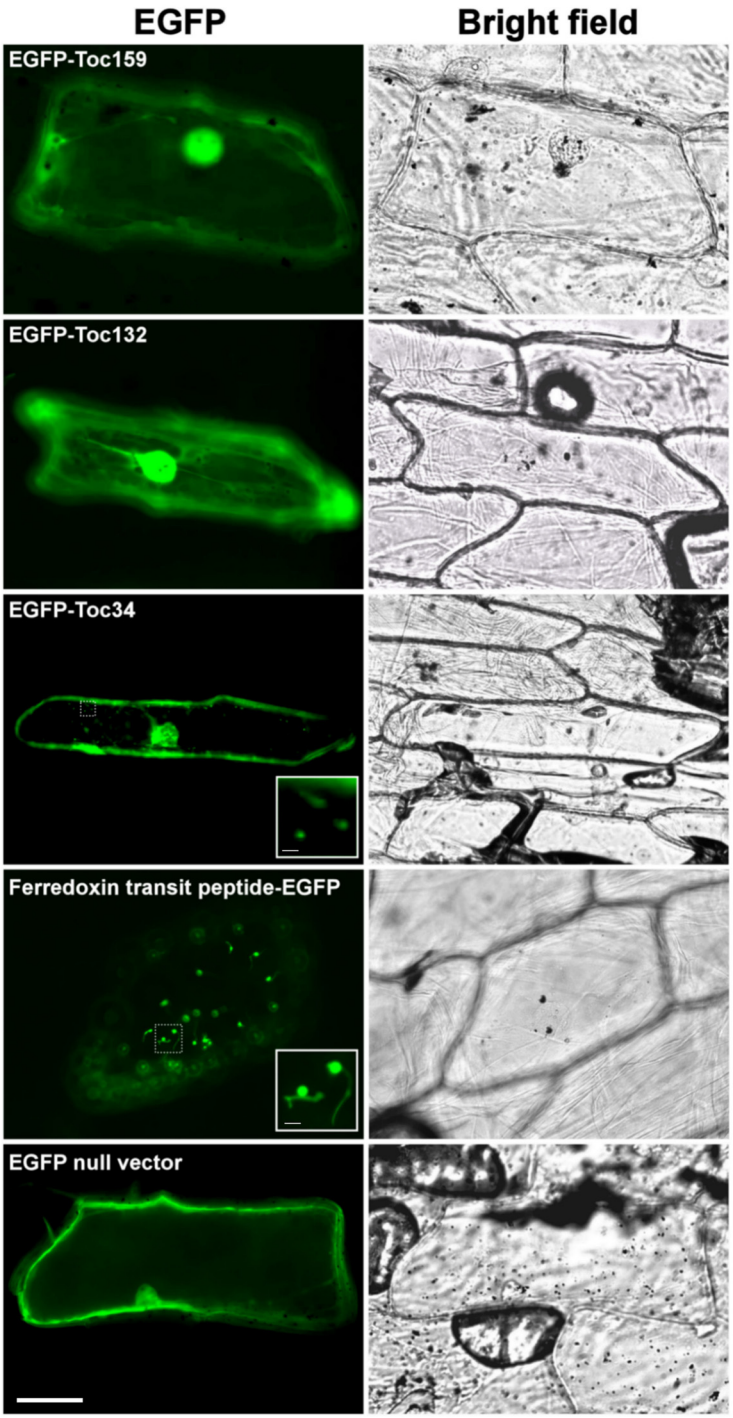

Figure 5.10 Transient expression of EGFP fusion proteins in onion epidermal cells

Entire Toc proteins were fused to the C-terminus of EGFP (i.e. EGFP-Toc159, EGFP-Toc132 and EGFP-Toc34) and the transit peptide of ferredoxin to the N-terminus of EGFP (i.e. Toc34-EGFP) for constitutive 35S-driven expression following biolistic bombardment of the expression constructs into onion epidermis. Scale bar = 40 μm or 10 μm (insets).

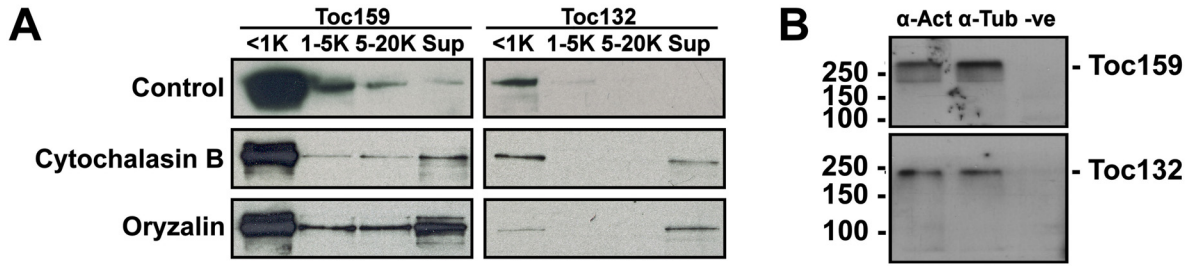

Figure 5.11 Association of BsToc159 and BsToc132 with the cytoskeleton

(A) Cytoskeleton-dissociating drug treatment of isolated protoplasts. Isolated *B. sinuspersici* chlorenchyma protoplasts were cultured overnight in the dark with 50 μM cytochalasin B (middle panels) or oryzalin (lower panels) or dimethyl sulfoxide only (upper panels). The treated protoplasts were lysed and sub-fractionated sequentially by differential speed centrifugation into 1,000*g* pellets (lane 1), 5,000*g* pellets (lane 2), 20,000*g* pellets (lane 3) and 20,000*g* supernatants (lane 4). The presence of BsToc159 and BsToc132 proteins in these fractions was detected by Western blot analysis with the respective antibodies.

(B) Co-immunoprecpitation of BsToc159 and BsToc132 with the cytoskeleton. Isolated chlorenchyma cells of *B. sinuspersici* were solubilized with a mild detergent, n-dodecyl maltoside, and the cell extracts were incubated with Protein-G-sepharose resin coupled to the anti-actin (lane 1) or anti-β-tubulin (lane 2) antibodies or without antibody (lane 3). The eluted proteins were subjected to Western blot analysis using the anti-BsToc159 and anti-Toc132 antibodies. Numbers to the left indicate the positions of marker proteins in kilodaltons.

observation suggested that the soluble form of Toc159 receptors might be associated with organelles or structures via ionic interaction with other proteins. In fact, Jouhet and Gray (2009a) have recently documented the *in vitro* interaction of Toc159 with actin filaments.

To confirm that the soluble form of Toc receptors is immobilized via interaction with the cytoskeleton *in planta*, the isolated *B. sinuspersici* chlorenchyma protoplasts were treated with the actin filament-dissociating drug, cytochalasin B, or the microtubule-dissociating drug, oryzalin, prior to the subfractionation experiments. Western blot analysis indicated that some signals of both Toc159 isoforms were "solubilized" after the treatment with cytochalasin B (Figure 5.11A, middle panels), and more prominently, with oryzalin (Figure 5.11A, lower panels). The co-immunoprecipitation of endogenous BsToc159 and BsToc132 from a crude cell extract with anti-actin or anti-β-tubulin antibodies further confirmed the association of Toc159 receptors with the cytoskeleton (Figure 5.11B).

5.4 Discussion

5.4.1 The conserved Toc receptors in single-cell C_4 species

The evolution of eukaryotic cells hinged on a sophisticated sorting mechanism to distribute newly synthesized proteins to their respective subcellular destinations. In plant cells, the acquisition of an additional endosymbiotic organelle and the massive transfer of genetic information from the endosymbiont to the host genomes added an extra level of complexity. While uncertainties and disagreements hold for the current chloroplast preprotein import models (Jarvis, 2008), the evolution of two distinct types of chloroplasts in terrestrial single-cell C_4 species poses further challenges for a thorough understanding of chloroplast biogenesis and differentiation at the biochemical level. The emerging evidence for signalling between the plastid and nuclear genomes (Nott et al., 2006) implies that the differential protein accumulation in dimorphic chloroplasts is not a single matter of concern during organelle differentiation, but rather a highly dynamic process throughout the lifetime of the plant. This notion implicates the existence of a differential protein import mechanism that accounts for the different subsets of proteins in the dimorphic chloroplasts. As a first step to aid future studies on the differential protein import hypothesis in the single-cell C_4 model, I sought to identify and characterize the preprotein import receptors at the chloroplast envelope in *B. sinuspersici*.

Two full-length Toc159-like cDNA sequences were identified in *B. sinuspersici*. Although their orthologies cannot be proven by computational methods (e.g. reciprocal BLAST search) because of the lack of genome sequence information from *B. sinuspersici* or its close

relatives, their homologies with current Toc159 orthologues are strongly supported by phylogenetic analysis (Figure 5.1), similarities in deduced amino acid sequences (Figure 5.3A and Table 5.1) and conservation of the signature tripartite structures of Toc159 (Figure 5.4). The separation of the two *B. sinuspersici* Toc159 isoforms into the "Toc159" and "Toc120/132" clades further suggests their functional similarities with the *A. thaliana* Toc159 homologues to mediate selective preprotein recognition (Figure 5.1). In fact, the protein expression profiles revealed that the protein expression of BsToc159 was up-regulated during the differentiation of proplastids into chloroplasts and remained at a high level during the further development of dimorphic chloroplasts, whereas the BsToc132 expression was maintained at a relatively steady level throughout the leaf development (Figure 5.6). These observations implicate the different substrate specificities of BsToc159 and BsToc132 for more abundant photosynthetic proteins and housekeeping proteins, respectively (Figure 5.6), as deduced from the previous molecular genetics and biochemical studies on *A. thaliana* Toc159 orthologues (Bauer et al., 2000; Ivanova et al., 2004; Kubis et al., 2004; Smith et al., 2004). Comparatively, the four moss (*Physcomitrella patens*) Toc159-like sequences were clustered into the same clade independent of the "Toc159" and "Toc120/132" clades in higher plants (Figure 5.1). In addition, the unicellular green (*Chlamydomonas reinhardtii*) and red (*Cyanidioschizon merolae*) algae apparently do not have multiple substrate-specific import pathways since their genomes only encode a single pair of Toc159 and Toc34 (Kalanon and McFadden, 2008). In spite of the exceptions in non-vascular plants and some other photosynthetic organisms, I showed that the evolution of *B. sinuspersici* in the C_4 lineage apparently has not altered the substrate-specific mechanism of preprotein recognition as elucidated in a C_3 species, *A. thaliana*.

5.4.2 The conserved tripartite structures of Toc159

Thorough analyses of the deduced amino acid sequences of BsToc159 and BsToc132 supported the presence of tripartite structures (i.e. A-, G- and M-domains) as observed in other Toc159 homologues (Figures 5.1, 5.3A, 5.4 and 5.5; Table 5.1). The conservation of GTPase motifs in the central G-domains is pertinent to their role in chloroplast preprotein import in terms of homotypic interaction with Toc34 (Smith et al., 2002a) and/or GTP-hydrolytic cycles for driving the preprotein translocation across the outer envelope (Schleiff et al., 2003b). Although the M-domain sequences are also conserved among the plant species, the physiological function of the M-domain has not been elucidated. As detailed in the next chapter, however, I showed that the C-terminal end in the M-domain contains important sorting information for the targeting of Toc159 to the chloroplast envelope.

Similar to other homologues in higher plants, the N-terminal regions (i.e. A-domains) of BsToc159 and BsToc132 exhibit a number of unusual properties, of which the physiological relevance is poorly understood due to the lack of knowledge regarding the function of the A-domains. First, the A-domains of both isoforms are highly variable in length and composition (Figures 5.1 and 5.3; Table 5.1), and characteristically enriched in acidic residues (one per 4.5 and 4.8 residues, respectively; Figure 5.4). In contrast, the genomes of unicellular green (*Chlamydomonas reinhardtii*) and red (*Cyanidioschizon merolae*) algae only encode a single Toc159 with an N-terminus not enriched in acidic residues (i.e. one per 8.4 and 7.1 residues, respectively; Kalanon and McFadden, 2008). In addition, the N-terminal sequence of the major isoform BsToc159, similar to PsToc159 and AtToc159, contains large blocks of

protein tandem repeats, although the number of repetitions and the degree of imperfections vary considerably among the homologues (Figure 5.5). While it has been estimated that half of the protein regions with tandem repeats are naturally unfolded (Tompa, 2003; Simon and Hancock, 2009), Richardson et al. (2009) have recently provided striking evidence that the A-domains of AtToc159 and AtToc132 are indeed intrinsically unstructured. Moreover, it has long been accepted that the A-domains are highly susceptible to proteolytic cleavage (Bölter et al., 1998), and the A-domains have also recently been found to be hyper-phosphorylated (Agne and Kessler, 2010). In an attempt to understand the physiological function of the A-domains, Inoue et al. (2010) complemented the *A. thaliana* Toc159 knock-out plants (*ppi2*) using mutant proteins of AtToc159 and AtToc132 with deleted and swapped A-domains, leading to the first evidence that the A-domains confer substrate selectivity of the receptors.

Taking together the unusual properties of the A-domains and the first insight into their function, it has recently been hypothesized that the substrate selectivity of the A-domains might be regulated by conformational changes (Inoue, 2011) and proteolytic cleavage upon phosphorylation (Agne and Kessler, 2010). Interestingly, my preliminary immunoblotting analysis of the purified dimorphic chloroplasts from *B. sinuspersici* suggested that the chloroplast envelope-associated form of BsToc159 might co-exist as various truncated versions, of which the molecular weights varied between the protein extracts from peripheral and central chloroplasts (data not shown). Unfortunately, this phenomenon could not be confirmed by the time of thesis submission due to the lack of plant materials. In the future, the multiple versions of BsToc159 can be affinity-purified individually from the protein

extracts of peripheral and central chloroplasts using the anti-BsToc159 antibody, and analyzed by tandem mass spectrometry for an explicit mapping of the proteolytic cleavage sites. Perhaps, the tandemly repeated sequences in the A-domain (Figure 5.5) might possibly account for the multiple cleavage events. Although the biological significance of the proteolytic cleavage is not known, considering the role of A-domains in governing preprotein substrate selection (Inoue et al., 2010), the truncated receptors may exhibit different substrate selectivity for the differential protein import into the specific type of dimorphic chloroplasts in a single-cell C_4 species. This hypothesis can be further tested using *in vitro* binding assays with recombinant proteins of Toc159 truncations in the future.

5.4.3 The existence of a soluble form of Toc159

Previously, Hiltbrunner et al. (2001) reported that the Toc159 receptor coexists in a soluble form, as evidenced by immunofluorescence labelling of isolated *A. thaliana* protoplasts using an antibody against the A-domain of AtToc159. Although Western blot analysis also revealed the existence of *P. sativum* Toc159 in the soluble fraction of the crude leaf extract, the precise subcellular location of the receptor was not determined (Hiltbrunner et al., 2001). Since it has been suggested that no single approach might ever be considered adequate for defining the *in vivo* location of a plant protein (Millar et al., 2009), I sought to define the subcellular locations for the targeting and accumulation of Toc159 in *B. sinuspersici* using multiple approaches. While fluorescent protein tagging indicated that Toc34 was primarily targeted to the plastids, diffuse signals of EGFP-BsToc159 and EGFP-BsToc132 were prominent in isolated chlorenchyma protoplasts of *B. sinuspersici* and onion epidermal cells (Figures 5.9 and 5.10). Both immunogold localization (Figure 5.7) and Western blot analysis

of the subfractionated protein extracts (Figure 5.8) further confirmed the accumulation of the endogenous BsToc159 and BsToc132 in the cytosolic fractions. Although the mechanism for chloroplast preprotein recognition has not been well elucidated, the partitioning of Toc159 between the soluble form and the chloroplast envelope-associated form will be important for understanding the functioning of the receptor. For instance, the concomitant observation of a homotypic interaction between the G-domains of Toc159 and Toc34 (Bauer et al., 2002; Smith et al., 2002a) has led to the current "targeting" model, which proposes that Toc159 functions as a cycling receptor for primary preprotein recognition and switches between the soluble and membrane-bound forms (Smith et al., 2004).

5.4.4 Interaction of Toc159 with the cytoskeleton

While the existence of a soluble form of Toc159 was evidenced, Jouhet and Gray (2009b) proposed that the intracellular trafficking of the soluble Toc159 receptor may involve the cytoskeleton. The authors recently documented that an anti-actin antibody co-immunoprecipitated PsToc159 from a preparation of detergent-solubilized pea chloroplast envelope (Jouhet and Gray, 2009a). The endogenous PsToc159 and the recombinant AtToc159 from a crude cell extract of *E. coli* were also co-sedimented with synthetic actin filaments (Jouhet and Gray, 2009a). In a photosynthetic cell, actin filaments are known to form a basket surrounding the chloroplasts (Kandasamy and Meagher, 1999; Higaki et al., 2007), as a means to regulate the intracellular positioning of the organelles (Kumatani et al., 2006) and their movement in response to light (Suetsugu and Wada, 2007; Schmidt and Schleiff, 2008). Given the interaction of Toc159 with the actin filament, Jouhet and Gray (2009b) further added that the actin filaments may assist in chloroplast preprotein import by

concentrating the soluble Toc159 receptors in close proximity to the chloroplast surface and/or providing a trackway for their intracellular movement.

The aforementioned hypotheses are in line with my observation at the electron microscopic level that the cytosolic forms of BsToc159 and BsToc132 were concentrated in the vicinity of the chloroplast envelopes (Figure 5.7). Concomitantly, the weak immunoreactive bands of BsToc159 and BsToc132 in the cytosolic fractions of crude cell extracts indicated that these receptors were not truly soluble but associated with some intracellular structures (Figure 5.11A, upper panels). In fact, BsToc159 and BsToc132 interact with actin filaments, as revealed from "solubilization" of the receptors in the presence of an actin filament-depolymerization drug (Figure 5.11A, middle panels) and co-immunoprecipitation of the receptors with anti-actin antibody (Figure 5.11B). Interestingly, in *B. sinuspersici*, the interaction of both Toc159 isoforms with microtubules was even more prominent, as revealed by the equivalent experiments using a microtubule-depolymerization drug (Figure 5.11A, lower panels) and anti-tubulin antibody (Figure 5.11B). While chloroplasts in a plant cell are typically surrounded by baskets of actin microfilaments (Kandasamy and Meagher, 1999; Higaki et al., 2007), previous immunofluorescence studies in *B. sinuspersici* also visualized clear association of microtubules with peripheral chloroplasts and the presence of a thick microtubular cage surrounding the CCC (Chuong et al., 2006). Cytoskeleton-disrupting drug treatments further suggested that microtubules are more critical than actin filaments for the intracellular compartmentation of the dimorphic chloroplasts (Chuong et al., 2006). Given the strong association of Toc159 with microtubules and actin filaments in *B. sinuspersici* (Figure 5.11), it might be interesting to further investigate if the cytoskeleton

contributes to the tight coordination of dimorphic chloroplast biogenesis simultaneously at the ultra-structural (i.e. organelle partitioning) and biochemical (i.e. differential preprotein import) levels. In the future, fundamental research can first be carried out to delineate the cytoskeleton-Toc159 interaction. For instance, the possible interaction between the cytoskeleton and the A-domains of Toc159 can be mapped using recombinant proteins of N-terminal truncation mutants by co-immunoprecipitation and co-sedimentation. In addition, the effects of cytoskeleton and organelle dynamics on chloroplast preprotein import can be studied *in planta* and *in vitro* using cytoskeleton-disrupting agents and chemical inhibitors of motor proteins (e.g. myosin and kinesin).

Chapter 6. A novel transit peptide-like sorting signal at the C-terminus directs Toc159 to the chloroplast outer membrane

6.1 Overview

Although Toc159 is known to be one of the key GTPase receptors for selective recognition of chloroplast preproteins, the exact mechanism for its targeting to the chloroplast surface remains unclear. Bioinformatics analyses indicated that the C-terminal tails (CTs) of Toc159 possess physicochemical and structural properties of chloroplastic transit peptides (cTPs). Fluorescent protein tagging studies showed that fusion proteins with the CTs of Toc159 homologues from a single-cell C_4 species, *Bienertia sinuspersici*, were localized at the chloroplast surface, whereas fusion with the C-terminally truncated mutants of Toc159 significantly abolished chloroplast targeting. The CT of BsToc159 in reverse orientation functioned as a cleavable cTP that guided the passenger protein to the stroma. Moreover, a BsToc34 mutant protein was re-targeted to the chloroplast envelope using the CTs of Toc159 or reverse sequences of other cTPs, suggesting their conserved functions. Together, the present study showed that the C-terminus and the central GTPase domain represent a novel dual domain-mediated sorting mechanism that might account for the partitioning of Toc159 between the cytosol and the chloroplast envelope for preprotein recognition.

Remark: A version of this chapter has been published in: **Lung SC, Chuong SDX** (2012) A transit peptide-like sorting signal at the C-terminus directs the *Bienertia sinuspersici* preprotein receptor Toc159 to the chloroplast outer membrane. Plant Cell, in press.

6.2 Introduction

The majority of plastid proteins are nuclear-encoded, synthesized on cytosolic ribosomes as precursor proteins (preproteins) and post-translationally imported into the organelles. Most of these preproteins possess an N-terminal cleavable chloroplastic transit peptide (cTP) that contains essential and sufficient information for chloroplast targeting via the general import pathway. This general pathway involves the translocon at the outer chloroplast membrane (Toc) and the translocon at the inner chloroplast membrane (Tic), which together mediate the coordinated events of preprotein recognition and translocation at the chloroplast envelope (for recent reviews, see Jarvis, 2008; Agne and Kessler, 2009; Andres et al., 2010). Toc75, Toc159 and Toc34 are core components of the Toc complex which play essential roles in the chloroplast protein import process (Kessler and Schnell, 2006). The early stages of import are mediated by two homologous GTPase proteins, Toc159 and Toc34, which are exposed on the cytosolic side of the chloroplast surface, pertinent to their roles in early preprotein recognition. The two receptors act in concert to regulate the initial interaction with cTPs and insertion of the preproteins into the β-barrel protein channel, Toc75, for translocation across the outer envelope membrane in an ATP- and GTP-dependent manner. Despite the sequence homology of their GTPase domains (G-domains), Toc159 and Toc34 receptors do not exhibit functional redundancy according to the studies of *A. thaliana* knockout mutants of Toc159 orthologues (Bauer et al., 2000; Ivanova et al., 2004; Kubis et al., 2004) and Toc34 orthologues (Jarvis et al., 1998; Kubis et al., 2003; Constan et al., 2004). Currently, there is no consensus on the specific role of the two receptors leading to the emergence of two contradictory models of protein translocation (Kessler and Schnell, 2004; Jarvis, 2008). Of particular interest in the present study is the "targeting" model, which proposes that Toc159

is the primary preprotein receptor as evidenced by the direct crosslinking of Toc159 with cTPs (Perry and Keegstra, 1994; Ma et al., 1996) and inhibition of preprotein binding *in vitro* after Toc159 antibody neutralization (Hirsch et al., 1994).

Resident proteins of the sub-chloroplast compartments which traffic across the membrane envelope of chloroplasts generally gain access through the Toc/Tic machinery. The targeting and integration of chloroplast outer membrane proteins, on the other hand, have been characterized to a much lesser extent and apparently involve multiple pathways (for reviews, see Hofmann and Theg, 2005; Bölter and Soll, 2011). To date, Toc75 is the only outer membrane protein known to contain an N-terminal cleavable cTP, and this signal is uniquely accompanied by a stretch of polyglycine that potentially functions as a stop signal to prevent its translocation into the stroma (Tranel et al., 1995; Tranel and Keegstra, 1996). Although both Toc75 and its paralogue, outer envelope protein 80 kDa (OEP80), are targeted with the assistance of some proteinaceous components on the chloroplast surface, the targeting of OEP80 is independent of the general import pathway, in agreement with the absence of an N-terminal cleavable cTP (Inoue and Potter, 2004; Huang et al., 2011). In fact, all other identified β-barrel proteins on the chloroplast outer membrane, including OEP21 (Bölter et al., 1999), OEP24 (Pohlmeyer et al., 1998) and OEP37 (Goetze et al., 2006), do not have a predicted cTP and are spontaneously integrated into the membrane. In addition to β-barrel proteins, chloroplasts have evolved α-helical integral proteins in the outer membrane, in spite of the endosymbiotic origin from a bacterial progenitor. Depending on the location of the transmembrane helix at the N- or C-terminus, these proteins are commonly referred to as signal-anchored proteins (e.g. OEP7/14 and OEP64) and tail-anchored proteins (e.g. OEP9

and Toc34), respectively. The targeting of these proteins and their efficient insertion with the correct topology depend on the information embedded in the transmembrane domains and the flanking charged regions, whereas the cytosolic G-domain of Toc34 also plays an essential role (Chen and Schnell, 1997; Schleiff et al., 2001; Qbadou et al., 2003; Hofmann and Theg, 2005; Dhanoa et al., 2010). Although two previous studies documented that the G-domain mediates the targeting and insertion of Toc159 to the outer chloroplast membrane (Bauer et al., 2002; Smith et al., 2002a), this domain per se presumably does not contain any sorting signal and the targeting specificity of this receptor to the chloroplast envelope has not been elucidated. The absence of any predicted β-barrel or α-helical transmembrane domains implies that Toc159 is targeted in a manner independent of the aforementioned pathways, critical to its function as a soluble preprotein receptor that partitions between the cytosol and the chloroplast envelope (Hiltbrunner et al., 2001). Previous protein truncation studies suggested that the specific sorting signal of Toc159 resides within its C-terminal transmembrane domain (M-domain; Muckel and Soll, 1996; Lee et al., 2003).

Focusing on plant organelles in a single-cell C_4 system such as *Bienertia sinuspersici* is of special interest to obtain information on the evolution of protein sorting mechanisms. Since plastid biogenesis and functions depend on the coordinated expression and import of thousands of nuclear-encoded proteins (Jarvis, 2008), the development and function of dimorphic chloroplasts in the single-cell C_4 system might involve distinct import pathways to regulate the selective import of proteins and mediate plastid differentiation. In the present study, analyses of the *B. sinuspersici* Toc159 sequences using various bioinformatics tools indicated that the C-terminal tails (CTs) possess general physicochemical and structural

properties similar to the transit sequences of chloroplast preproteins. I used various enhanced green fluorescent protein (EGFP) fusion constructs to demonstrate that the CTs directed the passenger protein to the chloroplast envelope, as evidenced by fluorescence microscopy and Western blot analysis following subcellular fractionation. Reciprocal fusion constructs of the CTs of Toc159 and various cTPs confirmed that these sequences behave as chloroplast-targeting signals. Considering the importance of the G-domain (Bauer et al., 2002; Smith et al., 2002a), this study led to the hypothesis of a dual domain-mediated pathway that may account for the partitioning of Toc159 receptors between the cytosol and the chloroplast envelope.

6.3 Results

6.3.1 Predicted transit peptide properties of the Toc159 C-terminus

In an attempt to unravel the chloroplast envelope-sorting signals of Toc159, I analyzed the amino acid sequences of the Toc159 homologues from *B. sinuspersici* (i.e. BsToc159 and BsToc132) and other plant species using various bioinformatics tools. A recurring observation is that the CT of BsToc159 exhibits features similar to those characteristic of cTPs, whilst other Toc159 homologues in the same region were also predicted to have moderate similarities. These similarities were generally with the physicochemical and structural properties of cTPs which are otherwise highly divergent in length, amino acid composition and organization (Bruce, 2001). First, I found that hydroxylated residues (i.e. serine and threonine) are overrepresented (20.3%) and acidic residues (i.e. aspartic and glutamic acids) are underrepresented (1.4%) in the BsToc159 CT leading to a basic (pI=10) (Table 6.1). A sequence logo representation of the aligned CTs of Toc159 homologues also illustrates a similar trend of amino acid occurrence (Figure 6.1), which is with a common feature of cTPs (von Heijne et al., 1989; Patron and Waller, 2007; Zybailov et al., 2008; Li and Chiu, 2010).

Next, I also observed structural similarities. cTPs primarily form random coils in an aqueous environment and yet might adopt amphipathic α-helical structure(s) at the aqueous/lipid bilayer interface at the chloroplast envelope, although the positions and degrees of amphipathicity may vary (Bruce, 2001). Secondary structure prediction analysis suggested that the CTs of both BsToc159 and BsToc132 have a tendency of forming an α- helix

Table 6.1 Physiochemical properties of Toc159 C-termini and chloroplastic transit peptides

Peptide(s)	Species	Terminus	Residues	Occurrence (%)		Calculated pI
				D+E[1]	S+T[2]	
BsToc159-1	*Bienertia sinuspersici*	Carboxyl	69	1.4	20.3	10.21
Other Toc159 (n=32)	Multiple	Carboxyl	60-77	4.0	15.4	10.63
Transit peptides (n=1,028)[3]	*Arabidopsis, Oryza*	Amino	12	2.4	26.6	N.D.

Remarks: [1] *The occurrence of acidic residues including aspartic (D) and glutamic (E) acids.*
[2] *The occurrence of hydroxylated residues including serine (S) and threonine (T).*
[3] *All values were previously reported by Patron and Waller (2007).*

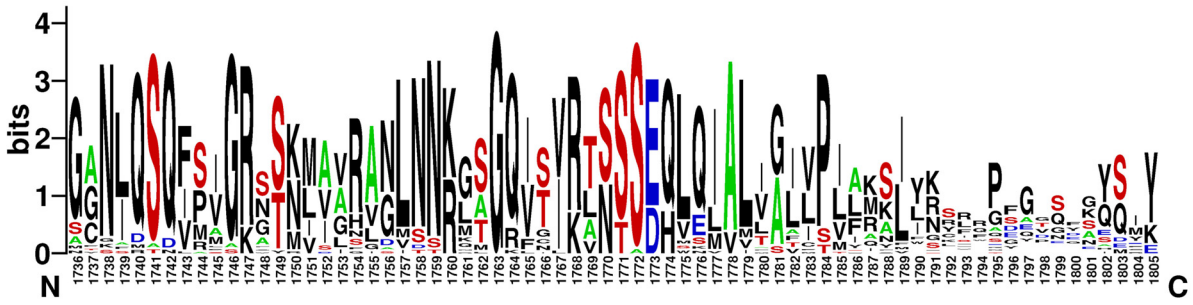

Figure 6.1 A WebLogo representation of the aligned C-terminal sequences from Toc159 homologues

Amino acid sequence alignment was performed using ClustalW algorithm. Sequence logos were generated from the alignment using WebLogo 2.8.2 (Crooks et al., 2004). Letter height is proportional to its frequency of occurrence. The graph illustrates high frequencies of hydroxylated residues (in red) and alanines (in green) and low frequencies of acidic residues (in blue).

adjacent to a random coil of 10~12 residues at the C-terminal end (Figure 6.2A). Helical wheel projections of the predicted α-helices depict a substantial hydrophobic moment to one side of the helices while hydrophilic residues largely comprise the other side (Figure 6.2B). The predicted amphipathic α-helices are somewhat conserved in the CTs of Toc159 homologues from other plant species (Table 6.2). I further evaluated their degrees of amphipathicity from the mean hydrophobicities and mean hydrophobic moments per residue (Table 6.2), using the structurally characterized α-helices of cTPs for comparison (Bruce, 2001). The resulting hydrophobic moment plot analysis depicts that all analyzed sequences have a similar range of mean hydrophobicities while the mean hydrophobic moments of the predicted α-helices of most Toc159 homologues are slightly above the values of the characterized cTPs (Figure 6.3). Thus, the structural prediction data suggest that Toc159 CTs tend to form amphipathic α-helical structures analogous to those of cTPs.

In addition to the evaluation based on the physicochemical and structural criteria, I wanted to confirm whether the Toc159 CTs contain a putative TP using a neural network-based approach. The ChloroP predictor is the most popular algorithm for predicting putative cTPs, and is also able to predict stromal processing peptidase cleavage independently of the cTP prediction results (Emanuelsson et al., 1999). Since cTPs all occur at the N-terminal ends of preproteins (hence the training data sets of chloroplast proteins used), I submitted the reverse sequences of full-length Toc159 homologues for ChloroP analysis. In agreement with the other bioinformatics results, ChloroP predicted a putative TP at the CT region of BsToc159 (Table 6.3). The average cTP score of 32 tested Toc159 homologues is, however, slightly below the threshold cut-off (Table 6.3). Interestingly, the program also predicted a cleavage

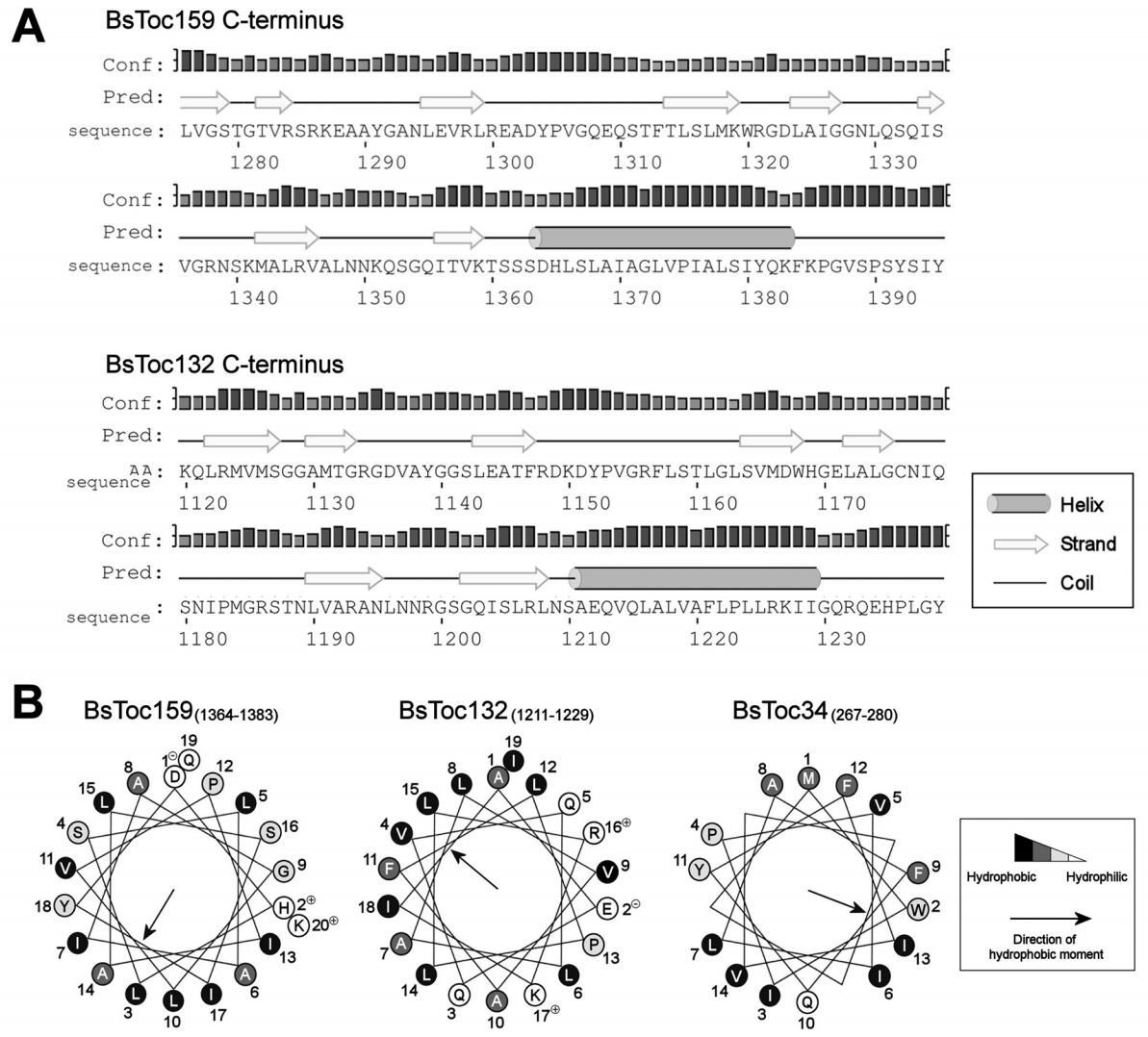

Figure 6.2 Structural predictions from the C-terminal sequences of *B. sinuspersici* Toc159 homologues

(A) Prediction of secondary structures at the C-termini of Toc159 homologues. Predictions were performed using the web-based program PSIPRED v3.0 (Jones, 1999). The height of the bar for each residue is proportional to the confidence level of prediction.

(B) Helical wheel projections of the predicted C-terminal helices of Toc159 homologues and the transmembrane helix of Toc34. Numbering designates the order of amino acid sequence. Hydrophobicities of residues are highlighted on the Kyte-Doolittle hydropathy scale (hydrophilic in white, neutral in light grey, hydrophobic in dark grey and very hydrophobic in black).

Table 6.2 Hydrophobic moment analysis of the predicted α-helices at the C-termini of Toc159 homologues

Isoform	Homologue	α-Helix position	Aligned sequence	Mean hydrophobicity per residue[1] <*H*>	Mean hydrophobic moment per residue[2] <μ*H*>
Toc159	*A. lyrata 1*	1483-1502	/ D Q L Q I A L T A I L P I A M S I Y K S	0.706	0.300
	A. thaliana 1	1471-1490	/ D Q L Q I A L T A I L P I A M S I Y K S	0.706	0.300
	B. rapa 1	1611-1630	/ D Q L Q I A L T A I L P I A M S I Y K M	0.770	0.299
	B. rapa 2	890-909	/ D Q L Q I A V M A I L P L A M S I Y K R	0.677	0.257
	B. sinuspersici 1	1364-1383	/ D H L S L A I A G L V P I A L S I Y Q K	0.705	0.267
	P. sativum	1438-1457	/ D Q L Q I A L I A I L P V A K A I Y K N	0.633	0.283
	S. lycopersicum	1372-1391	/ D H L S L A L T A I I P T A I G I Y R K	0.637	0.309
	R. communis 1	1021-1040	/ D Q L Q I A L V G L L P I A M S I Y K S	0.734	0.268
	V. vinifera 1	1344-1363	/ E Q L Q I A L V G I I P V V M A I Y K A	0.802	0.291
	R. communis 2	1351-1369	/ E / L Q V A L I S T L P M L I S M L R S	0.794	0.345
	H. vulgare 1	1395-1414	/ E Q V Q I A L L G L V P V I A S I Y R S	0.715	0.305
	O. sativa 1	1277-1296	/ E Q V Q I A L L G L I P V A A S I Y R S	0.669	0.241
	S. bicolor 1	1338-1357	/ E Q V Q I A L L G L I P V A A S I Y R S	0.669	0.241
	O. sativa 2	1178-1197	/ E Q L K I A L L G V C S M T M Y L W N R	0.705	0.264
	S. bicolor 2	1105-1124	/ E Q L N I A L F G T C S V I M Y L W N K	0.758	0.315
Toc120/132	*O. sativa 3*	985-1003	S E H L E I A L I A L V P I Y Q N I K / /	0.675	0.266
	S. bicolor 3	960-978	S E H L E I A L V A L V P I F Q N I M / /	0.805	0.354
	H. vulgare 2	1044-1062	S E H L Q I A L L A L V P I Y K N I R / /	0.650	0.292
	A. lyrata 3	1157-1175	S E Q L Q L A M V A I V P L F K K L L / /	0.737	0.386
	A. thaliana 2	1177-1195	S E Q L Q L A M V A I V P L F K K L L / /	0.737	0.386
	A. thaliana 3	1059-1077	S E Q L Q L A V V A L V P L F K K L L / /	0.731	0.381
	B. sinuspersici 2	1211-1229	A E Q V Q L A L V A F L P L L R K I I / /	0.784	0.399
	M. truncatula	1308-1326	S E Q L Q I A L I G L I P L L K K V I / /	0.782	0.376
	R. communis 3	1149-1167	S E Q L Q I A L V G L L P L L K K L F / /	0.771	0.409
	V. vinifera 2	1247-1265	S E Q L Q I A L I G L V P L L R K L L / /	0.770	0.378
Toc90	*O. sativa 4*	746-763	/ D H S E I A L V A A V T L F Q F F L R R	0.617	0.190
	A. thaliana 4	754-771	/ E H W E I A L I S A L T M F K A L V R R	0.609	0.346
	V. vinifera 3	769-786	/ E H M E I A L V A F F S I F R A L L R R	0.661	0.409
			Mean ± 1 S.D. :	0.715 ± 0.058	0.316 ± 0.059

Alignment of full-length protein sequences was performed using the Align X program of Vector NTI Advance™ 10.3.0 (Invitrogen). Regions of the predicted C-terminal α-helices are shown. Hydrophobicities of residues are highlighted on the Kyte-Doolittle hydropathy scale (hydrophilic in white, neutral in light grey, hydrophobic in dark grey and very hydrophobic in black). Asterisks indicate residues on the hydrophobic sides of the predicted helices. Hydrophobic moment analysis was performed with the web server HELIQUEST (http://heliquest.ipmc.cnrs.fr) using 19-residue (Toc120/132) or 20-residue (Toc90 and Toc159) windows.

Remarks: [1] *Mean hydrophobicities of residues were calculated based on their octanol/water partition (Fauchère and Pliska, 1983).*

[2] *Mean hydrophobic moments are the mean vector sum of the hydrophobicities of residues in a helix based on an alpha angle of 100°.*

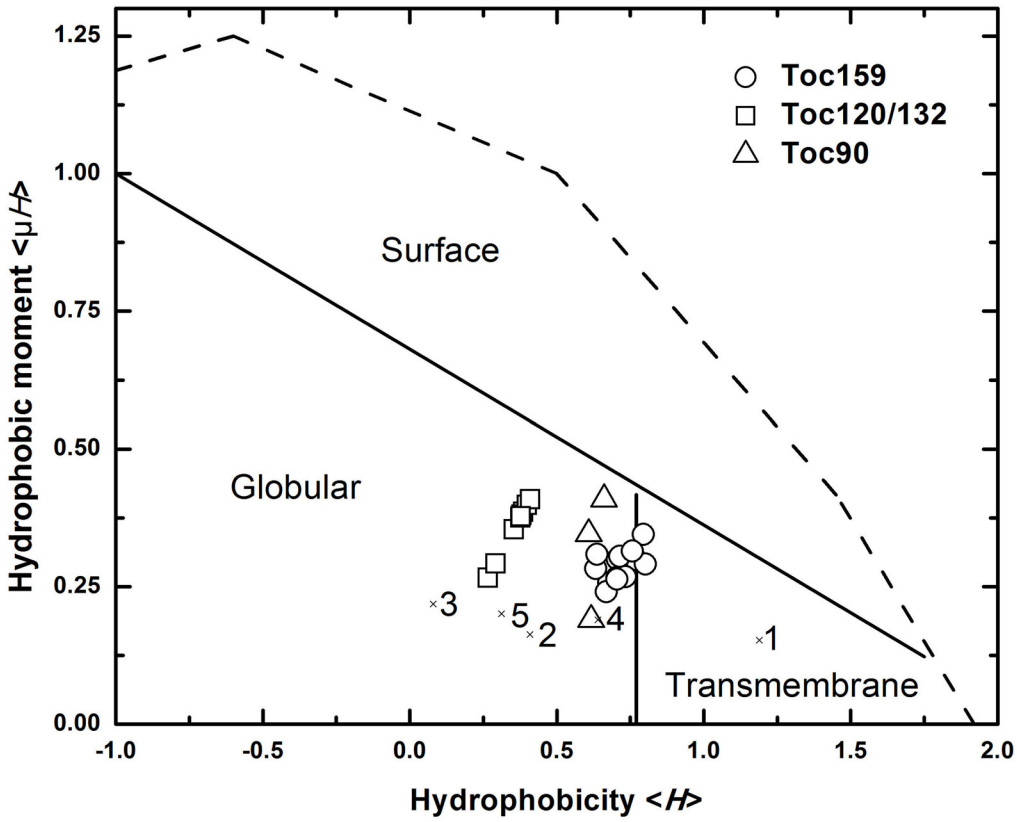

Figure 6.3 Hydrophobic moment plot analysis of Toc159 C-terminal α-helices

Each data point represents a predicted C-terminal α-helix of one Toc159 homologue. Values of the mean hydrophobicities and the mean hydrophobic moments for the plot are presented in Table 6.2. Hydrophobic moment plot was first created by Eisenberg et al. (1984) using the values from a data set of globular, surface-seeking and transmembrane proteins on a normalized Eisenberg scale (Eisenberg et al., 1984). The boundaries that define the three classes of proteins in the present study were based on a modified Eisenberg plot using Heliquest-generated values (Keller, 2011). The transmembrane helix of Toc34 (1) and structurally identified helices of chloroplast transit peptides (2-5; Bruce, 2001) are included for comparison. 1, *P. sativum* Toc34; 2, *C. reinhardtii* pre-ferredoxin; 3, *C. reinhardtii* pre-Rubisco activase; 4, *S. pratensis* pre-ferredoxin helix #1; 5, *S. pratensis* pre-ferredoxin helix #2.

Table 6.3 ChloroP prediction of putative chloroplast transit peptides

Protein	Orientation	cTP score[1]	cTP length[2]	CS score[3]
B. sinuspersici Toc159-1	Reverse	0.519	51	10.81
Other Toc159 (n=32)	Reverse	0.486 ± 0.024	48.3 ± 11.4	4.00 ± 3.30
A. thaliana Rubisco small-subunit	Forward	0.572	54	10.09

The values (±SD) were determined using the ChloroP 1.1 server (Emanuelsson et al., 1999).

Remarks: [1] *A value of greater than 0.5 predicts the presence of a transit peptide.*

[2] *The length is defined based on the cleavage site (CS) score.*

[3] *A more positive value indicates a higher probability of transit peptide cleavage.*

site of stromal processing peptidase within the BsToc159 CT sequence with a score comparable to that of Rubisco small-subunit (Table 6.3). Taken together, bioinformatics analyses predict a putative TP at the C-terminus of BsToc159.

6.3.2 Toc159 C-termini directed EGFP to the chloroplast surface

To complement the bioinformatics analyses, I evaluated the chloroplast-targeting function of Toc159 CTs by C-terminal truncation and EGFP fusion with the CTs of BsToc159 or BsToc132, of which the lengths were derived from the ChloroP prediction (Table 6.3) plus four additional residues. Since transient expression of EGFP fusion of full-length BsToc159 or BsToc132 in *B. sinuspersici* (Figure 5.9) and *A. thaliana* (Figures 6.4A and 6.4B) protoplasts produced identical subcellular localization patterns, I chose to express the EGFP fusion proteins in *A. thaliana* protoplasts due to the relative ease of subsequent chloroplast purification steps using standard and established protocols (Smith et al., 2002b), and given the intricate intracellular complexity of dimorphic chloroplast arrangement in *B. sinuspersici*. Fluorescence microscopy and Western blot analysis of the sub-fractions from total transfected protoplasts and isolated chloroplasts showed that the full-length BsToc159 fusion proteins were evenly distributed between the soluble and chloroplast-membrane-associated fractions (Figures 6.4A and 6.4B). The C-terminally truncated mutants, on the other hand, produced diffuse fluorescent signals and were detected primarily in the soluble fractions of total protoplasts (Figures 6.4C and 6.4D), similar to the null-vector control (Figure 6.4E). I also showed that the CTs of BsToc159 and BsToc132 directed a significant amount of EGFP protein close to the chloroplast exterior (Figures 6.4F and 6.4G).

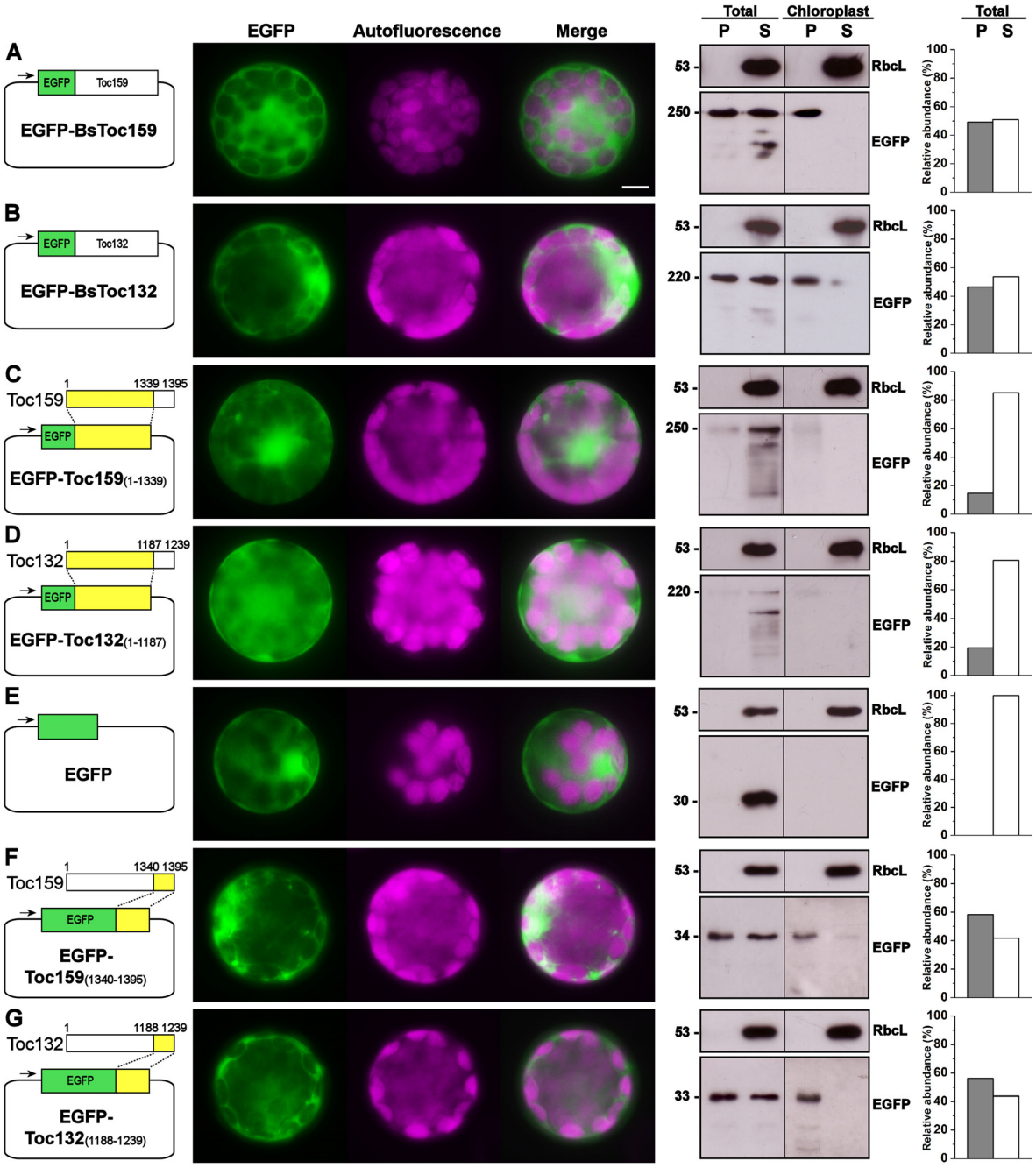

Figure 6.4

Figure legend on the next page

Figure 6.4 Transient expression of EGFP fusion proteins with full-length or partial sequences of Toc159

Isolated *A. thaliana* protoplasts were transfected with the EGFP fusion constructs for transient protein expression driven by the constitutive 35S promoter (left panels). For each construct, representative images of EGFP and chlorophyll fluorescence and a merge of the two channels are shown in the middle panel. The subcellular localization was confirmed by Western blot analysis with an anti-EGFP antibody after subfractionation of the total protoplasts or purified chloroplasts into pellet (P) and soluble (S) fractions, and analyzed by densitometric quantification (right panels). Detection with an antibody against Rubisco large-subunit (RbcL) served as loading controls for the S fractions. Numbers to the left indicate the positions of marker proteins in kilodaltons. Scale bar = 10 μm.

(A) Full-length BsToc159 fused to the C-terminus of EGFP.
(B) Full-length BsToc132 fused to the C-terminus of EGFP.
(C) C-terminally truncated BsToc159 fused to the C-terminus of EGFP
(D) C-terminally truncated BsToc132 fused to the C-terminus of EGFP.
(E) EGFP control in null vector.
(F) The C-terminal tail of *B. sinuspersici* Toc159 fused to the C-terminus of EGFP.
(G) The C-terminal tail of *B. sinuspersici* Toc132 fused to the C-terminus of EGFP.

Since further subfractionation of the insoluble chloroplast fractions into envelope and thylakoid membranes was impractical due to the number of transfected protoplasts required, I sought to rule out the possibility of thylakoid membrane localization of the fusion proteins by thermolysin treatments (Figure 6.5A). As expected, the immunoreactive signals of both EGFP-BsToc159CT and EGFP-BsToc132CT were completely abolished after thermolysin treatments, whereas the EGFP proteins were protected from protease degradation after ferredoxin TP-directed translocation into the stroma (Figure 6.5A). The observation that the CTs of BsToc159 and BsToc132 did not guide the translocation of the passenger protein across the outer chloroplast envelope is in line with the topology of Toc159 receptors which project the N-terminal acidic domain (A-domain) and central G-domain to the cytosolic side. To confirm that the CTs of BsToc159 and BsToc132 have high affinities for the chloroplast envelope but that these segments did not traverse the outer chloroplast membrane, I treated the isolated chloroplasts with alkaline extraction prior to Western blot analysis (Figure 6.5B). As expected, the immunoreactive signals of both EGFP-BsToc159CT and EGFP-BsToc132CT were abolished after the treatment, in contrast to those of the tail-anchored protein Toc34 and signal-anchored protein OEP7 (Figure 6.5B). In fact, the putative membrane anchor of Toc159 is likely to be found far upstream of the C-terminal end as predicted from the bulk size (e.g. ~50 kDa in *P. sativum* Toc159) of the fragment being protected from protease degradation (Kessler et al., 1994). From these experiments, I conclude that Toc159 CTs function as cTP-like sorting signals capable of directing passenger proteins to the chloroplast envelope but that the CT regions do not function as a membrane anchor.

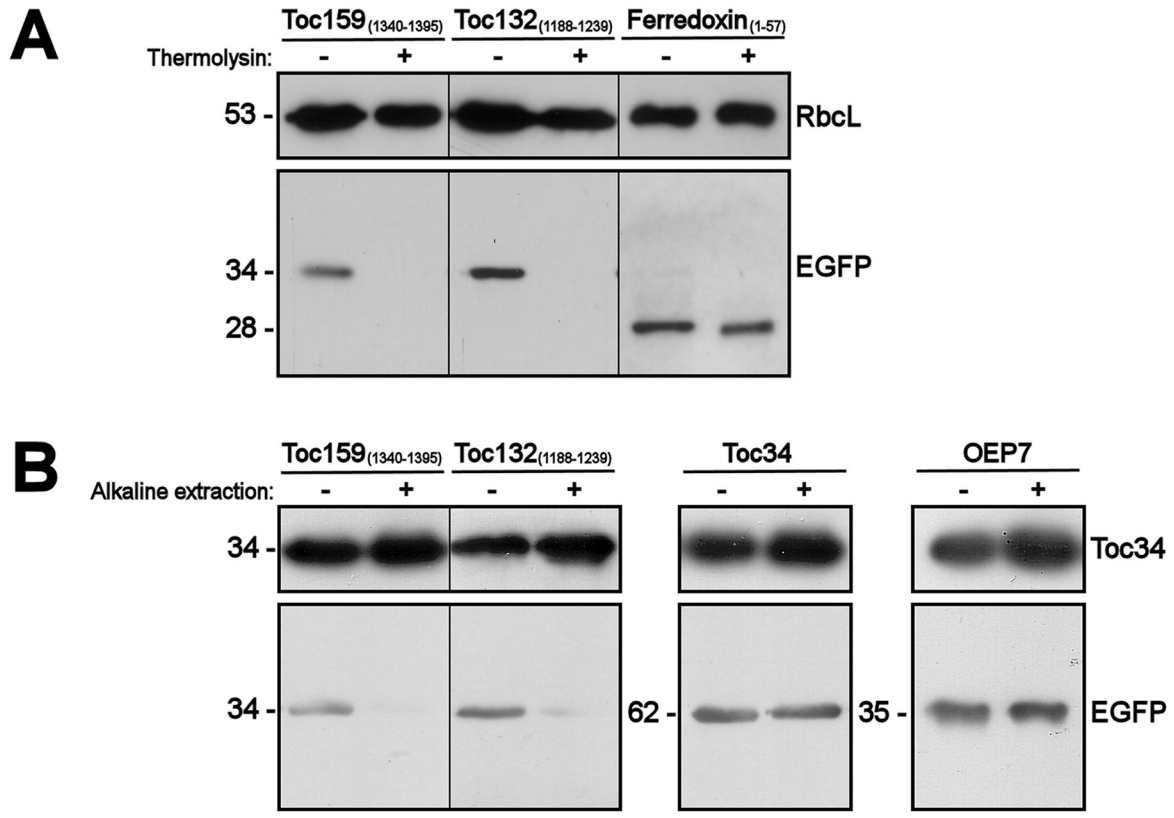

Figure 6.5 Thermolysin treatment and alkaline extraction of chloroplasts purified from transfected protoplasts

(A) Thermolysin treatment. Chloroplasts were isolated from transfected protoplasts that expressed the C-terminal tails of Toc159 or Toc132 fused to the C-terminus of EGFP or the transit peptide of ferredoxin fused to the N-terminus of EGFP. Purified chloroplasts were incubated with or without 10 µg of thermolysin on ice for 30 min prior to re-isolation of the chloroplasts on a Percoll gradient. The re-isolated chloroplasts were subjected to Western blot analysis using an anti-EGFP antibody and an antibody against Rubisco large-subunit (RbcL) as loading controls. Numbers to the left indicate the positions of marker proteins in kilodaltons.

(B) Alkaline extraction. Chloroplasts were isolated from transfected protoplasts that expressed the C-terminal tails of Toc159 or Toc132 or the entire Toc34 protein fused to the C-terminus of EGFP or OEP7 fused to the N-terminus of EGFP. Purified chloroplasts were incubated in carbonate buffer (pH 11.5) or Hepes buffer (pH 7.3) on ice for 10 min. The precipitated membrane pellets were subjected to Western blot analysis using an anti-EGFP antibody and an antibody against Toc34 as loading controls. Numbers to the left indicate the positions of marker proteins in kilodaltons.

6.3.3 Toc159 C-termini re-targeted the Toc34 mutant to the chloroplast envelope

As discussed earlier, thermolysin treatment data did not implicate the protein import machinery in the translocation of Toc159 CTs across the outer chloroplast membrane (Figure 6.5A), and alkaline extraction data further suggested the absence of membrane anchor signals in Toc159 CTs (Figure 6.5B). It is therefore plausible that the binding of Toc159 CTs to the chloroplast envelope is reversible, as evidenced by the considerable abundance of these fusion proteins detected in the soluble fractions (Figures 6.4F and 6.4G). In fact, in the case of cTP targeting, the initial docking of preproteins on the chloroplast envelope is also reversible (Perry and Keegstra, 1994; Kouranov and Schnell, 1997). Thus, I further investigated whether the Toc159 CTs can target passenger proteins known to reside at the chloroplast envelope. Previous truncation studies revealed that the C-terminal hydrophilic tail of Toc34 is essential for chloroplast envelope association (Chen and Schnell, 1997; Li and Chen, 1997; Dhanoa et al., 2010). I first confirmed that, while the EGFP-tagged full-length proteins of AtOEP7 and BsToc34 were exclusively localized to the chloroplast envelope (Figures 6.6A and 6.6B), C-terminal truncation of the hydrophilic tail from Toc34 resulted in diffuse signals throughout the cytosol (Figure 6.6C). Next, using this Toc34 mutant, I showed that the CTs of both BsToc159 and BsToc132 re-targeted the mutant Toc34 protein to the chloroplast envelope forming ring-like fluorescent patterns, with the majority of the fusion proteins found in the membrane fractions of transfected protoplasts and isolated chloroplasts as indicated by Western blot analysis (Figures 6.6D and 6.6E). Similar re-targeting of the Toc34 mutant to the chloroplast envelope was also achieved by fusion with the CTs of AtToc159 or AtToc132 (Figures 6.6F and 6.6G), suggesting that the chloroplast

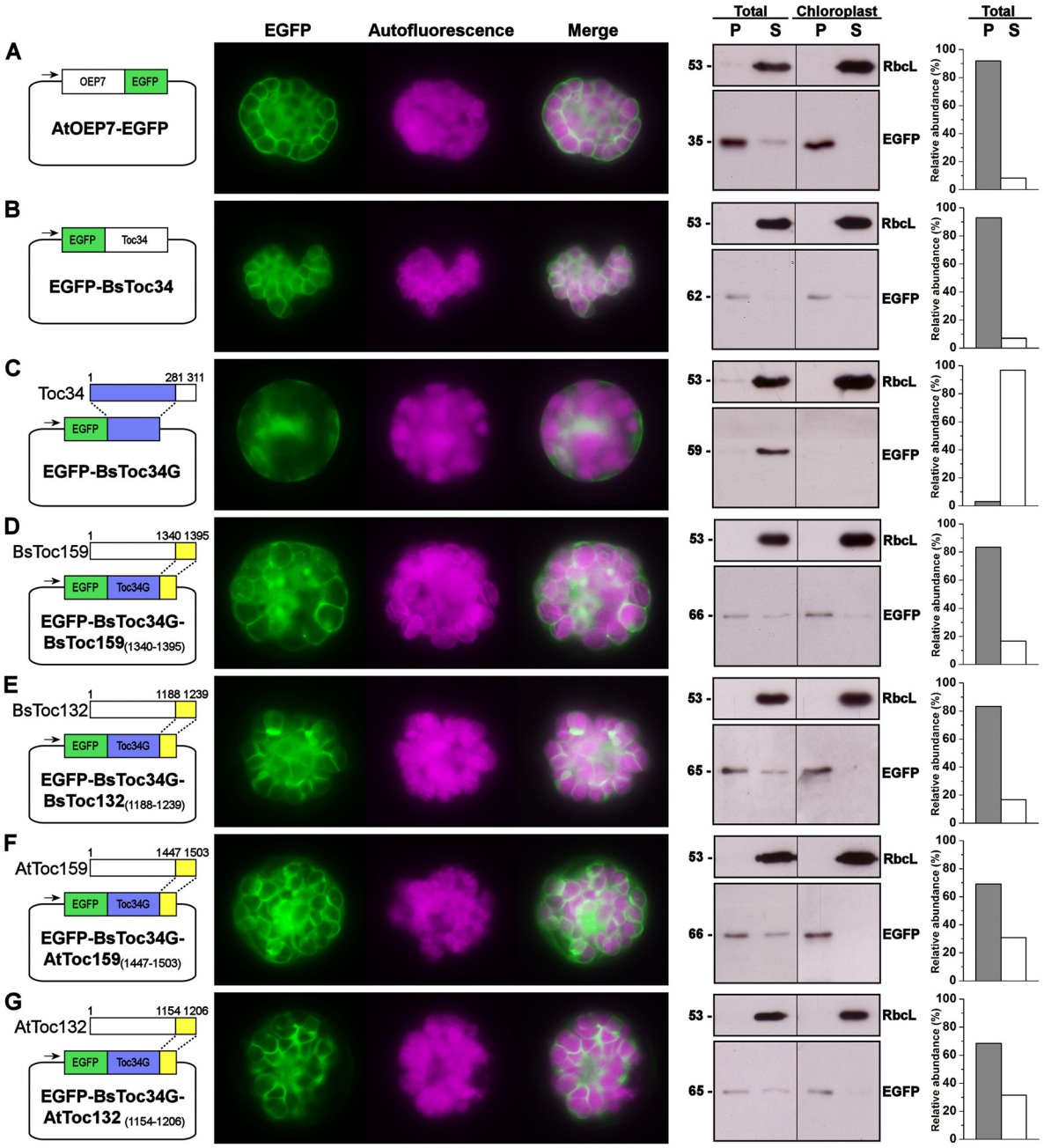

Figure 6.6

Figure legend on the next page

Figure 6.6 Re-targeting of the C-terminally truncated Toc34 to the chloroplast envelope by the Toc159 C-terminal tails

Isolated *A. thaliana* protoplasts were transfected with the EGFP fusion constructs for transient protein expression driven by the constitutive 35S promoter (left panels). For each construct, representative images of EGFP and chlorophyll fluorescence and a merge of the two channels are shown in the middle panel. The subcellular localization was confirmed by Western blot analysis with an anti-EGFP antibody after subfractionation of the total protoplasts or purified chloroplasts into pellet (P) and soluble (S) fractions, and analyzed by densitometric quantification (right panels). Detection with an antibody against Rubisco large-subunit (RbcL) served as loading controls for the S fractions. Numbers to the left indicate the positions of marker proteins in kilodaltons.

(A) Full-length *A. thaliana* OEP7 fused to the N-terminus of EGFP.
(B) Full-length *B. sinuspersici* Toc34 fused to the C-terminus of EGFP.
(C) C-terminally truncated *B. sinuspersici* Toc34 fused to the C-terminus of EGFP (EGFP-Toc34G).
(D) The C-terminal tail of *B. sinuspersici* Toc159 fused to the C-terminus of EGFP-Toc34G.
(E) The C-terminal tail of *B. sinuspersici* Toc132 fused to the C-terminus of EGFP-Toc34G.
(F) The C-terminal tail of *A. thaliana* Toc159 fused to the C-terminus of EGFP-Toc34G.
(G) The C-terminal tail of *A. thaliana* Toc132 fused to the C-terminus of EGFP-Toc34G.

envelope-targeting signals at the Toc159 CTs are universal at least in higher plant species. Based on these observations, I conclude that Toc159 CTs can complement the sorting signal of Toc34 CT for chloroplast envelope targeting.

6.3.4 Similar function of Toc159 C-termini and chloroplast transit peptides

Given the results of the bioinformatic analyses and EGFP fusion experiments, I hypothesized that the CTs of Toc159 receptors and cTPs of preproteins are in part functionally interchangeable. To test this hypothesis, I first produced reciprocal fusion constructs encoding the reverse TP sequence of Rubisco small-subunit fused to the C-terminus of the EGFP-tagged Toc34 truncation mutant. In spite of the lower targeting efficiency as judged by the intensities of immunoreactive bands, the association of this fusion protein with chloroplasts was evidenced in fluorescence microscopy and Western blot analysis (Figure 6.7A). More convincingly, the Toc34 mutant was efficiently re-targeted to the chloroplast envelope using the reverse TP sequences of pyruvate orthophosphate dikinase (Figure 6.7B) or ferredoxin (Figure 6.7C). Interestingly, the fusion of the Toc34 mutant with the reverse mitochondrial presequence of NAD-malic enzyme at the C-terminus resulted in some punctate signals (Figure 6.7D), which were similar with those localized to mitochondria (Figure 6.7E). In addition to re-targeting the Toc34 mutant, the EGFP fusion with the mature protein of ferredoxin, which otherwise appeared as a diffuse cytosolic signal (Figure 6.7F), was partially directed to the chloroplast envelope using its own TP sequence reversely fused at the C-terminus (Figure 6.7G).

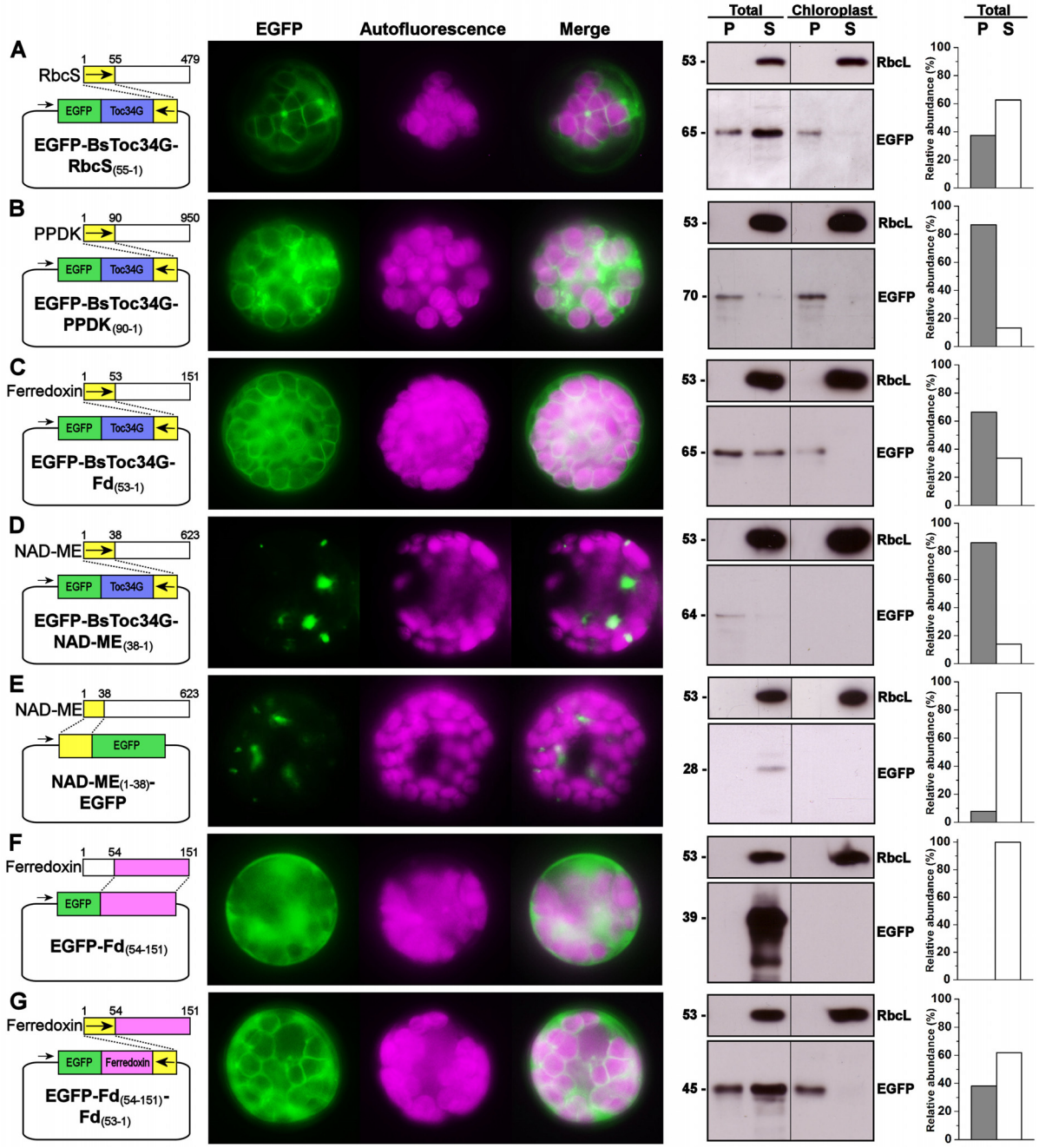

Figure 6.7

Figure legend on the next page

Figure 6.7 The targeting of EGFP fusion proteins to the chloroplast envelope by the reverse sequences of chloroplast transit peptides

Isolated *A. thaliana* protoplasts were transfected with the EGFP fusion constructs for transient protein expression driven by the constitutive 35S promoter (left panels). For each construct, representative images of EGFP and chlorophyll fluorescence and a merge of the two channels are shown in the middle panel. The subcellular localization was confirmed by Western blot analysis with an anti-EGFP antibody after subfractionation of the total protoplasts or purified chloroplasts into pellet (P) and soluble (S) fractions, and analyzed by densitometric quantification (right panels). Detection with an antibody against Rubisco large-subunit (RbcL) served as loading controls for the S fractions. Numbers to the left indicate the positions of marker proteins in kilodaltons.

(A) The reverse sequence of *A.thaliana* Rubisco small-subunit transit peptide fused to the C-terminus of EGFP-Toc34G.
(B) The reverse sequence of *B. sinuspersici* pyruvate orthophosphate dikinase transit peptide fused to the C-terminus of EGFP-Toc34G.
(C) The reverse sequence of *B. sinuspersici* ferredoxin transit peptide fused to the C-terminus of EGFP-Toc34G.
(D) The reverse sequence of *B. sinuspersici* NAD-malic enzyme mitochondrial presequence fused to the C-terminus of EGFP-Toc34G.
(E) The mitochondrial presequence of NAD-malic enzyme fused to the N-terminus of EGFP.
(F) The mature protein of *B. sinuspersici* ferredoxin fused to the C-terminus of EGFP.
(G) The reverse sequence of *B. sinuspersici* ferredoxin transit peptide fused to the C-terminus of the fusion protein as shown in (F).

I also produced reciprocal fusion constructs encoding the reverse sequences of BsToc159 CT and BsToc132 CT fused at the N-terminus of EGFP. Although the reversal of BsToc132 CT did not produce conclusive results due to the degradation of the CT tag for some unknown reason (Figure 6.8A), the N-terminal fusion of EGFP with the reverse sequence of BsToc159 resulted in translocation of the passenger protein into the stroma and subsequent maturation of the protein by stromal processing peptidase cleavage (Figure 6.8B). This observation is consistent with the ChloroP prediction suggesting that the BsToc159 CT is a putative cTP and possesses a cleavage site of stromal processing peptidase (Table 6.3). Taken together, I conclude that the function of Toc159 CTs is similar to that of characteristic cTPs.

6.3.5 Stromal processing degradation of the C-terminal targeting signals

Lastly, I investigated if the Toc159 CTs in the native, non-reversed orientation are susceptible to stromal processing peptidase degradation, which is a characteristic property of cTPs for the production of mature proteins after their translocation into the stroma. Purified recombinant EGFP fusion proteins with BsToc159 CT and BsToc132 CT were incubated in the presence of stromal protein extracts at 28 ^{o}C for 1.5 h. The subsequent Western blot analysis showed that a portion of EGFP-BsToc159CT, and more prominently, EGFP-BsToc132CT were processed to the shorter polypeptides of molecular weights comparable to that of the EGFP protein control (Figure 6.9). In the absence of stromal extracts, the degradation of fusion proteins was sparsely detectable (Figure 6.9). Thus, it can be concluded that the Toc159 CTs were partially susceptible to stromal processing *in vitro*.

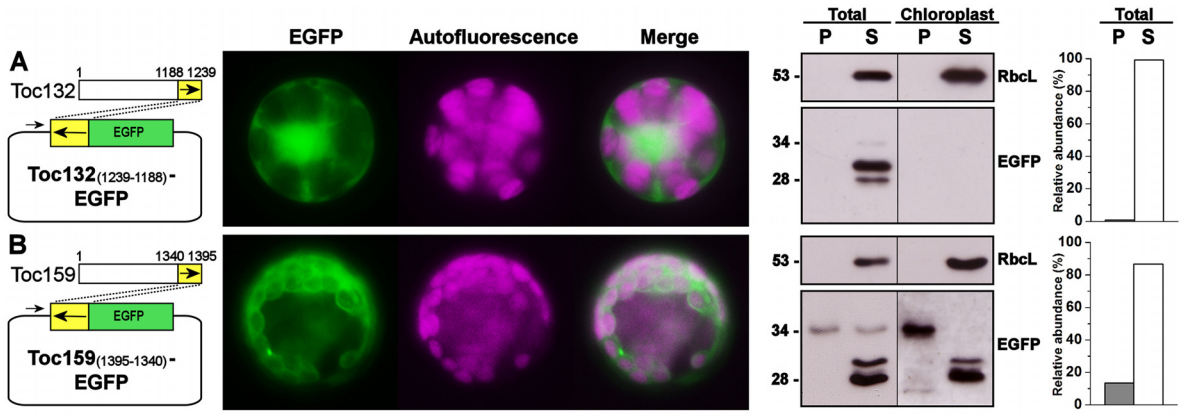

Figure 6.8 The reversal of Toc159 C-terminal tails and their fusion with EGFP

Isolated *A. thaliana* protoplasts were transfected with the EGFP fusion constructs for transient protein expression driven by the constitutive 35S promoter (left panels). For each construct, representative images of EGFP and chlorophyll fluorescence and a merge of the two channels are shown in the middle panel. The subcellular localization was confirmed by Western blot analysis with an anti-EGFP antibody after subfractionation of the total protoplasts or purified chloroplasts into pellet (P) and soluble (S) fractions, and analyzed by densitometric quantification (right panels). Detection with an antibody against Rubisco large-subunit (RbcL) served as loading controls for the S fractions. Numbers to the left indicate the positions of marker proteins in kilodaltons.

(A) The reverse sequence of the C-terminal tail of *B. sinuspersici* Toc132 fused to the C-terminus of EGFP.
(B) The reverse sequence of the C-terminal tail of *B. sinuspersici* Toc159 fused to the C-terminus of EGFP.

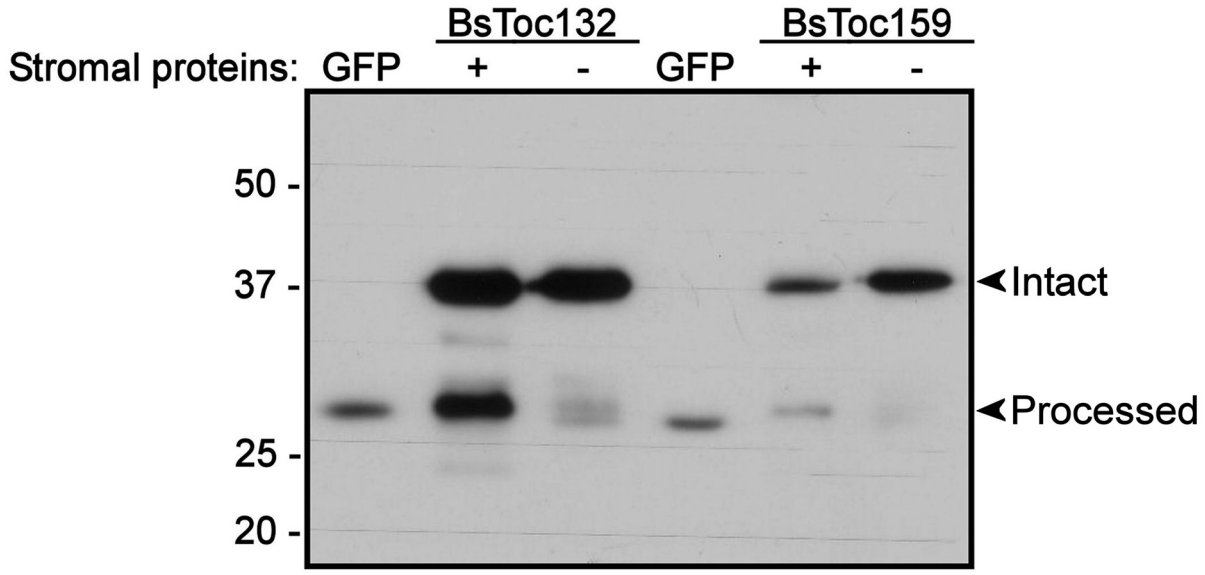

Figure 6.9 Stromal processing peptidase assays of recombinant EGFP fusion proteins withToc159 C-terminal tails

Purified recombinant proteins of EGFP-Toc159$_{(1340\text{-}1395)}$ or EGFP-Toc132$_{(1188\text{-}1239)}$ were incubated with or without crude protein extracts from *A. thaliana* chloroplast stroma, and analyzed by Western blot analysis with EGFP antibody. Purified EGFP proteins were loaded as controls. Numbers to the left indicate the positions of marker proteins in kilodaltons, and the positions of intact precursor proteins and processed proteins are indicated by arrowheads.

6.4 Discussion

6.4.1 The Toc159 targeting pathway awaited discovery of a sorting signal

The mechanisms for targeting and membrane integration of the two homologous GTPase receptors (i.e.Toc159 and Toc34) remain an important facet of chloroplast preprotein import studies. As detailed in the previous chapter, immunogold localization of the endogenous receptors in *B. sinuspersici* leaves, transient expression of EGFP fusion proteins in *B. sinuspersici* leaf-derived protoplasts as well as particle-bombarded onion epidermal cells clearly demonstrated the strict association of Toc34 with plastids, while Toc159 appeared to be a soluble receptor, which partitioned between the inter-chloroplastic space and the chloroplast envelope in photosynthetic cells (Figures 5.7-5.9). These unique patterns of subcellular localization point to the discrete sorting pathways for Toc159 and Toc34, respectively.

Similarly to other tail-anchored proteins, the targeting of Toc34 to the chloroplast envelope is dependent on its transmembrane domain plus the flanking hydrophilic C-terminus (Chen and Schnell, 1997; Li and Chen, 1997; Qbadou et al., 2003; Dhanoa et al., 2010). Li and Chen (1997) demonstrated that this C-terminal region is sufficient for targeting and efficient insertion of a passenger protein regardless of the location of fusion at the N- or C-terminus. A recent study, on the other hand, showed that GFP fusion with the transmembrane domain plus the N- and C-terminal flanking residues was localized to non-plastid punctate structures, and that the correct envelope targeting required the G-domain (Dhanoa et al., 2010). The importance of the G-domain in targeting is consistent with independent studies showing that

binding of GTP or GDP is required for membrane integration of Toc34 (Chen and Schnell, 1997; Qbadou et al., 2003). As expected, the assembly of its GTPase homologue, Toc159, into the Toc complex at the chloroplast envelope also depends on the G-domain (Bauer et al., 2002; Smith et al., 2002a). The efficient integration of Toc159 to the chloroplast envelope also depends on guanine nucleotide binding and is mediated by its homotypic interaction with the Toc34 G-domain (Smith et al., 2002a). Whilst both Toc GTPases are targeted to the chloroplast envelope with the assistance of their G-domains, the essential sorting information embedded in the transmembrane domain plus the hydrophilic tail of Toc34 is missing in the sequence of Toc159 (Figure 5.4). However, one should expect to find equivalent signals accompanying the Toc159 G-domain, which is otherwise ineffectively differentiated from diverse members of the GTPase superfamily for protein targeting to other subcellular compartments (e.g. nucleus, endoplasmic reticulum, endomembrane system).

Since the A-domain is fully dispensable for the targeting of Toc159 (Bauer et al., 2002; Smith et al., 2002a), the putative sorting signal of Toc159 that accompanies the G-domain is expected to reside within the C-terminal M-domain. In fact, earlier studies have documented that the C-terminal region or the entire M-domain of Toc159, to a certain extent, bound to the chloroplast surface *in vitro* and *in vivo*, whereas C-terminal truncations of Toc159 severely reduced their binding (Muckel and Soll, 1996; Bauer et al., 2002; Smith et al., 2002a). Wallas et al. (2003) demonstrated that the binding of AtToc159 to the chloroplast envelope was more efficient in the presence of both G- and M-domains. Interestingly, the albino phenotype of the A. *thaliana* Toc159 knockout mutant (*ppi2*) was rescued with almost fully developed chloroplasts by over-expression of the Toc159 M-domain, which was found

exclusively at the chloroplast envelope (Lee et al., 2003). Thus, numerous lines of evidence support the current finding that the C-terminal end contributes to the subcellular localization of Toc159.

6.4.2 The C-terminus of Toc159 is a transit peptide-like signal

Accordingly, I sought to unravel the chloroplast-sorting signal of Toc159. In view of the well-studied targeting pathways for chloroplast outer membrane proteins (Hofmann and Theg, 2005; Bölter and Soll, 2011), the sorting signals can be broadly classified into two types. Proteins with hydrophobic membrane-spanning regions (i.e. signal- and tail-anchored proteins) rely on their transmembrane α-helices and the flanking charged residues as the envelope-targeting signals (Bölter and Soll, 2011). In contrast, the preprotein translocation channel Toc75 is a β-barrel protein that is sorted to the chloroplast envelope in the presence of a cTP, which is similar to the signals generally found in other chloroplast preproteins (Tranel et al., 1995; Tranel and Keegstra, 1996). A similar cTP signal was also predicted at the N-terminus of a Toc75 paralogue, AtOEP80 (Eckart et al., 2002), although this putative signal was later shown to be non-cleavable and its physiological relevance is not known (Inoue and Potter, 2004). Given the absence of a transmembrane helix in the Toc159 sequences (Figure 5.4), I asked whether Toc159 has a cTP sorting signal. No N-terminal cTP was predicted which is in agreement with the irrelevance of the N-terminus in the targeting of Toc159 (Bauer et al., 2002; Smith et al., 2002a). On the other hand, bioinformatics analyses suggested that the C-terminal region of Toc159 exhibits properties of cTPs (Figures 6.1-6.3; Tables 6.1- 6.3).

cTPs are highly divergent in primary structures with no consensus sequence identified but exhibit similar physicochemical and structural properties (Bruce, 2001), which were also predicted for the Toc159 CTs, in agreement with their specific association with the chloroplast envelope. First, I found that Toc159 CTs are rich in hydroxylated residues and, in contrast to the N-termini, lack acidic residues, which lead to basic C-terminal ends (Figure 6.1; Table 6.1). The basicity of cTPs has been proposed to mediate their initial ionic interaction with the anionic phospholipids at the outer chloroplast membrane, whereas the hydroxylated residues forms hydrogen bonds with the galactose headgroups of the non-bilayer galactolipids, particularly the chloroplast-specific monogalactosyldiacylglycerol (MGDG) (Pinnaduwage and Bruce, 1996; Bruce, 2000). However, some studies did not support this hypothesis and suggest that MGDG may not be as important as previously indicated (Inoue et al., 2001; Schleiff et al., 2003c). Furthermore, a recent molecular genetics study of *Arabidopsis* mutants (*mgd1-1*) with reduced levels of MGDG showed no significant difference in protein targeting and import efficiency between wild-type and mutant chloroplasts (Aronsson et al., 2008). Thus, the lipid-interacting activity of cTPs that forms the basis of the initial association of preproteins specifically with the chloroplast surface may involve other lipid constituents or some unknown factors. The cTP-lipid interaction can also be predicted from a structural perspective. cTPs predominantly form random coils in the cytosol but, in the membrane-mimicking environments, adopted α-helical structures that exhibited various degrees of amphipathicity (Bruce, 2001). The formation of amphipathic α-helices is an important feature of proteins at the membrane interface for seeking a surface between hydrophobic and hydrophilic phases. The Eisenberg hydrophobic moment plot exemplified one of the earliest applications of bioinformatics to predict such surface-seeking

proteins (Eisenberg et al., 1984). I constructed an equivalent plot to illustrate the similar amphipathicity of the predicted α-helices from Toc159 CTs and the demonstrated cTPs (Figure 6.3). The lower values of their hydrophobic moments compared to those of surface proteins suggest the possibility of weak lipid-affinities of these sorting signals to the chloroplast surface (Figure 6.3 and Table 6.2), which is plausible due to the temporary and reversible nature of the association. The bioinformatic analyses therefore predicted the tendency of the Toc159 CTs to reversibly associate with the chloroplast surface in a manner resembling the cTP-lipid interaction. The subsequent insertion of Toc159 CTs into the outer membrane, analogous to the irreversible insertion of cTPs into the protein channel for translocation, might require both Toc34 and Toc75. This notion is supported by previous findings that the Toc159 M-domain associated with Toc34 and that both Toc34 and Toc75 were essential for the *in vitro* insertion of AtToc159 into reconstituted proteoliposomes (Wallas et al., 2003).

The cTP-like function of Toc159 CTs raises an interesting question regarding the evolutionary origin of this novel chloroplast envelope-routing signal which was found at the C-terminus for the first time. While Toc159 does not have proven homologues of prokaryotic or eukaryotic ancestry, hydrophobic cluster analysis suggested that both N- and C-terminal domains originated from a successive duplication of the central G-domain and subsequent evolution toward their distinctive functions (Torres et al., 2007). On the other hand, it has been proposed that cTPs were originally derived from the ancestral cyanobacterial genes encoding the putative secretion substrates of the voltage-gated channel SynToc75 by exon shuffling (McFadden, 1999). Thus, I speculate that the presence of a cTP-like signal in

Toc159 CTs represents an example of convergent evolution when a photosynthetic cell was under the selective pressure to target the gene products to the chloroplast envelope. Indeed, despite the independent endosymbiotic evolution of mitochondria and chloroplasts, their targeting of preproteins also shares considerable similarities, from the evolutionary mechanisms and properties of the sorting signals to the nature of translocon machineries (Bruce, 2000; Schleiff and Becker, 2011). Since the neural network-based ChloroP predicted a putative cTP in Toc159 (Table 6.3) but not in other polypeptides retrieved from the Plant Proteomics Database (http://ppdb.tc.cornell.edu), I believe that this C-terminal signal represents a unique product from the evolution of the receptor under special circumstances, that (1) the targeting could be reversible in nature enabling the receptor to partition between the cytosol and the chloroplast envelope; (2) the targeting signal must confer an N_{out}-C_{in} topology of the receptor; and (3) the targeting signal could not reside at the N-terminus due to the proteolytic processing from this end for regulation of the receptor (Agne and Kessler, 2010).

6.4.3 The unique chloroplast-targeting signal meets the needs of Toc159

In the present study, I used a number of EGFP fusion constructs to reveal the properties of the Toc159 CTs, which appear to fulfill the sorting signal criteria for reversible targeting of the receptor to the chloroplast envelope in such an orientation that permits preprotein recognition on the cytosolic side. First, the constructs confirmed the bioinformatics analyses predicting that the Toc159 CTs exhibit properties of cTPs. I showed that C-terminal truncations abolished the chloroplast localization of Toc159 receptors while Toc159 CTs alone sorted EGFP to the chloroplast envelope (Figure 6.4). In addition, the Toc159 CTs re-

directed the C-terminally truncated Toc34 mutant from the cytosol to the chloroplast (Figure 6.6). I also demonstrated that the Toc159 CTs and other cTPs were in part functionally interchangeable (Figures 6.7 and 6.8). Interestingly, when fused at the N-terminus in the reverse orientation, the Toc159 CTs functioned as a cleavable cTP that mediated translocation of EGFP into the chloroplast stroma (Figure 6.8B). The co-purified protein in the stroma extract of the isolated chloroplasts was processed to the molecular weight of EGFP (28 kDa; Figure 6.8B), confirming the ChloroP prediction of a cleavage site for the stromal processing peptidase (Table 6.3). The fusion of Toc159 CTs at the C-terminus of EGFP did not produce any difference between the theoretical and apparent molecular weights *in planta* (Figures 6.4F and 6.4G), which is plausible since the fusion proteins in this orientation did not gain access to the stroma (Figure 6.5A). Stromal processing peptidase assays, on the other hand, suggested that the Toc159 CTs are potentially susceptible to the protein maturation events if exposed to the stromal extracts *in vitro* (Figure 6.9). The assessment of whether the Toc159 CTs are processed at the chloroplast envelope requires insertion of the receptor to the outer membrane, which happens solely if both the G- and M-domains are present (Smith et al., 2002a). As a result, the subtle change in molecular weights of such fusion proteins after signal cleavage is not easily distinguishable by gel electrophoresis (Figures 6.4A and 6.4B). The possibility of Toc159 C-terminal cleavage, however, could be addressed in the future using other approaches such as mass spectrometry.

In addition, I showed that a fusion of EGFP to the C-terminus of Toc159 CTs was susceptible to thermolysin treatment of chloroplasts isolated from the transfected protoplasts, suggesting that the fusion proteins were exposed to the chloroplast exterior (Figure 6.5A).

This scenario is analogous to the A- and G-domains of endogenous Toc159 being projected to the cytosolic side of the chloroplast envelope. Thus, the sorting signal at the C-terminus contributes to conferring the favorable N_{out}-C_{in} topology of the receptor for preprotein recognition in the cytosol. Alkaline extraction of the isolated chloroplasts after expression of the same EGFP constructs further confirmed that the fusion proteins were not integrated into the chloroplast envelope (Figure 6.5B). This observation is consistent with the bioinformatic analyses predicting that the Toc159 CTs are not membrane anchors but rather function as cTP-like sorting signals that interact reversibly with the lipid components at the chloroplast surface. This reversible interaction might account for the abundance of fusion proteins that remained in the cytosol and the occasional contamination of the stromal extract due to the detachment of the fusion proteins from the envelope during the chloroplast lysis treatment (Figures 6.4F and 6.4G). In fact, Smith et al. (2002a) reported that initial docking of AtToc159 at the chloroplast envelope does not require bound nucleotide and the association is not stable until successful insertion occurs in a guanine nucleotide-dependent manner. Thus, the initial contacts of cTPs with the chloroplast envelope are reversible and energy-independent while subsequent insertion of the preproteins into the Toc complex is irreversible and dependent on ATP and GTP (Perry and Keegstra, 1994; Kouranov and Schnell, 1997).

Based on the affinity to the chloroplast envelope, the reversibility of the association, and the orientation of targeting, I conclude that Toc159 CT functions a sorting signal of the receptor.

6.4.4 A dual domain-mediated targeting pathway of Toc159

In our effort to identify a novel C-terminal cTP-like sorting signal, we have unravelled the fundamental components that account for the subcellular localization of Toc159. Incorporating the C-terminal signalling component into the current "targeting" model for preprotein import into chloroplasts (Smith, 2006), I now propose a dual domain-mediated targeting pathway for Toc159. First, the C-terminal sorting signal targets the soluble preprotein-bound Toc159 receptor to the chloroplast envelope. Second, the C-terminal sorting signal mediates reversible docking on the chloroplast surface through interaction with the lipids and/or other components of the Toc complex (i.e. Toc34 and Toc75). Third, the homotypic interaction between the GTP-bound G-domains of Toc159 and Toc34 stimulates GTP hydrolysis leading to the insertion of Toc159 into the outer membrane and initiation of preprotein translocation. Lastly, the G-domains of both Toc159 and Toc34 exchange GDP for GTP leading to the subsequent dissociation of Toc159 receptors from the Toc complex. In the future, structural studies of the Toc159 M-domain will provide insights into its functions as a membrane anchor and a chloroplast-targeting signal. *In vitro* targeting assays will also be performed to further characterize the novel targeting pathway of Toc159, particularly in relation to the requirement for proteinaceous components such as 14-3-3 proteins and molecular chaperones.

Chapter 7. Conclusions and future directions

The carbon-concentrating mechanism of terrestrial C_4 species has long intrigued scientists' efforts to boost productivity and nitrogen use efficiency of major crop plants by genetic engineering of similar C_4 machinery (Surridge, 2002). Whilst the anatomical complexity of the dimorphic chloroplast separation in a typical C_4 system remains one of the biggest hurdles toward the C_3-to-C_4 conversion, the more recent discovery of the intracellular compartmentation of dimorphic chloroplasts in three single-cell C_4 species has become a promising alternative without the need of engineering a dual-cell system. Over the past decade, fundamental research into the single-cell C_4 species has provided significant insights into the dimorphic chloroplast development at the anatomical and molecular levels. On the other hand, the differentiation of dimorphic chloroplasts, particularly the mechanism(s) leading to their differential protein accumulation, has yet to be explored at the biochemical level. Perhaps, thorough investigation of the single-cell C_4 species had been hindered by the technical limitations. To these ends, this thesis has made significant contributions as summarized below.

The first part of this thesis reported the establishment of multiple versatile techniques for the studies of single-cell C_4 model in *B. sinuspersici*. An efficient transient expression system was established for the first time in a single-cell C_4 species based on polyethylene glycol-mediated transfection of isolated chlorenchyma protoplasts. The high efficiency (i.e. over 80% of transfection rate) of this gene manipulation system suggests that over-expression and down-regulation of photosynthetic genes become a promising tool to unravel the novel

single-cell C_4 pathways. On the other hand, the established system opens a possibility that unknown functions of novel proteins be implicated through a subcellular localization approach, since the fluorescent protein fusions with a handful of different targeting signals were all targeted to their respective subcellular locations including the cytosol, nucleus, actin filaments, microtubules, peroxisomes, mitochondria and dimorphic chloroplasts. The observation of these subcellular structures using fluorescent protein markers also allows organelle dynamics studies, for instance, to explore the role of the cytoskeleton in light-oriented positioning of dimorphic chloroplasts in the future.

The successful isolation of a homogenous population of chlorenchyma protoplasts not only led to the establishment of a gene manipulation system, but also facilitated the purification of subcellular organelles. In analogy with the previous efforts of purifying the mesophyll and bundle sheath cells in Kranz-type C_4 plants over the past four decades, subcellular organelle fractionation of the single-cell C_4 species is indispensable for defining the relationship between the subcellular anatomical arrangements and the functional C_4 mechanisms. In a single-cell C_4 system, the complexity of subcellular organelle compartmentation implies that a gentle subfractionation approach is more preferable to mechanical treatments. As the first step, the present study was initiated to define the optimum conditions of cell wall digestion in an osmoticum- and pH-dependent manner for the best maintenance of organelle integrity as revealed by cytochemical staining under confocal laser scanning microscopy. The subsequent lysis of the intact chlorenchyma protoplasts has led to the success in dimorphic chloroplast purification. As a novel approach for plant organelle purification, the described procedures were empirically established based on the knowledge of the extraordinary subcellular

anatomy. Hypo-osmotically induced lysis of the isolated chlorenchyma protoplasts under the precise conditions resulted in the sedimentation of the central chloroplasts embedded in the central cytoplasmic compartments and the floatation of the peripheral chloroplasts adhered externally to the vacuole surface. The dimorphic chloroplasts were further purified on a Percoll step gradient to apparent homogeneity as confirmed by light microscopy and immunoblot analysis with antibodies against various protein markers. As a consequence, the potential applications of the two homogenous preparations of dimorphic chloroplasts from *B. sinuspersici* can be manifold. For instance, high-throughput comparative proteomics studies will help define the structure-function relationship and the physiological relevance of the dimorphic chloroplasts in relation to the proposed single-cell C_4 model as well as other plastid functions. In addition, to account for the differential protein accumulation in dimorphic chloroplasts, the two isolated chloroplast populations will also be useful in selective preprotein import research.

The second part of this thesis documented the characterization of the chloroplast preprotein import receptors in *B. sinuspersici*. Whilst the different proteomes of dimorphic chloroplasts in Kranz-type C_4 plants are attributable to the differential regulation of gene expression among the dual cell types at the transcriptional and translational levels, the same rationales cannot be applied to the similar phenomenon in the single-cell C_4 species which house the dimorphic chloroplasts within the cells. Since all C_4 enzymes and the vast majority of other plastidial proteins are universally encoded by the nuclear genomes, translated in the cytosol and translocated into the plastids, post-translational regulation of the chloroplast proteins is more probable in the single-cell C_4 species. Initial assessment using fluorescent fusion

proteins with various transit peptides indicated that multiple mechanisms might be interplaying. The transit peptides of Rubisco small-subunit and ferredoxin:$NADP^+$ reductase guided the passenger proteins efficiently into both types of chloroplasts, suggesting that these enzymes might not be selectively imported to the dimorphic chloroplasts. Instead, the mRNAs may be selectively targeted for translation in proximity to the respective chloroplast type and/or the imported proteins at the "wrong" destination may be selectively targeted for degradation. On the other hand, the transit peptides of pyruvate orthophosphate dikinase and ferredoxin sorted the passenger proteins more efficiently into the peripheral chloroplasts, implicating a possibility of selective protein targeting. As an initial step toward an ultimate goal of characterizing the selective protein import mechanism, I sought to identify the chloroplast protein import receptors Toc159 and Toc34 and determine their subcellular localization. In the present study, phylogenies and the conservation of domain structures confirmed the identification of three cDNA sequences encoding two Toc159 and one Toc34 homologues from *B. sinuspersici*. Phylogenetic analysis and protein expression profiling also implicated the different substrate selectivity of the two Toc159 homologues. Thus, the evolution of the single-cell C_4 species in the C_4 lineage apparently has not altered the universal substrate-specific mode of preprotein recognition as elucidated in C_3 species. Transient expression of fluorescent protein fusions revealed a cytosolic form of both Toc159 isoforms in isolated protoplasts of *B. sinuspersici* and *A. thaliana* and particle-bombarded onion epidermal cells, whereas the fusion protein with Toc34 was exclusively plastid-associated. To rule out the possibility of the cytosolic occurrence due to experimental artefacts from protein over-expression, the endogenous Toc159 proteins were also studied by immunogold localization and subcellular fractionation. Consistently, a considerable amount

of immunoreactive signals were not membrane-associated. The immunogold studies also revealed that the cytosolic Toc159 proteins were localized in close proximity to the chloroplast envelope, which might be attributed to their association with the cytoskeleton. While subcellular fractionation studies indicated that the cytosolic Toc159 proteins were not truly soluble, they could be "solubilized" with actin filament- or microtubule-disrupting drugs. Further experiments showed that both Toc159 isoforms co-immunoprecipitated with anti-actin and anti-β-tubulin antibodies.

The partitioning of Toc159 between the cytosolic- and envelope-associated forms is pertinent to my discovery that the receptors are reversibly targeted to the chloroplast surface by a C-terminal transit peptide-like sorting signal. Multiple computational analyses predicted the chloroplastic transit peptide properties of Toc159 C-terminal tails (CTs), including the abundance of hydroxylated residues, the rare occurrence of acidic residues and the presence of a putative amphipathic α-helix. The neural network-based ChloroP analysis also predicted the putative sorting signals at the Toc159 CTs. This prediction was confirmed using a number of fluorescent protein fusion constructs. Whilst the C-terminal truncations of Toc159 abolished chloroplast-targeting, the CTs were sufficient to guide passenger proteins and re-target the Toc34 mutant proteins to the chloroplast surface. On the other hand, the protein fusion with the CT of BsToc159 in the reverse orientation was translocated into the stroma. Further experiments suggested that the reverse sequences of chloroplastic transit peptides were in part interchangeable with the Toc159 CTs, implicating their conserved functions. Collectively, since it has been documented that the GTPase domain of Toc159 is crucial for its homotypic interaction with Toc34 as a docking site on the chloroplast surface, the

partitioning of Toc159 between the cytosolic and the chloroplast envelope for preprotein recognition might be attributable to a novel targeting mechanism which involves the central GTPase domain and the C-terminal sorting signal.

Therefore, incorporating my findings into the current "targeting" model for preprotein import into chloroplasts, I propose that a dual-domain-mediated mechanism that guides the movement of Toc159 receptors reversibly to and from the chloroplast surface possibly involving the cytoskeleton. In the future, this hypothetical model can be elucidated by investigating the missing link between Toc159-cytoskeleton interaction and chloroplast preprotein targeting. For instance, the chloroplast-targeting efficiency may be studied *in planta* and *in vitro* after the treatment of isolated protoplasts with cytoskeleton-disrupting agents and chemical inhibitors of motor proteins. With the fundamental knowledge of the identity, subcellular distribution and targeting mechanism of the Toc receptors, the selective protein import mechanism can be explored in the single-cell C_4 species in the future. While the selective preprotein targeting can be studied by *in vitro* import assays using homogenous preparations of dimorphic chloroplasts, the different selectivities of Toc34/159 subtypes can be implicated from antibody-neutralization and *in vitro* binding studies.

Appendix I - Vector maps

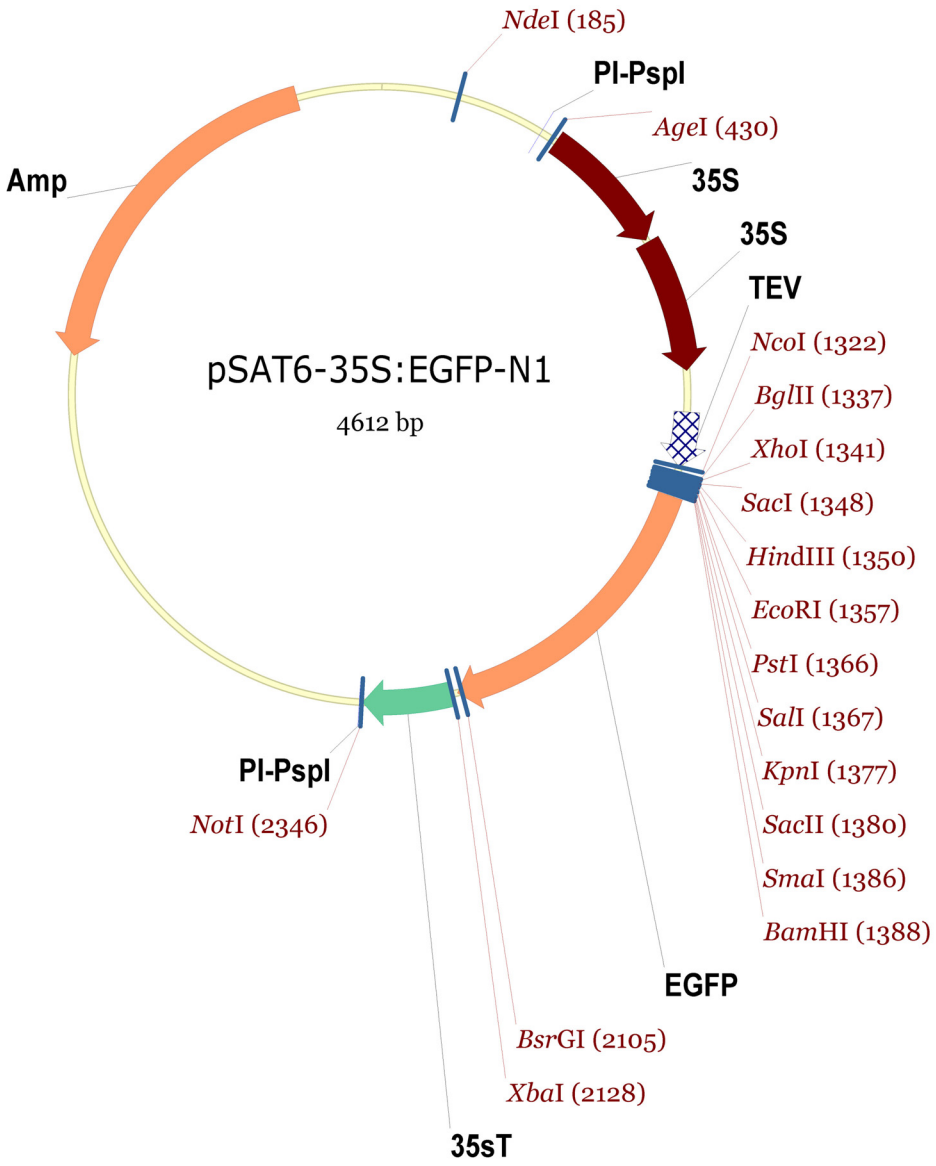

pSAT6-35S:EGFP-N1 sequence landmarks:

- Cauliflower mosaic virus 35S promoters (35S)	441 - 1,089
- Translational enhancer from tobacco etch virus (TEV)	1,190 - 1,320
- Enhanced green fluorescent protein (EGFP)	1,395 - 2,114
- Cauliflower mosaic virus 35S terminator (35sT)	2,133 – 2,343
- Ampicillin selection marker (Amp)	3,552 – 4,412

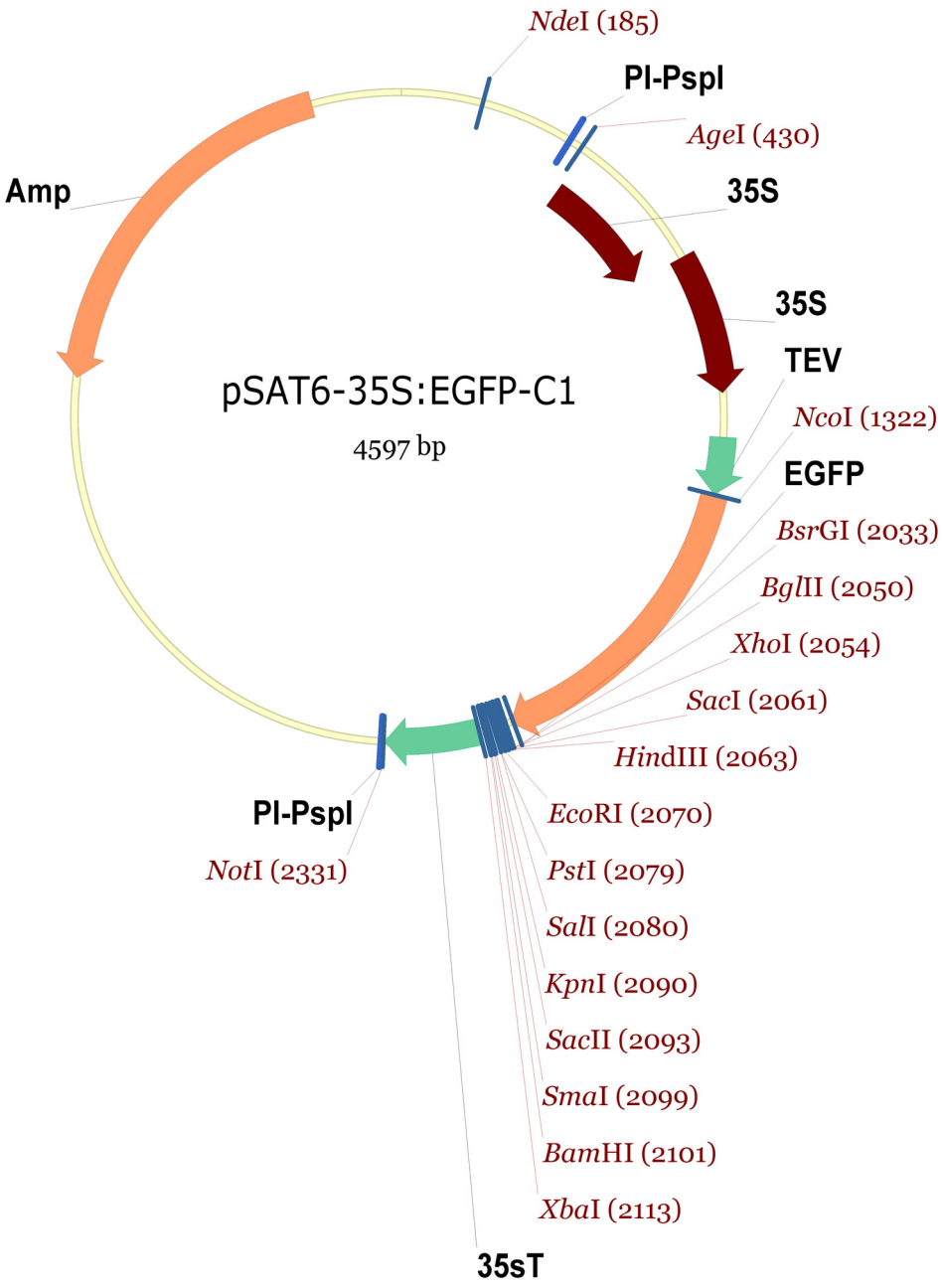

pSAT6-35S:EGFP-C1 sequence landmarks:

- Cauliflower mosaic virus 35S promoters (35S)	441 - 1,089
- Translational enhancer from tobacco etch virus (TEV)	1,190 - 1,320
- Enhanced green fluorescent protein (EGFP)	1,323 - 2,039
- Cauliflower mosaic virus 35S terminator (35sT)	2,118 – 2,328
- Ampicillin selection marker (Amp)	3,537 – 4,397

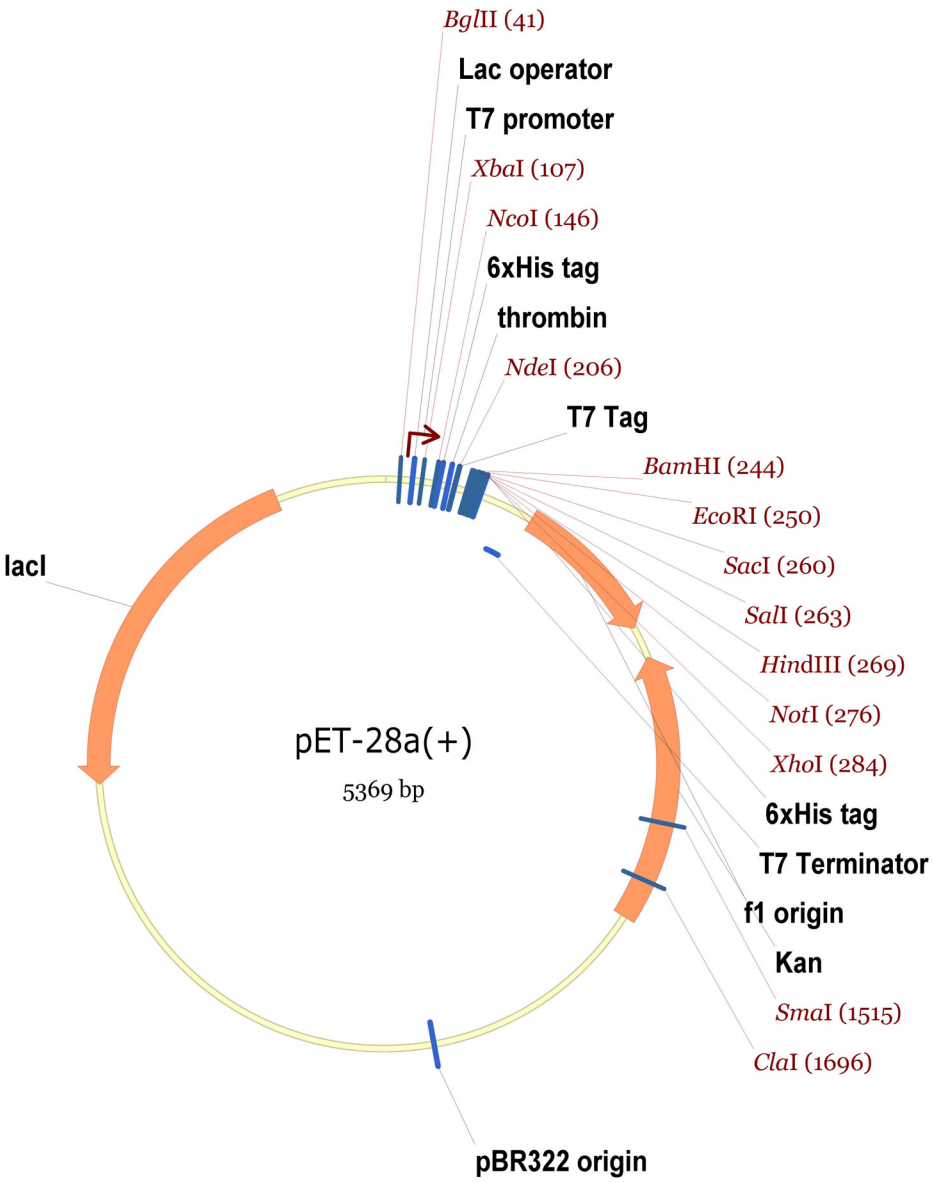

pET-28a(+) sequence landmarks

- T7 promoter	60 - 76
- T7 transcription start site	77
- N-terminal 6xHis tag coding sequence	159 - 176
- Thrombin cleavage site	186 - 203
- N-terminal T7 tag coding sequence	207 - 239
- C-terminal 6xHis tag coding sequence	289 - 306
- T7 terminator	374 - 420
- f1 origin	457 - 912
- Kanamycin selection marker (Kan)	1,008 – 1,820
- pBR322 origin	2,529
- *lacI* coding sequence	3,963 – 5,042

Appendix II

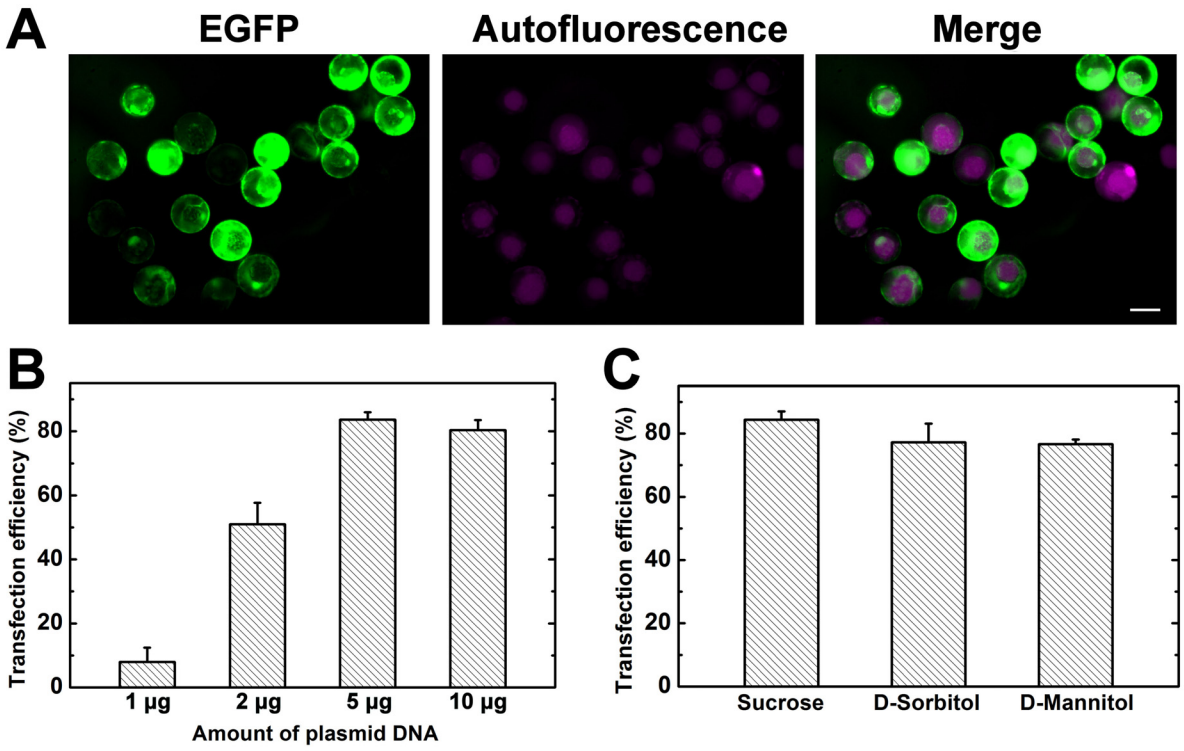

Appendix II. Optimization for transient expression in isolated chlorenchyma protoplasts from *B. sinuspersici*

Transfection efficiencies were determined as percentages of EGFP-expressing protoplasts over the total number of protoplasts randomly counted under epifluorescence microscopy. The depicted values represent means from at least four independent experiments (±SE).

(A) Isolated protoplasts were transfected with 5 µg of pSAT6-35S::EGFP-N1 plasmid DNA and imaged under epifluorescence microscopy. EGFP fluorescence (left panel), chlorophyll autofluorescence (middle panel) and a merged image (right panel) are shown. Scale bar = 20 µm.
(B) Effect of plasmid concentrations on protoplast transfection efficiencies.
(C) Effect of various osmotica on protoplast transfection efficiencies.

Remark: These experiments were performed by Dr. Makoto Yanagisawa.

Appendix III

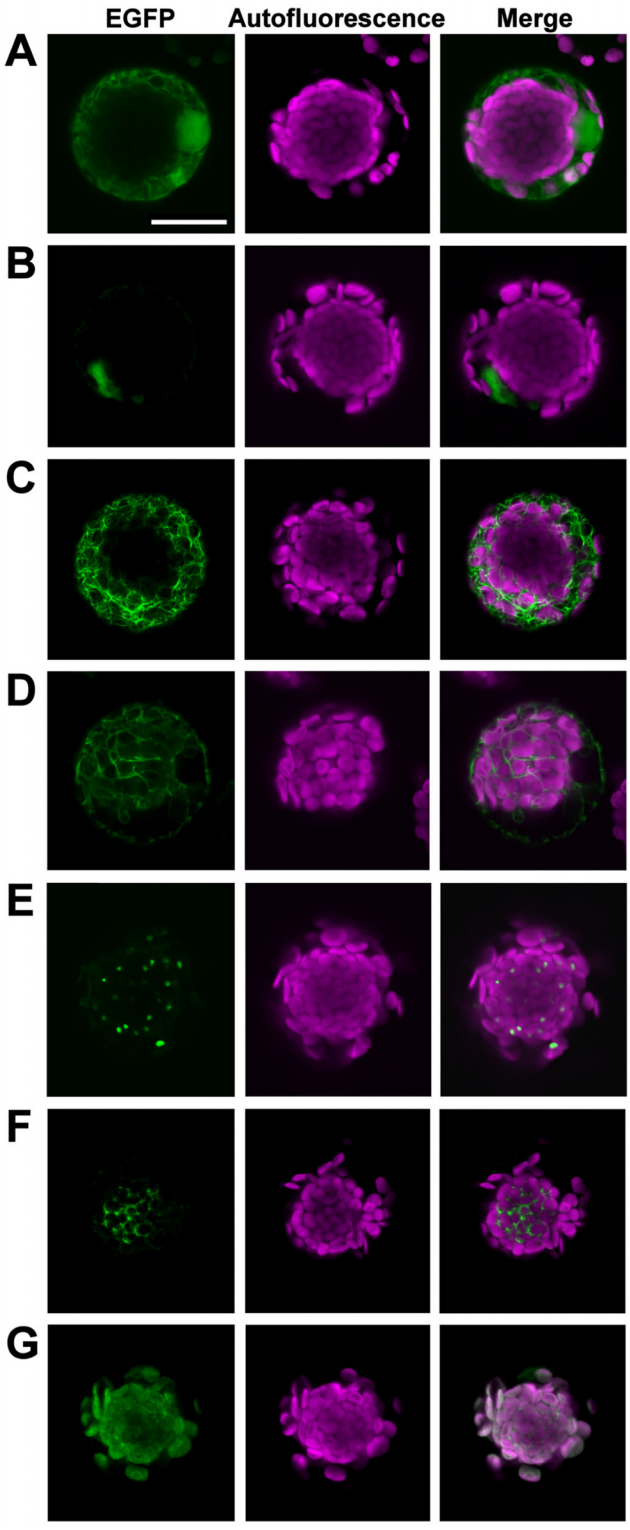

Figure legend on the next page

Appendix III. Transient expression of EGFP fusion proteins localized to various subcellular organelles of isolated protoplasts from *B. sinuspersici*

Isolated protoplasts were transfected with 5 µg of DNA of various plasmid constructs for transient expression of EGFP fusion proteins driven by the constitutive 35S promoter. Live protoplasts were visualized under confocal laser scanning microscopy. Each image shows a representative result from at least three independent experiments. EGFP fluorescence (left panels), chlorophyll autofluorescence (middle panels) and merged images (right panels) are shown.

(A) EGFP protein was unmodified.
(B) A nuclear localization signal was fused to the N-terminus of EGFP (NLS-EGFP).
(C) An actin-binding protein, talin, was fused to the C-terminus of GFP (GFP-talin).
(D) A microtubule-binding protein, MAP4, was fused to the C-terminus of GFP (GFP-MAP4).
(E) A peroxisomal targeting signal (SKL) was fused to the N-terminus of EGFP (EGFP-SKL).
(F) The mitochondrial presequence of NAD-malic enzyme was fused to the N-terminus of EGFP (tME-EGFP).
(G) The transit peptide of Rubisco small-subunit was fused to the N-terminus of EGFP (tRbcS-EGFP).

Remark: These experiments were performed in collaboration with Dr. Makoto Yanagisawa. Fluorescence images were acquired by Dr. Yanagisawa.

Appendix IV

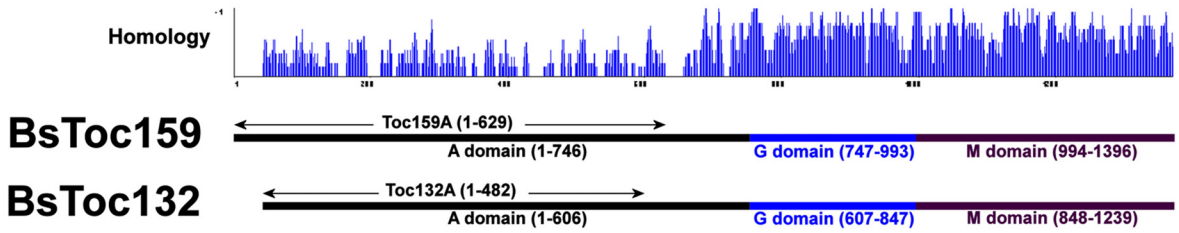

Appendix IV. Production of isoform-specific antibodies against the highly variable regions of Toc159 at the N-termini

The amino acid sequence variability along the sequences is illustrated by an absolute complexity plot of aligned Toc159, which indicates the average of pairwise alignment scores of each residue as computed using the AlignX module of Vector NTI Advance^{TM} 10.3.0 (Invitrogen) with the substitution matrix blosum62mt2. The more positive the value, the higher the degree of conservation is. The regions of BsToc159 and BsToc132 for over-expression of antigenic proteins are indicated by arrows.

Appendix V

A

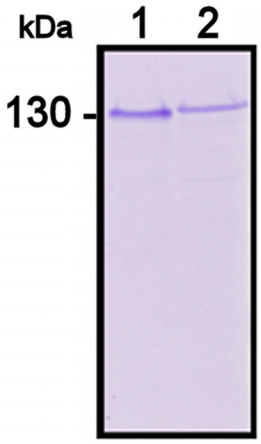

B

[Theoretical pI: 4.05 / Mw (average mass): 67745.62 / Mw (monoisotopic mass): 67705.56]

mass	position	#MC	artif.modification(s)		modifications	peptide sequence
4218.8683	120-162	0				DEEGVGEEEAVESLDVGSVAGNEETLAVENASEDSGAANGGVK
3705.6765	323-359	0				DLGAELESSVAENAGQVVENSDANGSAPEVGEFEGTK
3309.5484	538-570	0				SVELDGLDAAASDIPSPANGVNAEEENLGAQEK
3233.5211	445-475	0				VAENVTSANEFAALATANSSEIVDVDDEQPK
2930.2900	55-83	0				EPEVEEGNEETLAVENASEDSGAANGGVK

C

[Theoretical pI: 4.26 / Mw (average mass): 53949.78 / Mw (monoisotopic mass): 53917.61]

mass	position	#MC	artif.modification(s)		modifications	peptide sequence
3730.7293	368-403	0				VESSSSDISSSIDGNLTSEPQHSAPSLESSLNENVK
3547.5961	76-108	0				DSDGSEVFEEAVELAIDEGNDGLKPELDDVDAR
3475.5532	157-189	0	MSO:169	3491.5481		VESIEANDHEGSMITANEDSSVAIEGSETLGER
2688.2838	404-429	0				AESIASDLGTQTNANTLIQSPDTDAR
2635.2110	454-478	0				ASTQIQSPDTVHDSHALAEGEGTER

Figure legend on the next page

Appendix V. Aberrant electrophoretic motilities of recombinant BsToc159 and BsToc132 A-domains

Hexahistidine-tagged recombinant proteins of $BsToc159_{(1-629)}$ and $BsToc132_{(1-482)}$ were expressed in *E. coli* and purified by immobilized metal affinity chromatography. The purified proteins were run on SDS-PAGE and analyzed by tandem mass spectrometry (MS/MS). Briefly, the protein bands were excised, washed with water, destained with 50 mM NH_4HCO_3/50% acetonitrile, reduced with 10 mM DTT, alkylated with 55 mM iodoacetamide, and dehydrated with 100% acetonitrile. The rehydrated samples were digested with trypsin overnight, and the tryptic peptides were cleaned using the C-18 ZipTip system (Millipore, Billerica, MA, USA) and eluted with 5 μL of 50% acetonitrile with 0.2% formic acid. The protonated peptides were analyzed using a Waters Micromass Q-TOF Ultima with nanospray injection.

(A) Coomassie blue staining of purified recombinant proteins in a SDS-PAGE gel. Both BsToc159 and BsToc132 A-domains were run to the ca. 130 kDa positions, which deviated from the theoretical molecular weights of 68 and 54 kDa, respectively.
(B) Sample data from the MS/MS analysis of purified BsToc159 A-domain.
(C) Sample data from the MS/MS analysis of purified BsToc132 A-domain.

Remark: The MS/MS-based amino acid sequencing was performed by Dr. Zhenyu Cheng.

Appendix VI

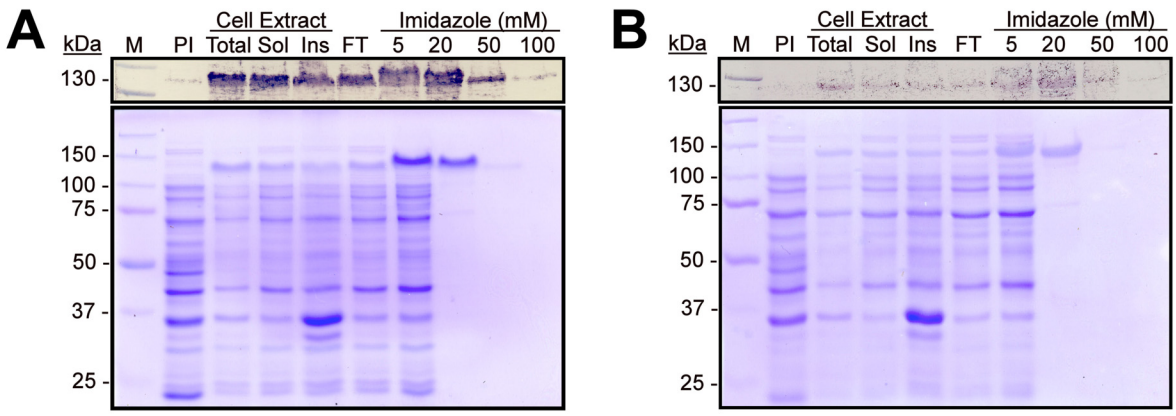

Appendix VI. Purification of recombinant Toc159 A-domains by immobilized metal affinity chromatography

Hexahistidine-tagged recombinant proteins of BsToc159$_{(1\text{-}629)}$ and BsToc132$_{(1\text{-}482)}$ were expressed in *E. coli* and purified by immobilized metal affinity chromatography. Immobilized proteins were eluted with a stepwise gradient of increasing concentrations of imidazole. Proteins resolved on 10%/SDS-PAGE were stained with Coomassie Blue R-250 (lower panels) and subjected to Western blot analysis. Immunoblots were probed with anti-His_6 antibody and anti-mouse alkaline phosphatase-conjugated antibody, and the signals were visualized with NBT/BCIP substrates. Lane 1, protein standard; lane 2, pre-induced cell extract; lane 3, induced cell extract; lane 4, soluble fraction; lane 5, insoluble fraction; lane 6, flow-through; lanes 7-10, eluents with 5-100 mM imidazole.

(A) Purification of BsToc159 A-domain.
(B) Purification of BsToc132 A-domain.

References

Agne B, Infanger S, Wang F, Hofstetter V, Rahim G, Martin M, Lee DW, Hwang I, Schnell D, Kessler F (2009) A Toc159 import receptor mutant, defective in hydrolysis of GTP, supports preprotein import into chloroplasts. J Biol Chem **284**: 8670-8679

Agne B, Kessler F (2009) Protein transport in organelles: The Toc complex way of preprotein import. FEBS J **276**: 1156-1165

Agne B, Kessler F (2010) Modifications at the A-domain of the chloroplast import receptor Toc159. Plant Signal Behav **5**: 1513-1516

Akhani H, Barroca J, Koteeva N, Voznesenskaya E, Franceschi V, Edwards G, Ghaffari SM, Ziegler H (2005) *Bienertia sinuspersici* (Chenopodiaceae): a new species from Southwest Asia and discovery of a third terrestrial C_4 plant without Kranz anatomy. Syst Bot **30**: 290-301

Akhani H, Trimborn P, Ziegler H (1997) Photosynthetic pathways in Chenopodiaceae from Africa, Asia and Europe with their ecological, phytogeographical and taxomomical importance. Plant Syst Evol **206**: 187-221

Akita M, Nielsen E, Keegstra K (1997) Identification of protein transport complexes in the chloroplastic envelope membranes via chemical cross-linking. J Cell Biol **136**: 983-994

America T, Hageman J, Guera A, Rook F, Archer K, Keegstra K, Weisbeek P (1994) Methotrexate does not block import of a DHFR fusion protein into chloroplasts. Plant Mol Biol **24**: 283-294

Andersson FI, Blakytny R, Kirstein J, Turgay K, Bukau B, Mogk A, Clarke AK (2006) Cyanobacterial ClpC/HSP100 protein displays intrinsic chaperone activity. J Biol Chem **281**: 5468-5475

Andres C, Agne B, Kessler F (2010) The TOC complex: Preprotein gateway to the chloroplast. Biochim Biophys Acta **1803**: 715-723

Aronsson J, Schottler MA, Kelly AA, Sundqvist C, Dormann P, Karim S, Jarvis P (2008) Monogalactosyldiacylglycerol deficiency in *Arabidopsis* affects pigment composition in the prolamellar body and impairs thylakoid membrane energization and photoprotection in leaves. Plant Physiol **148**: 580-592

Bae W, Lee YJ, Kim DH, Lee J, Kim S, Sohn EJ, Hwang I (2008) AKR2A-mediated import of chloroplast outer membrane proteins is essential for chloroplast biogenesis. Nat Cell Biol **10**: 220-227

Balsera M, Goetze TA, Kovács-Bogdan E, Schürmann P, Wagner R, Buchanan BB, Soll J, Bölter B (2009b) Characterization of Tic110, a channel-forming protein at the inner envelope membrane of chloroplasts, unveils a response to Ca^{2+} and a stromal regulatory disulfide bridge. J Biol Chem **284**: 2603-2616

Balsera M, Soll J, Bölter B (2009a) Protein import machineries in endosymbiotic organelles. Cell Mol Life Sci **66**: 1903-1923

Bauer J, Chen K, Hiltbunner A, Wehrli E, Eugster M, Schnell, D (2000) The major protein import receptor of plastids is essential for chloroplast biogenesis. Nature **403**: 203-207

Bauer J, Hiltbrunner A, Weibel P, Vidi PA, Alvarez-Huerta M, Smith MD, Schnell DJ, Kessler F (2002) Essential role of the G-domain in targeting of the protein import receptor atToc159 to the chloroplast outer membrane. J Cell Biol **159**: 845-854

Becker T, Jelic M, Vojta A, Radunz A, Soll J, Schleiff E (2004) Preprotein recognition by the Toc complex. EMBO J **23**: 520-530

Bédard J, Jarvis P (2005) Recognition and envelope translocation of chloroplast preproteins. J Exp Bot **56**: 2287-2320

Bédard J, Kubis S, Bimanadham S, Jarvis P (2007) Functional similarity between the chloroplast translocon component, Tic40, and the human co-chaperone, Hsp70-interacting protein (Hip). J Biol Chem **282**: 21404-21414

Bendtsen JD, Nielsen H, von Heijne G, Brunak S (2004) Improved prediction of signal peptides: SignalP 3.0. J Mol Biol **340**: 783-795

Benz JP, Soll J, Bölter B (2009) Protein transport in organelles: The composition, function and regulation of the Tic complex in chloroplast protein import. FEBS J **276**: 1166-1176

Bird MI, Haberie SG, Chivas AR (1994) Effect of altitude on the carbon-isotope composition of forest and grassland soils from Papua New Guinea. Global Biogeochem Cy **8**: 13-22

Bischof S, Baerenfaller K, Wildhaber T, Troesch R, Vidi PA, Roschitzki B, Hirsch-Hoffmann M, Hennig L, Kessler F, Gruissem W, Baginsky S (2011) Plastid proteome assembly without Toc159: photosynthetic protein import and accumulation of *N*-acetylated plastid precursor proteins. Plant Cell **23**: 3911-3928

Bölter B, May T, Soll J (1998) A protein import receptor in pea chloroplasts, Toc86, is only a proteolytic fragment of a larger polypeptide. FEBS Lett **441**: 59-62

Bölter B, Nada A, Fulgosi H, Soll J (2006) A chloroplastic inner envelope membrane protease is essential for plant development. FEBS Lett **580**: 789-794

Bölter B, Soll J (2001) Ion channels in the outer membranes of chloroplasts and mitochondria: open doors or regulated gates? EMBO J **20**: 935-940

Bölter B, Soll J (2011) Protein import into chloroplasts: dealing with the (membrane) integration problem. ChemBioChem **12**: 1655-1661

Bölter B, Soll J, Hill K, Hemmler R, Wagner R (1999) A rectifying ATP-regulated solute channel in the chloroplastic outer envelope from pea. EMBO J **18**: 5505-5516

Boyd CN, Franceschi VR, Chuong SDX, Akhani H, Kiirats O, Smith M, Edwards GE (2007) Flowers of *Bienertia cycloptera* and *Suaeda aralocaspica* (Chenopodiaceae) complete the life cycle performing single-cell C_4 photosynthesis. Funct Plant Biol **34**: 268-281

Bradford MM (1976) A rapid and sensitive method for quantitation of microgram quantities of protein utilizing the principle of protein-dye-binding. Anal Biochem **72**: 248-254

Bruce BD (2000) Chloroplast transit peptides: structure, function and evolution. Trends Cell Biol **10**: 440-447

Bruce BD (2001) The paradox of plastid transit peptides: conservation of function despite divergence in primary structure. Biochim Biophys Acta **1541**: 2-21

Caliebe A, Grimm R, Kaiser G, Lubeck J, Soll J, Heins L (1997) The chloroplastic protein import machinery contains a Rieske-type iron-sulfur cluster and a mononuclear iron-binding protein. EMBO J **16**: 7342-7350

Calvin M (1956) The photosynthetic carbon cycle. J Chem Soc **1956**: 1895-1915

Chan CX, Bhattacharya D (2010) The origin of plastids. Nat Educ **3**: 84

Chen D, Schnell DJ (1997) Insertion of the 34-kDa chloroplast protein import component, IAP34, into the chloroplast outer membrane is dependent on its intrinsic GTP-binding capacity. J Biol Chem **272**: 6614-6620

Chen K, Chen X, Schnell, DJ (2000) Initial binding of preproteins involving the Toc159 receptor can be bypassed during protein import into chloroplasts. Plant Physiol **122**: 813-822

Chen R, Rosen E, Masson PH (1999) Gravitropism in higher plants. Am J Plant Physiol **120**: 343-350

Chen S, Tao L, Zeng L, Vega-Sanchez M, Umemura K, Wang G (2006) A highly efficient transient protoplast system for analyzing defence gene expression and protein-protein interactions in rice. Mol Plant Pathol **7**: 417-427

Chen X, Smith MD, Fitzpatrick L, Schnell DJ (2002) In vivo analysis of the role of atTic20 in protein import into chloroplasts. Plant Cell **14**: 641-654

Chew O, Rudhe C, Glaser E, Whelan J (2003) Characterization of the targeting signal of dual-targeted pea glutathione reductase. Plant Mol Biol 53: 341-356

Chigri F, Soll J, Vothknecht UC (2005) Calcium regulation of chloroplast protein import. Plant J **42**: 821-831

Chou ML, Fitzpatrick LM, Tu SL, Budziszewski G, Potter-Lewis S, Akita M, Levin JZ, Keegstra K, Li HM (2003) Tic40, a membrane-anchored co-chaperone homolog in the chloroplast protein translocon. EMBO J **22**: 2970-2980

Chung SM, Frankman EL, Tzfira T (2005) A versatile vector system for multiple gene expression in plants. Trends Plant Sci **10**: 357-361

Chuong SDX, Franceschi VR, Edwards GE (2006) The cytoskeleton maintains organelle partitioning required for single-cell C_4 photosynthesis in Chenopodiaceae species. Plant Cell **18**: 2207-2223

Clark SA, Theg SM (1997) A folded protein can be transported across the chloroplast envelope and thylakoid membrane. Mol Biol Cell **8**: 923-934

Cocking EC (1960) A method for the isolation of plant protoplasts and vacuoles. Nature **187**: 962–963

Constan D, Patel R, Keegstra K, Jarvis P (2004) An outer envelope membrane component of the plastid protein import apparatus plays an essential role in *Arabidopsis*. Plant J **38**: 93-106

Crawford NM (1995) Nitrate: nutrient and signal for plant growth. Plant Cell **7**: 859-868

Crooks GE, Hon G, Chandonia JM, Brenner SE (2004) WebLogo: A sequence logo generator. Genome Res **14**: 1188-1190

Davey MR, Anthony P, Power JB, Lowe KC (2005) Plant protoplasts: status and biotechnological perspectives. Biotechnol Adv **23**: 131-171

Della-Cioppa G, Bauer SC, Klein BK, Shah DM, Fraley RT, Kishore GM (1986) Translocation of the precursor of 5-enolpyruvylshikimate-3-phosphate synthase into chloroplasts of higher plants *in vitro*. Proc Nat Acad Sci USA **83**: 6873-6877

Deruère J, Römer S, d'Harlingue A, Backhaus RA, Kuntz M, Camara (1994) Fibril assembly and carotenoid over accumulation: a model for supramolecular lipoprotein structures. Plant Cell **6**: 119-133

Dhanoa PK, Richardson LGL, Smith MD, Gidda SK, Henderson MPA, Andrews DW, Mullen RT (2010) Distinct pathways mediate the sorting of tail-anchored proteins to the plastid outer envelope. PLoS ONE **5**: e10098

Dörmann P (2006) Lipid synthesis, metabolism and transport. In: Wise RR, Hoober JK (eds) *The Structure and Function of Plastids,* Vol. 23. Springer, Dordrecht, The Netherlands, pp. 335-353

Duy D, Wanner G, Meda A, von Wirén N, Soll J, Philippara K (2007) PIC1, an ancient permease in *Arabidopsis* chloroplasts, mediates iron transport. Plant Cell **19**: 986-1006

Dyall SD, Brown MT, Johnson PJ (2004) Ancient invasions: from endosymbionts to organelles. Science **304**: 253-257

Eckart K, Eichacker L, Sohrt K, Schleiff E, Heins L, Soll J (2002) A Toc75-like protein import channel is abundant in chloroplasts. EMBO Rep **3**: 557-562

Edwards GE, Black CC (1971) Photosynthesis in mesophyll cells and bundle sheath cells isolated from *Digitaria sanguinalis* (L). Scop. Leaves. In: Hatch MD, Osmond CB, Slatyer RO (eds) *Photosynthesis and Photorespiration.* New York, John Wiley Inc., pp. 153-158

Edwards GE, Franceschi VR, Ku MSB, Voznesenskaya EV, Pyankov VI, Andreo, CS (2001) Compartmentation of photosynthesis in cells and tissues of C_4 plants. J Exp Bot **52**: 577-590

Edwards GE, Franceschi VR, Voznesenskaya EV (2004) Single-cell C_4 photosynthesis versus the dual-cell (Kranz) paradigm. Annu Rev Plant Biol **55**: 173-196

Edwards GE, Huber SC (1981) The C_4 pathway. In: Hatch MD, Boardman NK (eds) *The biochemistry of plants: a comprehensive treatise.* Photosynthesis vol 8. Academic Press, New York, pp 237-281

Edwards GE, Lee TM, Chen TM, Black CC (1970) Carboxylation reactions and photosynthesis of carbon compounds in isolated mesophyll and bundle sheath cells of *Digitaria sanguinalis* (L.) Scop. Biochem Biophys Res Commun **39**: 389-395

Edwards GE, Walker DA (1983) *C_3, C_4: mechanisms, and cellular and environmental regulation, of photosynthesis*. Oxford, Blackwell Scientific Publications.

Ehlert A, Weltmeier F, Wang X, Mayer CS, Smeekens S, Vicente-Carbojosa J, Dröge-Laser W (2006) Two-hybrid protein-protein interaction analysis in Arabidopsis protoplasts: establishment of a heterodimerization map of group C and group S bZIP transcription factors. Plant J **46**: 890-900

Eisenberg D, Schwarz E, Komaromy M, Wall R (1984) Analysis of membrane and surface protein sequences with the hydrophobic moment plot. J Mol Biol **179**: 125-142

Emanuelsson O, Brunak S, von Heijne G, Nielsen H (2007) Locating proteins in the cell using TargetP, SignalP and related tools. Nat Protoc **2**: 953-971

Emanuelsson O, Nielsen H, Brunak S, von Heijne G (2000) Predicting subcellular localization of proteins based on their N-terminal amino acid sequence. J Mol Biol **300**: 1005-1016

Emanuelsson O, Nielsen H, von Heijne G (1999) ChloroP a neural network-based method for predicting chloroplast transit peptides and their cleavage sites. Protein Sci **8**: 978-984

Ertel F, Mirus O, Bredemeier R, Moslavac S, Becker T, Schleiff E (2005) The evolutionarily related beta-barrel polypeptide transporters from *Pisum sativum* and *Nostoc* PCC7120 contain two distinct functional domains. J Biol Chem **280**: 28281-28289

Ferro M, Salvi D, Brugiere S, Miras S, Kowalski S, Louwagie M, Garin J, Joyard J, Rolland N (2003) Proteomics of the chloroplast envelope membranes from *Arabidopsis thaliana*. Mol Cell Proteomics **2**: 325-345

Fischer K, Weber A, Arbinger B, Brink S, Eckerskorn C, Flügge UI (1994) The 24 kDa outer envelope membrane protein from spinach chloroplasts: molecular cloning, in vivo expression and import pathway of a protein with unusual properties. Plant Mol Biol **25**: 167-177

Flügge UI, Benz R (1984) Pore-forming activity in the outer membrane of chloroplast envelope. FEBS Lett **169**: 85-89

Forde BG, Lea PJ (2007) Glutamate in plants: metabolism, regulation, and signaling. J Exp Bot **58**: 2339-2358

Franceschi VR, Nakata PA (2005) Calcium oxalate in plants: formation and function. Annu Rev Plant Biol **56**: 41-71

Freitag H, Stichler W (2000) A remarkable new leaf type with unusual photosynthetic tissue in a Central Asiatic genus of Chenopodiaceae. Plant Biol **2**: 154-160

Freitag H, Stichler W (2002) *Bienertia cycloptera* Bunge ex Boiss., Chenopodiaceae, another C_4 plant without Kranz tissues. Plant Biol **4**: 121-132

Froehlich JE, Itoh A, Howe GA (2001) Tomato allene oxide synthase and fatty acid hydroperoxide lyase, two cytochrome P450s involved in oxylipin metabolism, are targeted to different membranes of chloroplast envelope. Plant Physiol **125**: 306-317

Fromm M, Taylor LP, Walbot V (1985) Expression of genes transferred into monocot and dicot plant cells by electroporation. Proc Natl Acad Sci USA **82**: 5824-5828

Fukayama H, Tsuchida H, Agarie S, Nomura M, Onodera H, Ono K, Lee BH, Hirose S, Toki S, Ku MSB, Makino A, Matsuoka M, Miyao M (2001) Significant accumulation of C_4-specific pyruvate orthophosphate dikinase in a C_3 plant, rice. Plant Physiol **127**: 1136-1146

Gamaley YV, Voznesenskaya EV (1986) Structural-biochemical types of C_4 plants. Soviet Plant Physiol **33**: 616-630

Gavel Y, von Heijne G (1990) A conserved cleavage site motif in chloroplast transit peptides. FEBS Lett **261**: 455-458

Giglioli-Guivarc'h N, Pierre JN, Brown S, Chollet R, Vidal J, Gadal P (1996) The light-dependent transduction pathway controlling the regulatory phosphorylation of C_4 phosphoenolpyruvate carboxylase in protoplasts from *Digitaria sanguinalis*. Plant Cell **8**: 573-586

Gillion J, Yakir D (2001) Influence of carbonic anhydrase activity in terrestrial vegetation on the ^{18}O content of atmospheric CO_2. Science **291**: 2584-2587

Glockner G, Rosenthal A, Valentin K. (2000) The structure and gene repertoire of an ancient red algal plastid genome. J Mol Evol **51**: 382-390

Goetze TA, Philippar K, Ilkavets I, Soll J, Wagner R (2006) OEP37 is a new member of the chloroplast outer membrane ion channels. J Biol Chem **281**: 17989-17998

Gomez L, Chrispeels MJ (1993) Tonoplast and soluble vacuolar proteins are targeted by different mechanisms. Plant Cell **5**: 1113-1124

Gould SJ, Keller GA, Hosken N, Wilkinson J, Subramani S (1989) A conserved tripeptide sorts proteins to peroxisomes. J Cell Biol **108**: 1657-1664

Gray JC, Sullivan JA, Wang JH, Jerome CA, MacLean D (2003) Coordination of plastid and nuclear gene expression. Phil Trans R Soc Lond B **358**: 135-145

Gutierrez M, Gracen VE, Edwards GE (1974) Biochemical and cytological relationships in C_4 plants. Planta **119**: 279-300.

Haberlandt G (1884) Physiologische pflanzenanatomie (Physiological plant anatomy). Engelmann, Leipzig

Halperin T, Ostersetzer O, Adam Z (2001) ATP-dependent association between subunits of Clp protease in pea chloroplasts. Planta **213**: 614-619

Harris EH, Boynton JE, Gillham NW (1994) Chloroplast ribosomes and protein synthesis. Microbiol Rev **58**: 700-754

Hatch MD (1971) Mechanism and function of C_4 photosynthesis. In: Hatch MD, Osmond CB, Slatyer RO (eds) *Photosynthesis and photorespiration*. Wiley-Interscience, New York, pp 139-152

Hatch MD, Slack CR (1966) Photosynthesis by sugar-cane leaves: a new carboxylation reaction and the pathway of sugar formation. Biochem J **101**: 103-111

Hatch MD, Slack CR (1970) Photosynthetic CO_2-fixation pathways. Annu Rev Plant Physiol **21**: 141-162

Hedges SB, Blair JE, Venturi ML, Shoe JL (2004) A molecular timescale of eukaryotic evolution and the rise of complex multicellular life. BMC Evol Biol **4**: 2

Heiber T, Steinkamp T, Hinnah S, Schwarz M, Flugge UI, Weber A, Wagner R (1995) Ion channels in the chloroplast envelope membrane. Biochemistry **34**: 15906-15917

Heins L, Mehrle A, Hemmler R, Wagner R, Küchler M, Hörmann F, Sveshnikov D, Soll J (2002) The preprotein conducting channel at the inner envelope membrane of plastids. EMBO J **21**: 2616-2625

Higaki T, Sano T, Hasezawa S (2007) Actin microfilament dynamics and actin side-binding proteins in plant. Curr Opin Plant Biol **10**: 549-556

Hiltbrunner A, Bauer J, Vidi PA, Infanger S, Weibel P, Hohwy M, Kessler F (2001) Targeting of an abundant cytosolic form of the protein import receptor atToc159 to the outer chloroplast membrane. J Cell Biol **154**: 309-316

Hiltbrunner A, Grünig K, Alvarez-Huerta M, Infanger S, Bauer J, Kessler F (2004) AtToc90, a new GTP-binding component of the *Arabidopsis* chloroplast protein import machinery. Plant Mol Biol **54**: 427-440

Hinnah SC, Hill K, Wagner R, Schlicher T, Soll J (1997) Reconstitution of a chloroplast protein import channel. EMBO J **16**: 7351-7360

Hinnah SC, Wagner R, Sveshnikova N, Harrer R, Soll J (2002) The chloroplast protein import channel Toc75: pore properties and interaction with transit peptides. Biophys J **83**: 899-911

Hirsch S, Muckel E, Heemeyer F, von Heijne G, Soll J (1994) A receptor component of the chloroplast protein translocation machinery. Science **266**: 1989-1992

Hörmann F, Küchler M, Sveshnikov D, Oppermann U, Li Y, Soll J (2004) Tic32, an essential component in chloroplast biogenesis. J Biol Chem **279**: 34756-34762

Hofmann N, Theg, SM (2005) Protein- and energy-mediated targeting of chloroplast outer envelope membrane proteins. Plant J **44**: 917-927

Horniak L, Pilon M, van't Hof R, de Kruijff B (1993) The secondary structure of the ferredoxin transit sequence is modulated by its interaction with negatively charged lipids. FEBS Lett **334**: 241-246

Huang W, Ling Q, Bédard J, Lilley K, Jarvis P (2011) *In vivo* analysis of the roles of essential Omp85-related proteins in the chloroplast outer envelope membrane. Plant Physiol **157**: 147-159

Hust B, Gutensohn M (2006) Deletion of core components of the plastid protein import machinery causes differential arrest of embryo development in *Arabidopsis thaliana*. Plant Biol **8**: 18-30

Imaizumi N, Ku MSB, Ishihara K, Samejima M, Kaneo S, Matsuoka M (1997) Characterization of the gene for pyruvate, orthophosphate dikinase from rice, a C_3 plant, and a comparison of structure and expression between C_3 and C_4 genes for this protein. Plant Mol Biol **34**: 701-716

Inaba T, Alvarez-Huerta M, Li M, Bauer J, Ewers C, Kessler F, Schnell DJ (2005) *Arabidopsis* tic110 is essential for the assembly and function of the protein import machinery of plastids. Plant Cell **17**: 1482-1496

Inaba T, Li M, Alvarez-Huerta M, Kessler F, Schnell DJ (2003) atTic110 functions as a scaffold for coordinating the stromal events of protein import into chloroplasts. J Biol Chem **278**: 38617-38627

Inaba T, Schnell DJ (2008) Protein trafficking to plastids: one theme, many variations. Biochem J **413**: 15-28

Inoue H, Akita M (2008) Three sets of translocation intermediates are formed during the early stage of protein import into chloroplasts. J Biol Chem **283**: 7491-7502

Inoue H, Rounds C, Schnell DJ (2010) The molecular basis for distinct pathways for protein import into *Arabidopsis* chloroplasts. Plant Cell **22**: 1947-1960

Inoue K (2011) Emerging roles of the chloroplast outer envelope membrane. Trends Plant Sci **16**: 1360-1385

Inoue K, Demel R, de Kruijff B, Keegstra K (2001) The N-terminal portion of the preToc75 transit peptide interacts with membrane lipids and inhibits binding and import of precursor proteins into isolated chloroplasts. Eur J Biochem **268**: 4036-4043

Inoue K, Potter D (2004) The chloroplastic protein translocation channel Toc75 and its paralog OEP80 represent two distinct protein families and are targeted to the chloroplastic outer envelope by different mechanisms. Plant J. **39**: 354-365

Ishikawa S, Bang SW, Kaneko Y, Matsuzawa Y (2003) Production and characterization of intergeneric somatic hybrids between *Moricandia arvensis* and *Brassica oleracea*. Plant Breed **122**: 233-238

Ivanova Y, Smith MD, Chen K, Schnell DJ (2004) Members of the Toc159 import receptor family represent distinct pathways for protein targeting to plastids. Mol Biol Cell **15**: 3379-3392

Ivey RA, Bruce BD (2000) *In vivo* and *in vitro* interaction of DnaK and a chloroplast transit peptide. Cell Stress Chaperon **5**: 62-71

Jackson DT, Froehlich JE, Keegstra K (1998) The hydrophilic domain of Tic110, an inner envelope membrane component of the chloroplastic protein translocation apparatus, faces the stromal compartment. J Biol Chem **273**: 16583-16588

Jackson-Constan D, Akita M, Keegstra K (2001) Molecular chaperones involved in chloroplast protein import. Biochim Biophys Acta **1541**: 102-113

Jarvis P (2007) Intracellular signalling: chloroplast backchat. Curr Biol **17**: R552-R555

Jarvis P (2008) Targeting of nucleus-encoded proteins to chloroplasts in plants. New Phytol **179**: 257-285

Jarvis P, Chen LJ, Li H, Peto CA, Fankhauser C, Chory J (1998) An *Arabidopsis* mutant defective in the plastid general protein import apparatus. Science **282**: 100-103

Jelic M, Sveshnikova N, Motzkus M, Horth P, Soll J, Schleiff E (2002) The chloroplast import receptor Toc34 functions as preprotein-regulated GTPase. Biol Chem **383**: 1875-1883

Jones DT (1999) Protein secondary structure prediction based on position-specific scoring matrices. J Mol Biol **292**: 195-202

Jorrín-Novo JV, Maldonado AM, Echevarría-Zomeño S, Valledor L, Castillejo MA, Curto M, Valero J, Sghaier B, Donoso G, Redondo I (2009) Plant proteomics update (2007-2008): Second-generation proteomic techniques, an appropriate experimental design, and data analysis to fulfill MIAPE standards, increase plant proteome coverage and expand biological knowledge. J Proteomics **72**: 285-314

Jouhet J, Gray JC (2009a) Interaction of actin and the chloroplast protein import apparatus. J Biol Chem **284**: 19132-19141

Jouhet J, Gray JC (2009b) Is chloroplast import of photosynthesis proteins facilitated by an actin-TOC-TIC-VIPP1 complex? Plant Signal Behav **4**: 986-988

Joyard J, Block MA, Douce R (1991) Molecular aspects of plastid envelope biochemistry. Eur J Biochem **274**: 32351-32359

Kalanon M, McFadden GI (2008) The chloroplast protein translocation complexes of *Chlamydomonas reinhardtii*: a bioinformatic comparison of Toc and Tic components in plants, green algae and red algae. Genetics **179**: 95-112

Kanai R, Edwards GE (1973) Purification of enzymatically isolated mesophyll protoplasts from C_3, C_4 and Crassulacean acid metabolism plants using an aqueous dextran-polyethylene glycol two-phase system. Plant Physiol **52**: 484-490

Kandasamy MK, Meagher RB (1999) Actin-organelle interaction: Association with chloroplast in *Arabidopsis* leaf mesophyll cells. Cell Motil Cytoskeleton **44**: 110-118

Keeling PJ (2004) Diversity and evolutionary history of plastids and their hosts. Am J Bot **91**: 1481-1493

Keller RCA (2011) New user-friendly approach to obtain an Eisenberg plot and its use as a practical tool in protein sequence analysis. Int J Mol Sci **12**: 5577-5591

Kerber B, Soll J (1992) Transfer of a chloroplast-bound precursor protein into the translocation apparatus is impaired after phospholipase C treatment. FEBS Lett **306**: 71-74

Kessler F, Blobel G (1996) Interaction of the protein import and folding machineries of the chloroplast. Proc Nat Acad Sci USA **93**: 7684-7689

Kessler F, Blobel G, Patel HA, Schnell DJ (1994) Identification of two GTP-binding proteins in the chloroplast protein import machinery. Science **266**: 1035-1039

Kessler F, Schnell DJ (2004) Chloroplast protein import: solve the GTPase riddle for entry. Trends Cell Biol **14**: 334-338

Kessler F, Schnell DJ (2006) The function and diversity of plastid protein import pathways: A multilane GTPase highway into plastids. Traffic **7**: 248–257

Kim C, Apel K (2004) Substrate-dependent and organ-specific chloroplast protein import in planta. Plant Cell **16**: 88-98

Kim C, Ham H, Apel K (2005) Multiplicity of different cell- and organ-specific import routes for the NADPH-protochlorophyllide oxidoreductases A and B in plastids of *Arabidopsis* seedlings. Plant J **42**: 329-340

Kleffmann T, Russenberger D, von Zychlinski A, Christopher W, Sjolander K, Gruissem W, Baginsky S (2004) The *Arabidopsis thaliana* chloroplast proteome reveals pathway abundance and novel protein functions. Curr Biol **14**: 354-362

Koch KE (1996) Carbohydrate-modulated gene expression in plants. Annu Rev Plant Physiol Mol Biol **47**: 509-540

Kouranov A, Chen X, Fuks B, Schnell DJ (1998) Tic20 and Tic22 are new components of the protein import apparatus at the chloroplast inner envelope membrane. J Cell Biol **143**: 991-1002

Kortschak HP, Hartt CE, Burr GO (1965) Carbon dioxide fixation in sugarcane leaves. Plant Physiol **40**: 209-213

Kost B, Spielhofer P, Chua NH (1998) A GFP–mouse talin fusion protein labels plant actin filaments in vivo and visualizes the actin cytoskeleton in growing pollen tubes. Plant J **16**: 393-401

Kouranov A, Schnell DJ (1997) Analysis of the interactions of preproteins with the import machinery over the course of protein import into chloroplasts. J Cell Biol **139**: 1677-1685

Kovács-Bogdán E, Benz JP, Soll J, Bölter B (2011) Tic20 forms a channel independent of Tic110 in chloroplasts. BMC Plant Biol **11**: 133

Krens FA, Molendijk L, Wullems GJ, Schilperoort RA (1982) *In vitro* transformation of plant protoplasts with Ti-plasmid DNA. Nature **296**: 72-74

Krimm I, Gans P, Hernandez JF, Arlaud GJ, Lancelin JM (1999) A coil-helix instead of a helix-coil motif can be induced in a chloroplast transit peptide from *Chlamydomonas reinhardtii*. Eur J Biochem **265**: 171-180

Krogh A, Larsson B, von Heijne G, Sonnhammer EL (2001) Predicting transmembrane protein topology with a hidden Markov model: application to complete genomes. J Mol Biol **305**: 567-580

Krupinska K (2006) Fate and activities of plastids during leaf senescence. In: Wise RR, Hoober JK (eds) *The Structure and Function of Plastids,* Vol. 23. Springer, Dordrecht, The Netherlands, pp. 433-449

Ku MSB, Agarie S, Nomura M, Fukayama H, Tsuchida H, Ono K, Hirose S, Toki, Miyao M, Matsuoka M (1999) High-level expression of maize phosphoenolpyruvate carboxylase in transgenic rice plants. Nat Biotechnol **17**: 76-80

Kubis S, Baldwin A, Patel R, Razzaq A, Dupree P, Lilley K, Kurth J, Leister D, Jarvis P (2003) The *Arabidopsis ppi1* mutant is specifically defective in the expression, chloroplast import, and accumulation of photosynthetic proteins. Plant Cell **15**: 1859-1871

Kubis S, Patel R, Combe J, Bédard J, Kovacheva S, Lilley K, Biehl A, Leister D, Ríos G, Koncz C, Jarvis P (2004) Functional specialization amongst the *Arabidopsis* Toc159 family of chloroplast protein import receptors. Plant Cell **16**: 2059-2077

Küchler M, Decker S, Hörmann F, Soll J, Heins L (2002) Protein import into chloroplasts involves redox-regulated proteins. EMBO J **21**: 6136-6145

Kumatani T, Sakurai-Ozato N, Miyawaki N, Yokota, E, Shimmen T, Terashima I, Takagi S (2006) Possible association of actin filaments with chloroplasts of spinach mesophyll cells in vivo and in vitro. Protoplasma **229**: 45-52

Lam HM, Coschigano KT, Oliveira IC, Melo-Oliveira R, Coruzzi GM (1996) The molecular genetics of nitrogen assimilation into amino acids in higher plants. Annu Rev Plant Physiol Plant Mol Biol **47**: 569-593

Lara MV, Offermann S, Smith M, Okita TW, Andreo CS, Edwards GE (2008) Leaf development in the single-cell C_4 system in *Bienertia sinuspersici*: expression of genes and peptides levels for C_4 metabolism in relation to chlorenchyma structure under different light conditions. Plant Physiol **148**: 593-610

Larkin PJ (1976) Purification and viability determinations of plant protoplasts. Planta **128**: 213-216

Lee DW, Kim JK, Lee S, Choi S, Kim S, Hwang I (2008) *Arabidopsis* nuclear-encoded plastid transit peptides contain multiple sequence subgroups with distinctive chloroplast-targeting sequence motifs. Plant Cell **20**: 1603-1622

Lee DW, Lee S, Lee G, Lee KH, Kim S, Cheong GW, Hwang I (2006) Functional characterization of sequence motifs in the transit peptide of *Arabidopsis* small subunit of Rubisco. Plant Physiol **140**: 466-483

Lee KH, Kim SJ, Lee YJ, Jin JB, Hwang I (2003) The M domain of atToc159 plays an essential role in the import of proteins into chloroplasts and chloroplast biogenesis. J Biol Chem **278**: 36794-36805

Lee YJ, Kim DH, Kim YW, Hwang I (2001) Identification of a signal that distinguishes between the chloroplast outer envelope membrane and the endomembrane system in vivo. Plant Cell **13**: 2175-2190

Lee YJ, Sohn EJ, Lee KH, Lee DW, Hwang I (2004) The transmembrane domain of AtToc64 and its C-terminal lysine-rich flanking region are targeting signals to the chloroplast outer envelope membrane. Mol Cells **17**: 281-291

Leister D (2003) Chloroplast research in the genomic age. Trends Genet **19**: 47-56

Li HM, Chen LJ (1996) Protein targeting and integration signal for the chloroplastic outer envelope membrane. Plant Cell **8**: 2117-2126

Li HM, Chen LJ (1997) A novel chloroplastic outer membrane-targeting signal that functions at both termini of passenger polypeptides. J Biol Chem **272**: 10968-10974

Li HM, Chiu CC (2010) Protein transport into chloroplasts. Annu Rev Plant Biol **61**: 157-180

Li HM, Moore T, Keegstra K (1991) Targeting of proteins to the outer envelope membrane uses a different pathway than transport into chloroplasts. Plant Cell **7**: 709-717

Lieman-Hurwitz J, Rachmilevitch S, Mittler R, Marcus Y, Kaplan A (2003) Enhanced photosynthesis and growth of transgenic plants that express ictB, a gene involved in HCO_3^- accumulation in cyanobacteria. Plant Biotechnol J **1**: 43-50

Lung SC, Yanagisawa M, Chuong SDX (2011) Protoplast isolation and transient gene expression in the single-cell C_4 species, *Bienertia sinuspersici*. Plant Cell Rep **30**: 473-484

Lung SC, Yanagisawa M, Chuong SDX (2012) Isolation of dimorphic chloroplasts from the single-cell C_4 species *Bienertia sinuspersici*. Plant Methods **8**: 8.

Ma Y, Kouranov A, LaSala S, Schnell DJ (1996) Two components of the chloroplast protein import apparatus, IAP86 and IAP75, interact with the transit sequence during the recognition and translocation of precursor proteins at the outer envelope. J Cell Biol **134**: 1-13

Majeran W, Cai Y, Sun Q, van Wijk KJ (2005) Functional differentiation of bundle sheath and mesophyll maize chloroplasts determined by comparative proteomics. Plant Cell **17**: 3111-3140

Majeran W, van Wijk KJ (2009) Cell-type-specific differentiation of chloroplasts in C_4 plants. Trends Plant Sci **14**: 100-109

Majeran W, Zybailov B, Ytterberg AJ, Dunsmore J, Sun Q, van Wijk KJ (2008) Consequences of C_4 differentiation for chloroplasts membrane proteomes in maize mesophyll and bundle sheath cells. Mol Cell Proteomics **7**: 1609-1638

Malkin R, Niyogi K (2000) Photosynthesis. In: Buchanan B, Gruissem W, Jones R (eds) *Biochemistry and Molecular Biology of the Plants.* Am Soc Plant Biol, Rockville, MD, pp. 568-628

Maple J, Moller SG (2007) Plastid division: evolution, mechanism and complexity. Ann Bot **99**: 565-579

Marc J, Granger CL, Brincat J, Fisher DD, Kao TH, McCubbin AG, Cyr RJ (1998) A GFP-*MAP4* reporter gene for visualizing cortical microtubule rearrangements in living epidermal cells. Plant Cell **10**: 1927-1940

Martin T, Sharma R, Sippel C, Waegemann K, Soll J, Vothknecht UC (2006) A protein kinase family in *Arabidopsis* phosphorylates chloroplast precursor proteins. J Biol Chem **281**: 40216-40223

May T, Soll J (1998) Positive charges determine the topology and functionality of the transmembrane domain in the chloroplastic outer envelope protein Toc34. J Biol Chem **141**: 895-904

May T, Soll J (2000) 14-3-3 proteins form a guidance complex with chloroplast precursor proteins in plants. Plant Cell **12**: 53-63

McFadden GI (1999) Endosymbiosis and evolution of the plant cell. Curr Opin Plant Biol **2**: 513-519

Millar AH, Carrie C, Pogson B, Whelan J (2009) Exploring the function-location nexus: using multiple lines of evidence in defining the subcellular location of plant proteins. Plant Cell **21**: 1625-1631

Miras S, Salvi D, Ferro M, Grunwald D, Garin J, Joyard J, Rolland N (2002) Noncanonical transit peptide for import into the chloroplast. J Biol Chem **277**: 47770-47778

Miras S, Salvi D, Piette L, Seigneurin-Berny D, Grunwald D, Reinbothe C, Joyard J, Reinbothe S, Rolland N (2007) Toc159- and Toc75-independent import of a transit sequence-less precursor into the inner envelope of chloroplasts. J Biol Chem **282**: 29482-29492

Miyagishima SY, Froehlich JE, Osteryoung KW (2006) PDV1 and PDV2 mediate recruitment of the dynamin-related protein ARC5 to the plastid division site. Plant Cell **18**: 2517-2530

Muckel E, Soll J (1996) A protein import receptor of chloroplasts is inserted into the outer envelope membrane by a novel pathway. J Biol Chem **271**: 23846-23852

Nakai K, Horton P (1999) PSORT: a program for detecting sorting signals in proteins and predicting their subcellular localization. Trends Biochem Sci **24**: 34-36

Nakrieko KA, Mould RM, Smith AG (2004) Fidelity of targeting to chloroplasts is not affected by removal of the phosphorylation site from the transit peptide. Eur J Biochem **271**: 509-516

Nanjo Y, Oka H, Ikarashi N, Kaneko K, Kitajima A, Mitsui T, Muñoz FJ, Rodríguez-López M, Baroja-Fernández E, Pozueta-Romero J (2006) Rice plastidial *N*-glycosylated nucleotide pyrophosphatase/phosphodiesterase is transported from the ER-golgi to the chloroplast through the secretory pathway. Plant Cell **18**: 2582-2592

Nasr-Esfahani MH, Aitken JR, Johnson MH (1990) Hydrogen peroxide levels in mouse oocytes and early cleavage embryos developed in vitro or in vivo. Development **109**: 501-507

Neuhaus HE, Emes MJ (2000) Nonphotosynthetic metabolism in plastids. Annu Rev Plant Physiol Plant Mol Biol **51**: 111-140

Neuhaus G, Spangenberg G (1990) Plant transformation by microinjection techniques. Physiol Plant **79**: 213-217

Nielsen E, Akita M, Davila-Aponte J, Keegstra K (1997) Stable association of chloroplastic precursors with protein translocation complexes that contain proteins from both envelope membranes and a stromal Hsp100 molecular chaperone. EMBO J **16**: 935-946

Nott A, Jung HS, Koussevitzky S, Chory J (2006) Plastid-to-nucleus retrograde signalling. Annu. Rev Plant Biol **57**: 739-759

Offermann S, Okita TW, Edwards GE (2011a) Resolving the compartmentation and function of C_4 photosynthesis in the single-cell C_4 species *Bienertia sinuspersici*. Plant Physiol **155**: 1612-1628

Offermann S, Okita TW, Edwards GE (2011b) How do single cell C_4 species form dimorphic chloroplasts? Plant Signal Behav **6**: 762-765

Ogren WL (1984) Photorespiration: pathways, regulation, and modification. Ann Rev Plant Physiol **35**: 415-542

Ohlrogge JB, Jaworski JG, Post-Beittenmiller D (1993) De novo fatty acid biosynthesis. In: Moore TS Jr (ed) *Lipid Metabolism in Plants*. CRC Press, Boca Raton, FL, pp. 3-32

Oikawa K, Yamasato A, Kong SG, Kasahara M, Nakai M, Takahashi F, Ogura Y, Kagawa T, Wada M (2008) Chloroplast outer envelope protein CHUP1 is essential for chloroplast anchorage to the plasma membrane and chloroplast movement. Plant Physiol **148**: 829-842

Olsen LJ, Keegstra K (1992) The binding of precursor proteins to chloroplasts requires nucleoside triphosphates in the intermembrane space. J Biol Chem **267**: 433-439

Onda Y, Matsumura T, Kimata-Ariga Y, Sakakibara H, Sugiyama T, Hase T (2000) Differential interaction of maize root ferredoxin:$NADP^+$ oxidoreductase with photosynthetic and non-photosynthetic ferredoxin isoproteins. Plant Physiol **123**: 1037-1045

Orczyk W, Przetakiewicz J, Nadolska-Orczyk A (2003) Somatic hybrids of *Solanum tuberosum*—application to genetics and breeding. Plant Cell Tissue Organ Cult **74**: 1-13

Osteryoung KW, McAndrew RS (2001) The plastid division machine. Ann Rev Plant Physiol Plant Mol Biol **52**: 315-333

Pain D, Blobel G (1987) Protein import into chloroplasts requires a chloroplast ATPase. Proc Nat Acad Sci USA **84**: 3288-3292

Park J, Knoblauch M, Okita TW, Edwards GE (2009) Structural changes in the vacuole and cytoskeleton are key to development of the two cytoplasmic domains supporting single-cell C_4 photosynthesis in *Bienertia sinuspersici*. Planta **229**: 369-382

Paszkowski J, Shillito RD, Saul M, Mandák V, Hohn T, Hohn B, Potrykus I (1984) Direct gene transfer to plant. EMBO J **3**: 2717-2722

Patron NJ, Waller RF (2007) Transit peptide diversity and divergence: a global analysis of plastid targeting signals. BioEssays **29**: 1048-1058

Perry SE, Keegstra K (1994) Envelope membrane proteins that interact with chloroplastic precursor proteins. Plant Cell **6**: 93-105

Peterhansel C, Maurino VG (2011) Photorepiration redesigned. Plant Physiol **155**: 49-55

Pierre JN, Pacquit V, Vidal J, Gadal P (1992) Regulatory phosphorylation of phosphoenolpyruvate carboxylase in protoplasts from *Sorghum* mesophyll cells and the role of pH and Ca^{2+} as possible components of the light-transduction pathway. Eur J Biochem **210**: 531-537

Pilon-Smits EAH, Pilon M (2006) Sulfur metabolism in plastids. In: Wise RR, Hoober JK (eds) *The Structure and Function of Plastids*, Vol. 23. Springer, Dordrecht, The Netherlands, pp. 387-402

Pinnaduwage P, Bruce BD (1996) *In vitro* interaction between a chloroplast transit peptide and chloroplast envelope lipids is sequence-specific and lipid class-dependent. J Biol Chem **271**: 32907-32915

Pohlmeyer K, Soll J, Grimm R, Hill K, Wagner R (1998) A high-conductance solute channel in the chloroplastic outer envelope from pea. Plant Cell **10**: 1207-1216

Poincelot RP (1976) Lipid and fatty acid composition of chloroplast envelope membranes from species with differing net photosynthesis. Plant Physiol **58**: 595-598

Pollmann S, Springer A, Buhr F, Lahroussi A, Samol I, Bonneville JM, Tichtinsky G, von Wettstein D, Reinbothe C, Reinbothe S (2007) A plant porphyria related to defects in plastid import of protochlorophyllide oxidoreductase A. Proc Nat Acad Sci USA **104**: 2019-2023

Pottosin II (1992) Single channel recording in the chloroplast envelope. FEBS Lett **308**: 87-90

Pringle JR, Preston RA, Adams AEM, Stearns T, Drubin DG, Haarer BK, Jones EW (1989) Fluorescence microscopy methods for yeast. Methods Cell Biol **31**: 357-435

Pujol C, Marechal-Drouard L, Duchene AM (2007) How can organellar protein N-terminal sequences be dual targeting signals? In silico analysis and mutagenesis approach. J Mol Biol **369**: 356-367

Qbadou S, Becker T, Bionda T, Reger K, Ruprecht M, Soll J, Schleiff E (2007) Toc64 – A preprotein-receptor at the outer membrane with bipartite function. J Mol Biol **367**: 1330-1346

Qbadou S, Becker T, Mirus O, Tews I, Soll J, Schleiff E (2006) The molecular chaperone Hsp90 delivers precursor proteins to the chloroplast import receptor Toc64. EMBO J **25**: 1836-1847

Qbadou S, Tien R, Soll J, Schleiff E (2003) Membrane insertion of the chloroplast outer envelope protein, Toc34: constrains for insertion and topology. J Cell Sci **116**: 837-846

Rahim G, Bischof S, Kessler F, Agne B (2009) In vivo interaction between *at*Toc33 and *at*Toc159 GTP-binding domains demonstrated in a plant split-ubiquitin system. J Exp Bot **60**: 257-267

Raikhel N, Chrispeels MJ (2000) Protein sorting and vesicle traffic. In: Buchanan B, Gruissem W, Jones R (eds) *Biochemistry and Molecular Biology of the Plants*. Am Soc Plant Biol, Rockville, MD, pp. 160-201

Raines (2011) Increasing photosynthetic carbon assimilation in C_3 plants to improve crop yield: current and future strategies. Plant Physiol **155**: 36-42

Ranson SL, Thomas M (1960) Crassulacean acid metabolism. Annu Rev Plant Physiol **11**: 81-110

Rassow J, Dekker PJT, van Wilpe S, Meijer M, Soll J (1999) The preprotein translocase of the mitochondrial inner membrane: Function and evolution. J Mol Biol **286**: 105-120

Reinbothe C, Lebedev N, Apel K, Reinbothe S (1997) Regulation of chloroplast protein import through a protochlorophyllide-responsive transit peptide. Proc Nat Acad Sci USA **94**: 8890-8894

Reinbothe S, Runge S, Reinbothe C, van Cleve B, Apel K (1995) Substrate-dependent transport of the NADPH:protochlorophyllide oxidoreductase into isolated plastids. Plant Cell **7**: 161-172

Reumann S, Keegstra K (1999) The endosymbiotic origin of the protein import machinery of chloroplastic envelope membranes. Trends Plant Sci **4**: 302-307

Richardson LGL, Jelokhani-Niaraki, M, Smith MD (2009) The acidic domains of the Toc159 chloroplast preprotein receptor family are intrinsically disordered protein domains. BMC Biochem **10**: 35

Richter S, Lamppa GK (1998) A chloroplast processing enzyme functions as the general stromal processing peptidase. Proc Natl Acad Sci USA **95**: 7463-7468

Robert S, Zouhar J, Carter C, Raikhel N (2007) Isolation of intact vacuoles from Arabidopsis rosette leaf-derived protoplasts. Nat Protoc **2**: 259-262

Rydzanicz R, Zhao XS, Johnson, PE (2005) Assembly PCR oligo maker: a tool for designing oligodeoxynucleotides for constructing long DNA molecules for RNA production. Nucl Acids Res **33**: W521-525

Sage RF (2001) Environmental and evolutionary preconditions for the origin and diversification of the C_4 photosynthetic syndrome. Plant Biol **3**: 202-213

Sage RF (2002) C_4 photosynthesis in terrestrial plants does not require Kranz anatomy. Trends Plant Sci **7**: 283-285

Sage RF (2004) The evolution of C_4 photosynthesis. New Phytol **161**: 341-370.

Sage RF, Li MR, Monson RK (1999) The taxonomic distribution of C_4 photosynthesis. In: Sage RF, Monson RK (eds) *C_4 Plant Biology*. San Diego, Academic Press, pp. 551-584

Sanchez-Pulido L, Devos D, Genevrois S, Vicente M, Valencia A (2003) POTRA: a conserved domain in the FtsQ family and a class of beta-barrel outer membrane proteins. Trends Biochem Sci **28**: 523-526

Sanford JC, Smith FD, Russell JA (1993) Optimizing the biolistic process for different biological applications. Methods Enzymol **217**: 482-509

Schleiff E, Becker T (2011) Common ground for protein translocation: access control for mitochondria and chloroplasts. Nat Rev Mol Cell Biol **12**: 48-59

Schleiff E, Eichacker LA, Eckart K, Becker T, Mirus O, Stahl T, Soll J (2003a) Prediction of the plant beta-barrel proteome: a case study of the chloroplast outer envelope. Protein Sci **12**: 748-759

Schleiff E, Jelic M, Soll J (2003b) A GTP-driven motor moves proteins across the outer envelope of chloroplasts. Proc Natl Acad Sci USA **100**: 4604-4609

Schleiff E, Klösgen RB (2001) Without a little help from 'my' friends: direct insertion of proteins into chloroplast membranes? Biochim Biophys Acta **1541**: 22-33

Schleiff E, Soll J, Küchler M, Kuhlbrandt W, Harrer R (2003c) Characterization of the translocon of the outer envelope of chloroplasts. J Cell Biol **160**: 541-551

Schleiff E, Soll J, Sveshnikova N, Tien R, Wright S, Dabney-Smith C, Subramanian C, Bruce BD (2002) Structural and guanosine triphosphate/diphosphate requirements for transit

peptide recognition by the cytosolic domain of the chloroplast outer envelope receptor, Toc34. Biochemistry **41**: 1934-1946

Schleiff E, Tien R, Salomon M, Soll J (2001) Lipid composition of outer leaflet of chloroplast outer envelope determines topology of OEP7. Mol Biol Cell **12**: 4090-4102

Schnell DJ, Blobel G, Keegstra K, Kessler F, Ko K, Soll J (1997) A consensus nomenclature for the protein-import components of the chloroplast envelope. Trends Cell Biol **7**: 303-304

Schnell DJ, Kessler F, Blobel G (1994) Isolation of components of the chloroplast protein import machinery. Science **266**: 1007-1012

Seedorf M, Waegemann K, Soll J (1995) A constituent of the chloroplast import complex represents a new type of GTP-binding protein. Plant J **7**: 401-411

Shanklin J, DeWitt ND, Flanagan JM (1995) The stroma of higher plant plastids contain ClpP and ClpC, functional homologs of *Escherichia coli* ClpP and ClpA: an archetypal two-component ATP-dependent protease. Plant Cell **7**: 1713-1722

Sheen J (1990) Metabolic repression of transcription in higher plants. Plant Cell **2**: 1027-1038

Sheen J (1991) Molecular mechanisms underlying the differential expression of maize pyruvate, orthophosphate dikinase genes. Plant Cell **3**: 225-245

Sheen J (1995) Methods for mesophyll and bundle sheath cell separation. In: Galbraith DW, Bourque DP, Bohnert HJ (eds) *Methods in Cell Biology,* Part A. Academic Press, Orlando, pp. 305-314

Sheen J (2001) Signal transduction in maize and Arabidopsis mesophyll protoplasts. Plant Physiol **127**: 1466-1475

Siedow JN, David D (2000) Respiration and photorespiration. In: Buchanan B, Gruissem W, Jones R (eds) *Biochemistry and Molecular Biology of the Plants.* Am Soc Plant Biol, Rockville, MD, pp. 676-728

Simon M, Hancock JM (2009) Tandem and cryptic amino acid repeats accumulate in disordered regions of proteins. Genome Biol **10**: R59.1-R59.16

Small I, Peeters N, Legeai F, Lurin C (2004) Predotar: a tool for rapidly screening proteomes for N-terminal targeting sequences. Proteomics **4**: 1581-1590

Smith MD (2006) Protein import into chloroplasts: an ever-evolving story. Can J Bot **84**: 531-542

Smith MD, Fitzpatrick LM, Keegstra K, Schnell DJ (2002b) *In vitro* analysis of chloroplast protein import. In: Yamada KM (ed) *Current Protocols in Cell Biology*. John Wiley & Sons, New York, pp. 11.16.11-11.16.21

Smith MD, Hiltbrunner A, Kessler F, Schnell DJ (2002a) The targeting of the atToc159 preprotein receptor to the chloroplast outer membrane is mediated by its GTPase domain and is regulated by GTP. J Cell Biol **159**: 833-843

Smith MD, Rounds CM, Wang F, Chen K, Afitlhile M, Schnell DJ (2004) atToc159 is a selective transit peptide receptor for the import of nucleus-encoded chloroplast proteins. J Cell Biol **165**: 323-334

Sohrt K, Soll J (2000) Toc64, a new component of the protein translocon of chloroplasts. J Cell Biol **148**: 1213-1221

Stahl T, Glockmann C, Soll J, Heins L (1999) Tic40, a new 'old' subunit of the chloroplast protein import translocon. J Biol Chem **274**: 37467-37472

Stengel A, Benz P, Balsera M, Soll J, Bölter B (2008) TIC62 redox-regulated translocon composition and dynamics. J Biol Chem **283**: 6656-6667

Stitt M, Schulze D (1994) Does rubisco control the rate of photosynthesis and plant-growth —an exercise in molecular ecophysiology. Plant Cell Environ **17**: 465-487.

Suetsugu N, Wada M (2007) Chloroplast photorelocation movement mediated by phototropin family proteins in green plants. Biol Chem **388**: 927-935

Sun Q, Zybailov B, Majeran W, Friso G, Olinares PDB, van Wijk KJ (2009) PPDB, the Plant Proteomics Database at Cornell. Nucl Acids Res **37**: D969-D974

Sun YJ, Forouhar F, Li H, Tu SL, Yeh YH, Kao S, Shr HL, Chou CC, Chen C, Hsiao CD (2002) Crystal structure of pea Toc34, a novel GTPase of the chloroplast protein translocation. Nat Struct Biol **9**: 95-100

Surridge C (2002) The rice squad. Nature **416**: 576-578

Sveshnikova N, Grimm R, Soll J, Schleiff E (2000) Topology studies of the chloroplast protein import channel Toc75. Biol Chem **381**, 687-693

Taiz L, Zeiger E (2010) *Plant Physiology*, Fifth edition. Sinauer Associates, Sunderland, MA, USA

Takeuchi Y, Akagi H, Kamasawa N, Osumi M, Honda H (2000) Aberrant chloroplasts in transgenic rice plants expressing a high level of maize NADP-dependent malic enzyme. Planta **211**: 265-274

Tamura K, Peterson D, Peterson N, Stecher G, Nei M, Kumar S (2011) MEGA5: Molecular Evolutionary Genetic Analysis using maximum likelihood, evolutionary distance, and maximum parsimony methods. Mol Biol Evol **28**: 2731-2739

Teng YS, Su YS, Chen LJ, Lee YJ, Hwang I, Li HM (2006) Tic21 is an essential translocon component for protein translocation across the chloroplast inner envelope membrane. Plant Cell **18**: 2247-2257

Theg SM, Bauerle C, Olsen LJ, Selman BR, Keegstra K (1989) Internal ATP is the only energy requirement for the translocation of precursor proteins across chloroplastic membranes. J Biol Chem **264**: 6730-6736

Tieszen LL, Senyimba MM, Imbamba SK, Troughton JH (1979) The distribution of C_3 and C_4 grasses and carbon isotope discrimination along an altitudinal and moisture gradient in Kenya. Oecologia **37**: 337-350

Tolbert NE (1981) Metabolic pathways in peroxisomes and glyoxysomes. Annu Rev Biochem **50**: 133-157

Tompa P (2003) Intrinsically unstructured protein evolve by repeat expansion. Bioessays **25**: 847-855

Torres JH, Maldonado MAA, Chomilier J (2007) Tandem duplications of a degenerated GTP-binding domain at the origin of GTPase receptors Toc159 and thylakoidal SRP. Biochem. Biophys Res Commun **364**: 325-331

Tranel PJ, Froehlich J, Goyal A, Keegstra K (1995) A component of the chloroplastic protein import apparatus is targeted to the outer envelope membrane via a novel pathway. EMBO J **14**: 2436-2446

Tranel PJ, Keegstra K (1996) A novel, bipartite transit peptide targets OEP75 to the outer membrane of the chloroplastic envelope. Plant Cell **8**: 2093-2104

Tsai LY (1999) Insertion of atToc34 into the chloroplastic outer membrane is assisted by at least two proteinaceous components in the import system. J Biol Chem **274**: 18735-18740

Tu SL, Li HM (2000) Insertion of OEP14 into the outer envelope membrane is mediated by proteinaceous components of chloroplasts. Plant Cell **12**: 1951-1960

Tu SL, Chen LJ, Smith MD, Su YS, Schnell DJ, Li HM (2004) Import pathways of chloroplast interior proteins and the outer-membrane protein OEP14 converge at Toc75. Plant Cell **16**: 2078-2088

van Wijk KJ (2004) Plastid proteomics. Plant Physiol Biochem **42**: 963-977

van't Hof R, de Kruijff B (1995) Characterization of the import process of a transit peptide into chloroplasts. J Biol Chem **270**: 22368-22373

Villarejo A, Buren S, Larsson S, Dejardin A, Monne M, Rudhe C, Karlsson J, Jansson S, Lerouge P, Rolland N, von Heijne G, Grebe M, Bako L, Samuelsson G (2005) Evidence for a protein transported through the secretory pathway en route to the higher plant chloroplast. Nat Cell Biol **7**: 1124-1131

Voigt A, Jakob M, Klösgen RB, Gutensohn M (2005) At least two Toc34 protein import receptors with different specificities are also present in spinach chloroplasts. FEBS Lett **579**: 1343-1349

von Braun SS, Schleiff E (2008) The chloroplast outer membrane protein CHUP1 interacts with actin and profilin. Planta **227**: 1151-1159

von Heijne G, Nishikawa K (1991) Chloroplast transit peptides the perfect random coil? FEBS Lett **278**: 1-3

von Heijne G, Steppuhn J, Herman SG (1989) Domain structure of mitochondrial and chloroplast targeting peptides. Eur J Biochem **180**: 535-545

Vothknecht UC, Westhoff P (2001) Biogenesis and origin of thylakoid membranes. Biochim Biophys Acta **1541**: 91-101

Voznesenskaya EV, Edwards, GE, Kiirats O, Artyusheva EG, Franceschi VR (2003) Development of biochemical specialization and organelle partitioning in the single-cell C_4 system in leaves of *Borszczowia aralocaspica* (Chenopodiaceae). Am J Bot **90**: 1669-1680

Voznesenskaya EV, Franceschi VR, Kiirats O, Artyusheva EG, Freitag H, Edwards GE (2002) Proof of C_4 photosynthesis without Kranz anatomy in *Bienertia cycloptera* (Chenopodiaceae). Plant J **31**: 649-662

Voznesenskaya EV, Franceschi VR, Kiirats O, Freitag H, Edwards GE (2001) Kranz anatomy is not essential for terrestrial C_4 plant photosynthesis. Nature **414**: 543-546

Voznesenskaya EV, Franceschi VR, Pyankov VI, Edwards GE (1999) Anatomy, chloroplast structure and compartmentation of enzymes relative to photosynthetic mechanisms in leaves and cotyledons of species in the tribe Salsoleae (Chenopdiaceae). J Exp Bot **50**: 1779-1795

Voznesenskaya EV, Koteyeva NK, Chuong SDX, Akhani H, Edwards GE, Franceschi VR (2005) Differentiation of cellular and biochemical features of the single-cell C_4 syndrome during leaf development in *Bienertia cycloptera* (Chenopodiaceae). Am J Bot **92**: 1784-1795

Waegemann K, Soll J (1996) Phosphorylation of the transit sequence of chloroplast precursor proteins. J Biol Chem **271**: 6545-6554

Wallas TR, Smith MD, Sanchez-Nieto S, Schnell DJ (2003) The roles of Toc34 and Toc75 in targeting the Toc159 preprotein receptor to chloroplasts. J Biol Chem **278**: 44289-44297

Waters TM, Langdale JA (2009) The making of a chloroplast. EMBO J **28**: 2861-2873

Wang F, Agne, B, Kessler F, Schnell DJ (2008) The role of GTP binding and hydrolysis at the atToc159 preprotein receptor during protein import into chloroplasts. J Cell Biol **183**: 87-99

Wienk HL, Czisch M, de Kruijff B (1999) The structural flexibility of the preferredoxin transit peptide. FEBS Lett **453**: 318-326

Wienk HL, Wechselberger RW, Czisch M, de Kruijff B (2000) Structure, dynamics, and insertion of a chloroplast targeting peptide in mixed micelles. Biochemistry **39**: 8219-8282

Wiese A, Gröner F, Sonnewald U, Deppner H, Lerchl J, Hebbeker U, Flügge UI, Weber A (1999) Spinach hexokinase I is located in the outer envelope membrane of plastids. FEBS Lett **461**: 13-18

Winter K (1981) C_4 plants of high biomass in arid regions of Asia. Occurrence of C_4 photosynthesis in Chenopodiaceae and Polygonaceae from the Middle East and USSR. Oecologia **48**: 100-106

Wise RR (2006) The diversity of plastid form and function. In: Wise RR, Hoober JK (eds) *The Structure and Function of Plastids,* Vol. 23. Springer, Dordrecht, The Netherlands, pp. 3-26

Yamada M, Kawasaki M, Sugiyama T, Miyake H, Taniguchi M (2009) Differential positioning of C_4 mesophyll and bundle sheath chloroplasts: aggregative movement of C_4 mesophyll chloroplasts in response to environmental stresses. Plant Cell Physiol **50**: 1736-1749

Yanagisawa M (2012) Expression of photosynthetic genes and possible regulatory mechanisms in the single-cell C_4 species, *Bienertia sinuspersici*. PhD thesis, University of Waterloo

Yang Y, Glynn J, Olsen B, Schmitz A, Osteryoung KW (2008) Plastid division: across time and space. Curr Opin Plant Biol **11**: 577-584

Yoo SD, Cho YH, Sheen J (2007) *Arabidopsis* mesophyll protoplasts: a versatile cell system for transient gene expression analysis. Nat Protoc **2**: 1565-1572

Yoon HS, Hackett JD, Ciniglia C, Pinto G, Bhattacharya D (2004) A molecular timeline for the origin of photosynthetic eukaryotes. Mol Biol Evol **21**: 809-818

Young ME, Keegstra K, Froehlich JE (1999) GTP promotes the formation of early-import intermediates but is not required during the translocation step of protein-import into chloroplasts. Plant Physiol **121**: 237-244

Yu TS, Li HM (2001) Chloroplast protein translocon components atToc159 and atToc33 are not essential for chloroplast biogenesis in guard cells and root cells. Plant Physiol **127**: 90-96

Zachos J, Pagani M, Sloan L, Thomas E, Billups K (2001) Trends, rhythms and aberrations in global climate 65 Ma to present. Science **292**: 686-693

Zhang XP and Glaser E (2002) Interaction of plant mitochondrial and chloroplast signal peptides with the Hsp70 molecular chaperone. Trends Plant Sci **7**: 14-21

Zybailov B, Rutschow H, Friso G, Rudella A, Emanuelsson O, Sun Q, van Wijk KJ (2008) Sorting signals, N-terminal modifications and abundance of the chloroplast proteome. PLoS ONE **3**: e1994